

Investigation of a Non-Destructive System to Evaluate Critical Properties of Asphalt

Robert L. Schmitt, P.E., Ph.D.

Ahmed Faheem, Ph.D.

Department of Civil and Environmental Engineering
University of Wisconsin at Platteville

Imad L. Al-Qadi, P.E., Ph.D.

Department of Civil and Environmental Engineering
University of Illinois at Urbana-Champaign

WisDOT ID no. 0092-11-01

October 2013



RESEARCH & LIBRARY UNIT



WISCONSIN HIGHWAY RESEARCH PROGRAM

WISCONSIN DOT
PUTTING RESEARCH TO WORK

Technical Report Documentation Page

1. Report No. 0092-11-01		2. Government Accession No		3. Recipient's Catalog No	
4. Title and Subtitle Investigation and Development of a Non-Destructive System to Evaluate Critical Properties of Asphalt Pavements during the Compaction Process				5. Report Date October 2013	
				6. Performing Organization Code Wisconsin Highway Research Program	
7. Authors Robert L. Schmitt, Ahmed Faheem, and Imad L. Al-Qadi				8. Performing Organization Report No.	
9. Performing Organization Name and Address Department of Civil and Environmental Engineering University of Wisconsin-Platteville 1 University Plaza Platteville, WI 53818				10. Work Unit No. (TRAIS)	
				11. Contract or Grant No.	
12. Sponsoring Agency Name and Address Wisconsin Highway Research Program Wisconsin Department of Transportation WisDOT Research & Library Unit 4805 Sheboygan Avenue, Room 104 P.O. Box 7915 Madison, WI 53707				13. Type of Report and Period Covered Final Report. April 2010 – October 2013	
				14. Sponsoring Agency Code	
15. Supplementary Notes					
16. Abstract The purpose of this report is to present findings from a two-stage investigation to develop a non-destructive system to evaluate critical properties and characteristics of asphalt pavements during the compaction process. The first stage aligned critical properties and characteristics with available non-destructive testing (NDT) technologies. A quantitative ranking was created with an objective and unbiased scoring system to determine the most appropriate NDTs for field evaluation. Based upon this ranking system, the three higher-ranked NDTs for the evaluation and selected for a field evaluation were: Infrared Thermography (IR), Ground Penetrating Radar (GPR), and Portable Seismic Pavement Analyzer (PSPA). The nuclear density gauge was also used in the evaluation. The second stage of the investigation collected field data from three projects, analyzed the data using a variety of methods, and developed an implementation plan based upon the findings. Continuous infrared (IR) thermal readings measured mat temperature at 12 transverse offsets spaced 13 in apart, and at a 1 ft longitudinal spacing. Analysis of the data found greater variability along centerline of the paving mat. The average nuclear density on the three projects was nearly identical, ranging from 92.4% to 92.6%, and standard deviations of 2.21%, 1.66%, and 1.40%. The GPR density standard deviation was about half that of nuclear density. GPR thickness among the projects had a standard deviation ranging from 0.1 to 0.2 inches. Variability closer to the pavement centerline was generally higher. Average modulus normalized at 130°F on Project 1 was 3616 ksi, Project 2 at 3014 ksi, and Project 3 at 2530 ksi. Data from the three projects found no definitive relationship between continuous thermal temperatures behind the paver and final density measured by GPR and nuclear density gauge. Placement temperature did not appear to affect modulus; this finding is limited to the three projects in this study and may not be true for all mixes placed in Wisconsin or other states.					
17. Key Words Asphalt Pavement, Compaction, Non-Destructive Technologies, Infrared Thermography, Ground Penetrating Radar, Portable Seismic Pavement Analyzer			18. Distribution Statement No restriction. This document is available to the public through the National Technical Information Service 5285 Port Royal Road Springfield VA 22161		
18. Security Classif.(of this report) Unclassified		19. Security Classif. (of this page) Unclassified		20. No. of Pages 233	21. Price

Disclaimer

This research was funded through the Wisconsin Highway Research Program by the Wisconsin Department of Transportation and the Federal Highway Administration under Project 0092-11-01. The contents of this report reflect the views of the authors who are responsible for the facts and accuracy of the data presented herein. The contents do not necessarily reflect the official views of the Wisconsin Department of Transportation or the Federal Highway Administration at the time of publication.

This document is disseminated under the sponsorship of the Department of Transportation in the interest of information exchange. The United States Government assumes no liability for its contents or use thereof. This report does not constitute a standard, specification or regulation.

The United States Government does not endorse products or manufacturers. Trade and manufacturers' names appear in this report only because they are considered essential to the object of the document.

Executive Summary

The purpose of this final report is to present findings from a two-stage investigation to develop a non-destructive system to evaluate critical properties and characteristics of asphalt pavements during the compaction process.

Stage One of the investigation defined critical characteristics during compaction, investigated non-destructive testing (NDT) technologies to measure these characteristics, and ranked the NDTs to evaluate selected systems in the second stage of the study. A discussion with asphalt technologists in the state of Wisconsin ranked the critical characteristics in order as in-place compaction, thermal segregation, and modulus. NDT technologies capable of measuring asphalt pavement during compaction were investigated including: Deflectometers, Ground Penetration Radar, Impact Echo, Ultrasonic Pulse Velocity, Infrared Thermography, Intelligent Compaction, Lasers, Permeameters, and Ultrasonic Seismic. Each technology was evaluated against 12 specific attributes including: operational principle; measures and indicators; test equipment; portability of the test; complexity of execution in the field; testing time; environmental limitations; data reliability; committee-approved test protocols; degree of training required; cost; and states using the technology in practice. Critical properties and characteristics were aligned with available NDTs and quantitative ranking was created with an objective and unbiased scoring system to determine the most appropriate NDTs for field evaluation. Based upon this ranking system, the three higher-ranked NDTs for the evaluation and selected for a field evaluation were: Infrared Thermography, Ground Penetrating Radar, and Portable Seismic Pavement Analyzer. The nuclear density gauge was also used in the evaluation.

Stage Two of the investigation collected field data from three projects, analyzed the data using a variety of methods, and developed an implementation plan based upon the findings. Research test section lengths were 5,000 ft to 6,000 ft, having 500-ft sublots to manage data sampling and analysis. Five offsets from pavement centerline were established to evaluate measurements at both longitudinal joints, both wheel paths, and between the wheel paths.

Continuous infrared (IR) thermal readings measured mat temperature at 12 transverse offsets spaced 13 in apart, and at a 1 ft longitudinal spacing. Analysis of the data found greater variability along centerline of the paving mat. Average sensor temperatures varied among projects due to project-specific factors, such as mixing temperature that reported respective lower and upper measurements per project of 240 to 260°F, 288 to 303°F, and 287 to 327°F. Three sensors were out of calibration on the third project yielding high pavement temperatures that exceeded the plant mix temperature and the temperature of neighboring sensors by about 25 to 40°F. Average temperature of neighboring sensors were random (Project 1) or higher in the center and lower at the edges (Project 2). Variability was similar between adjoining sensors (Project 3) but greater at the outer sensors (Projects 1 and 2).

Graphs from the continuous thermal data and FLIR camera images consistently detected a distinctive V-shaped pattern at intervals equivalent to the length of a truckload of mix (80 to 135 ft) caused by cooler material spooling transversely by the augers as the paver moved longitudinally forward. The paver chain case was identified as a potential

cause of segregation in the paving operation creating a linear low-temperature streak in the mat.

Thermal camera images of the truck box, material transfer vehicle (MTV), and paver screed illustrated the mix temperature range using selected points and lines. The range of the material in the truck box was approximately 100°F to 160°F, and material behind the screed ranged from 8°F to 53°F. When a pass/fail criterion was set at a range of 25°F behind the screed, locations having an MTV were able to pass this requirement in 10 of 11 tests. Locations not having an MTV failed this requirement in 4 of 4 tests. Use of an MTV was able to reduce mat temperature variability. The range reduction ratio, as measured by the ratio of the truck temperature range to mat temperature range, was 2.1 up to 14.8. On Project 2, the standard deviation was reduced in half 9.4°F to 5.5°F when the MTV was added to the operation. The range also reduced from an average 66°F to 51°F.

Comparisons of the temperature range with the FLIR thermal image camera and Pave-IR sensor bar found that the thermal camera image measured a higher range than the sensor bar of up to 28°F. An issue when implementing the Pave-IR bar into practice is acknowledging this disparity, particularly if there is movement towards an allowable range, such as 25°F range found in some specifications. With respect to both thermal imaging techniques, it is important to note that in many instances the crust of the load was recorded and once the load is broke the underlying material will be much hotter.

GPR thickness among the projects had a standard deviation ranging from 0.1 to 0.2 inches, and coefficient of variation 2 to 9%. Variability closer to the pavement centerline was generally higher. GPR density on Project 1 at an offset of 2.5 ft from centerline averaged 93.8% with standard deviation 1.4%, while a 6-ft offset towards the middle of the lane averaged 94.7% and standard deviation of 1.1%. Density averages were fairly consistent at 94% for offsets of 9.5 ft and 11.5 ft on Project 2, and about 90.5% density at offsets of 6 ft, 9.5 ft and 11.5 ft on Project 3. However, the average GPR density values on Project 3 were 2 percentage points lower than the nuclear density gauge at 92.5% due to calibration.

The average nuclear density on the three projects was nearly identical, ranging from 92.4% to 92.6% and standard deviations of 2.21%, 1.66%, and 1.40%. Coefficient of variation for nuclear density was below 2.4% on all projects. By comparison, the project standard deviation of the GPR density were 1.4% and 1.1% (Project 1), 0.9% and 1.1% (Project 2), and 0.5% and 0.6% (Project 3). In other words, the GPR density standard deviation was about half that of nuclear density.

Modulus was investigated by offset location on the mat, as well as the sensitivity of the field test to pavement temperature (warm at about 140°F, or cool below 100°F). There was no effect in modulus by offset (centerline, between wheel path, right wheel path, etc.) even though density varied by offset. There was a reduction in modulus of 20 to 54 ksi for a 1°F increase, reflecting the viscoelastic nature of asphalt pavements with temperature, but also creating a complexity when measuring as-constructed modulus when the test is a function of the mat temperature.

Average modulus constructed on Project 1 was 3616.2 ksi, Projects 2 at 3014.1 ksi, and Project 3 at 2530.2 ksi. These modulus values were normalized at 130°F. Respective coefficient of variation (COV) values were at 17%, 14%, and 32%. In part, the relatively high variability in the modulus values is due to the technique of testing applied. A circle of 1 ft diameter was drawn at the test location. Five readings were taken, one in the center of the circle, and four around the circle circumference such that each test is 90° apart from the adjacent two.

Plots for the three projects found no definitive relationship between continuous thermal temperatures behind the paver and final density measured by GPR. Statistical correlations among NDTs using the average and standard deviation were computed for each NDT using all samples within each 500-ft subplot. The correlation slope among variables was inconsistent for any combination of variables, except for negative correlations between mean IR temperature and GPR thickness. This lack of consistency presents a challenge for developing a compaction system using these combinations of NDT test devices, in their current form, as interrelated quality control and acceptance tools. Additionally, previous research by Washington DOT found that temperature differentials were found to lead to significant density differentials in the finished mat (Willoughby et al. 2001). Over 40% of the jobs observed had temperature differentials of 25°F or greater. In this study, there was a very weak or no correlation between variability in IR temperature and nuclear density on the three projects.

An investigation assessed the ability of the proposed technologies to distinguish nonconforming sections of pavement using nuclear density as the baseline indicator. The average values for the densities for the conforming test points were consistently above 93%, while nonconforming test points ranged in average density values of 89.4 to 90.7%. The majority of the nonconforming test points were at the centerline edge of the pavement. The average modulus for nonconforming test points was lower than that of conforming except for one project where the nonconforming modulus was higher by 6.5%. Modulus at the outer edge of pavement was dependent on the pavement thickness. Density of the outer edge did not correlate with the pavement thickness.

Placement temperature does not appear to affect measured modulus or density. This could be due to the fact that the mixture is placed at suitable temperature for compaction, as well as prior research that has identified number of the passes at warmer temperatures as a key factor in achieving density. The results suggest that the final pavement quality is controlled by the compaction process behind the paver.

Recommendations for future implementation of these NDT technologies were enumerated using findings from the field data and previous research. Findings for thermal readings suggest that further research and development is necessary to create a structured system to generate reliable data, primarily due to calibration and differences between the thermal camera and Pave-IR sensor bar. Additionally, the relationship between temperature variability and performance is necessary for future implementation.

Findings for GPR indicate that the technology is state-of-the-art for HMA construction. This technology is valuable in mapping the thickness and density by offset and was able to detect more density variability along the centerline of the mat.

PSPA findings suggest that this technology is state-of-the-art for HMA construction, with a high level of variability (coefficient of variation). This technology is of interest in determining pavement strength with a seismic wave technique. It is, however, not a function of pavement density, but rather the layer thickness, which is plausible since there is generally greater pavement strength with added thickness.

Table of Contents

Disclaimer	ii
Executive Summary.....	iii
Acknowledgments	x
List of Tables.....	xi
List of Figures	xiii
Chapter 1 Introduction.....	1
1.1 Background.....	1
1.2 Challenge in Measuring In-Situ Asphaltic Concrete Density	1
1.3 Research Objectives	1
1.4 Report Structure.....	2
Chapter 2 Critical Characteristics and NDT Technologies.....	4
2.1 Introduction	4
2.2 Critical Characteristics	4
2.2.1 Mix Segregation	5
2.2.2 In-Place Compaction	5
2.2.3 Pavement Layer Thickness	6
2.2.4 Smoothness (Roughness).....	7
2.2.5 Temperature Segregation.....	7
2.2.6 Layer Interface Bonding	8
2.2.7 Pavement Layer Moduli	8
2.3 NDT Technologies	9
2.4 Ranking of Compaction Systems.....	14
2.4.1 Critical Characteristics and Non-Destructive Testing Technologies	14
2.4.2 Simplified Characteristics and Non-Destructive Testing Technologies	15
2.4.3 Ranking of Evaluation Systems.....	16
Chapter 3 Data Collection	21
3.1 Technologies and Models	21
3.2 Sampling Plan and Projects	21
3.3 Infrared Thermography.....	23
3.3.1 Sensors mounted to paver (Pave IR system)	23
3.3.2 Thermal Camera	25
3.4 Ground Penetrating Radar	28
3.5 Portable Seismic Pavement Analyzer	33
3.6 Project 1, U.S. Highway 2	36
3.7 Project 2, State Highway 75	38
3.8 Project 3, State Highway 42	42
Chapter 4 Data Summary	45
4.1 Introduction	45
4.2 Infrared Thermography.....	45
4.2.1 Project 1, USH 2.....	45
4.2.2 Project 2, STH 75	47
4.2.3 Project 3, STH 42	48
4.3 Ground Penetrating Radar	51
4.3.1 Project 1, USH 2.....	51
4.3.2 Project 2, STH 75	52
4.3.3 Project 3, STH 42	53
4.4 Portable Seismic Pavement Analyzer	55
4.4.1 Project 1, USH 2.....	55

4.4.2 Project 2, STH 75	60
4.4.3 Project 3, STH 42	62
4.5 Temperature Adjustment	65
4.6 Summary	66
4.6.1 Continuous Thermal Readings	66
4.6.2 Continuous GPR Thickness and Density Data	67
4.6.3 Point Measures for Seismic Modulus and Nuclear Density	68
Chapter 5 Thermal Analysis	70
5.1 Introduction	70
5.2 Project 1 Thermal Images	70
5.2.1 Stations 435+00 to 430+00	70
5.2.2 Stations 430+00 to 425+00	72
5.2.3 Station 422+00	77
5.2.4 Stations 420+00 to 415+00	80
5.2.5 Stations 415+00 to 400+00	82
5.2.6 Stations 400+00 to 390+00	87
5.3 Project 2 Thermal Images	89
5.3.1 Station 242+00, Start of Research Test Segment	91
5.3.2 Station 235+00, 700 ft into paving Research Test Segment	95
5.3.3 Station 230+00, 1200 ft into paving Research Test Segment	99
5.3.4 Station 220+00, 2200 ft into paving Research Test Segment	104
5.4 Project 3 Thermal Images	109
5.4.1 Stations 600+00 to 630+00	109
5.4.2 Stations 630+00 to 6??+00	114
5.5 Comparison of Continuous Thermal and GPR Data	123
5.5.1 Project 1, IR and GPR Comparison	123
5.5.2 Project 2, IR and GPR Comparison	127
5.5.3 Project 3, IR and GPR Comparison	130
5.6 Correlations by Sublot Averaging	133
5.6.1 Project 1 Correlations	135
5.6.2 Project 2 Correlations	139
5.6.3 Project 3 Correlations	142
5.6.4 Correlation Summary	146
5.7 Summary	146
5.7.1 Thermal Data and Images	146
5.7.2 Comparing Continuous Thermal and GPR Data	149
5.7.3 Correlations among NDTs using the Average and Standard Deviation	149
Chapter 6 Structural Analysis	151
6.1 Introduction	151
6.2 Conforming with Quality Analysis	151
6.2.1 Project 1, USH 2	154
6.2.2 Project 1, STH 75	155
6.2.3 Project 3, STH 42	156
6.3 Quality by Location	157
6.4 Mix Properties	161
6.5 Summary	164
Chapter 7 Implementation	165
7.1 Findings to Establish Guidelines	165
7.2 Thermal Measurements	168
7.3 Ground Penetrating Radar	169
7.4 Portable Seismic Pavement Analyzer	171

Chapter 8 Conclusions & Recommendations	174
8.1 Conclusions	174
8.1.1 Defining Critical Properties and Selecting NDT Technologies	174
8.1.2 Field Data Collection.....	174
8.1.3 Basic Statistical Summaries.....	175
8.1.4 Thermal Analysis.....	176
8.1.5 Structural Analysis of Point Measures.....	178
8.2 Recommendations	179
8.2.1 Thermal Readings.....	179
8.2.2 GPR Technology	180
8.2.3 PSPA for Modulus.....	181
8.2.4 Technology Selection Process	182
References	183
Appendix A – Infrared Thermography Sublot Data Summary.....	A-1
Appendix B – Ground Penetrating Radar Sublot Data Summary.....	B-1
Appendix C – Project Correlations.....	C-1

Acknowledgments

The authors thank Wisconsin DOT for sponsoring this research, and for members of the Wisconsin Highway Research Program Flexible Technical Committee for their time and input. They also thank the contractors for their assistance during field testing, including Mathy Construction, Payne & Dolan, and Northeast Asphalt. A special thanks to Jim Hedderich, Erv Dukatz, Brett Stanton, and John Stevens for assistance in acquiring thermal data and assisting the research team. UW-Platteville civil engineering students were a valuable resource during this research, including Cayleigh Snodgrass, James Des Jarlais, Tyler LeClair, William McElroy, and Alexander Popp. An additional thanks to Mark Baker at Geomedia Research and Development for assistance with PSPA setup; Paul Angerhofer, James Lano, and Jon Lano with assistance with Moba Pave-IR setup; and Rich Aguinaga at ATS, Inc. for furnishing a reliable nuclear density gauge.

List of Tables

Table 2.1	Summary of impact of critical characteristics on pavement performance	4
Table 2.2	Rating scale for NDT attributes	10
Table 2.3	Summary Attributes of Non-Destructive Testing Technologies.....	11
Table 2.4	Non-Destructive Testing Technologies for Measuring Critical Characteristics	14
Table 2.5	NDT Technologies for Pavement Condition Assessment	15
Table 2.6	NDT Technologies for measuring Wisconsin Critical Characteristics	16
Table 2.7	Score Values and Scoring Levels for Each Parameter.....	18
Table 2.8	Score Values and Levels for Project Objectives.....	18
Table 2.9	Scores for the evaluated NDTs.....	19
Table 2.10	Evaluated Non-Destructive Technology Ranking	20
Table 3.1	NDT Models for Field Testing	21
Table 3.2	Projects for Data Collection	22
Table 3.3	Project Mixture Properties.....	23
Table 3.4	Selected Scan Lines for each project.....	29
Table 3.5	Selection of the Scan Lines for Density and Air Void Content Profiles.....	30
Table 3.6	Paving equipment for Project 1	37
Table 3.7	Drift in Paver DMI and Project Stationing	38
Table 3.8	Paving spread for the Highway 75 project on August 11 th	39
Table 3.9	Paving equipment for the third project	43
Table 4.1	Infrared Temperature Basic Statistics for Project 1	45
Table 4.2	Infrared Temperature Statistics for Project 1 Sublot 1	46
Table 4.3	Infrared Temperature Basic Statistics for Project 1 Sublot 10.....	46
Table 4.4	Infrared Temperature Basic Statistics for Project 2	47
Table 4.5	Infrared Temperature Basic Statistics for Project 2 Sublot 1	48
Table 4.6	Infrared Temperature Basic Statistics for Project 2 Sublot 10.....	48
Table 4.7	Infrared Temperature Basic Statistics for Project 3	49
Table 4.8	Infrared Temperature Basic Statistics for Project 3 Sublot 1	49
Table 4.9	Infrared Temperature Basic Statistics for Project 3 Sublot 12.....	50
Table 4.10	GPR Basic Statistics for Project 1	51
Table 4.11	GPR Basic Statistics for Project 1 Sublot 1.....	51
Table 4.12	GPR Basic Statistics for Project 1 Sublot 10.....	52
Table 4.13	GPR Basic Statistics for Project 2	52
Table 4.14	GPR Basic Statistics for Project 2 Sublot 1	53
Table 4.15	GPR Basic Statistics for Project 2 Sublot 10.....	53
Table 4.16	GPR Basic Statistics for Project 3	54
Table 4.17	GPR Basic Statistics for Project 3 Sublot 1	54
Table 4.18	GPR Basic Statistics for Project 3 Sublot 12.....	54
Table 4.19	Statistical Summary of Modulus and Nuclear Density for Project 1	55
Table 4.20	Statistical Summary for PSPA and Nuclear Density on Project 2	60
Table 4.21	Statistical Summary of Testing Section for Project 3	63
Table 4.22	Adjusted Modulus Values and Variability at 130°F.....	66
Table 4.23	Summary of Continuous Thermal Readings.....	67
Table 4.24	Summary of Continuous GPR Thickness and Density Readings	68
Table 4.25	Statistical Summary of Modulus and Nuclear Density	69
Table 4.26	Seismic Modulus with Location and Mat Temperature.....	69
Table 5.1	Thermal Measurement comparison at Station 432+00	72
Table 5.2	Thermal Measurement comparison at Station 429+00	77
Table 5.3	Thermal Measurement comparison at Station 422+00	77
Table 5.4	Without-MTV IR Summary Statistics Sta. 242+00 to 209+80.....	90
Table 5.5	With-MTV IR Summary Statistics Sta. 209+80 to 192+00.....	91
Table 5.6	Thermal Measurement comparison at Station 242+00	91
Table 5.7	Thermal Measurement comparison at Station 235+00	95
Table 5.8	Thermal Measurement comparison at Station 230+00	99

Table 5.9 Thermal Measurement comparison at Station 220+00	104
Table 5.10 Thermal Measurement comparison at Station 628+00	111
Table 5.11 Thermal Measurement comparison at Station 630+00	113
Table 5.12 Thermal Measurement comparison at Station 634+00	116
Table 5.13 Thermal Measurement comparison at Station 637+50	118
Table 5.14 Thermal Image comparison at Stations 673, 787, and 790	120
Table 5.15 Summary of Project Correlations	134
Table 5.16 Project 1 Statistics for Correlation Analysis.....	135
Table 5.17 Project 2 Statistics for Correlation Analysis.....	139
Table 5.18 Project 3 Statistics for Correlation Analysis.....	142
Table 5.19 Thermal Range and Pass/Fail Comparison by MTV	148
Table 5.20 Range Comparison of Thermal Camera and Sensor Bar	148
Table 5.21 Summary of Project Correlations	150
Table 6.1 Station and Offset for Nonconforming Tests on Project 1.....	154
Table 6.2 Quality Indicators for Conforming and Nonconforming Tests on Project 1	155
Table 6.3 Station and Offset for Nonconforming Tests on Project 2.....	155
Table 6.4 Quality Indicators for Conforming and Nonconforming Tests on Project 2	156
Table 6.5 Station and Offset for Nonconforming Tests on Project 3.....	157
Table 6.6 Quality Indicators for Conforming and Nonconforming Tests on Project 3	157
Table 6.7 Correlation Coefficient for Modulus at 130°F versus the Placement Temperature	160
Table 8.1 Project Continuous Thermal Readings	175
Table 8.2 Continuous GPR Measurements.....	176
Table 8.3 Summary of Project Correlations	178

List of Figures

Figure 2.1 Scoring Scheme for NDT Testing Equipment.....	17
Figure 3.1 Spatial Data Collection Plan	22
Figure 3.2 Pave-IR system mounted to rear of paver	24
Figure 3.3 Pave-IR Display Screen	25
Figure 3.4 Thermal hand-held camera recording image inside truck box on Project 2 at Station 242+00.....	26
Figure 3.5 Data presentation for thermal image taken on Project 2 at Station 242+00	27
Figure 3.6 GPR equipment ready to scan a pavement layer	28
Figure 3.7 GPR pavement reference scan on a pulverized base layer	29
Figure 3.8 GPR offset reference scan lines	30
Figure 3.9 GPR thickness calibration site with aluminum foil	31
Figure 3.10 Hot mix securing aluminum foil ahead of paver	31
Figure 3.11 GPR density and thickness measurement.....	32
Figure 3.12 PSPA (Geomed 2010)	33
Figure 3.13 PSPA testing the asphalt layer near longitudinal construction joint.....	34
Figure 3.14 Typical SPA signal waves (Geomed 2010).....	34
Figure 3.15 Sample Display of PSPA Manager Software (Geomed 2010)	35
Figure 3.16 Cedarapids paver on Project 1.....	36
Figure 3.17 Pave-IR system with display panel on Project 1	37
Figure 3.18 Project 2 Sta. 244+70 start of paving with MTV	39
Figure 3.19 Project 2 Station 242+00 with MTV removed from paving train	40
Figure 3.20 Project 2 Station 240+00 paving without MTV	40
Figure 3.21 Project 2 Station 213+00 delivery of replacement MTV	41
Figure 3.22 Project 2 Station 209+80 with replacement MTV in paving train.....	41
Figure 3.23 Paving train on third project.....	42
Figure 3.24 Pave-IR system with display panel	43
Figure 3.25 Sensors out of calibration on the third project.....	44
Figure 4.1 Distribution of Test Points for Project 1	56
Figure 4.2 Modulus of the Testing Temperature by Station/Offset for Project 1	57
Figure 4.3 Average Recorded Modulus by Station/Offset for Project 1	57
Figure 4.4 Relationship of Pavement Seismic Modulus with Temperature (Adapted from Nazarian et al. 2005).....	58
Figure 4.5 Change in Modulus as the Testing Temperature Varies for Project 1.....	59
Figure 4.6 Nuclear Density Measurements by Station/Offset for Project 1	59
Figure 4.7 Distribution of Test Points for Project 2	60
Figure 4.8 Testing Temperature by Station/Offset for Project 2	61
Figure 4.9 Average Recorded Modulus Values by Location for Project 2.....	61
Figure 4.10 Change in Modulus as Testing Temperature Varies for Project 2.....	62
Figure 4.11 Nuclear Density by Station/Offset for Project 2.....	62
Figure 4.12 Distribution of Test Points for Project 3	63
Figure 4.13 Distribution of the Testing Temperature by Station/Offset for Project 3	64
Figure 4.14 Average Modulus Values by Station/Offset for Project 3	64
Figure 4.15 Change in Modulus as Testing Temperature Range Varies for Project 3	65
Figure 4.16 Nuclear Density by Station/Offset for Project 3.....	65
Figure 5.1 Pave-IR measurement from Station 435+00 to 428+00	70
Figure 5.2 FLIR Thermal Image at Station 432+00	71
Figure 5.3 Pave-IR measurement from Station 432+00 to 425+00	72
Figure 5.4 Mix accidentally dumped in front of remix hopper at Station 426+80.....	73
Figure 5.5 Station 429+00 Truck Box	74
Figure 5.6 Station 429+00 Paver Hopper Insert	75
Figure 5.7 Station 429+00 Paver Screed	76
Figure 5.8 Station 422+00 Truck Box	78
Figure 5.9 Station 422+00 Paver Hopper	79
Figure 5.10 Station 422+00 Paver Screed	80
Figure 5.11 Pave-IR measurement from Station 420+00 to 414+00	81

Figure 5.12	Paver screed segments for Roadtec model #RP 195	81
Figure 5.13	Pave-IR measurement from Station 415+00 to 408+00	82
Figure 5.14	Pave-IR measurement from Station 408+00 to 401+00	82
Figure 5.15	Station 402+00 Paver Screed after paving resumed (Image #1)	83
Figure 5.16	Station 402+00 Paver Screed after paving resumed (Image #2)	84
Figure 5.17	Station 402+00 Paver Screed after paving resumed (Image #3)	85
Figure 5.18	Longitudinal crack in center of paving lane	86
Figure 5.19	Longitudinal crack in center of paving lane	86
Figure 5.20	Pave-IR measurement from Station 402+00 to 392+00	87
Figure 5.21	Pave-IR measurement from Station 392+00 to 381+00	88
Figure 5.22	Graphical Display of Paving Mat Temperature on Project 2	89
Figure 5.23	End of Truckload Segregation on Project 2	90
Figure 5.24	Station 242+00 Truck Box	92
Figure 5.25	Station 242+00 Paver Hopper	93
Figure 5.26	Station 242+00 Paver Screed	94
Figure 5.27	Station 235+00 Truck Box	96
Figure 5.28	Station 235+00 Paver Screed (Image #1)	97
Figure 5.29	Station 235+00 Paver Screed (Image #2)	98
Figure 5.30	Station 230+00 Truck Box	100
Figure 5.31	Station 230+00 Paver Hopper	101
Figure 5.32	Station 230+00 Paver Screed (left side)	102
Figure 5.33	Station 230+00 Paver Screed (Right side)	103
Figure 5.34	Station 220+00 Truck Box	105
Figure 5.35	Station 220+00 Paver Hopper	106
Figure 5.36	Station 220+00 Paver Screed	107
Figure 5.37	Station 209+00 Paver Screed (with MTV)	108
Figure 5.38	Pave-IR measurement from Station 604+00 to 613+00	109
Figure 5.39	Pave-IR measurement from Station 614+00 to 623+00	110
Figure 5.40	Pave-IR measurement from Station 624+00 to 632+00	110
Figure 5.41	Station 628+00 Truck Box	111
Figure 5.42	Station 628+00 Paver Screed	112
Figure 5.43	Station 630+00 Paver Screed	113
Figure 5.44	Pave-IR measurement from Station 634+00 to 642+00	114
Figure 5.45	Pave-IR measurement from Station 643+00 to 652+00	115
Figure 5.46	Pave-IR measurement from Station 653+00 to 661+00	115
Figure 5.47	Station 634+00 MTV Discharge Chute	116
Figure 5.48	Station 634+00 Paver Screed	117
Figure 5.49	Station 637+50 Truck Box	118
Figure 5.50	Station 637+50 Paver Screed	119
Figure 5.51	Station 673+00 Paver Screed	120
Figure 5.52	Station 787+00 Paver Screed	121
Figure 5.53	Station 790+00 Paver Screed	122
Figure 5.54	IR Temperature (2.1 ft) and GPR Density (2.5 ft) Project 1, Full Length	124
Figure 5.55	IR Temperature (6.4 ft) and GPR Density (6 ft) Project 1, Full Length	124
Figure 5.56	IR Temperature (2.1 ft) and GPR Density (2.5 ft) Project 1, Sublot 1	125
Figure 5.57	IR Temperature (6.4 ft) and GPR Density (6 ft) Project 1, Sublot 1	126
Figure 5.58	IR Temperature (8.6 ft) and GPR Density (9.5 ft) Project 2, Full Length	127
Figure 5.59	IR Temperature (10.8 ft) and GPR Density (11.5 ft) Project 2, Full Length	128
Figure 5.60	IR Temperature (8.6 ft) and GPR Density (9.5 ft) Project 2, Sublot 1	129
Figure 5.61	IR Temperature (10.8 ft) and GPR Density (11.5 ft) Project 2, Sublot 1	129
Figure 5.62	IR Temperature (6.4 ft) and GPR Density (6 ft) Project 3, Full Length	130
Figure 5.63	IR Temperature (9.7 ft) and GPR Density (9.5 ft) Project 3, Full Length	131
Figure 5.64	IR Temperature (11.8 ft) and GPR Density (11.5 ft) Project 3, Full Length	131
Figure 5.65	IR Temperature (6.4 ft) and GPR Density (6 ft) Project 3, Sublot 1	132
Figure 5.66	IR Temperature (9.7 ft) and GPR Density (9.5 ft) Project 3, Sublot 1	132
Figure 5.67	IR Temperature (11.8 ft) and GPR Density (11.5 ft) Project 3, Sublot 1	133
Figure 5.68	Correlation between Average GPR Thickness and IR Temperature on Project 1	136

Figure 5.69 Correlation between Average GPR Density and IR Temperature on Project 1	136
Figure 5.70 Correlation between Average Nuclear Density and IR Temperature on Project 1	137
Figure 5.71 Correlation between Average Seismic Modulus and IR Temperature on Project 1	137
Figure 5.72 Correlation between Seismic Modulus and GPR Thickness on Project 1	138
Figure 5.73 Correlation between Average GPR Density and Nuclear Density on Project 1	138
Figure 5.74 Correlation between Average GPR Density and IR Temperature on Project 2	140
Figure 5.75 Correlation between Average Nuclear Density and IR Temperature on Project 2	140
Figure 5.76 Correlation between Average Seismic Modulus and IR Temperature on Project 2	141
Figure 5.77 Correlation between Standard Deviations of Seismic Modulus and GPR Thickness on Project 2	141
Figure 5.78 Correlation between GPR Density and Thickness Standard Deviations on Project 2	142
Figure 5.79 Correlation between Average GPR Thickness and IR Temperature on Project 3	143
Figure 5.80 Correlation between Average GPR Density and IR Temperature on Project 3	144
Figure 5.81 Correlation between Average Nuclear Density and IR Temperature on Project 3	144
Figure 5.82 Correlation between Average Seismic Modulus and IR Temperature on Project 3	145
Figure 5.83 Correlation between the Standard Deviations of the Seismic Modulus and the GPRadar Thickness on Project 3	145
Figure 5.84 Correlation between Nuclear Density Variability and IR Temperature Variability	146
Figure 6.1 Average of Density Values for Conforming and Nonconforming Tests	152
Figure 6.2 Average Modulus Values for Conforming and Nonconforming Tests	152
Figure 6.3 Average IR Temperature for Conforming and Nonconforming Tests	153
Figure 6.4 Average GPR Thicknesses for Conforming and Nonconforming Test Points	153
Figure 6.5 Density Average of all Projects by Transverse Locations	158
Figure 6.6 Modulus Values of all Projects by Transverse Locations	159
Figure 6.7 GPR Pavement Thickness of all Projects by Transverse Location	159
Figure 6.8 Pavement Placement Temperature of all Projects by Transverse Location	160
Figure 6.9 Comparison of Average Pavement Modulus and Mixture VMA	161
Figure 6.10 Comparison of Average Pavement Modulus and Mixture VMA for Compacted and Under-compacted Test Points	162
Figure 6.11 Comparison of Average Pavement In-Place Density and Mixture VMA, for Compacted and Under-compacted Test Points	163
Figure 7.1 Flow Chart of NDT Quality Plan during HMA Pavement Construction	166
Figure 7.2 GPR setup for compaction status monitoring	170
Figure 7.3 Procedure of compaction operation monitoring using GPR: collecting data between compactor passes	171
Figure 7.4 Comparison of Rate of Change in Modulus per Unit Temperature Increase and Asphalt Binder Content	172

Chapter 1 Introduction

1.1 Background

During the mid-1990's, WisDOT specifications shifted from the primary use of cored samples to a nondestructive measurement of asphalt pavement density. While the current system has served to maintain a defined level of acceptance, concerns have been raised surrounding increased variability when attempting to properly evaluate the following: (a) the influx of new materials going into bituminous pavements (e.g., recycled products, binder additives, SMA, WMA, etc.); (b) uniformity of mat compaction and densification as related to impacts on service life; (c) a change in department direction towards emphasis on pavement textures; (d) increase awareness of construction zone safety issues as related to trying to reduce time and number of personnel needed to occupy the zone, as well as implementing safety standards; and (e) joint constructability and associated acceptance methods. All of these concerns suggest an opportunity to re-evaluate and enhance the current quality management system.

1.2 Challenge in Measuring In-Situ Asphaltic Concrete Density

Presently, WisDOT employs the use of nuclear density gauges in its Quality Management and Acceptance Programs to provide rapid density readings and allowing non-destructive pavement evaluation for spot locations on-site. However, the current system has drawbacks, namely the procurement and handling of radioactive materials and using discrete point measurements to characterize the density of the entire pavement layer.

Recent advancements in non-destructive testing (NDT) technologies suggest an opportunity for the Department to expand beyond density as the sole parameter used to evaluate and accept flexible pavements. These NDTs provide the potential to develop a system capable of collecting an increased number of diverse measurements, efficient data, off-site data retrieval, and real-time corrective actions during construction. Traditional knowledge combined with newer technologies also presents opportunities to define methods assessing entire pavement sections.

1.3 Research Objectives

The objectives of this research study are presented in two stages as follows:

Stage 1

- (a) Define critical properties for measurement during compaction and justify their importance. Identify technology available to measure these products including potential suppliers and an estimate of cost.
- (b) Develop evaluation systems using single or multiple technologies capable of measuring these critical material properties. Rank potential systems based on technical merits, cost, practicality, and other discerning factors.

- (c) Prepare an interim report and present to the TOC within 6 months of the project start date, including a detailed description of a minimum two highest-ranked evaluation systems. The researcher and TOC will discuss the merits of each of these systems and select the system that will be used in field experiment specified in Stage 2.

Stage 2

- (d) Develop additional detailed plan to complete a field experiment designed to evaluate the system selected by the researcher and TOC at the completion of Stage 1.
- (e) Perform fieldwork, collect and analyze supporting data.
- (f) Develop specifications and guidance for implementation of the defined system.
- (g) Prepare a final report documenting Stage 1 and 2 actions.

1.4 Report Structure

The scope of this report is to summarize the research investigation from Stage 1 and Stage 2 of the project. The first chapters describe work in Stage 1, while the latter chapters summarize research in Stage 2.

Chapter 2 summarizes critical properties and NDT technologies during the asphalt compaction process. A detailed investigation from the Interim Report is presented in an abbreviated form. Candidate NDTs for measuring compaction characteristics during and immediately after final compaction are critically evaluated. The evaluation process of the candidate technologies/tests includes key parameters that are important to field measurement, as well as relevance of data output. Critical properties and characteristics are aligned with available NDTs for volumetric, structural, and functional features.

Chapter 3 illustrates the data collection plan approved by the WHRP Flexible Pavement Committee. Three projects tested for the field evaluation are described, including mixture properties, paving mat, and construction equipment. The NDT technologies chosen for evaluation are described, including Infrared Thermography, Ground Penetration Radar, and Portable Seismic Pavement Analyzer. The nuclear density gauge was also used in the evaluation.

Chapter 4 summarizes basic statistics for each NDT technology for the full length of project research testing, and 500-ft test sublots. The purpose of the 500-ft sublots was to better manage field data collection and provide a within-project comparison of devices. Basic summary statistics include the mean, standard deviation, coefficient of variation, maximum, minimum, and range.

Chapter 5 present a detailed analysis of thermal temperature data collected by the Pave-IR sensors and the FLIR imaging camera. A comparison is made with data from the other NDT devices including continuous GPR thickness and density data, and point measures from PSPA modulus and nuclear density.

Chapter 6 focuses on the ability of the proposed technologies to distinguish nonconforming sections of pavement using nuclear density as the baseline indicator. This is to establish the ability of the non-destructive technologies to serve as quality control and/or acceptance tools during pavement construction. This chapter also explores the interrelationship between the different NDT technology measures and illustrate the presence of strong correlations is applicable using point measures.

Chapter 7 incorporates data findings to recommend implementation of the NDT guidelines for these three systems on actual construction projects. Barriers for implementing the technologies into practice are identified.

Chapter 8 summarizes the research work with conclusions and recommendations. Recommendations for future work are enumerated by NDT technology.

Chapter 2 Critical Characteristics and NDT Technologies

2.1 Introduction

The purpose of this chapter is to summarize research in the first stage of the study for critical characteristics measurable in the field using available non-destructive testing (NDT) technologies. An interim report published by UWP-Bloom (2011) presents detailed findings of this investigation. The following sections summarize critical characteristics and NDT technologies to measure those characteristics from the Interim Report.

2.2 Critical Characteristics

Critical field construction-related characteristics that influence the pavement quality were identified in the first stage of this project and published in an interim report by UWP-Bloom (2011). A review of literature from numerous sources disclosed findings and expert opinion on the role of each characteristic with its effect on long-term pavement performance. Over 40 sources were cited during this review. Table 2.1 summarizes the impact of the critical characteristics on the pavement performance as indicated in the literature. A brief summary of each critical characteristic is presented in the following sections.

Table 2.1 Summary of impact of critical characteristics on pavement performance

Critical Characteristic (1)	Impact on Pavement (2)
Mix Segregation	Pavement permeability, mechanical stability, rutting, raveling, bleeding
In Place Compaction	Pavement mechanical stability, rutting, permeability
Smoothness	Safety, comfort
Temperature Segregation	Densification, mechanical stability
Layer Thickness	Pavement density, permeability, structural capacity
Layer Interface Bonding	Structural capacity, slippage, compaction difficulty, premature fatigue, near-surface cracking, moisture damage
Pavement Modulus	Structural capacity, various distresses

2.2.1 Mix Segregation

The state of Washington defined mix segregation as aggregate segregation having non-uniform distribution of coarse and fine aggregate components within the HMA (Willoughby and Mahoney 2007). This includes two basic types of aggregate segregation defined by Williams et al. (1996): (1) *coarse segregation* when gradation is shifted to excessive coarse aggregate and insufficient fine aggregate as characterized by low asphalt content, low density, high air voids, rough surface texture, and accelerated rutting and fatigue failure, and (2) *fine segregation* when gradation is shifted to include excessive fine aggregate and not enough coarse aggregate characterized by high asphalt content, low density, smooth surface texture, and accelerated rutting.

NCHRP Project 9-11, *Segregation in Hot-Mix Asphalt Pavements*, concluded there are three types of segregation that may be detected by infrared measurement, including gradation, temperature, and aggregate-asphalt segregation (Stroup-Gardiner and Brown 2000). A survey of agencies found that estimated loss of pavement life from segregation varied from a 2 to 7 years in an anticipated 15-year life. A life-cycle cost analysis estimated that the agency cost because of segregation was approximately 10% of the original cost of the HMA for a low level of segregation and about 20% for medium levels of segregation. High levels of segregation resulted in additional costs of close to 50%.

A quantitative aggregate segregation definition varies. Since coarse segregation is generally accepted as most destructive, a general quantitative definition is a sample at least 10% coarser than the JMF on the No. 4 or No. 8 sieve (Brown and Brownfield 1988; Cross and Brown 1993; Williams et al. 1996).

Von Quintus recommends the use of the portable seismic pavement analyzer (PSPA), or impact echo technologies to control the presence of mix segregation. The author confirmed this recommendation in another publication sponsored by the NCHRP, and at an AAPT symposium (Von Quintus 2009 et al.; Von Quintus 2009).

2.2.2 In-Place Compaction

A reasonable goal of field densification is to achieve approximately 7% air voids in the compacted mat. This is based on numerous studies that show an increase in mechanical stability and durability for in-place air voids less than 7% (Linden et al. 1989; Brown 1990; Brown and Cross 1991; Cominsky et al. 1998; Cooley et al. 2002). According to the Asphalt Institute (2003), the air void content for compaction of flexible pavements should be controlled between 7% and 3%. Once voids reach 8% or higher, interconnected voids result, which allow air and moisture to penetrate the pavement.

One of the more common compaction challenges is related to the construction of longitudinal joints. Kandhal et al. (2001) reported that the likely cause of longitudinal cracking is a lower material density at the joint. This is due to the initial pavement lane having an unconfined edge that is not fully compacted, because it is not restrained by

adjacent material. The initial edge has cooled when the adjoining mat is placed and cannot be compacted further, creating a cold joint.

Von Quintus et al. (2009), using non-destructive testing techniques, consistently found deviations in pavement density when comparing the longitudinal joint and the middle of a driving lane. This was confirmed by Hand (2009). The author reported that the governing factor in achieving good longitudinal joint performance is the compaction of the joint to a density of about 2% within mat density.

2.2.3 Pavement Layer Thickness

Work by Florida DOT indicated that layer thickness can have an influence on density (Musselman et al. 1998). Florida DOT constructed numerous pavement test sections that suggested increased layer thicknesses could lead to better pavement density, and hence, structural stability. In addition, increased layer thickness has been shown to allow desirable density levels to be more easily achieved. Choubane et al. (1998) and Musselman et al. (1998) have all suggested that a thickness to NMA ratio (t/NMA) of 4.0 is preferred. The National Asphalt Pavement Association issued a special report in 1997 providing Superpave construction guidelines recommending that a minimum t/NMA of 3.0 be used.

A study conducted for the WHP evaluated the effect of layer thickness to maximum aggregate size ratio on compaction of Superpave mixtures (Paye and Bahia 2001). This study showed the effect of size to the thickness ratio and indicates that density is highly dependent on size and gradation in the laboratory when the Superpave Gyratory Compactor is used. It was also found that the optimal size to thickness ratio varies according to the angularity and source of the aggregates. In a later study sponsored by the WHP, Russell et al. (2005) found that for fine-graded mixes, the t/NMA ratio showed an influence on achieving density, particularly below a ratio of 2 for gravel-source mixes and a ratio of 3 for limestone-source mixes. No clear relationship was found between t/NMA ratios and permeability. For coarse-graded mixes, those compacted at smaller t/NMA ratios for limestone-source were more permeable than higher ratios, but no trend was observed for the gravel-source mixes.

Brown et al. (2004) reconfirmed important layer thickness criteria in NCHRP Report 531. The recommendations for achieving improved compactability are:

- Fine graded mixes should have t/NMA ratios ≥ 3.0 ; and
- Coarse graded and SMA mixes should have t/NMA ratios ≥ 4.0 .

Monismith and Harvey (2009) included a list of factors influencing the pavement performance. Among the list, layer thickness and compaction were the only construction related properties. In their discussion, the authors recommended that the minimum layer thickness should be at least 3 times the maximum aggregate size.

2.2.4 Smoothness (Roughness)

Pavement roughness is measured using the International Roughness Index (IRI). It is calculated using a quarter-car vehicle math model, whose response is accumulated to yield a roughness index with units of inches/mile (Sayers and Karamihas 1998). According to the FHWA, the performance goal is to qualify 95% of the amount of travel on the National Highway System with a reported IRI of 170 inches/mile (or less) by 2008. Additionally, a secondary performance goal was established which focused on increasing the amount of travel on roadways considered with good ride quality, a reported IRI of 95 inches/mile (or less).

The current practice in Wisconsin requires a comprehensive evaluation of the pavement smoothness. According to the Wisconsin Quality Management Plan (QMP), if the IRI is more than 175 inches/mile, a pay reduction is imposed on the contractor.

2.2.5 Temperature Segregation

The temperature differential within the pavement usually leads to inconsistent compaction. It is important to follow construction practices that will maintain the uniform temperature within the pavement. Infrared temperature devices are now available to monitor the paving process in real time to identify the presence of thermal segregation, and thus, provide needed remedies to achieve the needed density.

Von Quintus (2009), in an AAPT symposium, mentioned in-place compaction within temperature sensitive zones as one of the factors that may reduce the service life of pavements. Temperature-sensitive zones, also called tender zones, are typically defined as a temperature window where pavement compaction does not achieve density. The temperature range is usually between 240°F and 193°F. If this behavior is observed, the further compaction of the pavement may cause the development of cracks, or lateral shoving within the fresh pavement, in addition to the lack of density.

Buchanan and Cooley (2003) studied factors affecting tender mixes. The authors postulated that the temperature differential within the pavement mat is one of the leading causes of this phenomenon. A similar temperature differential relationship could be assumed to occur in Superpave mixtures with various layer thicknesses. The authors mentioned that the tender zone tends to occur when breakdown rolling is nearing completion, generally corresponding to approximately 5 to 10 minutes after the initial placement of the mixture.

Willoughby et al. (2001) conducted a study for Washington State DOT where temperature differentials were found to lead to significant density differentials in the finished mat. Over 40% of the jobs observed in this study had temperature differentials 25°F or greater. The need to minimize the effects of temperature differentials is readily apparent if a 15-year overlay life is to be achieved.

2.2.6 Layer Interface Bonding

Bonding between pavement various layers is very important. A loss of bonding causes slippage where the surface layer is shoved horizontally. Hand (2009) suggested that the application of tack coat to improve bonds between HMA layers will improve fatigue performance. Furthermore, in the cases of thin overlays of 1½ to 2½ inches thick, or slightly thicker HMA on aggregate base of up to 4 inches thick, the author noticed several slippage failures. This behavior is attributed primarily to inadequate tensile and shear strength in the pavement, and secondarily to lack of bonding or tack coat application. The combination of these factors, with opening the pavement to traffic at high ambient and pavement temperatures, can have detrimental effects.

Von Quintus (2009) in the same symposium stated that the loss of bond within the pavement will result in accelerated cracking or premature rehabilitation. The use of tack coat and appropriately applying it are the recommendations for the authors. These recommendations mirror other researchers who mentioned this construction related issue. The author recommends the use of portable seismic pavement analyzer (PSPA), or impact echo technologies, to monitor layer bonds.

Mohammad et al. (2009) conducted a study as part of NCHRP 9-40, *Optimization of Tack Coat for HMA Placement*, on the level of tack coat for HMA placement. Several factors determined to influence the effectiveness of the tack coat, including tack coat type, tack coat application rate, tack coat curing time, surface condition, and pavement temperature. In 2010, the same research group published a study on the effects of surface type on tack coat interface shear strength. The conclusions included that an application rate of 0.70 l/m² yielded the highest shear strength. In addition, the existing surface roughness shows a strong direct relationship with the shear strength at the interface. (Mohammed et al. 2010).

2.2.7 Pavement Layer Moduli

The measurement of pavement layer moduli provides a valuable fundamental mechanical property. In fact, field density measurements are used as surrogate measures for the structural stability of the pavement. It is a challenging and tricky process to measure the pavement layer moduli in the field non-destructively. Some technologies are available that can provide an estimate of the pavement modulus using either deflection or ultrasonic-based techniques. Although Von Quintus et al. (2009) and Noureldin et al. (2005) indicated that the measured values using these tests do not match laboratory measurements and coring was needed, similar trends exist between lab and field values.

An additional challenge with determining the pavement modulus is the lack of acceptable limits in the literature. To develop such limits, a comprehensive field and laboratory study is required. A Texas DOT study by Nazarian et al. (2005) investigated the comparison of laboratory and field modulus values to control final pavement strength. Traditional HMA design was expanded to include curves for lab air void versus modulus, and then in the field, the actual pavement modulus was measured so that the design values were met. The comparison proved successful, but highlighted the challenges of controlling

as-built field modulus with the effect of pavement temperature, where higher temperatures produced a correspondingly lower modulus.

2.3 NDT Technologies

There are several state-of-the-art and state-of-the-practice NDTs for evaluating those characteristics in the previous section. Technologies considered state-of-the-art are the most advanced stage of development whether ready for practical use or not, while state-of-the-practice technologies have been refined for practical field use and accepted in state specifications and/or procedures. A listing of NDT technologies investigated in this study to measure asphalt pavement compaction include the following:

- Deflectometers
- Ground Penetration Radar
- Impact Echo
- Ultrasonic Pulse Velocity
- Infrared Thermography
- Intelligent Compaction
- Lasers
- Permeameters
- Ultrasonic Seismic

A detailed breakdown of 12 specific attributes for each NDT technology was reported in the interim report by UWP-Bloom (2011) for the following:

- Operational principle
- Measures and indicators
- Test equipment
- Portability of the test
- Complexity of execution in the field
- Time required to conduct each test
- Environmental limitations
- Reliability of collected data
- Committee-approved test protocols
- Degree of training required
- Cost
- States using technology in practice

A qualitative rating scale is shown in Table 2.2 for four NDT technology attributes. The purpose of this table is to provide a formal rating scale of attributes for portability of test equipment on the jobsite, complexity of execution in the field, reliability of the data, and degree of training to operate and interpret data from the technology.

Table 2.2 Rating scale for NDT attributes

Rating (1)	Portability (2)	Complexity in Field (3)	Reliability of Data (4)	Degree of Training (5)
Excellent	Can be moved rapidly between test sites. Test unit is self-contained.	Easy to operate.	Highly accurate.	Minimal training.
Good	Can be moved rapidly between test sites. Test unit is attached to a vehicle or other equipment, or a computer cable.	Multiple steps are required to operate within two or more primary phases.	Good accuracy but requires calibration.	Multiple phases, and steps within each phase, are necessary to operate the test equipment.
Fair	Can be moved rapidly between test sites. Test unit requires trailering.	Multiple steps within a series of phases to operate, along with knowledge of calibration.	Higher testing variability with known bias or needed calibration.	Capability for both field data collection and statistical analysis procedures is necessary.
Poor	Requires trailering, considerable set up time, and connection to a computer to operate.	Very complex to operate. Requires multiple phases, knowledge of relatively sophisticated equipment systems.	Inaccurate with technology considered at experimental phase for asphaltic materials.	Requires an in-depth understanding of pavement engineering principles and concepts.

Table 2.3 presents a summary matrix for attributes for the NDT technologies. The features of the NDTs are then used to develop a system to evaluate pavement compaction in the next section.

Table 2.3 Summary Attributes of Non-Destructive Testing Technologies

Attribute (1)	Deflectometer FWD (2)	Deflectometer LWD (3)	GPR (4)	Impact Echo (5)	Infrared Thermography (6)	Intelligent Compactor (7)	Laser (8)	Permeameter (9)	SPA (10)	PSPA (11)
Operational Principle	Layer stiffness under controlled static, vibratory, or impulse loading.	Layer stiffness under controlled impulse loading.	Electromagnetic waves measure the reflection amplitude to characterize the material.	Stress waves propagate and reflect material to set up resonances.	Rate of radiation energy and emissivity map thermal contour of surface.	Adjust the vibration amplitude and frequency based on the measured material stiffness.	Infrared light projected onto surface is scattered then detected using receiving lens.	Flow rate of air or fluid through a substance; Darcy's Law is applied.	Ultrasonic energy waves radiate to detect material properties and dimensions.	Ultrasonic energy waves radiate to detect material properties and dimensions.
Measures and Indicators	Moduli	Moduli	Thickness, density, defects (segregation and possibly stripping), moisture content.	Layer thickness; internal flaws, delamination.	Temperature detects segregation, stripping, changes in air voids relative to aggregate gradation and asphalt content.	Stiffness, compactor indicator or index, compaction meter value, vibration modulus.	Surface texture and surface distresses.	Permeability measured as distance over time (cm/sec).	Moduli, layer thickness, moisture, voids, delamination.	Moduli, layer thickness, moisture, voids, delamination.
Test Equipment	Trailer-mounted or vehicle-mounted test device, computer.	Hand-held device, computer.	Vehicle (may be needed), control unit, pulse generator, antenna(e), computer.	PSPA, Impact Echo Scanning Unit (PCC), computer	Infrared camera, sensor bar (optional attached behind paver), computer.	Roller compactor and sensing equipment.	Area-scan or line-scan laser mounted to vehicle.	NCAT water permeameter. ROMUS air permeameter.	Trailer-mounted test kit with pneumatic hammers and receivers, and computer.	Small suitcase-sized test kit with source and receivers, and computer.
Portability of the test	Fair	Excellent	Good	Excellent	Excellent	Good	Good	Excellent	Good	Excellent
Complexity of execution in the field	Fair	Good	Fair	Good	Good	Good	Fair	Excellent	Fair	Fair

Table 2.3 Summary Attributes of Non-Destructive Testing Technologies (cont.)

Attribute (1)	Deflectometer FWD (2)	Deflectometer LWD (3)	GPR (4)	Impact Echo (5)	Infrared Thermography (6)	Intelligent Compactor (7)	Laser (8)	Permeameter (9)	SPA (10)	PSPA (11)
Time required to conduct each test (not including setup)	2 min	1 to 5 min	Continuous. 1 hour for complete coverage of one lane-mile using 8-inch wide scan.	1 min	30 sec (with paver rate of 60 fpm)	Continuous	Continuous. 50 mph maximum speed.	20 min water perm. 10 minutes air perm.	1 min	45 sec
Environmental limitations	Sensitive to pavement temperature; correction advised. (moisture not a factor).	Sensitive to pavement temperature; correction advised. (moisture not a factor).	Sensitive to wet surface and/or layer.	Not advisable on thicker, softer HMA at elevated temperatures	High temperature gradients are required.	Not affected by temperature or surface moisture.	Dry pavement is required.	Pavement temperature less than 140°F. Moisture okay for water permeameter. Dry pavement is required for air permeameter test.	Pavement temperature of 32 to 120 °F. Moisture not a proven factor.	Pavement temperature of 32 to 120 °F. Moisture not a proven factor.
Reliability of collected data	Good	Fair	Good with calibration to cores. Better with calibration to cores.	Poor for new HMA. Good for aged HMA and PCC.	Excellent	Excellent	Excellent	Fair. Erroneous if leakage. Water perm. has trial errors.	Fair	Good

Table 2.3 Summary Attributes of Non-Destructive Testing Technologies (cont.)

Attribute (1)	Deflectometer FWD (2)	Deflectometer LWD (3)	GPR (4)	Impact Echo (5)	Infrared Thermography (6)	Intelligent Compactor (7)	Laser (8)	Permeameter (9)	SPA (10)	PSPA (11)
Committee- approved test protocols	ASTM D4695- 03 (2008)	ASTM E2583-07	ASTM D4748-06	ASTM C1383-04	ASTM D4788- 03(2007). ASTM E1543- 00 (2006). ASTM E1213- 97 (2009).	None	ASTM E1845-09. ASTM E2157-09.	Field has none. Lab: ASTM PS 129-01 (withdrawn 2003). ASTM D5084-10.	ASTM STP1375, Third Volume, 2000	ASTM STP1375, Third Volume, 2000
Degree of training	Poor	Good	Poor	Good	Good	Fair	Fair	Excellent	Poor	Fair
Cost	\$100,000 to \$150,000 purchase excluding the tow vehicle	\$20,000 purchase	\$50,000 purchase (excluding vehicle) \$100,000 to \$150,000 for vehicle plus GPR kit.	\$30,000 purchase. \$3,000 per month rental.	\$4,000 to \$50,000 purchase. \$28,000 for sensor bar, cameras, software.	\$175,000 to \$280,000 for a new compactor with IC technology.	\$150,000 to \$180,000 for vehicle, cameras, and on-board software.	\$800 for NCAT water perm. \$6,000 for ROMUS air perm. (est.).	None available	\$30,000 purchase. \$3,000 per month rental.

2.4 Ranking of Compaction Systems

2.4.1 Critical Characteristics and Non-Destructive Testing Technologies

The ability of current NDT technologies to measure critical characteristics is illustrated in matrix form in Table 2.4. The rank order of critical characteristics from Mahoney and Backus (1999) is noted in this table with more critical characteristics in the left-most columns. Continuous or point coverage is also stated. Full coverage increases the ability to measure mat areas for uniformity. Point measures, on the other hand, require sufficient sample size.

Table 2.4 Non-Destructive Testing Technologies for Measuring Critical Characteristics

NDT	Continuous coverage?	Mix Segregation	Compaction	Smoothness	Temp. Segregation	Thickness	Bond	Moduli
Rank (Mahoney and Backus 1999)	---	1	2	3	4	5	6	7
Falling Weight Deflectometer	No							√
Light Weight Deflectometer	No							√
Seismic Pavement Analyzer	No					√	√	√
Portable Seismic Pavement Analyzer	No					√	√	√
Impact Echo	No					√	√	
Ultrasonic Pulse Velocity	No					√	√	
Nuclear and Non-nuclear Density Gauges	No		√					
Ground Penetrating Radar	Yes	√	√		√	√		
Infrared Thermography	Yes	√			√			
Laser Profiler	Yes			√				
Intelligent Compactor	Yes		√					√
Permeameters	No	√			√			

It is clear that only four NDTs are capable of continuously measuring all locations on the mat, and that not one single technology can measure all critical characteristics. The most important property from the survey, mix segregation, can only be measured by GPR, infrared thermography, and permeameters. The minimum combination of NDTs to measure all critical characteristics is three, and each combination must include laser profilers.

2.4.2 Simplified Characteristics and Non-Destructive Testing Technologies

Non-destructive testing technologies are compared amongst each other in Table 2.5 according to a simplified classification of measured pavement characteristics for volumetric, structural, and functional measurements. Full coverage is only provided by ground penetrating radar (GPR), infrared thermography, laser profilers, and intelligent compaction (IC). A combination of at least two of these NDTs will provide volumetric, structural, and functional evaluation. Laser profilers combined with either GPR or IC are two viable options. Since IC technology is generally limited to the breakdown roller at this time, and not capable of measuring final as-built pavement characteristics, by deduction, GPR and laser profiler combination is one option for final quality assurance and acceptance measurement.

Table 2.5 NDT Technologies for Pavement Condition Assessment

Method Category	Method Name	Type of Measured Property			Full-Coverage Measurement? Width
		Volumetric	Structural	Functional	
Deflection-Based	Falling Weight Deflectometer		√		No
	Light Weight Deflectometer		√		No
	Seismic Pavement Analyzer		√		No
	Portable Seismic Pavement Analyzer		√		No
Stress Wave	Impact Echo		√		No
	Ultrasonic Pulse Velocity		√		No
Electro-Magnetic	Nuclear and Non-nuclear Density Gauges	√			No
	Ground Penetrating Radar	√	√		Yes, 1-foot
	Infrared Thermography	√			Yes, lane
	Laser Profiler			√	Yes, wheel
Mechanical or Hydraulic	Intelligent Compactor	√	√		Yes, drum
	Permeameters	√			No

2.4.3 Ranking of Evaluation Systems

With many critical characteristics and NDT technologies currently available, input was sought from the WHRP Project Oversight Committee to rank the seven critical characteristics from the state of Washington survey in terms in Wisconsin practices and experiences. The top three critical characteristics from WHRP input in rank order were compaction, thermal segregation, and moduli. Based on this ranking, a reduced matrix of critical characteristics and NDT technologies was prepared, as shown in Table 2.6.

Table 2.6 NDT Technologies for measuring Wisconsin Critical Characteristics

NDT	Continuous coverage?	Com- paction	Temp. Segregation	Moduli
Wisconsin Rank	---	1	2	3
Falling Weight Deflectometer	No			√
Light Weight Deflectometer	No			√
Seismic Pavement Analyzer	No			√
Portable Seismic Pavement Analyzer	No			√
Impact Echo	No			
Ultrasonic Pulse Velocity	No			
Nuclear and Non-nuclear Density Gauges	No	√		
Ground Penetrating Radar	Yes	√	√	
Infrared Thermography	Yes		√	
Laser Profiler	Yes			
Intelligent Compactor	Yes	√		√
Permeameters	No		√	

The ranking of the technologies is conducted based on a scoring system that reflects an objective and unbiased evaluation of the NDTs, while incorporating the Wisconsin ranking. Thus, the overall score of the testing equipment is calculated as the interaction of the equipment properties, with their ability to achieve the goals of the project. There are seven parameters used to evaluate the NDTs characteristics including portability, complexity, testing time, environmental limitations, data reliability, degree of training, and purchase cost. There are two parameters used to evaluate the NDTs ability to meet the project objectives, including the measured pavement characteristics, and utilization during the construction process. This scheme is assuming that the equipment characteristics are

independent of the project objectives, and allows for the calculation of an unbiased scoring system. Figure 2.1 presents the conceptual multiplicative approach for calculating the overall score of a particular NDT technology.

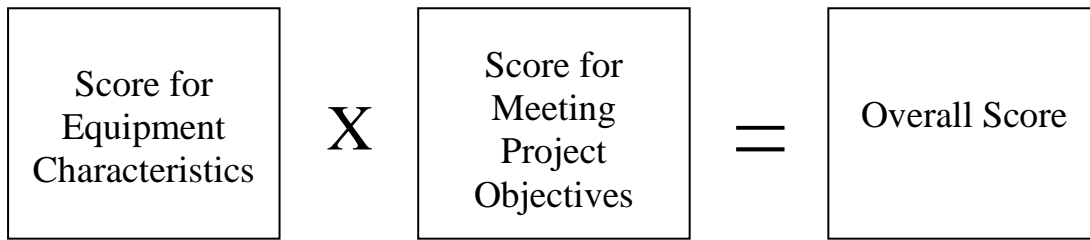


Figure 2.1 Scoring Scheme for NDT Testing Equipment

Tables 2.7 and 2.8 include the details of these parameters with explanation of the scoring range. It is important to note that the levels are selected based on the information collected and illustrated in Chapter 3. Therefore, the score range for each parameter represents the range for the subset of technologies studied in this report, not an absolute range. For the evaluation of the equipments, a score value is assigned to each parameter according to the scale shown in the Table 2.7.

Each parameter is scored on a scale of 4, where a score of 4 represents most favorable. Each test equipment is evaluated against the scoring scheme to obtain a cumulative value representing the NDTs equipment suitability for collecting compaction evaluation data. The next step is to determine the contribution of the equipment to the project objective.

In Table 2.8, the two parameters are the pavement performance indicator measured by the equipment, and the utilization during the construction process. The levels of scoring are determined through the Wisconsin ranking of critical characteristics. The range of "4" could not be achieved for the construction process utilization; since the focus is to determine which side of the construction process a given technology is used (during compaction or after compaction). The cumulative score for the equipment is then multiplied by the score for meeting the objective to calculate the overall score for the every technology included. Table 2.9 includes the cumulative scores assigned to the NDTs according to the scheme in Figure 2.1.

Table 2.7 Score Values and Scoring Levels for Each Parameter

Equipment Parameter	Score Values and Levels			
	4	3	2	1
Portability of the test	Excellent: 1 - Hand held 2 - Easy to maneuver 3 - Small size	Good: Two attributes are present	Moderate: One attribute is present	Poor: None present
Complexity of execution in the field	Excellent: 1 - Simple test setup. 2 - Easy to collect data 3 - Easy to interpret the results	Good: Two attributes are present	Moderate: One attribute is present	Poor: None present
Time required to conduct each test (not including setup)	Excellent: Continuous data collection of the mat	Good: < 1 minute	Moderate: 1 - 5 minutes	Poor: > 5 minutes
Environmental limitations	Excellent: 1 - No temperature effect 2 - No moisture effect	Good: 1 - Applicable at warm temperatures ~120°F 2 - No moisture effect	Moderate: 1 - Effect of temperature can be corrected. 2 - No moisture effect.	Poor: 1- Ambient temperature 2- Dry
Reliability of collected data	Excellent: 1 - High accuracy 2 - Good repeatability 3 - High resolution	Good: Two attributes are present.	Moderate: One attribute is present	Poor: None present
Degree of Training	Excellent: Minimum training to 1 – operate. 2 –analyze data 3 –interpret data	Good: Two attributes are present.	Moderate: One attribute is present	Poor: None present
Purchase Price	Excellent: \$0-\$50k	Good: \$50k-\$100k	Moderate: \$100k-\$150k	Poor: >\$150k

Table 2.8 Score Values and Levels for Project Objectives

Objectives	Score Values and Levels			
	4	3	2	1
Measures and Indicators	Compaction	Thermal Segregation	Modulus	Other Characteristics
Construction Process Utilization	X	X	During Compaction	After Compaction

Table 2.9 Scores for the evaluated NDTs

	Attribute	FWD	LWD	GPR	Impact Echo	Infrared Thermography	Intelligent Compactor	Laser	Permeameter	SPA	PSPA
Equipment	Portability of the test	2	4	4	3	4	4	4	3	2	4
	Complexity of execution in the field	1	2	1	2	2	2	1	2	2	2
	Time required to conduct each test (not including setup)	2	2	4	3	3	4	4	1	3	3
	Environmental limitations	2	2	1	2	4	4	1	3	3	3
	Reliability of collected data	3	2	4	1	3	3	3	2	2	3
	Degree of training	1	1	1	2	2	2	1	2	1	1
	Purchase price	2	4	2	4	4	1	1	4	2	4
Objective	Measures and indicators	2	2	4	1	3	4	1	1	2	2
	Construction process utilization	1	2	1	1	2	2	1	1	1	2
Equipment Score		13	17	17	17	22	20	15	17	15	20
Objective Score		3	4	5	2	5	6	2	2	3	4
Overall Score		39	68	85	34	110	120	30	34	45	80

To illustrate the calculation process for the overall score, the following example is prepared. The example illustrates the steps used to calculate the overall score for the FWD. The first step is to calculate the “Equipment” cumulative score based on the attribute scores:

$$\text{Equipment score} = 2 + 1 + 2 + 2 + 3 + 1 + 2 = 13$$

The second step is to calculate the score for meeting the project objectives:

$$\text{Objective score} = 2 + 1 = 3$$

The third step is to calculate the overall score by multiplying the “Equipment” score by the “Objective” score:

$$\text{Overall score} = 13 \times 3 = 39$$

The overall score calculated in Table 2.9 is used to rank the different NDTs. The ranking allows a selection of minimum two NDTs to proceed to Stage 2 of this study. Table 2.10 lists the ranking of the technologies including the score for the equipment, objective, and overall score. The overall ranking of the NDTs shows the intelligent compactor and infrared thermography are closely ranked at the top two spots while maintaining a wide range with the lesser ranked NDTs.

Table 2.10 Evaluated Non-Destructive Technology Ranking

Technology	Rank	Equipment	Objective	Overall Score
Intelligent Compactor	1	20	6	120
Infrared Thermography	2	22	5	110
Ground Penetrating Radar	3	17	5	85
Portable Seismic Pavement Analyzer	4	20	4	80
Light Weight Deflectometer	5	17	4	68
Seismic Pavement Analyzer	6	15	3	45
Falling Weight Deflectometer	7	13	3	39
Impact Echo	8	17	2	34
Permeameter	9	17	2	34
Laser	10	15	2	30

At a meeting with the WHRP Technical Oversight Committee, a decision was made to evaluate infrared thermography (IR), GPR, and the PSPA. IR allows continuous coverage across the mat, GPR a 1-foot wide continuous strip, and PSPA as a point measure. The following chapter describe the data collection with these three technologies.

Chapter 3 Data Collection

3.1 Technologies and Models

This chapter describes the data collection for the field evaluation of the three NDT technologies: infrared thermography (IR), ground penetrating radar (GPR), and portable seismic pavement analyzer (PSPA). Infrared thermography included two acquisition methods: the Pave-IR system mounted on the rear of the paver for continuous readings, and a hand-held FLIR (Forward Looking Infrared Radiometer) thermal camera for discrete readings. A nuclear density gauge also collected data for comparative purposes. Table 3.1 summarizes the NDT technologies and chosen manufacturer and model for field testing.

Table 3.1 NDT Models for Field Testing

NDT Technology (1)	Manufacturer (2)	Model (3)
Infrared Thermography, paver-mounted system	Moba Automation Corp.	Pave-IR
Infrared Thermography, hand-held camera	FLIR Systems, Inc. (Forward Looking Infrared Radiometer)	Reporter v8.5
Ground Penetrating Radar, mounted to test vehicle	Geophysical Survey Systems, Inc.	RADAN
Portable Seismic Pavement Analyzer	Geomeia Research and Development, Inc.	PSPA-PU
Nuclear Density Gauge	Campbell Pacific Nuclear	M1DCP

3.2 Sampling Plan and Projects

Figure 3.1 illustrates the spatial data collection plan where a 500-foot subplot length was created to manage data sampling and analysis. Five offsets from pavement reference centerline were established to evaluate measurements at the longitudinal joints, both wheel paths, and between the wheel paths. This approach leveraged the ability of the IR and GPR to measure continuously in a path and detect any changes transversely and longitudinally.

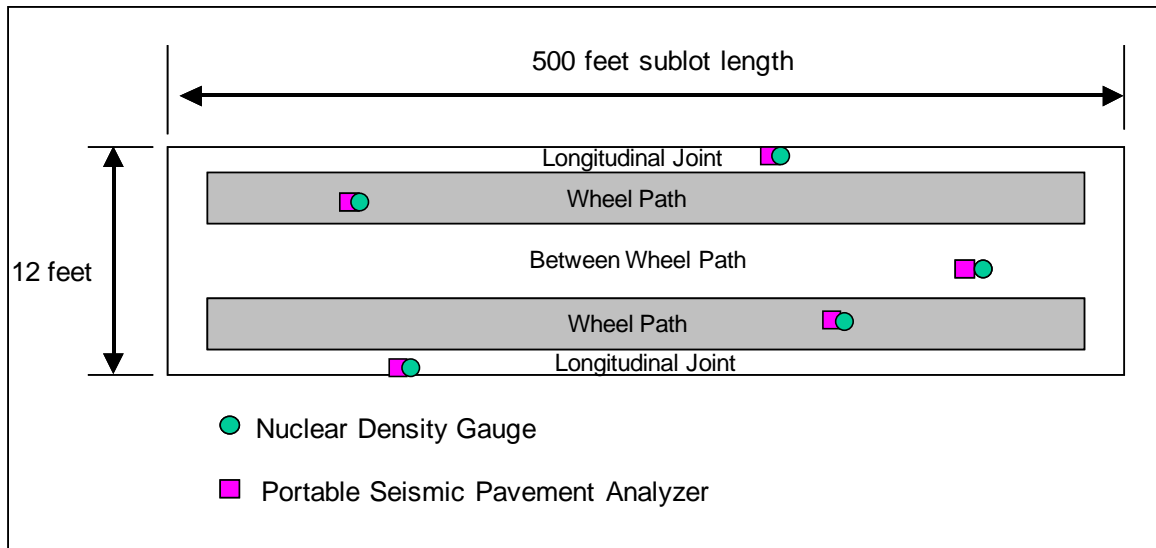


Figure 3.1 Spatial Data Collection Plan

Projects for field data collection are reported in Table 3.2. It was a stated goal to collect data from at least three projects, with emphasis on the gradation and surface texture. Scheduling and rental of all test equipment in August 2011 allowed only three fine-graded mixes to be tested. The budget permitted one day of testing on the three projects. Total length of research test sections was limited by the ability to collect GPR data after the pavement cooled and before darkness. This test window for the GPR and PSPA was in a 1-hr to 2-hr range, presenting a practical consideration for implementing this technology in a future specification or construction manual.

Table 3.2 Projects for Data Collection

Roadway	Project Location	Project ID	Data Collection Date	Begin Test Station	End Test Station	Test Section Length
USH 2	Ashland County, east of Ashland	1180-00-73	August 4	435+00	385+00	5000 ft
STH 75	Kenosha County, southeast of Burlington	2420-02-70	August 11	242+00	192+00	5000 ft
STH 42	Manitowoc County, southwest of Manitowoc	4570-05-71	August 18	600+00	660+00	6000 ft

Project selection was also based upon scheduling of the test equipment, whether the contractor would use their Pave-IR system on the project, and project locations having different aggregate sources. Since candidate projects were fine graded, unique aggregate sources and paving crews were explored. The Job Mix Formula and traditional QMP data were collected from the project staff for plant-produced mixture properties, with a summary of select mix properties shown in Table 3.3.

Table 3.3 Project Mixture Properties

Mix Property	Project		
	USH 2	STH 75	STH 42
ESAL classification	E-3	E-1	E-3
NMAS, mm	19	19	12.5
Coarse Aggregate ¹	Basalt	Dolostone	Dolostone
Gsb aggregate	2.706	2.663	---
Gmb	2.380	2.411	2.450
Gmm	2.501	2.512	2.552
Voids, %	4.9	4.0	4.0
VMA, %	16.3	13.6	15.0
VFA, %	---	70.6	73.3
AC, %	4.8	4.6	5.2
PG	58-28	58-28	58-28
P19mm, %	99.4	98.6	100.0
P12.5mm, %	91.1	87.6	94.2
P9.5mm, %	81.8	78.6	89.6
P4.75mm, %	60.0	55.4	63.4
P2.36mm, %	45.1	41.2	49.6
P1.18mm, %	35.7	---	---
P600um, %	27.7	23.9	28.9
P300um, %	14.0	10.9	13.8
P150um, %	7.3	---	---
P75um, %	5.5	4.7	4.5
¹ Source: http://tin.er.usgs.gov/geology/state/			

3.3 Infrared Thermography

Infrared thermography data were collected using two methods: (1) the Pave-IR system manufactured by the Moba Automation Corp. mounted to the rear of the paver, and (2) a hand-held thermal camera manufactured by FLIR Systems, Inc. (Forward Looking Infrared Radiometer). Use of two thermal measurement techniques allowed the research study to report how these methods could measure mat temperature and potential segregated areas during construction.

3.3.1 Sensors mounted to paver (Pave IR system)

The Pave-IR system manufactured by the Moba Automation Corp. is the leading continuous infrared thermography measurement system currently available for the asphalt industry. As reported in the interim report (UWP-Bloom 2011), thermal measurements behind the paver are specified by the Texas and Washington Departments of Transportation. With this new technology, paving contractors are beginning to actively use

the Pave-IR system for quality control. The paving contractors participating in this study were very cooperative and furnished the generated Pave-IR data for research purposes.

Pave-IR hardware consisted of 12 thermal cameras spaced 13 in. and mounted on an aluminum support bar. The bar extended from the centerline longitudinal joint towards the shoulder edge, effectively measuring temperature across a 13-ft width behind the screed. On all projects, the screed width exceeded the 13-ft measurement width since an integral 12-ft drive lane and paved shoulder were paved simultaneously. Readings are collected at an operator-specified interval of 6 inches or greater. Although a 6-in increment was programmed for each project, only 12-in increments were retained for analysis.

Figure 3.2 shows the Pave-IR mounted to the rear of the paver. As this photo illustrates, attaching the system to a paver adds complexity with multiple other attachments, such as a longitudinal joint roller and external grade control sensors (ski and shoe).



Figure 3.2 Pave-IR system mounted to rear of paver

Temperature readings from the sensors are displayed on a multi-colored screen to visually monitor the temperature profile directly behind the paver (Figure 3.3). Forward progress of the paver, GPS coordinates, paver speed, and other selected output are reported in real time. Operators can periodically scan the display to monitor the temperature profile and possibly detect any temperature anomalies.



Figure 3.3 Pavement-IR Display Screen

Data collected during paving is stored on a jump drive for later downloading to a computer. Data are encrypted and must be decoded for post-processing data analysis in text format. If using Moba's post processing software known as Pavement Project Manager™, data is automatically decoded and displayed. Pavement Project Manager™, displays thermal image, a histogram of measured temperatures, data playback, and histogram display of temperatures for the entire project (Moba 2011). Typical data fields reported in the output file are project set-up, time, distance, speed, GPS location, and temperature measures for the 12 infrared sensors.

Pavement-IR software, known as PavementApp™, performs multiple functions including calibration of the sensors at certified calibration center, calibration of the distance measurement instrument (DMI), collection of transverse scans at user-defined distances, real-time analysis of temperature range as defined by the PavementApp™ software, real-time display of thermal image and temperature differentials.

3.3.2 Thermal Camera

A hand-held FLIR (Forward Looking Infrared Radiometer) thermal camera recorded asphalt mixture temperatures on each of the projects. Images were recorded on an approximate one-hour interval to provide comparative data or when changes occurred on the project, such as an equipment delay, or addition of a material transfer vehicle. Experienced operators in FLIR thermal cameras recorded the images. The FLIR camera was calibrated: (1) on an annual basis from the manufacturer (exact date was not

documented), and (2) a daily calibration during the start of paving. The daily calibration included a comparison of a point reading with the FLIR camera and a point reading with a handheld infrared thermometer (“heat gun”). The FLIR camera and handheld infrared thermometer were within 5 °F in all comparisons. Two handheld infrared thermometers were compared on each project to ensure calibration and were also within 5 °F in all comparisons.

On a typical project, the camera can record temperatures in the truck box, material transfer vehicle receiving hopper, paver receiving hopper, and behind the screed. Figure 3.4 is the camera recording the temperature in the truck box, and Figure 3.5 is the resulting image and data presentation. FLIR version 8.5 software processes the thermal image and presents a data summary. During post-processing, the operator is able to specify locations of temperatures using lines (Li), areas (Ar), and specific points (Sp). It is important to note that in many instances the crust of the load is recorded and once the load is broken the underlying material will be much hotter. The camera has a "point-sample" approach where every pixel in the photo has an associated temperature. It is possible to export the data to a spreadsheet and view hundreds of temperature data points.



Figure 3.4 Thermal hand-held camera recording image inside truck box on Project 2 at Station 242+00

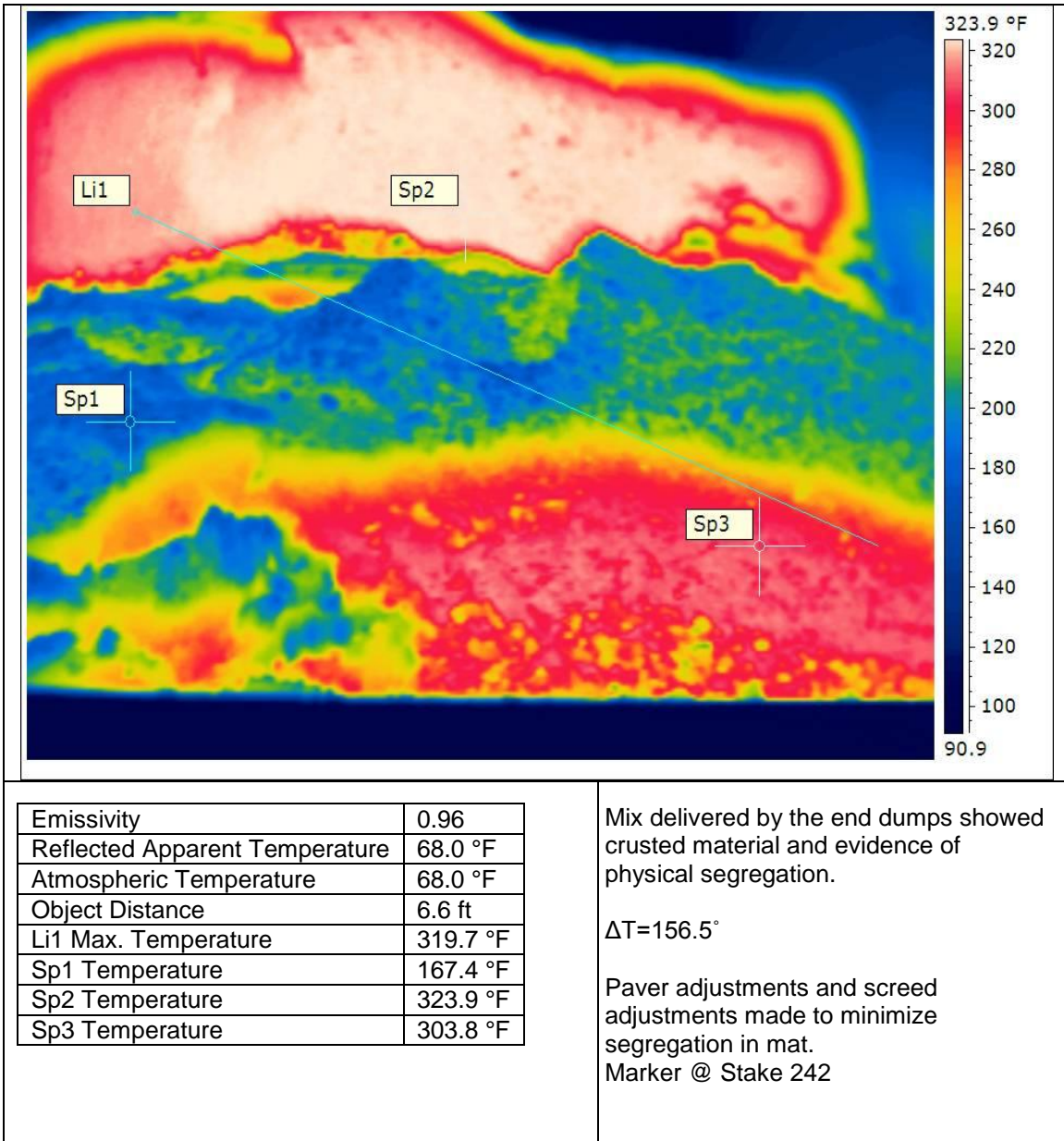


Figure 3.5 Data presentation for thermal image taken on Project 2 at Station 242+00

3.4 Ground Penetrating Radar

A ground penetrating radar (GPR) manufactured by Geophysical Survey Systems, Inc. (GSSI) and operated by the University of Illinois tested the newly-placed asphalt layer. GPR is based on electromagnetic (EM) wave theory. It typically has two antennas: (1) a transmitter that sends EM wave signals to the pavement, and (2) a receiver that collects the signals reflected by the pavement. Information concerning the pavement, such as layer thickness and density, can be obtained from the reflected signals. Figure 3.6 is the GPR antennas measuring thickness and density on the first project.



Figure 3.6 GPR equipment ready to scan a pavement layer

When selecting a GPR antenna for a project, survey speed and the trade-off between signal resolution and penetration depth is considered. Compared to the ground-coupled antenna, which is in contact with the ground, the air-coupled antenna suspended in the air allows greater survey speed; hence, the air-coupled method was selected for this study. In addition, the signal of the higher central frequency has greater resolution, but lower penetration depth. On the other hand, for lower frequency signal, the resolution is lower, but the penetration depth is higher (Leng et al. 2009). The air-coupled antennae with a central frequency of 2 GHz has enough resolution and penetration depth (up to 2.5 ft) for a freshly placed layer, and thus was used in this study. To synchronize the GPR data with survey distance and location, a distance measuring instrument (DMI) was also used.

GPR scan data were collected from centerline offset as listed in Table 3.4. In order to evaluate pavement layer thickness and density at various locations in a lane, multiple survey lines were established at varying offset distances from the centerline. The lines were marked on the lower base or existing asphalt layer for the initial pre-paving scan (Figure 3.7), and on the freshly paved layer (Figure 3.8) to align the start of each scan. While scanning, the driver visually maintained the desired offset by periodically referencing the center longitudinal joint. There is the potential for lane wander during the scan, and this variability has been naturally built into the data set. It was not possible to scan all five offsets on each project due to opposing vehicle traffic near the centerline joint or layer edge drop off.

Table 3.4 Selected Scan Lines for each project

Project No.	Project Location	Distance between Centerline and Scan Line				
		0.5 ft	2.5 ft	6 ft	9.5 ft	11.5 ft
1	USH 2, Ashland County	No	Yes	Yes	Yes	No
2	STH 75, Kenosha County	Yes	Yes	Yes	Yes	Yes
3	STH 42, Manitowoc County	No	Yes	Yes	Yes	Yes



Figure 3.7 GPR pavement reference scan on a pulverized base layer

Since there is horizontal curvature on every project, the potential exists for a disagreement between project stationing and the test vehicle distance measurement

instrument (DMI). As a precaution, project stationing and the GPR test vehicle DMI were compared every 1,000 ft. Adjustments up to 10 ft were necessary on some scans.



Figure 3.8 GPR offset reference scan lines

Pre-paving scan data were stored and compared to post-paving scan data to enhance the dielectric constant resolution of the existing base layer and new asphalt layer. The software estimates the dielectric constant of the layers, and thus, the thickness of the detected layers can be calculated (Al-Qadi and Lahouar 2005; Lahouar 2003; Lahouar et al. 2008). In addition, by implementing the ALL density model (Al-Qadi, Lahouar, and Leng model), the densities of the tested layers (represented by G_{mb}) were also estimated using previous work by Leng et al. (2011). Scan lines shown in Table 3.5 were selected for reporting the pavement densities, as well as the air void contents. It was not possible to report densities on each scan due to processing error.

Table 3.5 Selection of the Scan Lines for Density and Air Void Content Profiles

Project (1)	Project Location (2)	Scan Lines for Density and Air Void Content Profiles (3)
1	USH 2, Ashland County	2.5 ft and 6 ft
2	STH 75, Kenosha County	9.5 ft and 11.5 ft
3	STH 42, Manitowoc County	6 ft, 9.5 ft and 11.5 ft

The GPR measurements were obtained within hours after the final compaction and after the pavement had cooled to withstand traffic. Measurement lengths were 5,000 ft on first two projects and 6,000 ft on the third project. Moving traffic control and/or darkness limited testing length. The GPR collected data were then used to obtain layer thickness and density.

The nuclear density gauge was used to calibrate the GPR to a known reference density at a minimum of five comparative test sites per project. Pavement cores were not taken due to logistics and the smaller comparison size, such as 2 sites per project. GPR thickness measurements were calibrated by placing aluminum foil on the base ahead of the paver, paving and compacting over the foil, then actuating GPR signal pulses over the foil to yield a strong reflective signal. Figures 3.9 and 3.10 show the GPR calibration site on

the second project where aluminum was placed on the pulverized-and-relay base ahead of the paver. Figure 3.11 is the GPR actuating signal pulses to estimate layer thickness and pavement density.



Figure 3.9 GPR thickness calibration site with aluminum foil



Figure 3.10 Hot mix securing aluminum foil ahead of paver



Figure 3.11 GPR density and thickness measurement

3.5 Portable Seismic Pavement Analyzer

A portable seismic pavement analyzer (PSPA) developed and manufactured by Geomeia Research and Development, Inc., recorded modulus measurements on all projects. Model #PSPA-PU included a seismic test unit, software, maintenance kit, carrying case, and lengthy USB cable for connecting to a laptop computer.

The PSPA device is controlled by software titled SPA Manager™. After connecting the PSPA hardware and starting the SPA Manager™, the field operator inputs data to collect data for a test site. The PSPA source then initiates a test by tapping the surface with an electromagnetic hammer. This "tap" creates vibrations (stress waves) which travel and propagate outward from the contact point through the asphalt mat. These vibrations are detected by two accelerometer receivers and translated into a signal. These signals are then transferred to an electronics box that uses acquisition and data conditioning hardware to process the signals and forward to the computer. Figure 3.12 illustrates the PSPA hardware. Members of the research team operated the PSPA-PU on all projects; the device is shown testing compacted asphalt near the longitudinal joint in Figure 3.13.

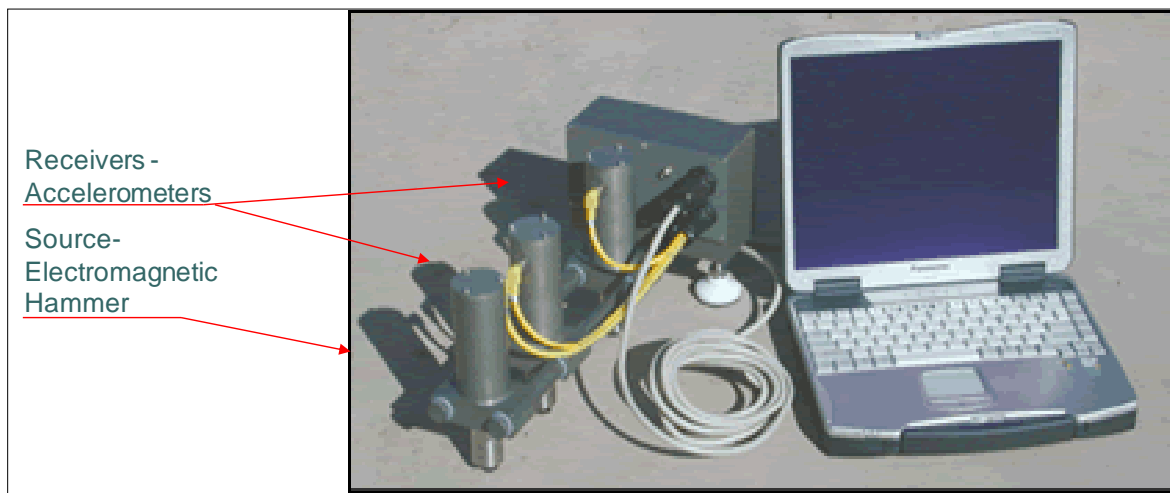


Figure 3.12 PSPA (Geomeia 2010)

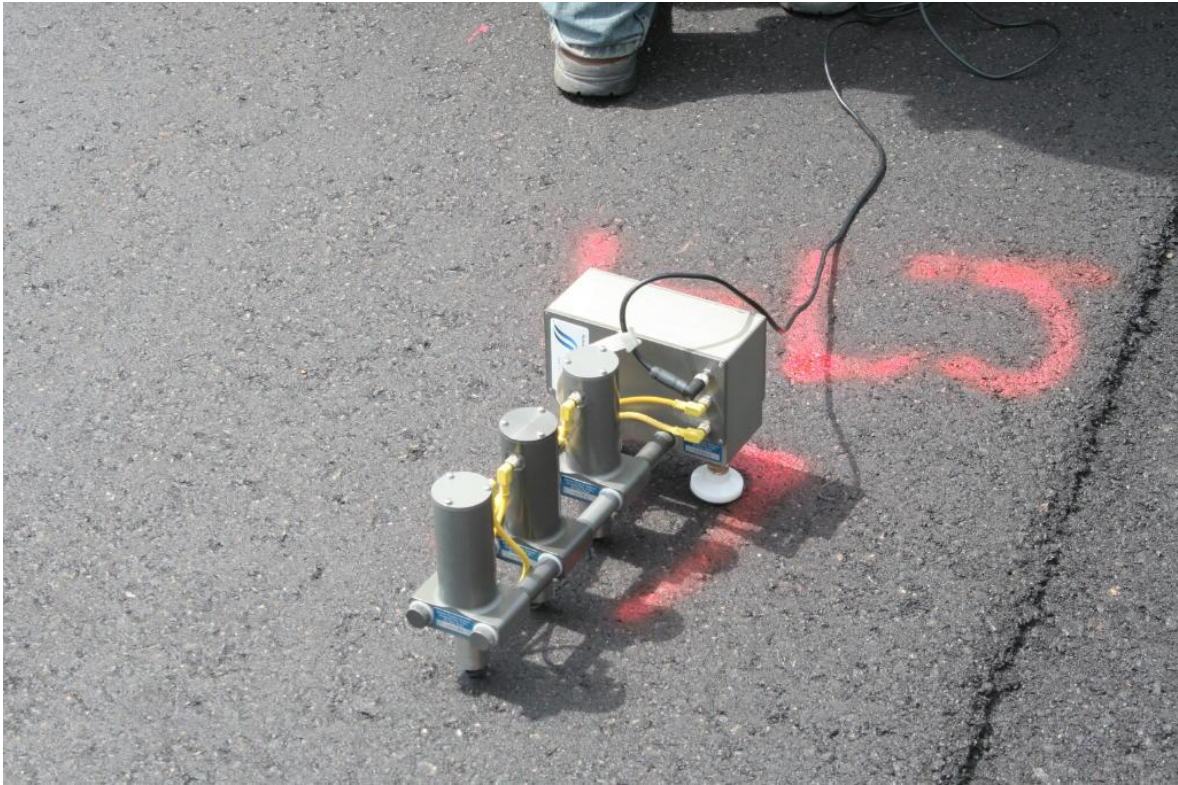


Figure 3.13 PSPA testing the asphalt layer near longitudinal construction joint

Stress waves are propagated through a solid or liquid media where the propagation depends on the mechanical properties (as density or modulus) of the excited media. The PSPA measures the motion of the surface at each receiver as the vibration travels past the receiver. A typical measurement of the vibrations is shown in Figure 3.14. The signal represents the motion of the surface under a sensor as time changes. The arrival of the P, S and R disturbances are also indicated. Figure 3.15 is an output displayed by the PSPA software after testing at one point.

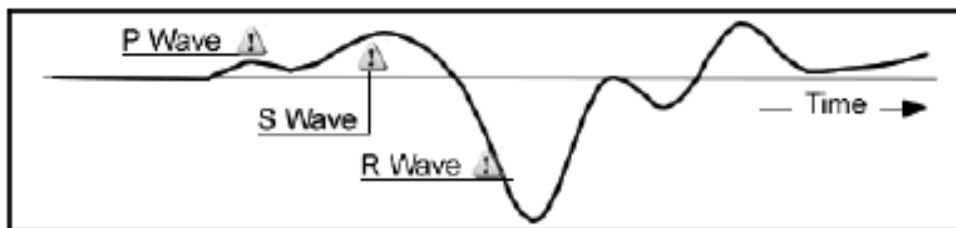


Figure 3.14 Typical SPA signal waves (Geomedia 2010)

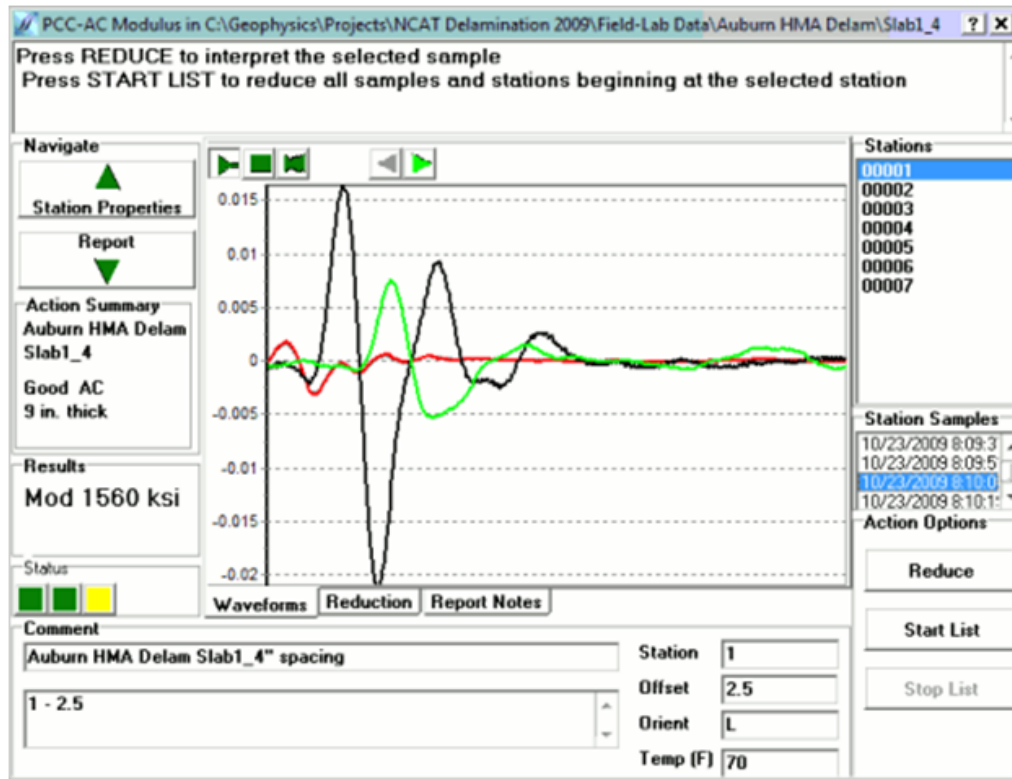


Figure 3.15 Sample Display of PSPA Manager Software (Geomedia 2010)

In order to calculate the seismic modulus, the time records of both the near and far receivers are used. The measured difference in time between the arrival of the “S” wave is used to calculate the modulus as shown by Equation 3.1:

$$E = cV^2 = c(x/t)^2s \quad (3.1)$$

Where,

- E = seismic modulus of the medium;
- c = constant;
- V = velocity;
- x = distance between receivers;
- t = derived distance; and
- s = spacing of signals.

A thermistor sensor limits testing in a pavement temperature range of 32 to 120°F. At some sites, the PSPA was able to measure modulus with pavement temperature exceeding 120°F. Since asphalt pavement strength is temperature dependent, comparative data were collected at 10 test sites at warmer and cooler temperatures. Warmer temperatures were soon after finish rolling at temperatures of about 120°F to 130°F, while cooler temperatures of about 90°F to 100°F were recorded during dusk hours.

3.6 Project 1, U.S. Highway 2

U.S. Highway 2 paving consisted of an 18-ft wide, 2.5-in thick mat placed on a milled asphalt base. Total paving width was 18 ft incorporating an integral 12 ft driving lane and 6 ft shoulder. The bar was positioned over the driving lane. The eastbound lane was paved in a westward direction, away from the mix plant. A tapered joint was placed with the screed extension and externally mounted roller. The Pave-IR system and FLIR imaging camera recorded temperatures throughout the day.

The Pave-IR system had a 13-ft long aluminum bar mounted on the rear of the paver with 12 sensors spaced at 13 inches each. The right sensor (#12) was approximately 1 ft left of the longitudinal taper. Sensor #1 was 13 ft left of the longitudinal taper. Screed control included a right ski and two shoes. Figures 3.16 and 3.17 show the paver on Project 1.



Figure 3.16 Cedarapids paver on Project 1



Figure 3.17 Pave-IR system with display panel on Project 1

Paving equipment on the first project is summarized in Table 3.6. A material transfer vehicle (MTV) was included in the operation. Trucks with rear dumps hauled material from a mix plant approximately 20 miles east.

Table 3.6 Paving equipment for Project 1

Equipment (1)	Manufacturer or Description (2)
Trucks	Rear dumps
Material Transfer Vehicle	Terex Roadmix C6250, tracked
Paver	Cedarapids
Paver receiving hopper	Cedarapids CR662
Breakdown roller	Ingersoll-Rand DD-130
Intermediate pneumatic roller	Dynapac
Finish roller	Hypac

Total research test section length for August 4th was 5,000 ft, while actual paving was well over a mile. Research testing began at 435+00 with paving down station to 385+00. Only 5,000 ft were tested due to the time constraints to collect GPR and PSPA under single-lane traffic control before darkness.

A comparison was made between project stationing lathe along the alignment and the distance measurement instrument (DMI) mounted on the paver drive axle that supplies movement data to the Pave-IR system. The purpose of this comparison was to ensure

correct locations of Pave-IR data with respect to the GPR, PSPA, and nuclear density data. Table 3.7 compares the paver DMI with the project stationing. Unfortunately, there were no comparisons made until after Station 395+00, which was 4,000 ft into the research test section (start of Sublot #9), and it is unclear when the difference began to occur. The change from comparisons #1 to #2 was 177 ft across 4,226 ft (4.2% change in ft/ft), while from comparisons #2 to #8 the change was 97 ft across 1,774 ft (5.5% change in ft/ft). A lengthy left horizontal curve and right horizontal curve could also explain the change in difference. With lack of comparison sites in the first 4,000 ft, it was not possible to correctly adjust the Pave-IR locations, and thus, no adjustments were made to the data set.

Table 3.7 Drift in Paver DMI and Project Stationing

Comparison Location (1)	Station from lathe (2)	Pave-IR Station (3)	Difference, Feet (4)
1	435+00	435+00	0
2	392+74	394+51	177
3	390+00	391+87	187
4	387+00	389+07	207
5	384+00	386+19	219
6	381+00	383+39	239
7	378+00	380+57	257
8	375+00	377+74	274

3.7 Project 2, State Highway 75

State Highway 75 paving consisted of a 17-ft wide, 2.5-in thick mat placed on a pulverized-and-relay base. Total paving width was 17 ft incorporating an integral 12 ft driving lane and 5 ft shoulder. Both the Pave-IR and FLIR imaging camera recorded temperatures throughout the day; however, the Pave-IR recorded temperatures from only six sensors spaced 26 inches due to the operational set-up (not 12 sensors spaced 13 inches). The right sensor (#6) was 2 ft from the centerline longitudinal joint, while the left sensor (#1) was 2 feet from the shoulder longitudinal joint.

The paving spread by stationing is summarized in Table 3.8. Paving on August 11th offered a unique opportunity to analyze changes in asphalt mix temperatures during laydown both with and without a material transfer vehicle (MTV). At the start of paving, the MTV had a mechanical failure with a bent conveyor slat and was removed from the operation. Trucks then began dumping directly into the paver hopper. Paving continued without the MTV until about mid-day when a replacement arrived and begin transferring material at Station 209+80. Prior to this location, the plant mixing temperature was lowered 10°F, from an estimated 320°F to 310°F. A higher initial mixing temperature was designed to blend 3% recycled asphalt shingles into the mixture.

Table 3.8 Paving spread for the Highway 75 project on August 11th

Equipment	Morning paving Station 242+00 to 210+00*	Afternoon paving Station 210+00 to 192+00**
Paver, Volvo/Blaw-Know PF6160	Yes	Yes
Paver receiving hopper, Weiler	No	Yes
Material transfer vehicle, Roadtec SB25000 “Shuttle Buggy”	No	Yes
Breakdown roller, Hypac	Yes	Yes
Intermediate pneumatic roller, Bomag	Yes	Yes
Finish roller, Bomag	Yes	Yes
*Paving started at 244+70; Research testing started at 242+00. **Paving stopped for day at 146+80; Research testing ended at 192+00.		

Total research test section length for August 11th was 5,000 ft, the first 3,220 ft without the MTV and latter 1,780 ft with the MTV. Figures 3.18 through 3.22 sequentially illustrate the operation.



Figure 3.18 Project 2 Sta. 244+70 start of paving with MTV



Figure 3.19 Project 2 Station 242+00 with MTV removed from paving train



Figure 3.20 Project 2 Station 240+00 paving without MTV



Figure 3.21 Project 2 Station 213+00 delivery of replacement MTV



Figure 3.22 Project 2 Station 209+80 with replacement MTV in paving train

3.8 Project 3, State Highway 42

The third project for evaluating the NDT devices was STH 42 southwest of Manitowoc. Final surface layer paving consisted of a 15-ft wide, 1.75-in thick mat placed on a leveling layer and existing asphalt base. Total paving width was 15 ft incorporating an integral 12 ft driving lane and 3 ft shoulder. The westbound lane was paved in an eastward direction (compass northeast), away from the mix plant. A tapered longitudinal joint was paved along the right side of the paver.

The Pave-IR system and FLIR imaging camera recorded temperatures throughout the day. The Pave-IR system had a 13-ft long aluminum bar mounted on the rear of the paver with 12 sensors spaced 13 in. The right sensor (#12) was approximately 2 ft from the centerline longitudinal joint, and 1 ft from the longitudinal taper. Sensor (#1) was 13 ft from the longitudinal joint taper. Screed control included a right ski and two shoes. Figures 3.23 and 3.24 show the paving train and temperature bar.



Figure 3.23 Paving train on third project



Figure 3.24 Pave-IR system with display panel

Paving equipment on the third project is summarized in Table 3.9. A material transfer vehicle (MTV) was included in the operation. Trucks with rear dumps hauled material from a mix plant approximately 25 miles to the east.

Table 3.9 Paving equipment for the third project

Equipment (1)	Manufacturer (2)
Trucks	Various rear dumps
Material transfer vehicle	Roadtec SB2500 “Shuttle Buggy”
Paver	Blaw-Know PF3200
Paver receiving hopper	Weiler
Breakdown roller	Ingersoll-Rand DD-110HF
Finish roller	Bomag

Total research test section length for August 18th was 6,000 ft, while actual paving was about three miles in length. Research testing began at station 600+00 and continued to station 660+00. Similar to the other projects, test section length was limited by daylight.

It was observed at the start of paving that three temperature sensors appeared to be out of calibration with respect to the other sensors. Sensors #5 and #6 near the center of the bar, and Sensor #2 near the left side of the bar, had a consistently higher temperature than the neighboring sensors. Figure 3.25 illustrates the higher temperature sensors designated by red and orange colors. Temperature resolution was adjusted so that lower

temperature sensors had a monolithic green appearance. Because of this project, calibration is a fundamental concern if the sensing bar is to be used in any future construction manual or specification.



Figure 3.25 Sensors out of calibration on the third project

Chapter 4 Data Summary

4.1 Introduction

This chapter presents the data summary from the three projects for the evaluated NDT devices: infrared thermography (IR), ground penetrating radar (GPR), portable seismic pavement analyzer (PSPA), and nuclear density gauge. The purpose of this summary is to present the fundamental project statistics for each NDT device by entire project research section length and by individual 500-ft subplot lengths. Sections have been created for the NDT devices in the order data would be collected on a typical project, beginning with the IR thermal bar and ending with the PSPA. Statistics were computed using commercially available software package including SAS™ v9.1, Minitab™ v15, and Microsoft Excel™. Descriptive statistics are provided for each test device to offer a basic understanding of the data, and include sample size, mean, standard deviation, coefficient of variation, maximum, minimum, and range. Data were summarized to one decimal for conciseness and interpretability. Then, in the Chapters 5 and 6, an in-depth investigation is conducted for thermal data and structural data, respectively.

4.2 Infrared Thermography

4.2.1 Project 1, USH 2

The full research test section length on Project 1 was 5,000 ft, having ten 500-ft sublots. Continuous IR data were collected every 6 in, but only 1-ft intervals were retained for ease in interpretation. Thus, a total of 5,000 thermal readings were retained from each sensor. Table 4.1 summarizes basic statistics for the continuous IR readings by sensor and offset from reference centerline.

Table 4.1 Infrared Temperature Basic Statistics for Project 1

Offset Location	N	Mean	Std. Dev.	Coeff. Var.	Maximum	Minimum	Range
Sensor 12 at 1.0 ft, °F	5000	248.4	22.8	9.2	287.1	95.0	192.1
Sensor 11 at 2.1 ft, °F	5000	249.9	22.1	8.9	291.6	98.4	193.2
Sensor 10 at 3.2 ft, °F	5000	249.4	23.0	9.2	294.3	95.9	198.4
Sensor 9 at 4.3 ft, °F	5000	241.8	22.6	9.4	284.5	85.1	199.4
Sensor 8 at 5.3 ft, °F	5000	243.5	22.0	9.0	288.5	91.8	196.7
Sensor 7 at 6.4 ft, °F	5000	244.1	19.7	8.1	283.6	96.8	186.8
Sensor 6 at 7.5 ft, °F	5000	247.7	19.1	7.7	280.2	97.7	182.5
Sensor 5 at 8.6 ft, °F	5000	250.7	19.0	7.6	295.5	96.3	199.2
Sensor 4 at 9.7 ft, °F	5000	246.1	19.6	7.9	290.8	97.9	192.9
Sensor 3 at 10.8 ft, °F	5000	244.8	20.1	8.2	285.6	91.9	193.7
Sensor 2 at 11.8 ft, °F	5000	260.3	21.6	8.3	303.8	101.7	202.1
Sensor 1 at 12.9 ft, °F	5000	254.1	21.4	8.4	302.0	104.0	198.0

Average sensor temperature was between 240 and 260°F with no trend detected among average readings across the thermal bar; however, greater variability occurred at the

outer sensors. Highest reading was 304°F while the lowest was 85°F. The range among the sensors was relatively consistent, with a lower range of 183°F and upper range of 202°F. Higher pavement temperatures were measured towards the left side of the paver (sensors 2 and 5), while more variability occurred along the right side (sensors 8-12).

Basic statistics for the individual 500-ft sublots were also calculated to understand any trends in the data during paving operations. Summaries are provided for the first and final 500-ft sublots for comparative purposes in Tables 4.2 and 4.3, respectively. Summaries for all 10 sublots are found in Appendix A.

Table 4.2 Infrared Temperature Statistics for Project 1 Sublot 1

Offset Location	N	Mean	Std. Dev.	Coeff. Var.	Maximum	Minimum	Range
Sensor 12 at 1.0 ft, °F	500	232.8	31.6	13.6	252.3	95.0	157.3
Sensor 11 at 2.1 ft, °F	500	235.9	30.3	12.9	252.7	98.4	154.3
Sensor 10 at 3.2 ft, °F	500	233.6	34.6	14.8	253.2	95.9	157.3
Sensor 9 at 4.3 ft, °F	500	225.6	34.8	15.4	247.5	85.1	162.4
Sensor 8 at 5.3 ft, °F	500	227.6	32.9	14.5	248.4	91.8	156.6
Sensor 7 at 6.4 ft, °F	500	231.2	25.4	11.0	248.2	96.8	151.4
Sensor 6 at 7.5 ft, °F	500	239.6	18.9	7.9	255.2	97.7	157.5
Sensor 5 at 8.6 ft, °F	500	240.1	15.2	6.3	253.0	96.3	156.7
Sensor 4 at 9.7 ft, °F	500	236.4	16.2	6.9	252.3	97.9	154.4
Sensor 3 at 10.8 ft, °F	500	233.9	17.5	7.5	248.0	91.9	156.1
Sensor 2 at 11.8 ft, °F	500	248.8	19.1	7.7	262.6	101.7	160.9
Sensor 1 at 12.9 ft, °F	500	242.5	5.0	2.1	253.4	227.5	25.9

Table 4.3 Infrared Temperature Basic Statistics for Project 1 Sublot 10

Offset Location	N	Mean	Std. Dev.	Coeff. Var.	Maximum	Minimum	Range
Sensor 12 at 1.0 ft, °F	500	258.9	7.3	2.8	274.1	229.3	44.8
Sensor 11 at 2.1 ft, °F	500	260.3	7.4	2.8	276.4	231.3	45.1
Sensor 10 at 3.2 ft, °F	500	259.3	9.0	3.5	281.3	233.8	47.5
Sensor 9 at 4.3 ft, °F	500	251.5	8.1	3.2	272.1	225.3	46.8
Sensor 8 at 5.3 ft, °F	500	253.2	7.6	3.0	273.6	227.7	45.9
Sensor 7 at 6.4 ft, °F	500	253.2	6.8	2.7	269.8	225.3	44.5
Sensor 6 at 7.5 ft, °F	500	253.2	7.5	2.9	271.4	225.5	45.9
Sensor 5 at 8.6 ft, °F	500	258.6	7.2	2.8	279.1	230.2	48.9
Sensor 4 at 9.7 ft, °F	500	254.6	8.2	3.2	274.6	227.7	46.9
Sensor 3 at 10.8 ft, °F	500	252.7	7.1	2.8	271.9	225.3	46.6
Sensor 2 at 11.8 ft, °F	500	269.1	8.6	3.2	291.6	239.2	52.4
Sensor 1 at 12.9 ft, °F	500	267.1	7.2	2.7	285.1	234.3	50.8

The 150°F to 160°F range of the first subplot was nearly three times that of the final subplot. The accompanying standard deviation and coefficient of variation were also high. Lower readings were caused by an 8-minute paver stop at Station 433+00 with cooler readings for a distance of about 30 ft (details in Chapter 5). To compound this event, a stack test was conducted at the mix plant in the morning causing a fluctuation in temperatures.

Statistics in Table 4.3 were more representative of the other sublots; however, a 20-minute paver stop in the second subplot also increased the range. Note the similar coefficient of variation values in Table 4.3.

An important consideration in interpreting the data is using the standard deviation or range. The standard deviation allows all readings equal weight in determining variability, while the range is substantially influenced by a single maximum or minimum value. In fact, placing an object between the sensor and mat, such as a tool or hand, immediately effects the range.

4.2.2 Project 2, STH 75

The full research test section length on Project 2 was also 5,000 ft, having ten 500-ft sublots. Project research testing began at Station 242+00 with downward stationing, so the first subplot extended from 242+00 to 237+00, second subplot from 237+00 to 232+00, and so on. This project was different from the others with only 6 of 12 sensors operating, each spaced at 26 in. A total of 5,000 thermal readings were retained for each sensor. Table 4.4 summarizes basic statistics for the continuous IR readings by sensor and offset from centerline joint. Higher mean temperatures were recorded by the central sensors (#3 and #4) and cooler temperatures towards the edges. Variability, as measured by the standard deviation, was inconsistent across the mat. More variability and a higher coefficient of variation was detected on the right side of the paver (centerline side).

Table 4.4 Infrared Temperature Basic Statistics for Project 2

Offset Location	N	Mean	Std. Dev.	Coeff. Var.	Maximum	Minimum	Range
Sensor 6 at 2.0 ft, °F	5000	288.4	9.3	3.2	312.8	238.3	74.5
Sensor 5 at 4.2 ft, °F	5000	295.0	11.1	3.8	321.8	239.9	81.9
Sensor 4 at 6.4 ft, °F	5000	303.4	9.0	3.0	323.2	251.1	72.1
Sensor 3 at 8.6 ft, °F	5000	300.5	7.7	2.6	323.6	257.5	66.1
Sensor 2 at 10.8 ft, °F	5000	291.8	8.4	2.9	312.8	250.9	61.9
Sensor 1 at 13.0 ft, °F	5000	282.9	6.4	2.3	302.2	253.9	48.3

Summaries for the first and final 500-ft sublots are presented in Tables 4.5 and 4.6, respectively. Detailed summary tables for the 10 sublots are reported in Appendix A. Similar to the first project, a higher range and standard deviation occurred at the start of paving as compared to nearly 5,000 ft into the day's paving. There was no consistent trend

in variation from the start to the end. Less variability was detected (and lower coefficient of variation) at the center of the paver.

Table 4.5 Infrared Temperature Basic Statistics for Project 2 Sublot 1

Offset Location	N	Mean	Std. Dev.	Coeff. Var.	Maximum	Minimum	Range
Sensor 6 at 2.0 ft, °F	500	290.0	11.3	3.9	306.0	241.2	64.8
Sensor 5 at 4.2 ft, °F	500	291.9	15.5	5.3	309.9	239.9	70.0
Sensor 4 at 6.4 ft, °F	500	302.9	12.7	4.2	316.6	251.1	65.5
Sensor 3 at 8.6 ft, °F	500	298.0	8.4	2.8	313.0	264.4	48.6
Sensor 2 at 10.8 ft, °F	500	294.2	9.4	3.2	309.4	259.2	50.2
Sensor 1 at 13.0 ft, °F	500	282.7	7.1	2.5	294.3	257.7	36.6

Table 4.6 Infrared Temperature Basic Statistics for Project 2 Sublot 10

Offset Location	N	Mean	Std. Dev.	Coeff. Var.	Maximum	Minimum	Range
Sensor 6 at 2.0 ft, °F	500	280.3	5.4	1.9	291.4	264.6	26.8
Sensor 5 at 4.2 ft, °F	500	290.8	5.5	1.9	304.3	278.1	26.2
Sensor 4 at 6.4 ft, °F	500	299.8	4.7	1.6	311.4	288.3	23.1
Sensor 3 at 8.6 ft, °F	500	297.5	4.7	1.6	310.3	286.7	23.6
Sensor 2 at 10.8 ft, °F	500	285.9	6.1	2.1	300.7	272.5	28.2
Sensor 1 at 13.0 ft, °F	500	279.7	4.8	1.7	292.3	270.9	21.4

4.2.3 Project 3, STH 42

The full research test section length on Project 3 was 1,000 ft longer than the first two projects, having a total length of 6,000 ft. A total of 6,000 thermal readings were retained for each sensor, having a transverse spacing of 13 in. Table 4.7 summarizes basic statistics for the 12 sensors and offset from centerline joint.

The data in the project summary indicate higher averages with Sensors 2, 5, and 6, supporting the graphical display in Figure 3.22. Heat gun readings taken periodically during paving operation verified that these 3 sensors were out of calibration, reading a higher pavement temperature. In fact, the pavement temperature recorded by these sensors exceeded the plant mixing temperature. This particular Pave-IR hardware was sent back to the manufacturer for calibration after project completion. Aside from those sensors, the right side of the paver (sensor 12) near the tapered longitudinal joint had the highest variability. Adjoining sensors had similar variability levels.

Table 4.7 Infrared Temperature Basic Statistics for Project 3

Offset Location	N	Mean	Std. Dev.	Coeff. Var.	Maximum	Minimum	Range
Sensor 12 at 1.0 ft, °F	6000	287.0	7.5	2.6	299.1	83.8	215.3
Sensor 11 at 2.1 ft, °F	6000	298.3	4.3	1.4	309.2	257.5	51.7
Sensor 10 at 3.2 ft, °F	6000	296.1	4.7	1.6	307.9	273.4	34.5
Sensor 9 at 4.3 ft, °F	6000	289.8	4.3	1.5	300.7	264.6	36.1
Sensor 8 at 5.3 ft, °F	6000	297.6	4.2	1.4	310.1	275.0	35.1
Sensor 7 at 6.4 ft, °F	6000	299.9	3.3	1.1	309.4	271.6	37.8
Sensor 6 at 7.5 ft, °F	6000	326.7	6.2	1.9	341.6	100.6	241.0
Sensor 5 at 8.6 ft, °F	6000	310.9	5.6	1.8	320.4	91.6	228.8
Sensor 4 at 9.7 ft, °F	6000	291.7	3.9	1.3	301.6	267.8	33.8
Sensor 3 at 10.8 ft, °F	6000	291.7	3.9	1.3	301.6	267.8	33.8
Sensor 2 at 11.8 ft, °F	6000	320.1	5.5	1.7	329.7	91.2	238.5
Sensor 1 at 12.9 ft, °F	6000	298.5	5.8	1.9	311.7	155.1	156.6

Summaries for the first and final 500-ft sublots are shown in Tables 4.8 and 4.9, respectively. Detailed summary tables for the 10 sublots are found Appendix A. Similar to the previous projects, variability was higher in the first test section subplot when compared to the final subplot. This implies that there should be an initial allowable distance for establishing contractor process control, then closer monitoring of thermal readings to make necessary corrections during the paving operation. A similar finding with Projects 1 and 3 was higher variability measured at the edge of the sensor bar, with the largest standard deviation found at the centerline joint.

Table 4.8 Infrared Temperature Basic Statistics for Project 3 Sublot 1

Offset Location	N	Mean	Std. Dev.	Coeff. Var.	Maximum	Minimum	Range
Sensor 12 at 1.0 ft, °F	500	279.8	18.3	6.5	288.5	83.8	204.7
Sensor 11 at 2.1 ft, °F	500	293.6	2.2	0.8	298.2	288.5	9.7
Sensor 10 at 3.2 ft, °F	500	289.3	2.6	0.9	294.3	284.4	9.9
Sensor 9 at 4.3 ft, °F	500	285.8	2.7	0.9	290.1	278.1	12.0
Sensor 8 at 5.3 ft, °F	500	291.0	2.1	0.7	295.0	284.2	10.8
Sensor 7 at 6.4 ft, °F	500	296.7	1.8	0.6	300.7	292.8	7.9
Sensor 6 at 7.5 ft, °F	500	320.9	2.8	0.9	325.8	313.0	12.8
Sensor 5 at 8.6 ft, °F	500	308.8	3.5	1.1	314.4	299.3	15.1
Sensor 4 at 9.7 ft, °F	500	289.5	3.4	1.2	294.8	280.2	14.6
Sensor 3 at 10.8 ft, °F	500	289.5	3.4	1.2	294.8	280.2	14.6
Sensor 2 at 11.8 ft, °F	500	315.0	13.9	4.4	322.7	91.2	231.5
Sensor 1 at 12.9 ft, °F	500	292.3	6.8	2.3	298.6	155.1	143.5

Table 4.9 Infrared Temperature Basic Statistics for Project 3 Sublot 12

Offset Location	N	Mean	Std. Dev.	Coeff. Var.	Maximum	Minimum	Range
Sensor 12 at 1.0 ft, °F	500	290.5	3.7	1.3	299.1	276.6	22.5
Sensor 11 at 2.1 ft, °F	500	301.3	3.9	1.3	309.2	289.2	20.0
Sensor 10 at 3.2 ft, °F	500	299.2	4.6	1.5	307.9	286.2	21.7
Sensor 9 at 4.3 ft, °F	500	291.9	4.7	1.6	300.0	268.3	31.7
Sensor 8 at 5.3 ft, °F	500	300.9	4.0	1.3	310.1	287.6	22.5
Sensor 7 at 6.4 ft, °F	500	302.0	3.0	1.0	309.2	291.7	17.5
Sensor 6 at 7.5 ft, °F	500	331.2	4.5	1.4	341.6	320.4	21.2
Sensor 5 at 8.6 ft, °F	500	312.9	3.7	1.2	319.6	295.2	24.4
Sensor 4 at 9.7 ft, °F	500	294.2	4.1	1.4	300.9	276.3	24.6
Sensor 3 at 10.8 ft, °F	500	294.2	4.1	1.4	300.9	276.3	24.6
Sensor 2 at 11.8 ft, °F	500	323.1	3.4	1.0	329.5	308.7	20.8
Sensor 1 at 12.9 ft, °F	500	304.3	3.9	1.3	311.7	292.3	19.4

4.3 Ground Penetrating Radar

4.3.1 Project 1, USH 2

Research test section length on Project 1 was 5,000 ft with 10 equal-length 500-ft sublots. Table 4.10 summarizes basic statistics for thickness and density the entire test section length. A total of 5,000 GPR readings were collected at an interval of 1 ft; however, there was a processing error for GPR thickness and density data from 1,500 to 2,000 feet from the start of the test section, creating a sample size less than 5,000. A final GPR trace at 12-ft offset was not possible due to darkness.

Table 4.10 GPR Basic Statistics for Project 1

Offset Location	N	Mean	Std. Dev.	Coeff. Var.	Maximum	Minimum	Range
Thickness at 0.5 ft, in.	4600	1.9	0.2	8.9	2.4	1.5	0.9
Thickness at 2.5 ft, in.	5000	1.8	0.1	4.0	2.0	1.7	0.4
Thickness at 6.0 ft, in.	5000	1.8	0.1	3.3	2.0	1.6	0.4
Thickness at 9.5 ft, in.	5000	1.6	0.1	3.9	1.9	1.5	0.4
Density at 2.5 ft, %	4500	93.8	1.4	1.5	97.4	90	7.4
Density at 6.0 ft, %	4500	94.7	1.1	1.2	97.1	92	5.2

Thickness variability and coefficient of variation close to the centerline joint (0.5 ft offset) was greater than the other offsets at 2.5 ft, 6 ft, and 9.5ft. Density at an offset of 2.5 ft averaged 93.8%, while a 6-ft offset towards the middle of the lane averaged 94.7%. Variability closer to the centerline joint was also much higher.

Tables 4.11 and 4.12 report statistics from the first and final sublots, respectively. Statistics for all sublots are reported in Appendix B. Average thickness and variability was very similar among the first and last sublots. Density by offset was similar at the start of paving, but much higher towards the middle of the mat a mile into paving. GPR density subplot statistics in Appendix B disclosed a consistent finding with higher density at a 6-ft offset compared to a 2.5-ft offset.

Table 4.11 GPR Basic Statistics for Project 1 Sublot 1

Offset Location	N	Mean	Std. Dev.	Coeff. Var.	Maximum	Minimum	Range
Thickness at 0.5 ft, in.	500	2.0	0.1	4.3	2.3	1.9	0.3
Thickness at 2.5 ft, in.	500	1.8	0.1	6.4	2.0	1.7	0.3
Thickness at 6.0 ft, in.	500	1.7	0.0	2.3	1.8	1.7	0.2
Thickness at 9.5 ft, in.	500	1.6	0.0	2.5	1.7	1.5	0.2
Density at 2.5 ft, %	500	95.4	1.0	1.1	97.4	93	4.4
Density at 6.0 ft, %	500	95.5	0.5	0.5	96.3	94.6	1.7

Table 4.12 GPR Basic Statistics for Project 1 Sublot 10

Offset Location	N	Mean	Std. Dev.	Coeff. Var.	Maximum	Minimum	Range
Thickness at 0.5 ft, in.	500	1.9	0.1	5.1	2.1	1.6	0.5
Thickness at 2.5 ft, in.	500	1.8	0.0	1.9	1.8	1.7	0.1
Thickness at 6.0 ft, in.	500	1.7	0.0	2.5	1.8	1.7	0.2
Thickness at 9.5 ft, in.	500	1.6	0.0	2.5	1.6	1.5	0.2
Density at 2.5 ft, %	500	93.9	0.2	0.2	94.4	93.7	0.8
Density at 6.0 ft, %	500	96.2	0.6	0.6	97.1	94.6	2.5

4.3.2 Project 2, STH 75

Research test section length on the second project was also 5,000 ft having ten 500-ft sublots. A total of 5,000 GPR readings were collected at an interval of 1 ft with data processing errors for density at 0.5, 2.5, and 6.0 ft. Table 4.13 reports statistics for the entire 5,000-ft test section length. Thickness mean and variability were fairly consistent across the mat; however, thickness offsets of 2.5 ft and 6 ft had higher coefficients of variation. Density statistics were fairly consistent at offsets of 9.5 ft and 11.5 ft.

Table 4.13 GPR Basic Statistics for Project 2

Offset Location	N	Mean	Std. Dev.	Coeff. Var.	Maximum	Minimum	Range
Thickness at 0.5 ft, in.	5000	2.6	0.1	4.8	2.8	2.3	0.4
Thickness at 2.5 ft, in.	5000	2.4	0.2	9.1	2.8	2.0	0.8
Thickness at 6.0 ft, in.	5000	2.6	0.2	6.3	2.8	2.0	0.7
Thickness at 9.5 ft, in.	5000	2.7	0.1	2.6	2.8	2.3	0.4
Thickness at 11.5 ft, in.	5000	2.7	0.1	2.0	2.8	2.5	0.3
Density at 9.5 ft, %	5000	94.0	0.9	1.0	96.1	91.7	4.4
Density at 11.5 ft, %	5000	94.2	1.0	1.1	96.6	92.3	4.3

Tables 4.14 and 4.15 summarize statistics from the first and last sublots, respectively. Appendix B reports statistics for all 10 sublots. A comparison of thicknesses among sublots measured a thicker mat closer to the edges. Density was similar at 9.5-ft and 11.5-ft offsets at the start of paving, and higher at a 9.5-ft offset a mile into paving.

Table 4.14 GPR Basic Statistics for Project 2 Sublot 1

Offset Location	N	Mean	Std. Dev.	Coeff. Var.	Maximum	Minimum	Range
Thickness at 0.5 ft, in.	500	2.6	0.1	3.8	2.8	2.3	0.4
Thickness at 2.5 ft, in.	500	2.4	0.2	9.8	2.7	2.0	0.7
Thickness at 6.0 ft, in.	500	2.5	0.2	7.4	2.7	2.0	0.7
Thickness at 9.5 ft, in.	500	2.7	0.1	2.6	2.8	2.5	0.2
Thickness at 11.5 ft, in.	500	2.7	0.1	2.2	2.8	2.6	0.2
Density at 9.5 ft, %	500	94.9	0.1	0.1	95.1	94.6	0.5
Density at 11.5 ft, %	500	95.1	0.4	0.4	95.8	94.6	1.2

Table 4.15 GPR Basic Statistics for Project 2 Sublot 10

Offset Location	N	Mean	Std. Dev.	Coeff. Var.	Maximum	Minimum	Range
Thickness at 0.5 ft, in.	500	2.6	0.1	4.6	2.8	2.3	0.4
Thickness at 2.5 ft, in.	500	2.3	0.1	6.0	2.6	2.0	0.5
Thickness at 6.0 ft, in.	500	2.6	0.1	4.2	2.7	2.4	0.3
Thickness at 9.5 ft, in.	500	2.7	0.0	1.0	2.8	2.6	0.1
Thickness at 11.5 ft, in.	500	2.7	0.0	1.4	2.8	2.6	0.1
Density at 9.5 ft, %	500	93.4	0.3	0.3	93.9	93.0	0.9
Density at 11.5 ft, %	500	92.8	0.3	0.4	93.4	92.3	1.1

4.3.3 Project 3, STH 42

Test section length on the third project was 6,000 ft producing 6,000 readings for each GPR offset. Table 4.16 reports statistics for the 6,000-ft test section length. Thickness mean and variability were consistent across the mat, while the 9.5-ft and 11-ft offsets had a higher coefficient of variation. A consistent thickness would be expected with final surface layer paving. A high 1-in thickness range could be explained by measurement error at Sublots 3 and 7 (see Appendix B for statistics). Density statistics were fairly consistent at the offsets of 6 ft, 9.5 ft and 11.5 ft. However, the density values were about 90-91%, while nuclear density readings averaged 92-93%. GPR readings were calibrated to the nuclear density gauge at 5 test sites; however, there could have been an offset error.

Table 4.16 GPR Basic Statistics for Project 3

Offset Location	N	Mean	Std. Dev.	Coeff. Var.	Maximum	Minimum	Range
Thickness at 2.5 ft, in.	6000	1.5	0.1	8.1	2.0	1.3	0.7
Thickness at 6.0 ft, in.	6000	1.6	0.2	11.0	2.4	1.3	1.1
Thickness at 9.5 ft, in.	6000	1.6	0.2	14.0	2.5	1.3	1.2
Thickness at 11.5 ft, in.	6000	1.6	0.2	12.9	2.4	1.3	1.1
Density at 6.0 ft, %	6000	90.1	0.5	0.6	91.1	88.8	2.3
Density at 9.5 ft, %	6000	90.3	0.6	0.6	91.6	88.9	2.7
Density at 11.5 ft, %	6000	90.6	0.5	0.5	91.4	89.4	2.0

Tables 4.17 and 4.18 summarize basic statistics from the first and last sublots, respectively. Statistics for all 12 sublots are reported in Appendix B. Overall, statistics between the first and last test sublots were very similar. Final surface paving likely reduced variability from that on the first and second projects which were paved on a milled asphaltic surface and pulverized surface, respectively.

Table 4.17 GPR Basic Statistics for Project 3 Sublot 1

Offset Location	N	Mean	Std. Dev.	Coeff. Var.	Maximum	Minimum	Range
Thickness at 2.5 ft, in.	500	1.5	0.1	5.8	1.6	1.4	0.3
Thickness at 6.0 ft, in.	500	1.6	0.1	5.8	1.8	1.4	0.4
Thickness at 9.5 ft, in.	500	1.6	0.1	6.0	1.7	1.4	0.3
Thickness at 11.5 ft, in.	500	1.6	0.1	5.3	1.7	1.4	0.3
Density at 6.0 ft, %	500	90.1	0.1	0.1	90.3	90.0	0.3
Density at 9.5 ft, %	500	90.6	0.4	0.5	91.2	90.0	1.2
Density at 11.5 ft, %	500	90.9	0.2	0.3	91.4	90.6	0.8

Table 4.18 GPR Basic Statistics for Project 3 Sublot 12

Offset Location	N	Mean	Std. Dev.	Coeff. Var.	Maximum	Minimum	Range
Thickness at 2.5 ft, in.	500	1.5	0.1	3.8	1.6	1.4	0.2
Thickness at 6.0 ft, in.	500	1.5	0.1	4.0	1.7	1.4	0.2
Thickness at 9.5 ft, in.	500	1.5	0.1	3.9	1.6	1.4	0.2
Thickness at 11.5 ft, in.	500	1.5	0.1	4.0	1.6	1.4	0.2
Density at 6.0 ft, %	500	90.6	0.1	0.1	90.8	90.4	0.4
Density at 9.5 ft, %	500	90.0	0.4	0.5	90.5	89.2	1.3
Density at 11.5 ft, %	500	90.5	0.3	0.3	91.0	90.0	1.0

4.4 Portable Seismic Pavement Analyzer

Seismic modulus measurements were recorded within sublots of 500-ft length, with a sample of 5 per subplot. A stratified random sampling approach was employed having one test site within each of the 5 offsets. The reason for stratification was twofold: (1) the IR and GPR readings use a stratification approach by sampling by offset, and (2) offset location allowed an investigation into areas of the mat with different properties (thermal, thickness, density, and modulus). The designated five transverse locations included:

- Left Joint in direction of vehicle travel (i.e., centerline);
- Left Wheel Path;
- Between Wheel Paths;
- Right Wheel Path; and
- Right Joint.

4.4.1 Project 1, USH 2

Table 4.19 presents the basic statistical information of this project. The average modulus constructed in the pavement was 1,462 ksi, with a relatively high standard deviation of 382 ksi. This modulus is based upon an average surface temperature test of 108°F, and nuclear density of 92.6%. The coefficient of variation (COV) for the measured nuclear density was lowest compared to modulus and temperature. The range of the density is relatively wide due to the presence of one test point with a measured density of 81.5%; however, the average was above the standard minimum of 91.5% on a milled surface. As highlighted earlier, the range is very sensitive to a single outlier reading, while the standard deviation is more robust to single data points. But overall, the recorded density values for this project demonstrate consistency. In addition, the standard deviation of 2.21%, indicating that over 84% of the tested locations will be above 92% density assuming a normally-distributed data set.

Table 4.19 Statistical Summary of Modulus and Nuclear Density for Project 1

Measure	N	Mean	Standard Deviation	Coeff. Of Var., %	Minimum	Maximum	Range
Offset	50	6.7	4.38	65.6%	1	12	11
Average Modulus, ksi	50	1426	382	26.8%	452	2123	1672
Warm Temp., °F	50	108.4	4.24	3.9%	100	117	17
Nuclear Density, %	50	92.6	2.21	2.4%	81.5	95.5	14

Further examining the seismic modulus statistics, the COV is more than 10 times that of the density. This higher variability in the measured modulus values could be due to variability within the device, or due to other material and construction related issues. The report will investigate the possibility of correlating this wide range of variability to different possible factors in Chapter 6.

The distribution of all data points tested for the first project are plotted in Figure 4.1. As shown, the data points are randomized longitudinally by station and offset.

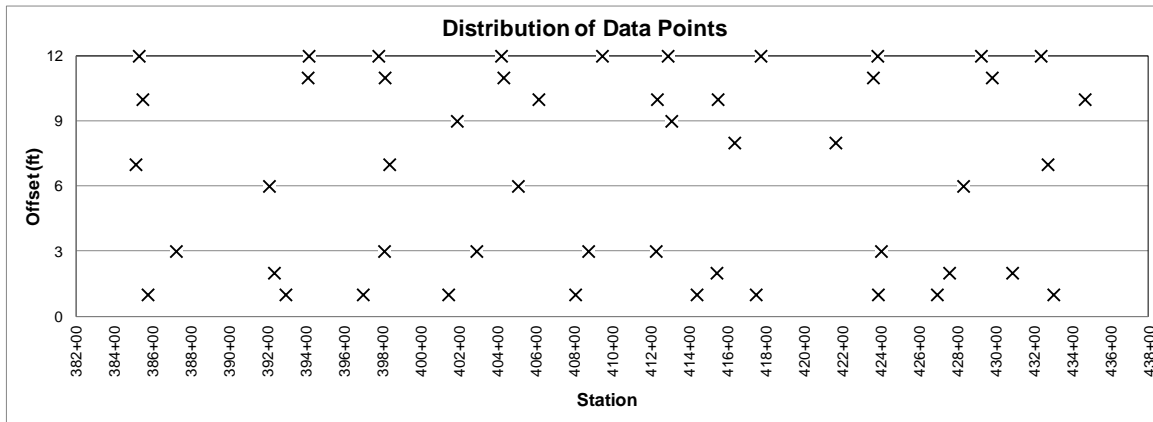


Figure 4.1 Distribution of Test Points for Project 1

Temperature-related PSPA testing occurred after the finish roller was completed (warm mat) and after the pavement cooled below 100°F (cool mat). The cold test points were sampled several hours later at the same location and limited to a sample of 10 data points due to darkness and traffic control. This data comparison of the modulus readings at warm and cold mat temperatures permitted insight into the dependency of the PSPA readings on the pavement temperature.

Figure 4.2 distributes the temperatures for all the tested data points. Paving was downstation from 435+00 to 385+00 (right to left in Figure 4.2). Modulus readings were at higher mat temperatures early into paving to begin collecting the data and moving with traffic control. A downward temperature trend occurred after 412+00 with testing later in the day. It is clear that the warm mat did not show dependency on the location of the test point as demonstrated by the continuous trend of the testing temperatures. The testing at each data point was conducted such that five test trials are taken, the maximum and minimum recorded values are eliminated, and the remaining three values are averaged with coefficient of variation (COV) calculated and recorded.

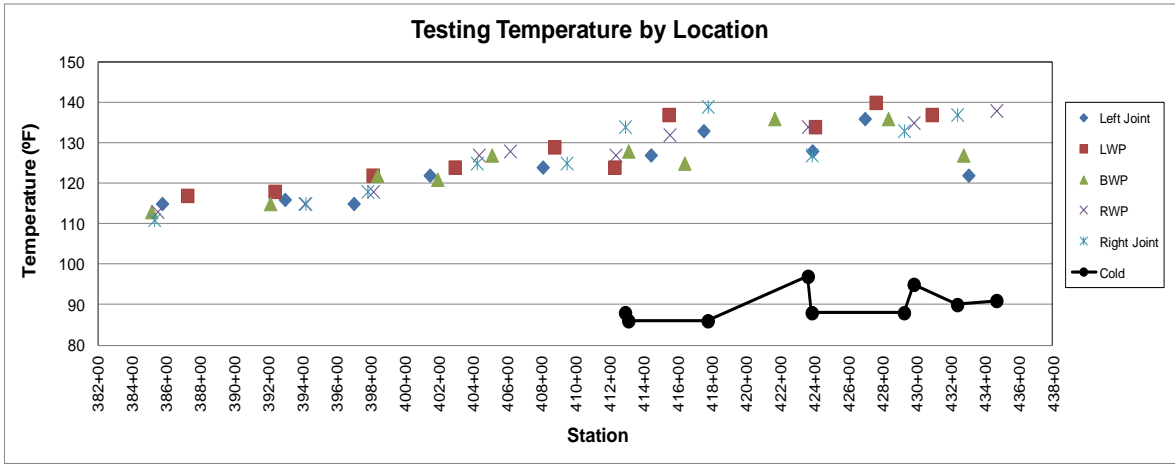


Figure 4.2 Modulus of the Testing Temperature by Station/Offset for Project 1

Figure 4.3 shows the average modulus values recorded for every test point by offset. Again, the testing location did not cause apparent shifts in modulus since the scatter appeared random in nature. It is evident that the modulus at lower temperatures is undistinguishable from the range of warm modulus values.

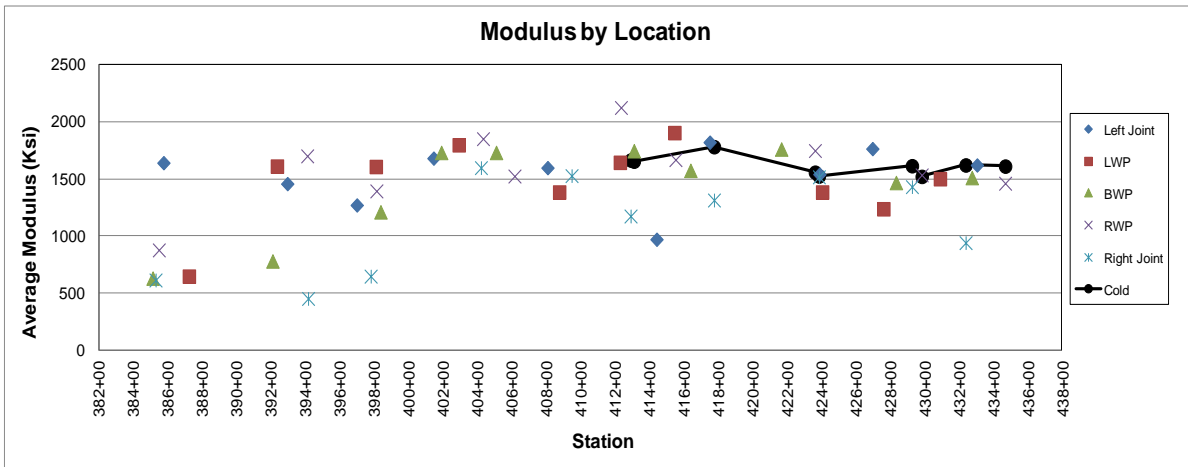


Figure 4.3 Average Recorded Modulus by Station/Offset for Project 1

A Texas DOT study by Nazarian et al. (2005) has reported a trend among field mixes where the seismic modulus followed a trend where the modulus increases as the pavement temperature decreases. It is important to note that this study was not conducted on fresh pavements but on existing and aged pavements. Figure 4.4 shows the results with PSPA modulus collected in the Texas DOT study where a clear negative correlation exists, with higher temperatures lowering the seismic modulus. Modulus results collected for the three projects will be analyzed in more detail in Chapter 6 with a comparison among devices at the same test site.

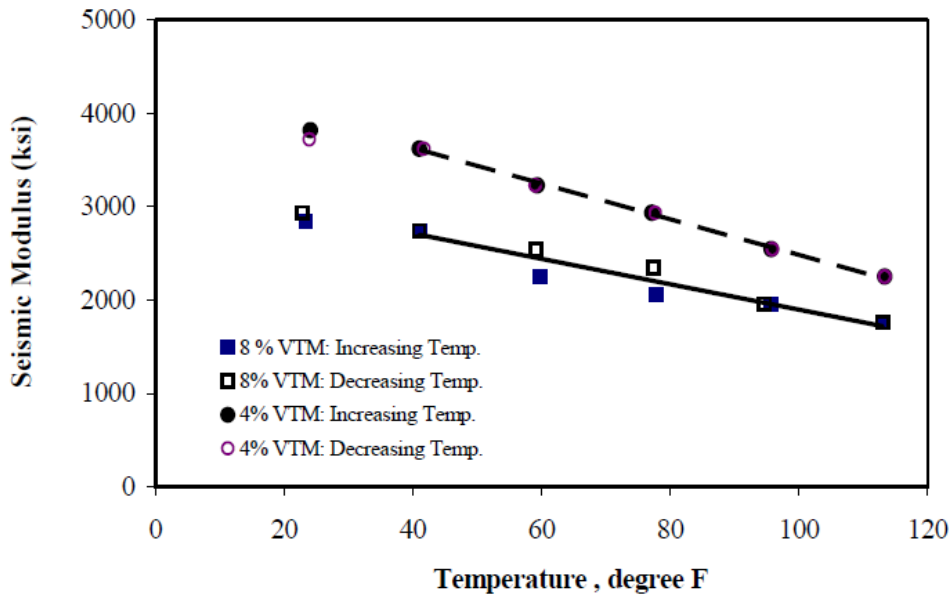


Figure 4.4 Relationship of Pavement Seismic Modulus with Temperature (Adapted from Nazarian et al. 2005)

The modulus values measured by the PSPA at warm and cold temperatures were compared to detect any differences. Measured modulus values were not acquired at a controlled temperature, but rather random values under field conditions, such as between 120°F and 140°F, while the cold testing was conducted with pavement temperatures below 100°F. Although the pavement modulus is expected to vary with temperature and unrealistic to control, the strategy behind this approach was confining the testing temperatures to a typical field range to evaluate the sensitivity to temperatures immediately after final compaction, and several hours after final compaction.

Figure 4.5 quantifies the modulus decrease per unit increase in temperature. This figure shows moderate trend in measured modulus as the temperature varies indicating that the modulus drops by about 51.5 ksi for every 1°F increase. This is a logical trend given the viscoelastic nature of asphalt mixtures. The consistency of this trend as the other projects are presented will provide the needed basis for developing modulus-temperature dependency models to ultimately assign future construction quality control and acceptance values.

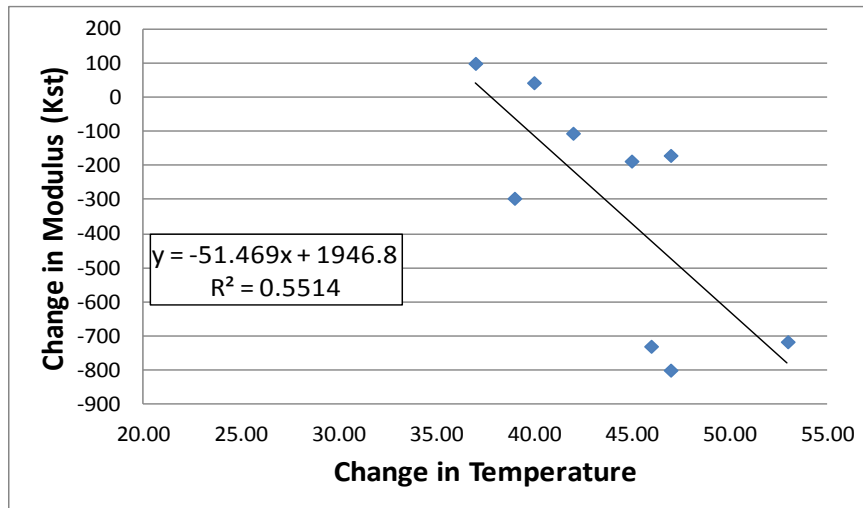


Figure 4.5 Change in Modulus as the Testing Temperature Varies for Project 1

The testing locations for the PSPA were used to measure the pavement final density. Figure 4.6 shows the distribution of the measured density values by station and transverse location. Standard WisDOT procedures were followed with a 4-minute nuclear test duration per test site.

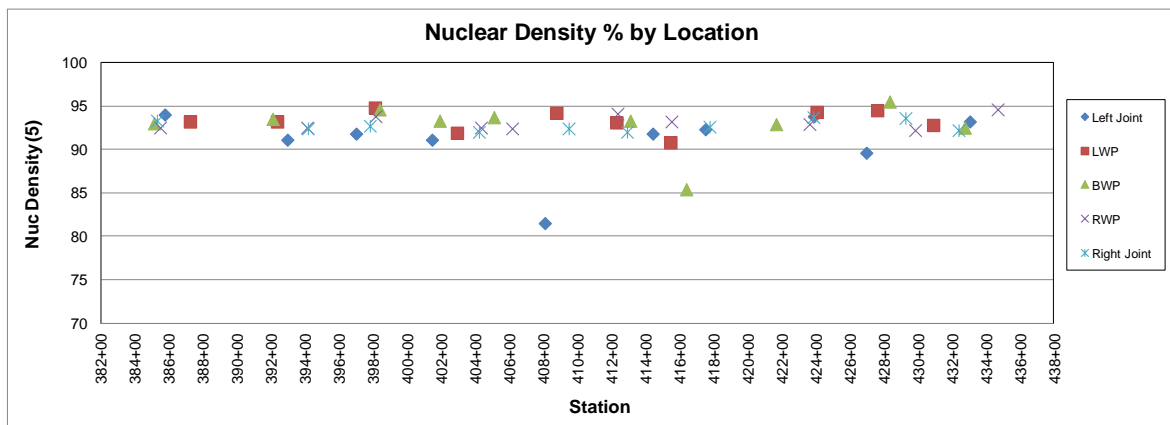


Figure 4.6 Nuclear Density Measurements by Station/Offset for Project 1

The recorded density values show a consistency in the measured density except for few locations, where the average density values converged around 92%. This is understandable, since the construction process is design to target this density. Therefore, it does not allow for variability in the recorded values and eliminates the independence of the density measures to be included in statistical analysis. On the other hand, since the density defines an acceptable product based on the current state of practice, it will be used to investigate the nonconforming locations. This investigation is detailed in Chapter 6.

4.4.2 Project 2, STH 75

Table 4.20 is the summary statistics for seismic modulus and nuclear density readings across the 5,000-ft test length. The basic statistical information for this pavement section shows that the coefficient of variation continues to be lower than the modulus and surface test temperature. It is important to note this project had the greatest variability in terms of the average modulus values, with an average modulus of 1,272 ksi and standard deviation of 585 ksi. This relatively high level of variability is supported by a coefficient of variation of 64%. Average density was 92.6%, exceeding the specified minimum average of 90.5% on pulverized base.

Table 4.20 Statistical Summary for PSPA and Nuclear Density on Project 2

	N	Mean	Standard Deviation	COV	Range	Minimum	Maximum
Offset, ft	50	6.54	4.21	10%	11	1	12
Average Modulus, ksi	50	1272	585	64%	1807	420	2227
Warm Temp., °F	50	123.6	12.9	46%	40	103	143
Density, %	50	92.6	1.66	1.79%	6.9	88.0	94.9

The testing for the second project followed the same stratified randomization procedure, with results plotted in Figure 4.7.

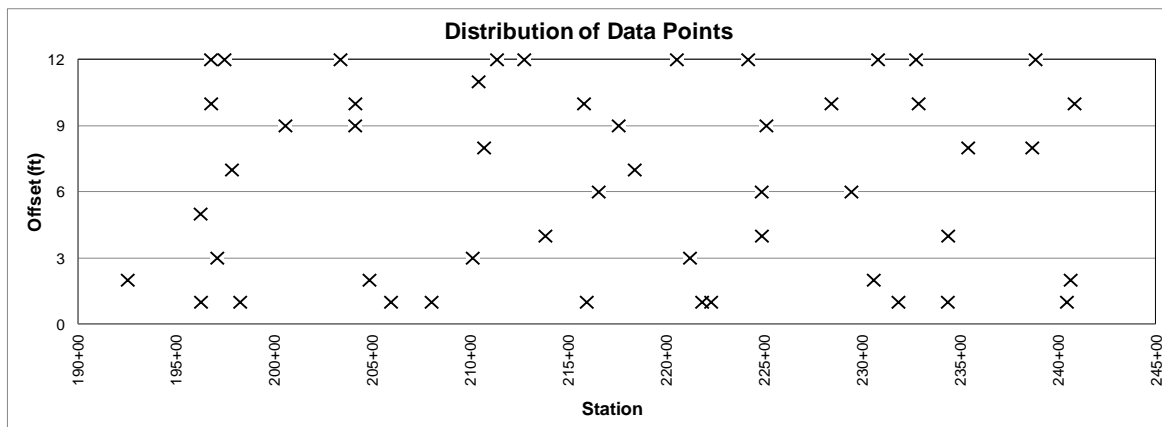


Figure 4.7 Distribution of Test Points for Project 2

Figures 4.8 and 4.9 show the distribution of the testing temperature and the measured modulus per station and transverse location. Paving was downstation from 245+00 to 190+00, with a similar trend from the first project where testing began at higher temperature at the start of paving and lower at the end of paving.

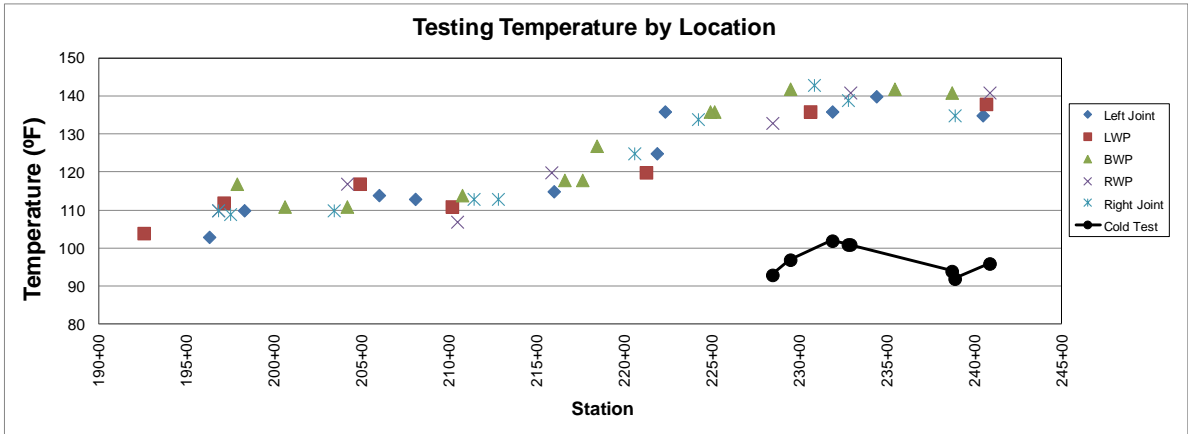


Figure 4.8 Testing Temperature by Station/Offset for Project 2

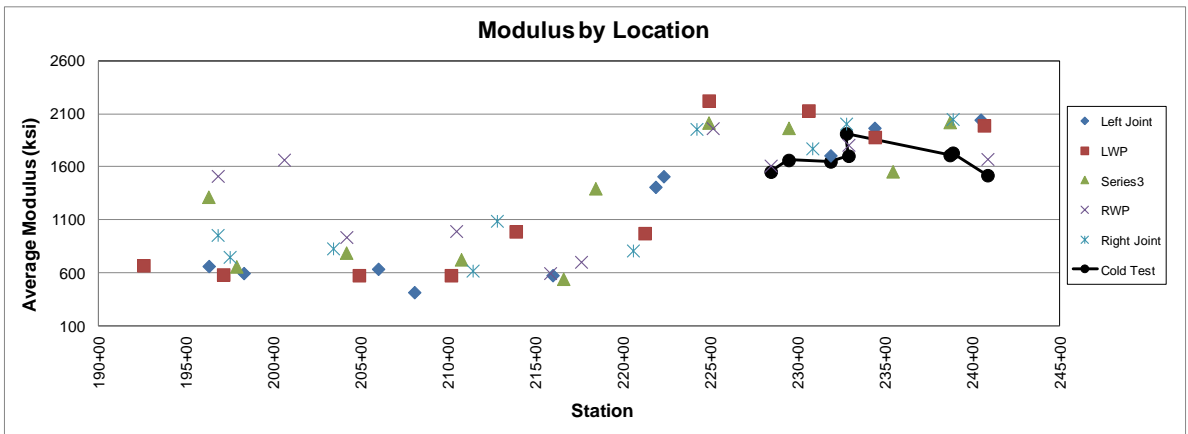


Figure 4.9 Average Recorded Modulus Values by Location for Project 2

The distribution of the data points show no dependence on the transverse location. On the other hand, average modulus values show a transition at Station 225+00 and beyond. Near this location, the plant mixing temperature was lowered about 10°F.

The relationship between the change in temperature and change in modulus is illustrated in Figure 4.10. This relationship shows the least drop in modulus with the increase of unit temperature compared with the first project. It also shows that the modulus drops by only 20 ksi for every 1°F increase.

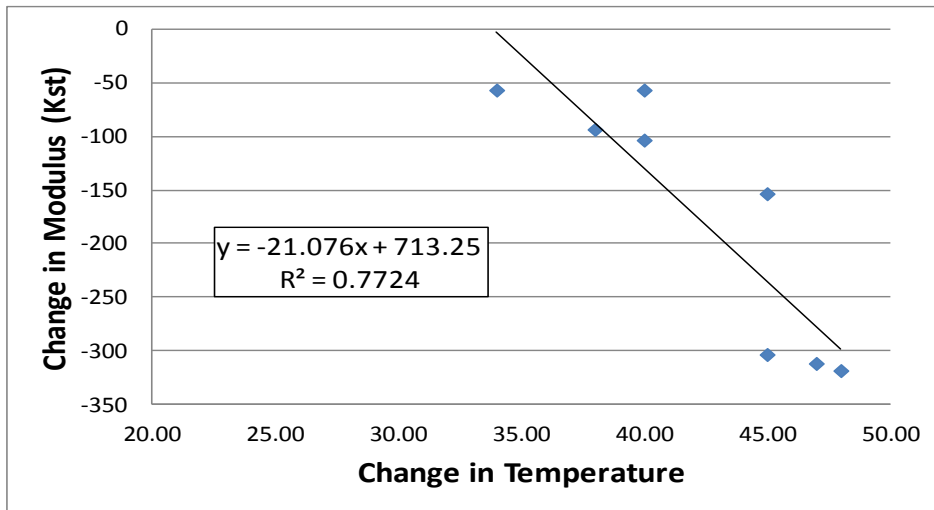


Figure 4.10 Change in Modulus as Testing Temperature Varies for Project 2

The distribution of the modulus values show that the left joint locations are less dense compared to the other testing locations. In fact, 80% of the left joint (outside joint) test points are below 92% density.

Figure 4.11 is the nuclear density reading plots by station and offset on Project 2. As mentioned earlier, the nuclear density measurements will be used in Chapter 6 to further investigate locations where the density requirements were not met, providing a basis to assess the potential benefit of the non-destructive technologies as quality control indicators. Testing in different transverse locations for nuclear density values, seem to reveal a trend of less densification at the centerline joint of the pavement.

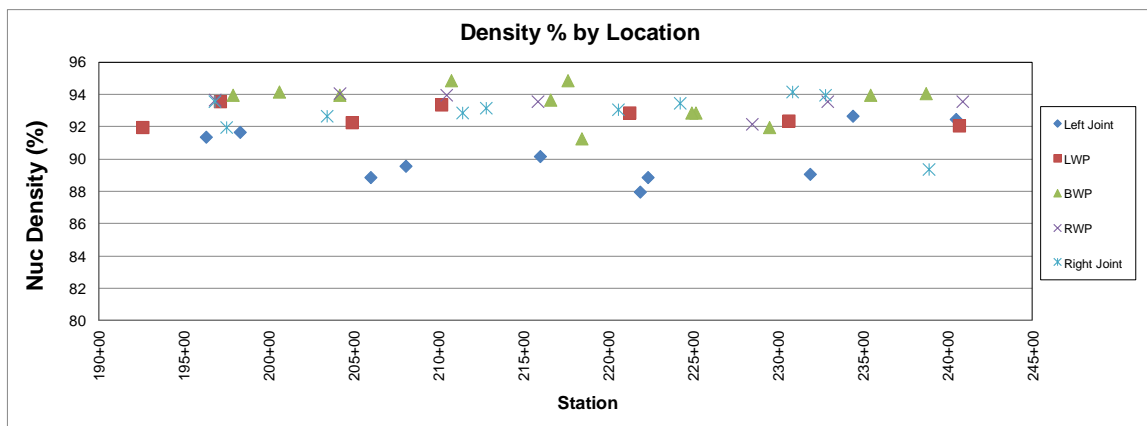


Figure 4.11 Nuclear Density by Station/Offset for Project 2

4.4.3 Project 3, STH 42

The basic statistical information of the seismic modulus, mat test temperature, and nuclear density for Project 3 is summarized in Table 4.21. The average pavement modulus as 1,276 ksi with a relatively high standard deviation of 405 ksi (similar to the previous project). This modulus is with average density shows an acceptable value of 92.4%, exceeding the 91.5% minimum. As with the previous projects, the nuclear density readings had a lower coefficient of variation than modulus and mat testing temperature.

Table 4.21 Statistical Summary of Testing Section for Project 3

Measure	N	Mean	Standard Deviation	COV	Range	Minimum	Maximum
Offset, ft	60	6.6	4.31	65.2%	11	1	12
Average Modulus, ksi	60	1276	405	31.7%	1333	527	1860
Warm Temp., °F	60	124.1	12.34	9.9%	44	97	141
Nuclear Density, %	60	92.34	1.40	1.5%	5.4	89.5	94.9

Similar to first projects, the assigned testing locations within the 6,000-ft test section length were randomized as shown in Figure 4.12.

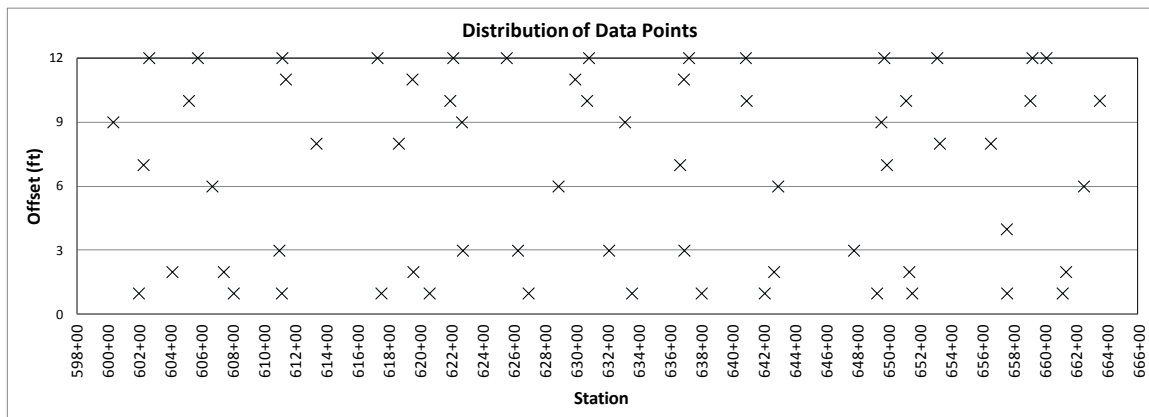


Figure 4.12 Distribution of Test Points for Project 3

A subset of the test section was tested at cooler temperatures. The distribution of the testing temperatures (warm and cold) is shown in Figure 4.13. The results show no trend in terms of transverse location. However, with respect to stations, the testing temperatures drop at higher station locations. This is due the fact that the research team arrived to these stations after a longer time gap.

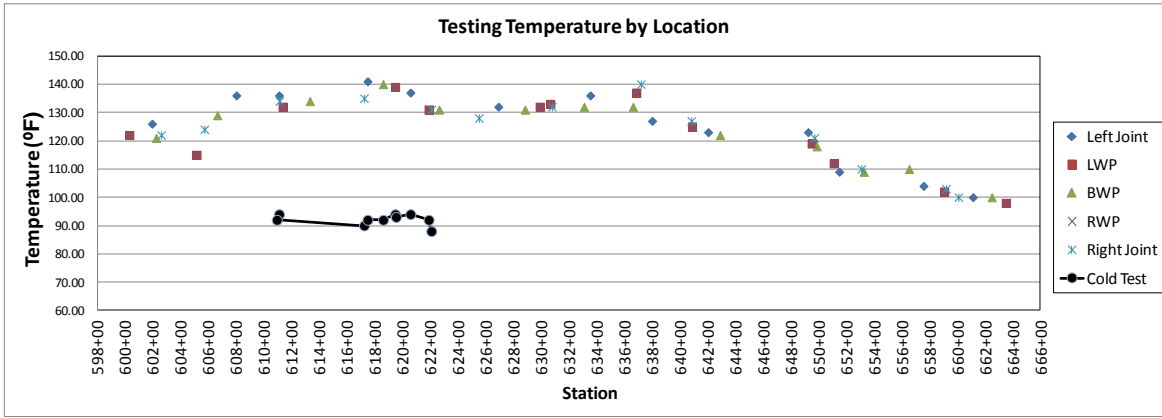


Figure 4.13 Distribution of the Testing Temperature by Station/Offset for Project 3

While the testing temperature shows minimal variability in the transverse location, the modulus values show a wider scatter of values for both warm and cold tests as shown in Figure 4.14.

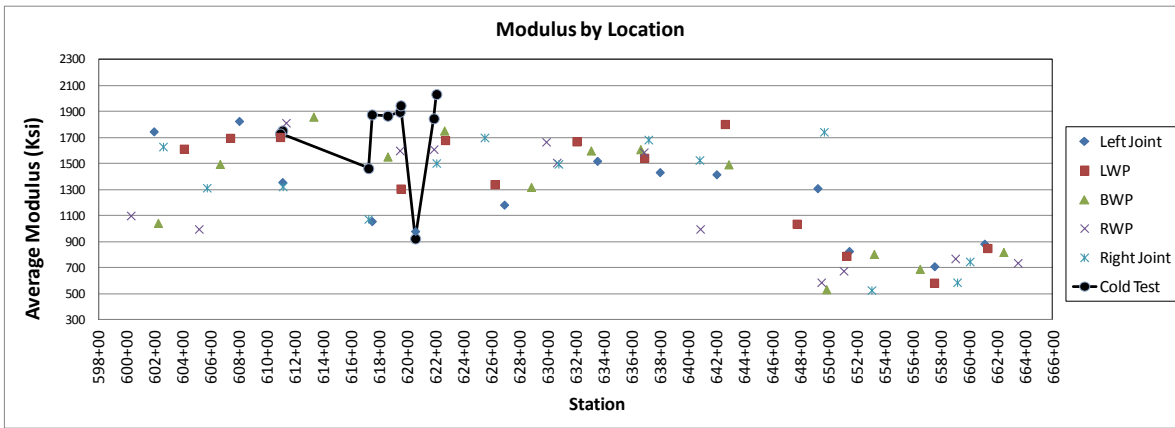


Figure 4.14 Average Modulus Values by Station/Offset for Project 3

Since the testing was not conducted at controlled temperature, the change in modulus per unit temperature serves to evaluate the temperature dependency of the modulus values. Figure 4.15 shows the correlation of the change in modulus against the change in testing temperature.

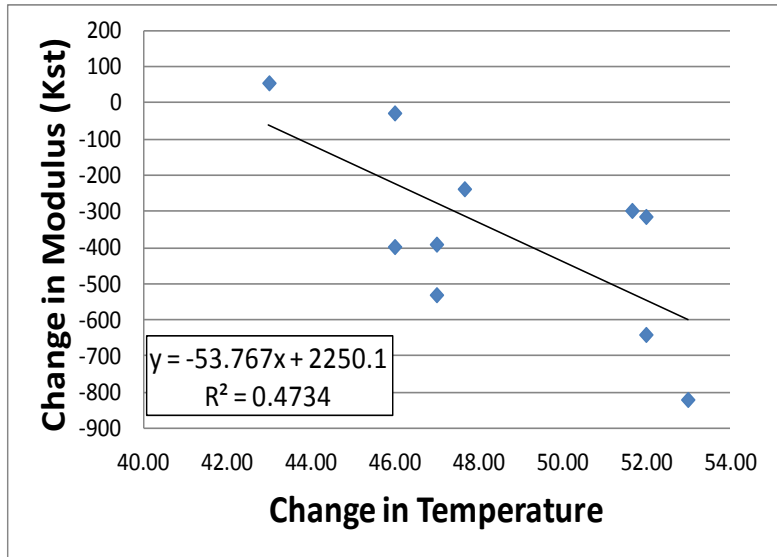


Figure 4.15 Change in Modulus as Testing Temperature Range Varies for Project 3

The trend shown in Figure 4.15 indicates that the modulus drops by about 54 ksi per 1°F. This trend also follows fundamental material behavior. It is important to note that the slope of the correlation is similar to that observed from the first project.

The recorded density values for this project are shown in Figure 4.16, and show more scatter in the transverse direction. Most of the measured values near the left joint are the least within each subplot.

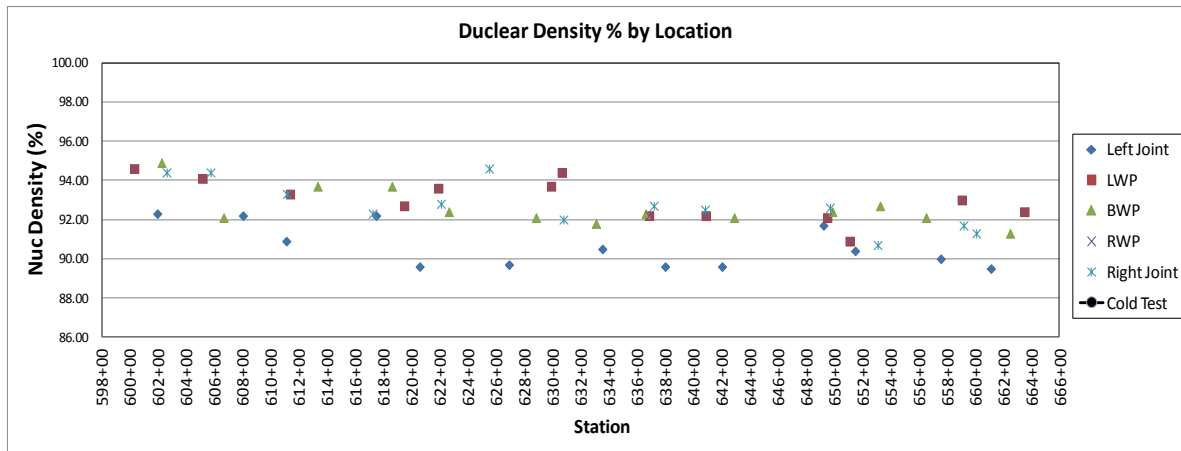


Figure 4.16 Nuclear Density by Station/Offset for Project 3

4.5 Temperature Adjustment

The information presented in Section 4.4 clearly shows the dependency of the measured modulus on the temperature of the mat. Therefore, the modulus versus temperature relationships provided above for each project is used to normalize the

measured modulus values at all locations for the three projects at 130°F. Table 4.22 lists the variability of the measured modulus values.

Table 4.22 Adjusted Modulus Values and Variability at 130°F

Project	N	Seismic Modulus @130°F			Nuclear Density		
		Average, ksi	Std. Dev., ksi	COV, %	Average, %	Std. Dev., %	COV, %
Project 1	50	3616.2	640.6	17.7	92.6	2.2	2.4
Project 2	50	3014.1	428.3	14.2	92.6	1.3	1.5
Project 3	50	2530.2	818.8	32.4	92.6	1.7	1.8

Normalizing the modulus values reduced the variability of the modulus values significantly compared to the values reported in Section 4.4. This is because the variability due to temperature is omitted. However, the variability of the PSPA is still much higher than that of the nuclear density. This can be attributed to the fact that the compaction operation is controlled by the pavement density. The construction crew is typically targeting a density measure of 92%, therefore, the end product is expected to have a narrow range in density. On the other hand, PSPA measurements are not used as quality control process during the construction. This also affected by the testing method and variation in testing temperatures. In addition, variability within the mix will result in a variation in the modulus even if the density remains constant. The results show that Projects 1 and 2 yield coefficients of variation (COV) values of less than 20% while Project 3 shows a COV of 32.4%. The range of variability for the first two projects is reasonable given the variability in the testing process, especially since the results show logical dependency on the rheological properties of the HMA as shown in Section 4.4. Yet the results indicate the need for fine-tuning the process.

One proposed approach to minimizing the variability is discovered after all testing is conducted in a verbal discussion with the manufacturer. The research team conducted five spot testing per location in a circle of a one foot diameter by moving the device along the diameter of the circle. The manufacturer indicated that this will add more variability in the measurement. The recommended procedure is to take the measurement at the same spot five times without moving the device. However, this recommendation was not mentioned earlier to the research team nor included in the user manual. According to the manufacturer, the observed variability would reduce significantly compared to the recorded values.

4.6 Summary

This chapter presented data summaries from the three projects for IR continuous temperature, GPR density and thickness, PSPA seismic modulus, and nuclear density. Fundamental project statistics for each NDT device by entire project research section length and by individual 500-ft subplot lengths were reported. The following sections are specific findings relative to each device.

4.6.1 Continuous Thermal Readings

Table 4.23 provides a summary of the continuous thermal readings on the three projects. There were mixed findings due to project-specific factors, such as plant mixing temperature, delivered truck temperature, paver operation, and Pave-IR device calibration. One consistent finding among projects was higher temperature variability along the centerline side of the mat.

An important consideration in interpreting the data is use of the standard deviation or range. The standard deviation allows all readings equal weight in determining variability, while the range is substantially influenced by a single maximum or minimum value.

Table 4.23 Summary of Continuous Thermal Readings

Project	Thermal Findings
1	<ul style="list-style-type: none"> • Average sensor temperature was between 240 and 260°F. • No trend detected among average readings across the thermal bar. • Highest reading was 304°F while the lowest was 85°F. • Range among the sensors was relatively consistent, with a lower range of 183°F and upper range of 202°F. • Greater variability occurred at the outer sensors. • Higher pavement temperatures were measured towards the left side of the paver (Sensors 2 and 5), while more variability occurred along the right side (Sensors 8-12).
2	<ul style="list-style-type: none"> • Average sensor temperature was between 288 and 303°F. • Higher mean temperatures were recorded by the central sensors and cooler temperatures towards the edges. • Variability was inconsistent across the mat. • More variability and a higher coefficient of variation was detected on centerline side of the paver.
3	<ul style="list-style-type: none"> • Average sensor temperature was between 287 and 327°F. • 3 sensors were out of calibration (Sensors 2, 5, and 6) recording a higher pavement temperature of about 25°F to 40°F than neighboring sensors. • Right side of the paver (Sensor 12) near the tapered longitudinal joint had the highest variability. • Adjoining sensors had similar variability levels.

4.6.2 Continuous GPR Thickness and Density Data

Table 4.24 summarizes of the continuous thermal readings on the three projects. There were mixed findings due to project-specific factors, such as the base layer including a milled surface on the first project, pulverized base on the second project and two lower layers on the third project. One consistent finding was higher thickness variability along the centerline side of the mat.

Table 4.24 Summary of Continuous GPR Thickness and Density Readings

Project	GPR Findings
1	<ul style="list-style-type: none"> • Average thickness was 1.9 in at 0.5 ft, 1.8 in and 2.5 ft and 6.0 ft, and 1.6 in at 9.5 ft. • Thickness variability and coefficient of variation close to the centerline joint 0.5-ft offset ($\sigma = 0.2$ in) was greater than the other offsets at 2.5 ft, 6 ft, and 9.5ft ($\sigma = 0.1$ in). • Density at an offset of 2.5 ft averaged 93.8%, while a 6-ft offset towards the middle of the lane averaged 94.7%. • Density variability closer to the centerline joint was higher ($\sigma = 1.4\%$) than center of the mat ($\sigma = 1.1\%$).
2	<ul style="list-style-type: none"> • Thickness mean was fairly consistent across the mat for a pulverized base, with 2.6 in at 0.5 ft and 6.0 ft, 2.4 in at 2.5 ft, and 2.7 in at 9.5 ft and 11.5 ft. • Thickness variability at offsets of 2.5 ft and 6 ft ($\sigma = 0.2$ in) was higher than the other offsets. • Density statistics were fairly consistent at the only two offsets of 9.5 ft and 11.5 ft, with $\mu=94.0\%$ and $\mu=94.2\%$, and $\sigma = 0.9\%$ and $\sigma = 1.0\%$. No data were available at the centerline joint for comparison.
3	<ul style="list-style-type: none"> • Average thickness was very consistent for this surface layer, with 1.5 in at 2.5 ft, and 1.6 in at offsets of 6.0 ft, 9.5 ft, and 11.5 ft. • Thickness variability was also consistent across the mat, with a lower variability of $\sigma = 0.1$ in at 2.5 ft and $\sigma = 0.2$ in at the other offsets. • GPR density average was fairly consistent with 90.1%, 90.3%, and 90.6% at respective offsets of 6 ft, 9.5 ft and 11.5 ft. • GPR density averages were about 2 percentage points lower than nuclear density readings that averaged 92-93%. GPR readings were calibrated to the nuclear density gauge at 5 test sites; however, there could have been an offset error. • GPR standard deviations for density were 0.5%, 0.6%, and 0.5% at respective offsets of 6 ft, 9.5 ft and 11.5 ft.

4.6.3 Point Measures for Seismic Modulus and Nuclear Density

Seismic modulus measurements and nuclear density readings were recorded within sublots of 500-ft length, with a sample of 5 per subplot. A stratified random sampling approach was employed having one test site within each of the five offsets at two longitudinal joints, both wheel paths, and between wheel paths.

Table 4.25 summarizes the basic statistics for seismic modulus and nuclear density on the three projects. The average modulus constructed on Project 1 was 1,462 ksi, with a relatively high standard deviation of 382 ksi. This modulus is based upon an average surface temperature test of 108°F, and nuclear density of 92.6%. The seismic modulus coefficient of variation (COV) is more than 10 times that of the density. Project 2 had the greatest variability in terms of the average modulus values, with an average modulus of 1,272 ksi, standard deviation of 585 ksi, and COV of 64%. Average density was 92.6% with a standard deviation of 1.66%. and COV of 1.8%. The average pavement modulus on

Project 3 was 1,276 ksi with a relatively high standard deviation of 405 ksi (similar to the previous project) with COV of 32%, while density averaged 92.4%, standard deviation of 1.4%, and COV of 1.5%.

Table 4.25 Statistical Summary of Modulus and Nuclear Density

Project	N	Seismic Modulus			Nuclear Density		
		Average, ksi	Std. Dev., ksi	Coeff. of Var., %	Average, %	Std. Dev., %	Coeff. of Var., %
1	50	1426	382	27	92.6	2.21	2.4
2	50	1272	585	64	92.6	1.66	1.8
3	60	1276	405	32	92.4	1.40	1.5

Modulus was investigated by offset location on the mat, as well as the sensitivity of the field test to pavement temperature (warm at about 120°F, or cool below 100°F). Table 4.26 summarizes the findings presented earlier in this chapter. There was no effect in modulus by offset (centerline, between wheel path, right wheel path, etc.) and a drop in modulus of 20 to 54 ksi for a 1°F increase.

Table 4.26 Seismic Modulus with Location and Mat Temperature

Project	Effect of Offset Location	Viscoelastic Effect of Warm vs. Cold Mat Temperature
1	None	51.5 ksi decrease for 1°F increase
2	None	20 ksi decrease for 1°F increase
3	None	54 ksi decrease for 1°F increase

Chapter 5 Thermal Analysis

5.1 Introduction

The purpose of this chapter is to present a detailed analysis of thermal temperatures during paving with Pave-IR sensor data and FLIR imaging camera data. A comparison is made with data from the other NDT devices, including continuous GPR thickness and density data, and point measures from PSPA seismic modulus and nuclear density.

The analysis begins with a visual presentation of the continuous thermal data using Mobile Automation’s “Paving Project Manager™” software. Data collected from the temperature sensing bar were transferred to a laptop, then converted from an encrypted log file to a graphical display file. Screen captures for lengths of the project were created to illustrate the mat temperature and paver stop duration.

FLIR camera images were recorded periodically during paving either at a random time, or after a lengthy paver stop of 10 minutes or more. Images were recorded at the truck box, material transfer vehicle (if in the paving train), and behind the paver screed. Specific locations were referenced using project stationing.

The following sections present thermal image analysis from the three projects. Then, correlations among NDT devices are reported and an overall summary is presented in the final section.

5.2 Project 1 Thermal Images

5.2.1 Stations 435+00 to 430+00

Paving was downstation beginning at 437+00 and ending at approximately two miles, with research testing occurring from 435+00 to 385+00. Figure 5.1 illustrates the continuous temperatures behind the paver from Stations 435+00 to 428+00.

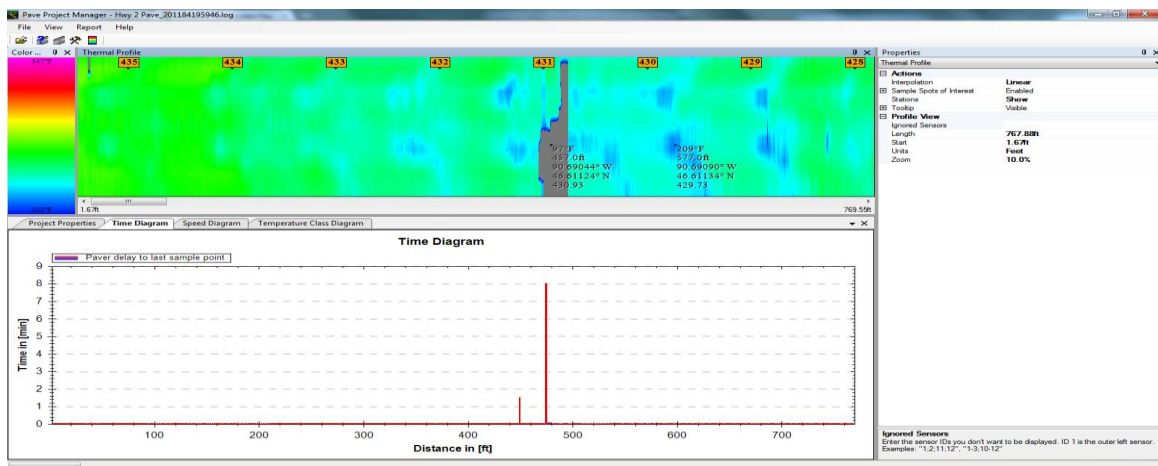


Figure 5.1 Pave-IR measurement from Station 435+00 to 428+00

A standard default color scale was applied to identify cooler areas in the mat. Generally, temperatures above 275°F are orange or red, while yellow, green and blue colors are cooler temperatures. The gray region at Station 431+00 was a paver stop, with estimated time to be 1.5 minutes and then 8 minutes. Note the distinctive V-shaped pattern (blue) at intervals of about 80 ft where cooler material spools transversely with the augers as the paver moves forward. A 22-ton mix payload placed 2.5-in thick and 18-ft wide at 150 lb/ft³ has a yield length of 78 ft.

The mat temperature at Station 432+00 using the FLIR image is shown in Figure 5.2. Specific temperature at a given point are numbered Sp (e.g., Sp1 = Spot 1), and the maximum temperature across a line is denoted Li (e.g., Li1 = Line 1).

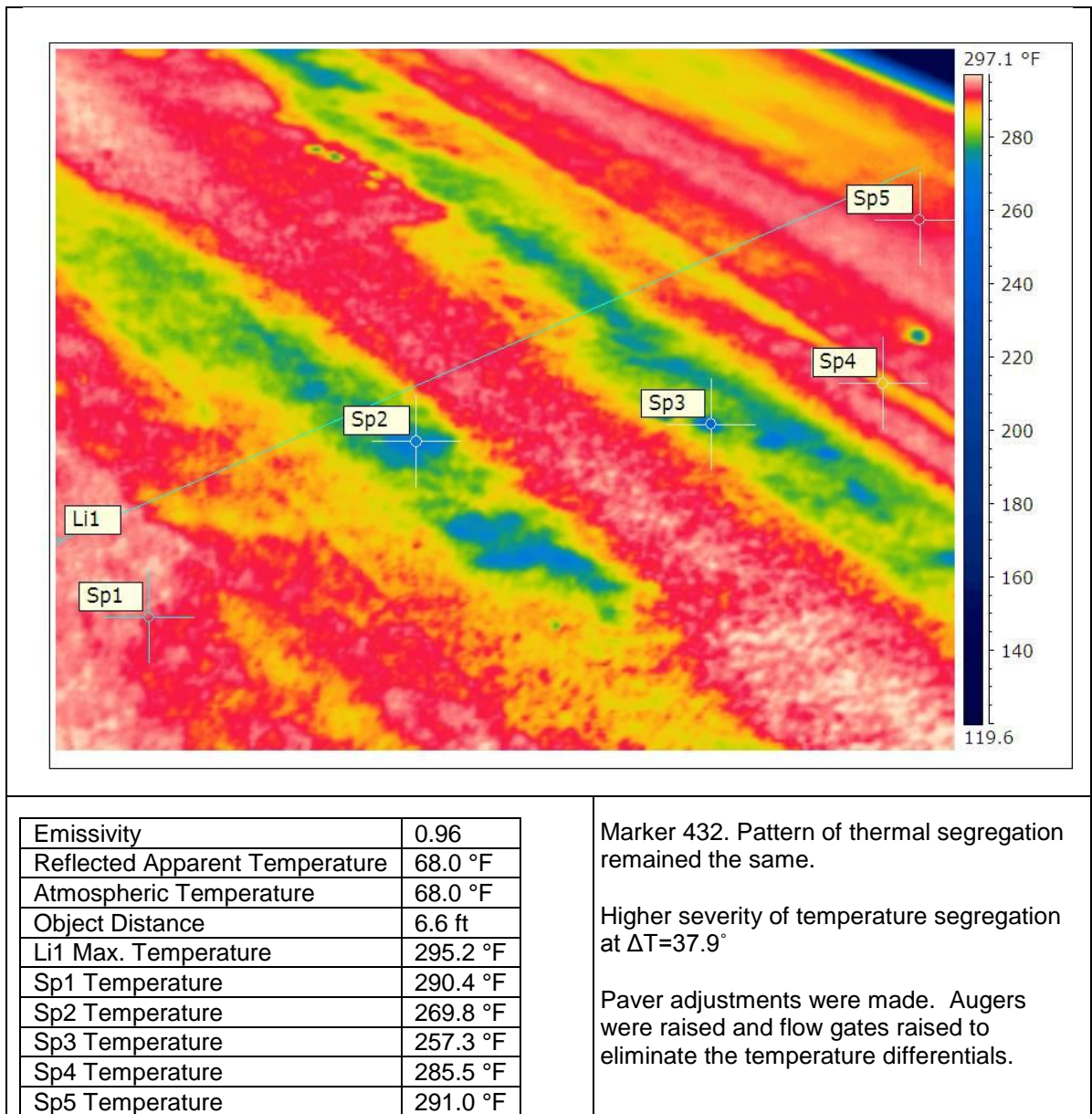


Figure 5.2 FLIR Thermal Image at Station 432+00

Temperatures with both thermal measurement methods were compared at Station 432+00, as shown in Table 5.1. The data indicate a disagreement between the bar sensors and thermal camera of about 50°F, where the camera recorded higher temperatures. The reason for this temperature bias is unexplained. The 24°F sensor range is in general agreement with the Pave-IR graph. The cooler blue regions on both sides of the paver center are equally represented by the FLIR image.

Table 5.1 Thermal Measurement comparison at Station 432+00

Measurement	Minimum, °F	Maximum, °F	Δ Temp., °F
Sensors	223	247	24
Camera	257	295	38

5.2.2 Stations 430+00 to 425+00

Figure 5.3 illustrates the continuous temperatures behind the paver from Stations 432+00 to 425+00, transitioning from the thermal graph in Figure 5.1. The gray region at Station 431+00 was a paver stop, with the actual time estimated to be about 8 minutes. In the region immediately after the paver stop, several truckloads with cooler mix were observed at Stations 430+00 and 429+00. Distance between trucks was approximately 80 ft, resembling a 22-ton mix payload. Again, a V-shaped pattern is evident with cooler material spooling transversely as the paver moves longitudinally (left to right in this figure).

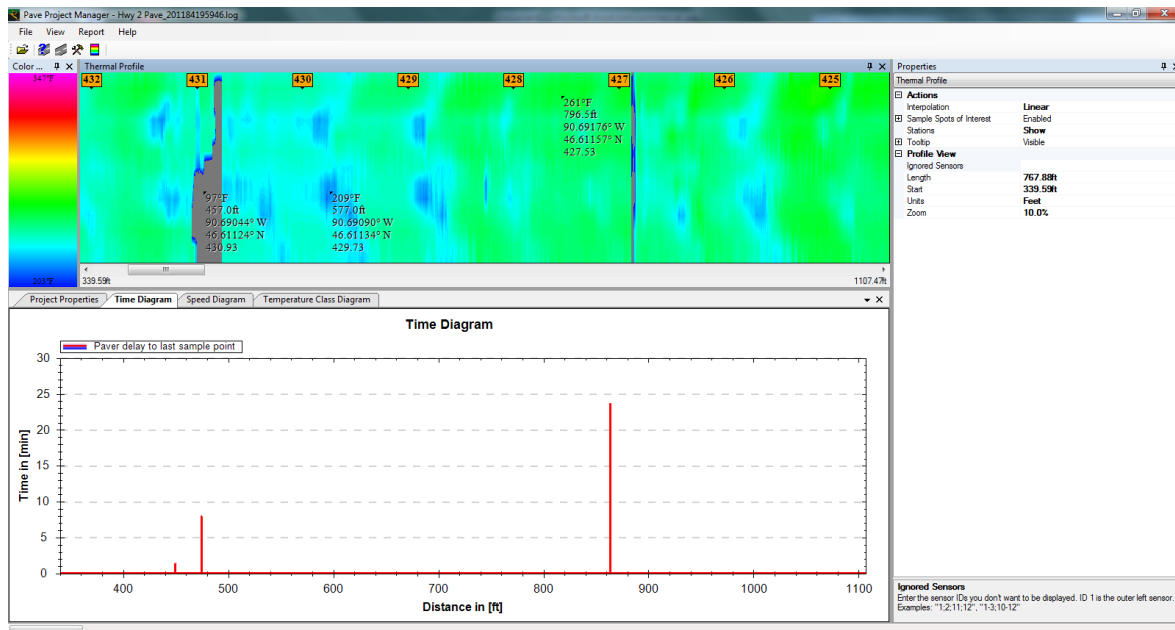


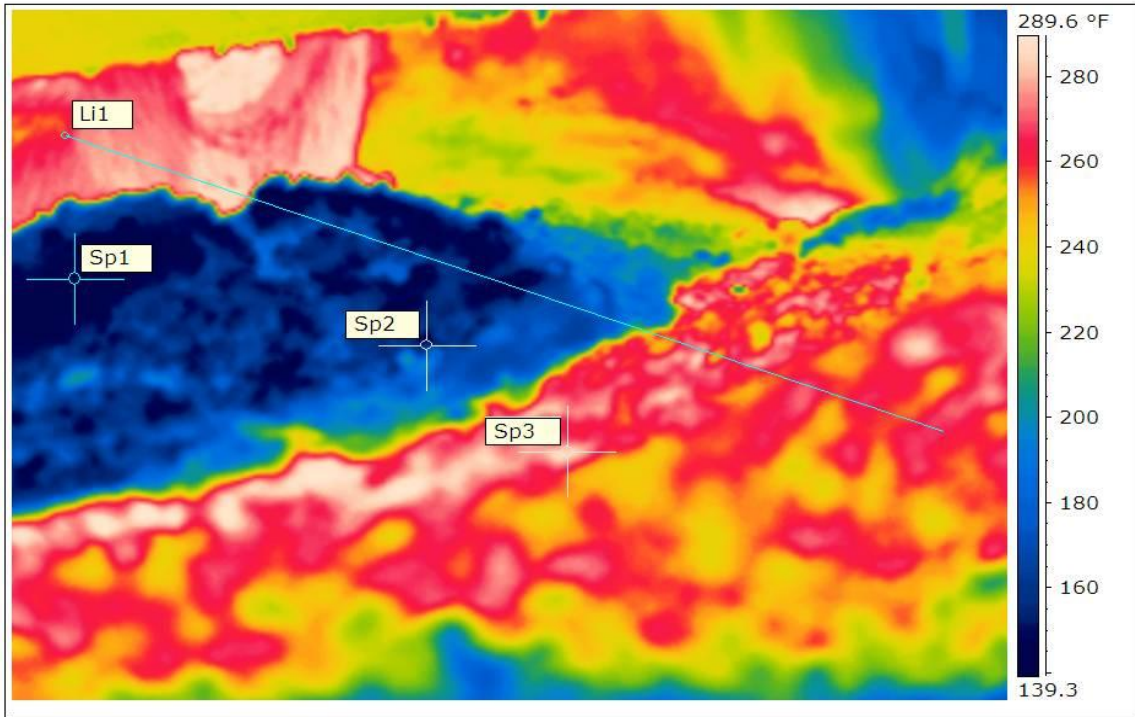
Figure 5.3 Pave-IR measurement from Station 432+00 to 425+00

Station 426+80 recorded an approximate 23-minute paver stop where a truck load was accidentally discharged in front of the paver hopper effectively stopping paving, as shown in Figure 5.4. Despite this lengthy delay, the mat temperature soon after paving resumed was similar to the temperature before the stop.



Figure 5.4 Mix accidentally dumped in front of remix hopper at Station 426+80

At Station 429+00, the material temperature was monitored from the truck box to behind the paver screed with the FLIR camera. Figures 5.5 through 5.7 document the material in the truck box, paver hopper insert, and paver screed, respectively.



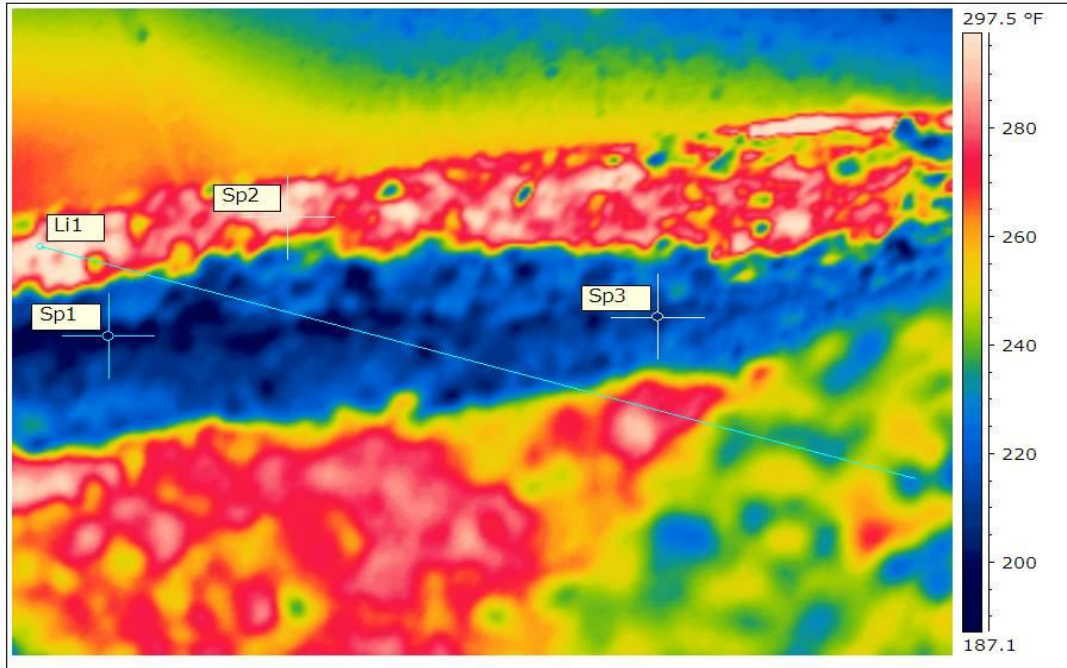
Emissivity	0.96
Reflected Apparent Temperature	68.0 °F
Atmospheric Temperature	68.0 °F
Object Distance	6.6 ft
Li1 Max. Temperature	285.7 °F
Sp1 Temperature	136.9 °F
Sp2 Temperature	162.3 °F
Sp3 Temperature	284.0 °F

Marker 429 minus. Second truck showed same material flow in receiving hopper of remix transfer device. Temperature differentials were reduced

These were typical differentials from delivery trucks which were mitigated by the remix process.

$\Delta T = 148.8^\circ$ contributing to the differentials in the mat created by the screed.

Figure 5.5 Station 429+00 Truck Box

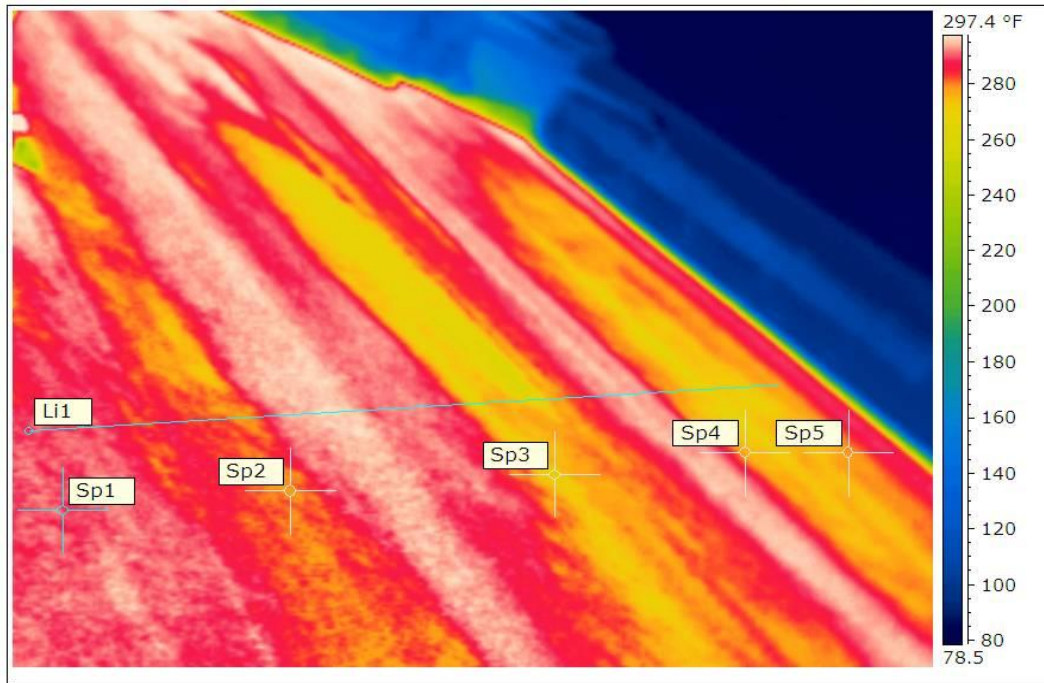


Emissivity	0.96
Reflected Apparent Temperature	68.0 °F
Atmospheric Temperature	68.0 °F
Object Distance	6.6 ft
Li1 Max. Temperature	304.1 °F
Sp1 Temperature	197.0 °F
Sp2 Temperature	293.8 °F
Sp3 Temperature	205.8 °F

The hopper material flow caused material to remain in the hopper wings until dumped as in standard paver operation. Cold material existed in the outside wings and contributed to the cold material placed in the wheel paths of the mat.

$\Delta T = 107.1^\circ$ Remixing and the paver hopper insert reduced these very severe differentials to marginal levels in the mat placed by the paver.
Marker #429.

Figure 5.6 Station 429+00 Paver Hopper Insert



Emissivity	0.96
Reflected Apparent Temperature	68.0 °F
Atmospheric Temperature	68.0 °F
Object Distance	6.6 ft
Li1 Max. Temperature	296.2 °F
Sp1 Temperature	289.9 °F
Sp2 Temperature	277.8 °F
Sp3 Temperature	270.8 °F
Sp4 Temperature	275.1 °F
Sp5 Temperature	277.9 °F

Pattern of temperature segregation behind paver at Marker 429.

Further adjustments made to raise paver augers and open right (crown) side flow gate.

$\Delta T = 25.4^\circ$. Delivered mix temperature varied due to stack testing being conducted at the asphalt plant
 1 to 2% additional air voids could be expected at the centerline (Sp3).
 Left wheel path Sp4 at 21.1 degrees (marginal).

Figure 5.7 Station 429+00 Paver Screed

A comparison of temperature readings at Station 429+00 for the FLIR camera and sensors are reported in Table 5.2. An approximate 30°F bias was measured between the camera and sensors, with the Pave-IR sensor measuring a lower temperature than the camera (reason for bias unknown). Variability was reduced with a 149°F range in the truck to 107°F in the hopper, to 25°F behind the screed. This indicates that the remix paver was able to reduce the temperature range about 40°F, or about 40%. The paver was able to further reduce the range from 107°F to 25°F, a reduction ratio of about 4.3-to-1. The overall temperature range reduction ratio from the truck box to the screed was about 6-to-1 (149°F to 25°F). This indicates that the operation is able to operate with a 25°F specified

range found in Washington and Texas DOT specifications. A caution when viewing this data is the spot (Sp) sampling approach, where the temperature points (including Area or Line) can be selected without randomization.

Table 5.2 Thermal Measurement comparison at Station 429+00

Measurement	Minimum, °F	Maximum, °F	Δ Temp., °F	Change between stages, °F
Camera-Truck	137	286	149	---
Camera-Hopper	197	304	107	-42
Camera-Screed	271	296	25	-83
Sensors	243	260	17	---

5.2.3 Station 422+00

A similar comparison was made at Station 422+00 between the FLIR images and the Pave-IR sensor. Table 5.3 summarizes the temperature ranges at the truck box, hopper insert (after remixing), and paver screed. There remained a similar 30°F bias in the sensors and camera where the sensors were continually reading a lower temperature. At this location, variability was reduced with a 91°F range in the truck to 85°F in the hopper, to 24°F behind the screed. This indicates that the remix paver was able to reduce the temperature range only 4°F, or about 5%. The paver was able to further reduce the range from 85°F to 24°F, a reduction ratio of about 3.5-to-1. The overall temperature range reduction ratio from the truck box to the screed was about 3.8-to-1 (91°F to 24°F). Variability behind the paver was higher with the camera since it is able to sample specific points while the sensors uses a standard 13-in spacing. The FLIR camera images to support this data are shown in Figures 5.8 through 5.10.

Table 5.3 Thermal Measurement comparison at Station 422+00

Measurement	Minimum, °F	Maximum, °F	Δ Temp., °F	Change between stages, °F
Camera-Truck	170	261	91	---
Camera-Hopper	157	304	85	-6
Camera-Screed	271	296	24	-61
Sensors	243	260	17	---

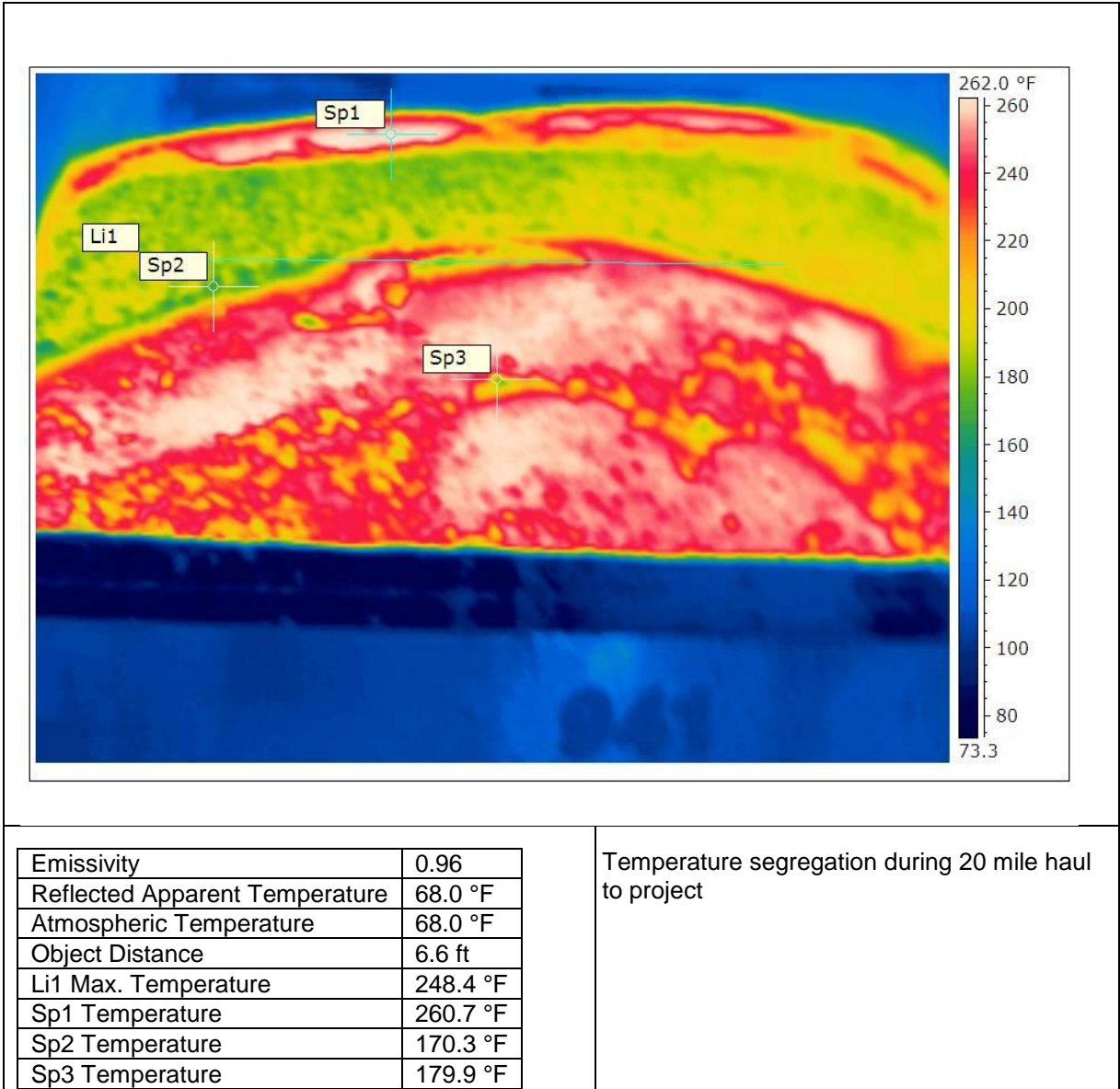
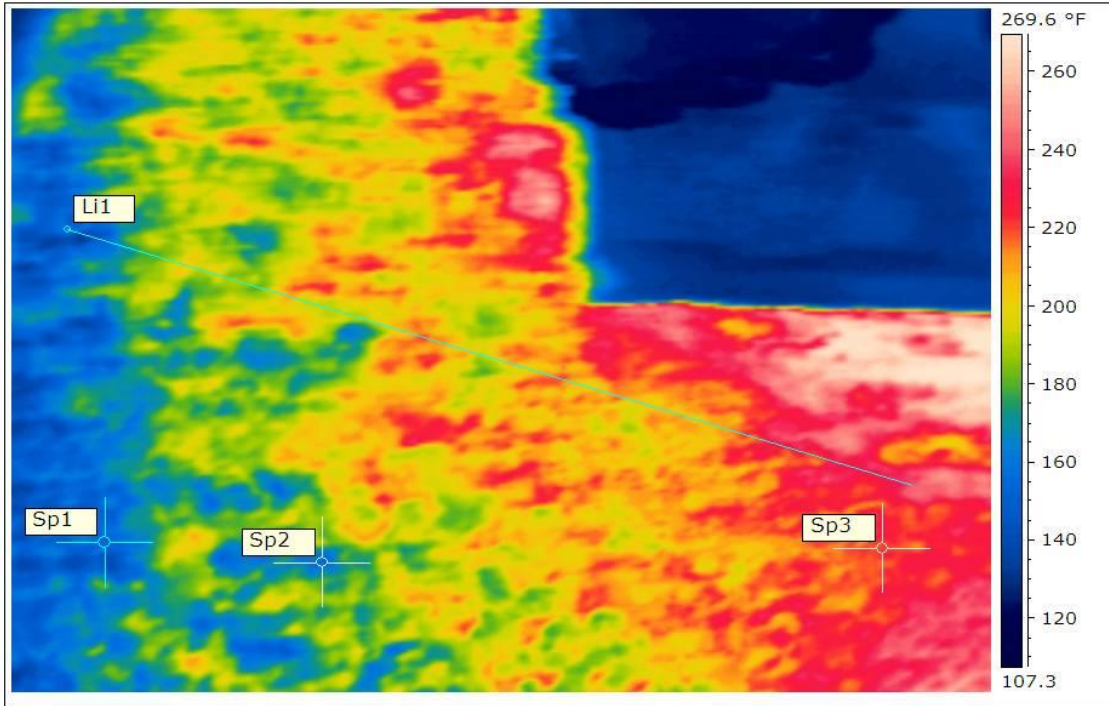


Figure 5.8 Station 422+00 Truck Box



Emissivity	0.96
Reflected Apparent Temperature	68.0 °F
Atmospheric Temperature	68.0 °F
Object Distance	6.6 ft
Li1 Max. Temperature	242.2 °F
Sp1 Temperature	156.9 °F
Sp2 Temperature	159.3 °F
Sp3 Temperature	221.2 °F

Colder material on shoulder side of receiving hopper contributed to the cooler mix placed in the shoulder and right wheel path.

Figure 5.9 Station 422+00 Paver Hopper

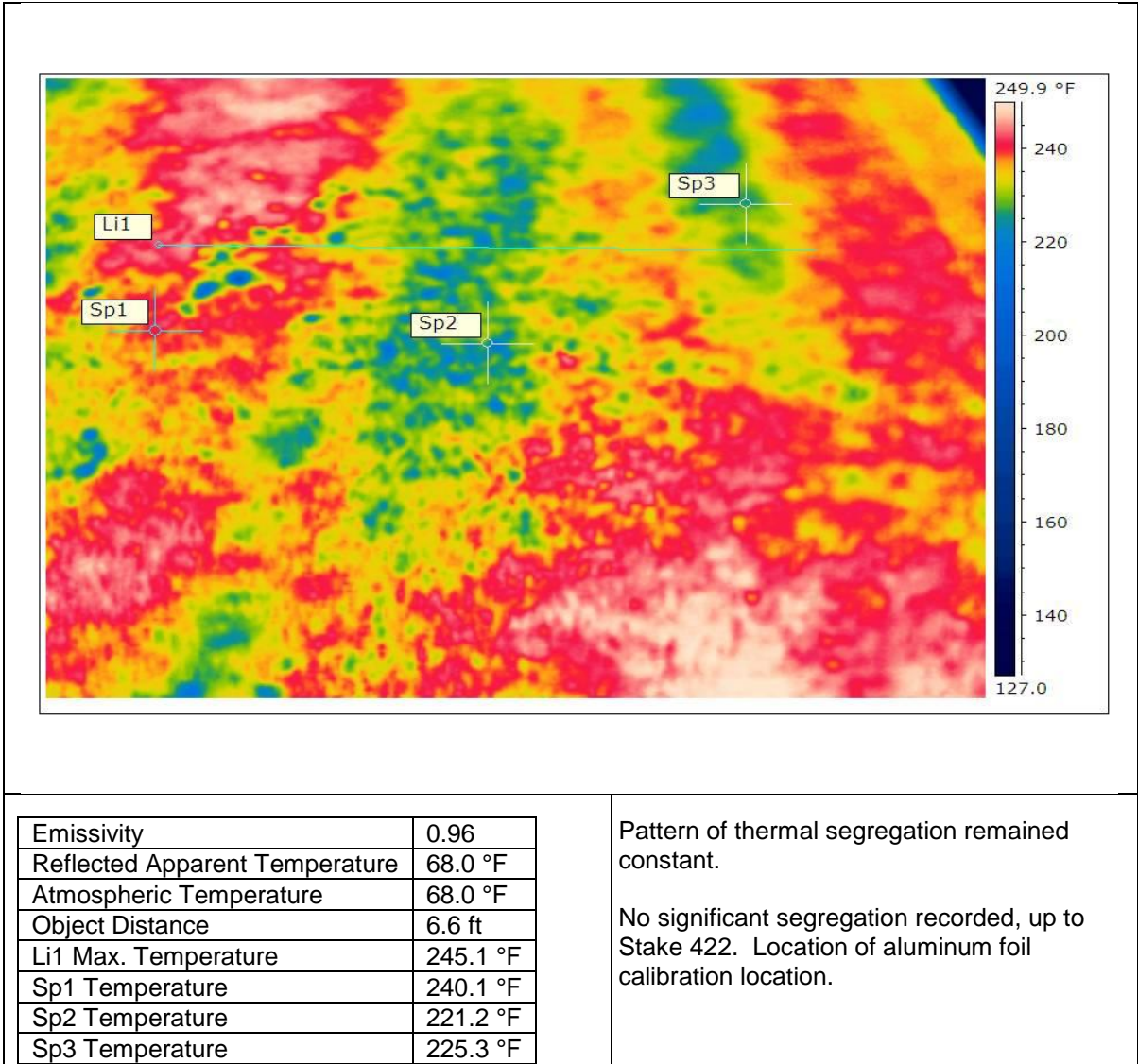


Figure 5.10 Station 422+00 Paver Screed

5.2.4 Stations 420+00 to 415+00

Figure 5.11 is the thermal profile from Stations 420+00 to 414+00. This graph reports multiple paver stops due to dumped material or other delays. V-shaped segregation at 80-ft intervals is again clearly evident with warmer green areas and cooler blue areas. A large gray region at Station 417+00 was a documented material dump in front of the paver. No FLIR images were recorded in this area.

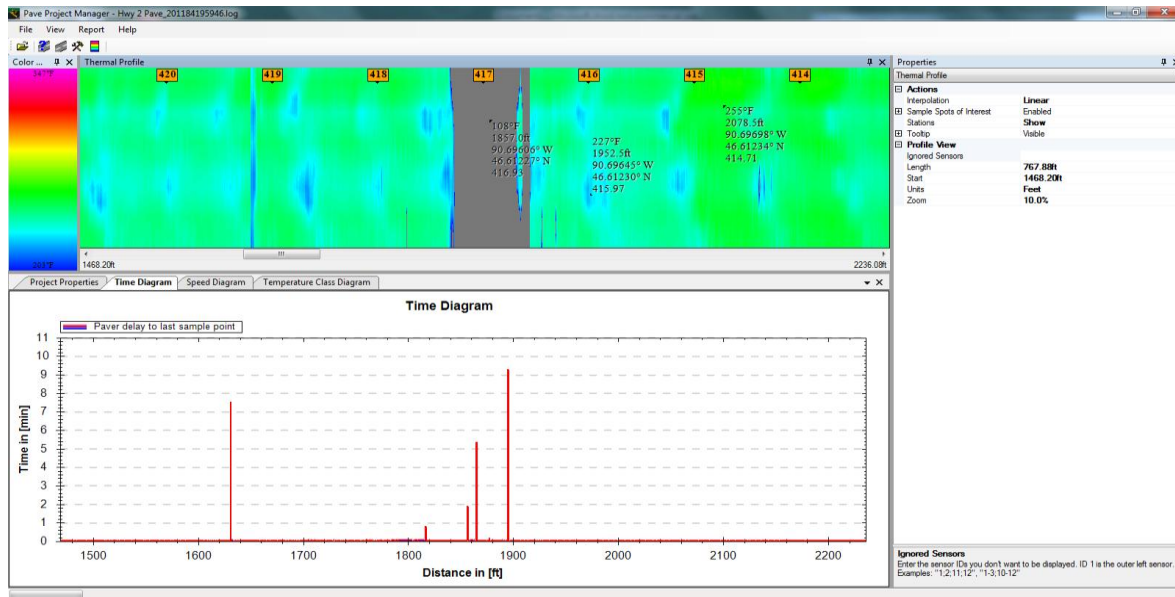


Figure 5.11 Pavement IR measurement from Station 420+00 to 414+00

The cooler V-shaped blue areas were systemic in nature at an 80-ft interval and symmetrical across the mat. To help understand the causes of the cooler areas, a photo of the screed and auger assembly for a Roadtec paver model #RP 195 is shown in Figure 5.12. Although this is not the exact Cedarapids model in Project 1, it does show a similar three-screed configuration having one main screed in the middle of the chassis capable of variable slope and crown shaping, and two extension screeds on each side of the main screed. It appears the cooler areas may be near the ends of the screed tubes in an overlap region. The Cedarapids paver was equipped with diesel-fueled screed heaters, and all were operable during the start of the operation. A more detailed investigation is recommended to understand this possible operational behavior and corrective field actions if appropriate.



Figure 5.12 Paver screed segments for Roadtec model #RP 195

5.2.5 Stations 415+00 to 400+00

Figures 5.13 and 5.14 are the thermal profile from Stations 415+00 to 408+00, and 408+00 to 400+00, respectively. The repeated end-of-truck V-shaped segregation pattern is still visible. A paver productivity graph is shown in Figure 5.13 where incremental 2-second lags are recorded. A 17-minute paver stop was recorded at Station 404+50 where material was dumped in front of the paver. Figures 5.15 through 5.17 document the material at Station 402+00 using FLIR images after paving resumed.

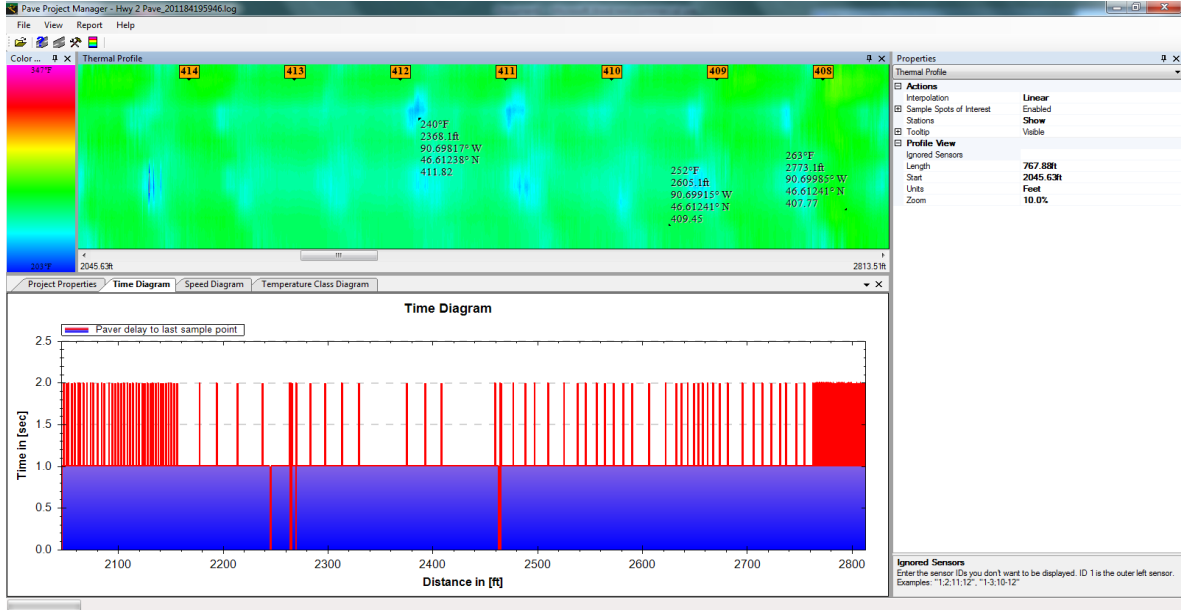


Figure 5.13 Pave-IR measurement from Station 415+00 to 408+00

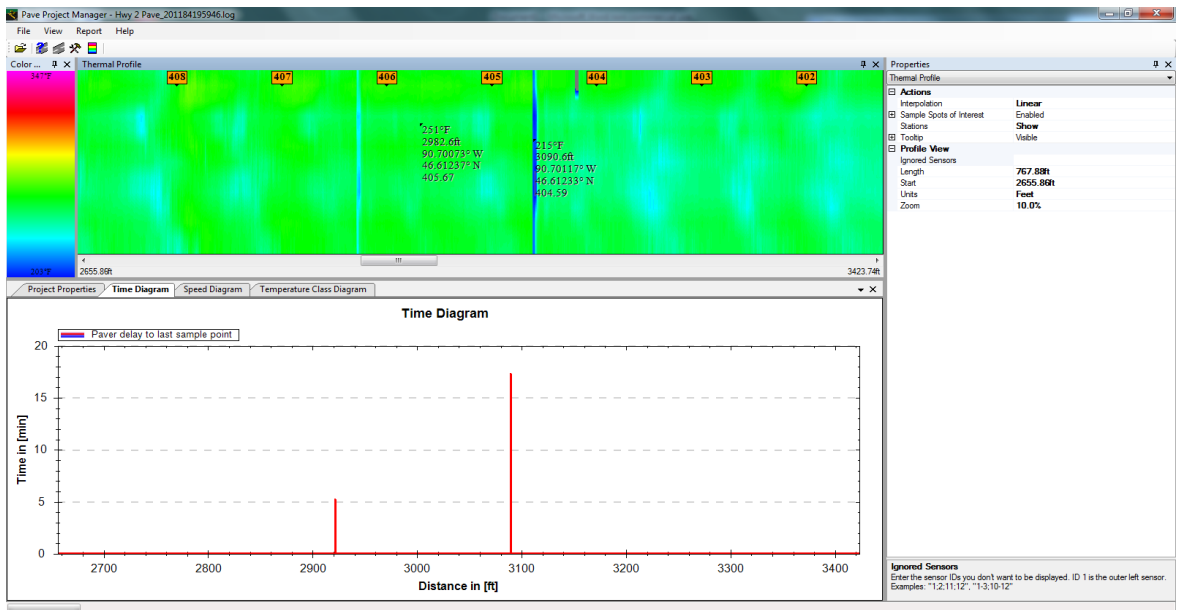
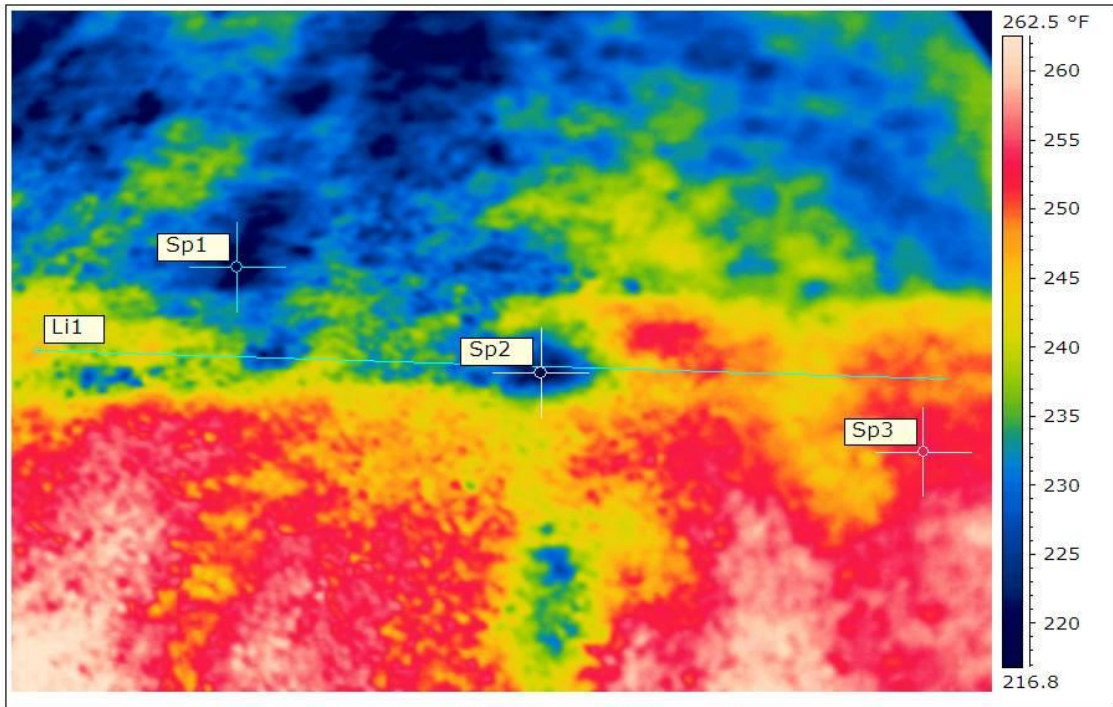


Figure 5.14 Pave-IR measurement from Station 408+00 to 401+00



Emissivity	0.96
Reflected Apparent Temperature	68.0 °F
Atmospheric Temperature	68.0 °F
Object Distance	6.6 ft
Li1 Max. Temperature	252.0 °F
Sp1 Temperature	214.7 °F
Sp2 Temperature	218.1 °F
Sp3 Temperature	252.9 °F

Fifteen to twenty minute paver stop due to dumped material in front of remix.

Temperatures and the cold unrolled material is all of the Sp1 and above material.

High potential for low density and roughness in the ride numbers through this area.

Figure 5.15 Station 402+00 Paver Screed after paving resumed (Image #1)

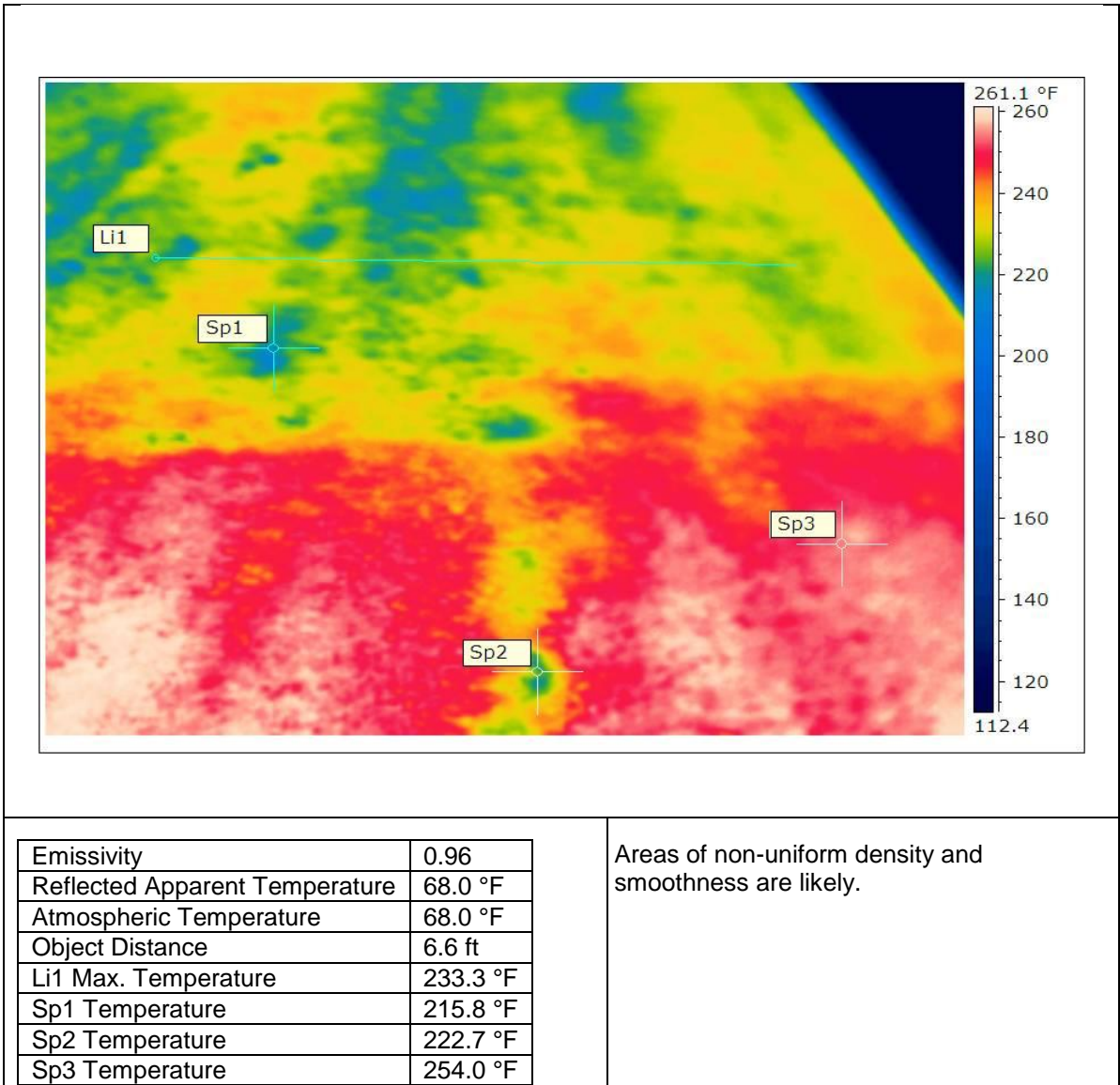


Figure 5.16 Station 402+00 Paver Screed after paving resumed (Image #2)

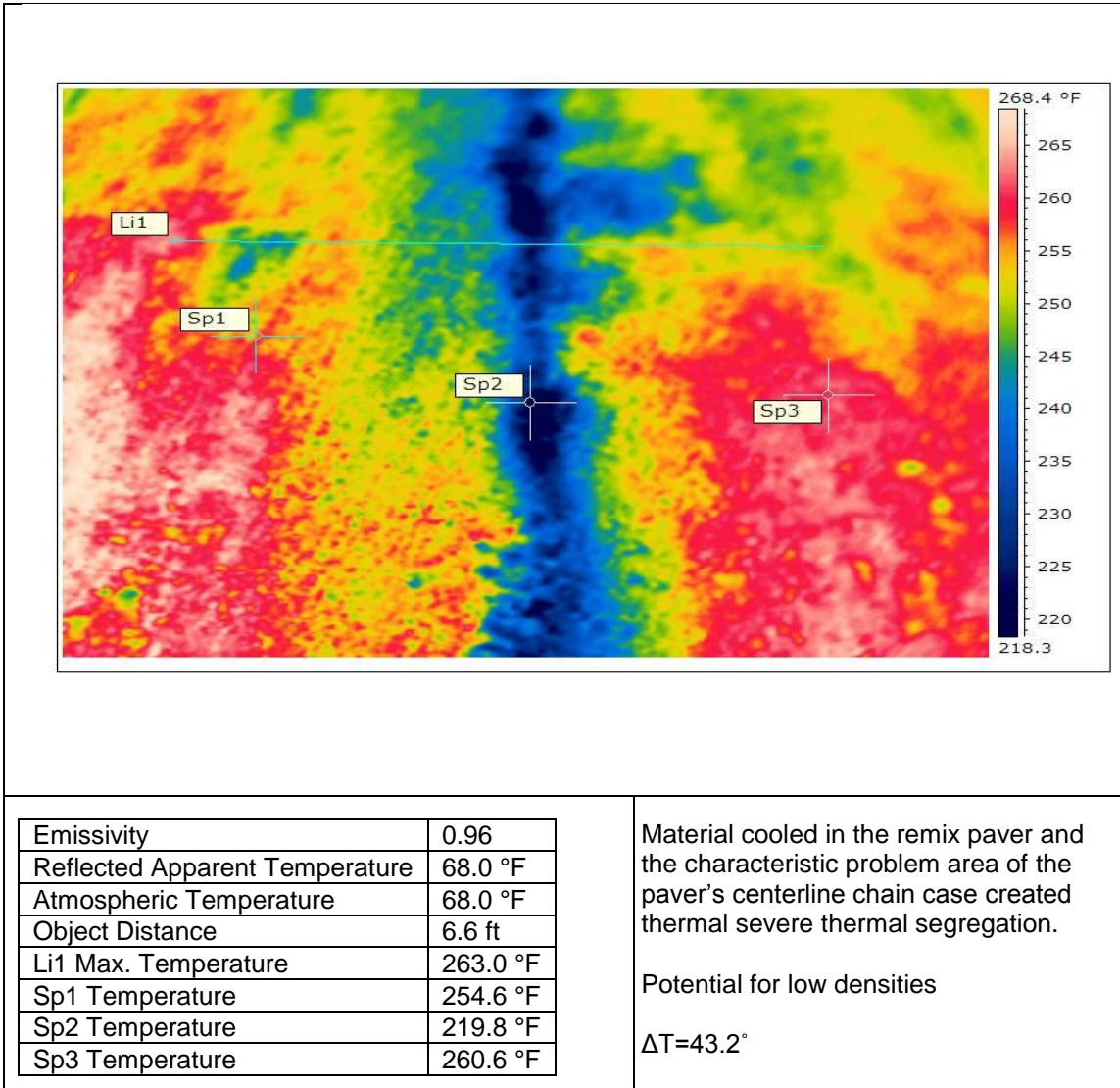


Figure 5.17 Station 402+00 Paver Screed after paving resumed (Image #3)

As Figure 5.17 illustrates, the paver chain case is a potential cause of segregation in the paving operation. The chain case houses a torque drive to turn the augers and slat conveyors. Its close proximity to the mat and variable temperature from the mix passing overhead, along with the case in direct alignment with the articulation pin in the main screed, combine to potentially cause a linear low temperature streak in the mat. The chain case strip in Figure 5.17 measured 220°F temperature while the adjoining areas exceeded 250°F. The sensor bar is unable to detect this linearly segregated section.

A linear segregated location on a 7-year old STH 77 asphalt pavement west of Minong, Wisconsin, was most likely caused by chain case thermal segregation, as shown in Figures 5.18 and 5.19. Pavement width from centerline to pavement edge is 17 ft, with the longitudinal crack midway between the centerline and edge. At first it would appear that

the longitudinal crack is directly under right wheel path loading, however, the figures show a personal vehicle and truck straddling the sealed crack.



Figure 5.18 Longitudinal crack in center of paving lane



Figure 5.19 Longitudinal crack in center of paving lane

5.2.6 Stations 400+00 to 390+00

Figures 5.20 and 5.21 illustrate thermal profiles from Stations 402+00 to 381+00. A speed diagram graph illustrates the paver speed, generally ranging from 20 to 25 ft/min, except for a few paver stops. The repeated end-of-truck V-shaped pattern at 80-ft truckload intervals is visible. Research testing of all NDT devices ended at 385+00. These figures conclude Pave-IR thermal images for Project 1.

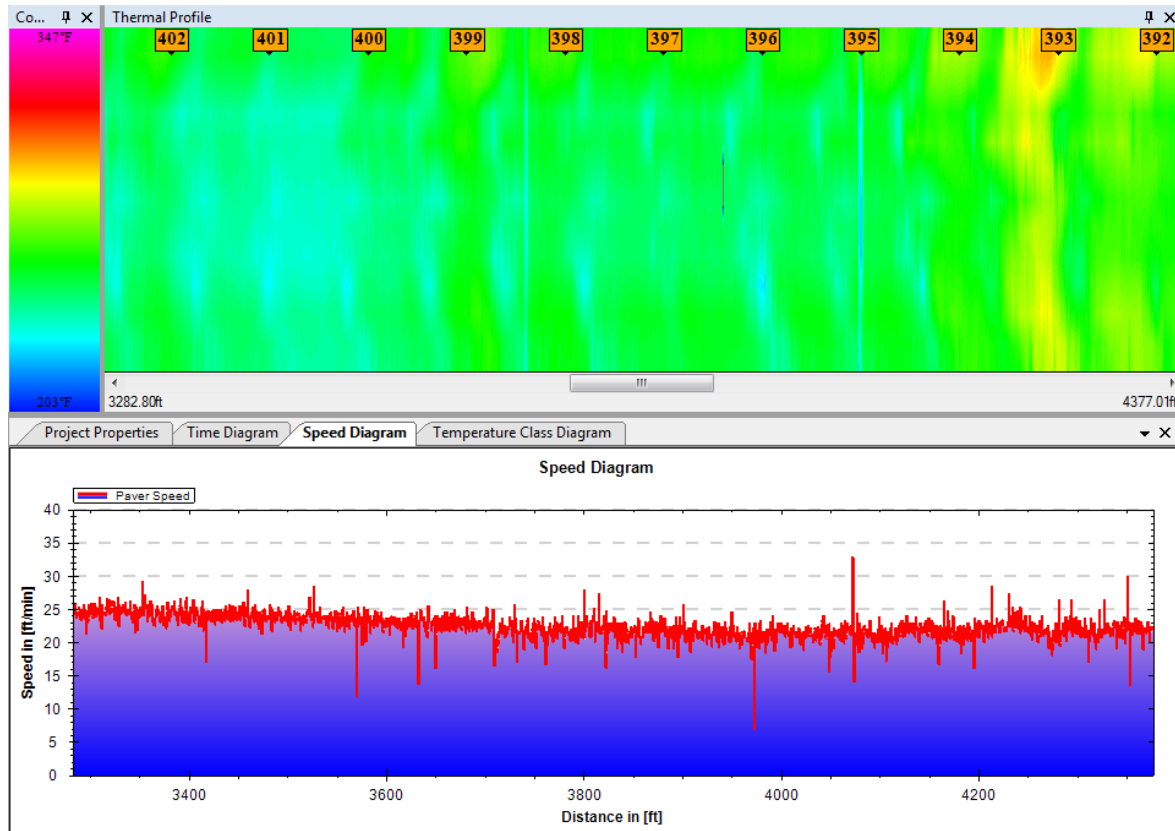


Figure 5.20 Pave-IR measurement from Station 402+00 to 392+00

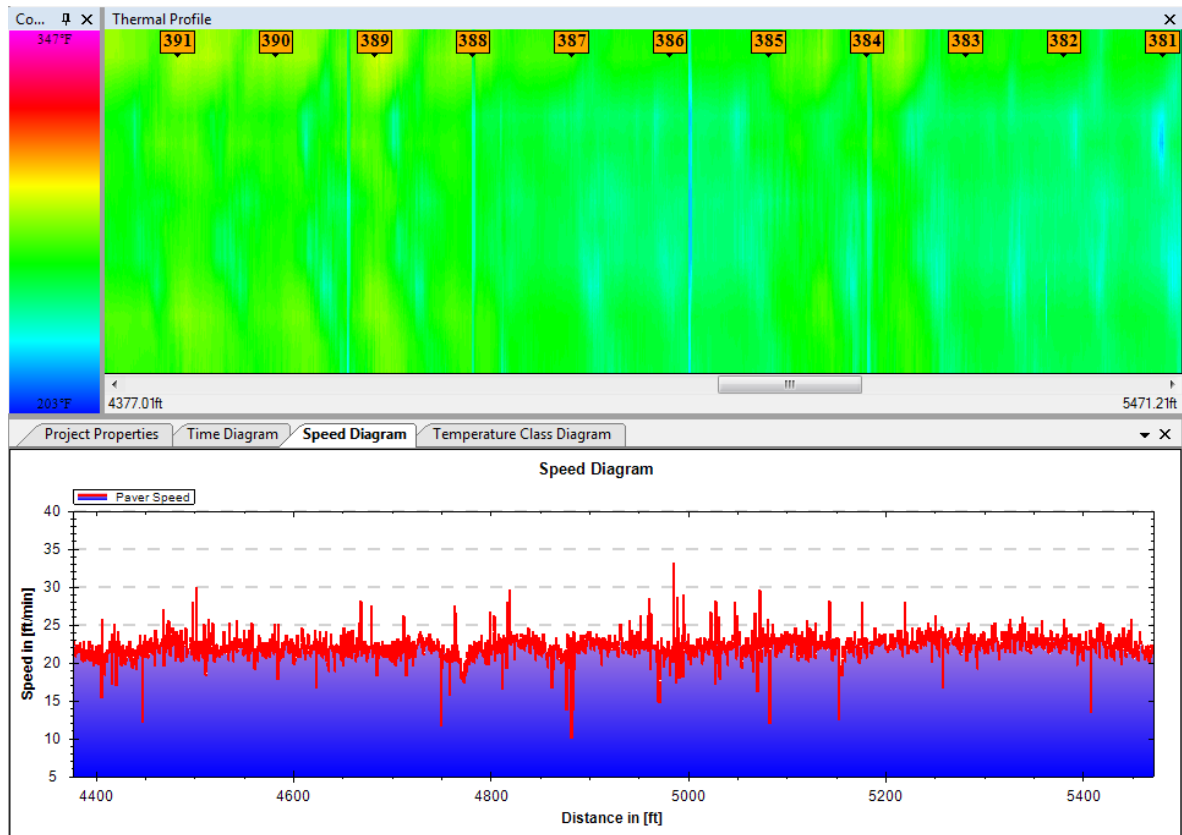


Figure 5.21 Pave-IR measurement from Station 392+00 to 381+00

5.3 Project 2 Thermal Images

Project 2 was STH 75 in Kenosha and Racine Counties with paving a 2.5-in 17-ft mat over pulverized base on August 11th. Figure 5.22 illustrates the entire graphical display of August 11th mat temperatures directly behind the paver from Stations 244+70 to 146+70 (paving was downstation). Transversely, the temperatures were warmest in the mat center and cooler near the edges. The thermal bar was centered on the paver with ends approximately 2 feet from each slipformed edge. The beginning of each truckload is defined by cooler light green colors bordering warmer red/orange temperatures. The length of paving with a 22-ton mix payload placed 2.5-in thick and 17-ft wide at densified 150 lb/ft³ is estimated at 83 ft. This interval is well defined in the figure.

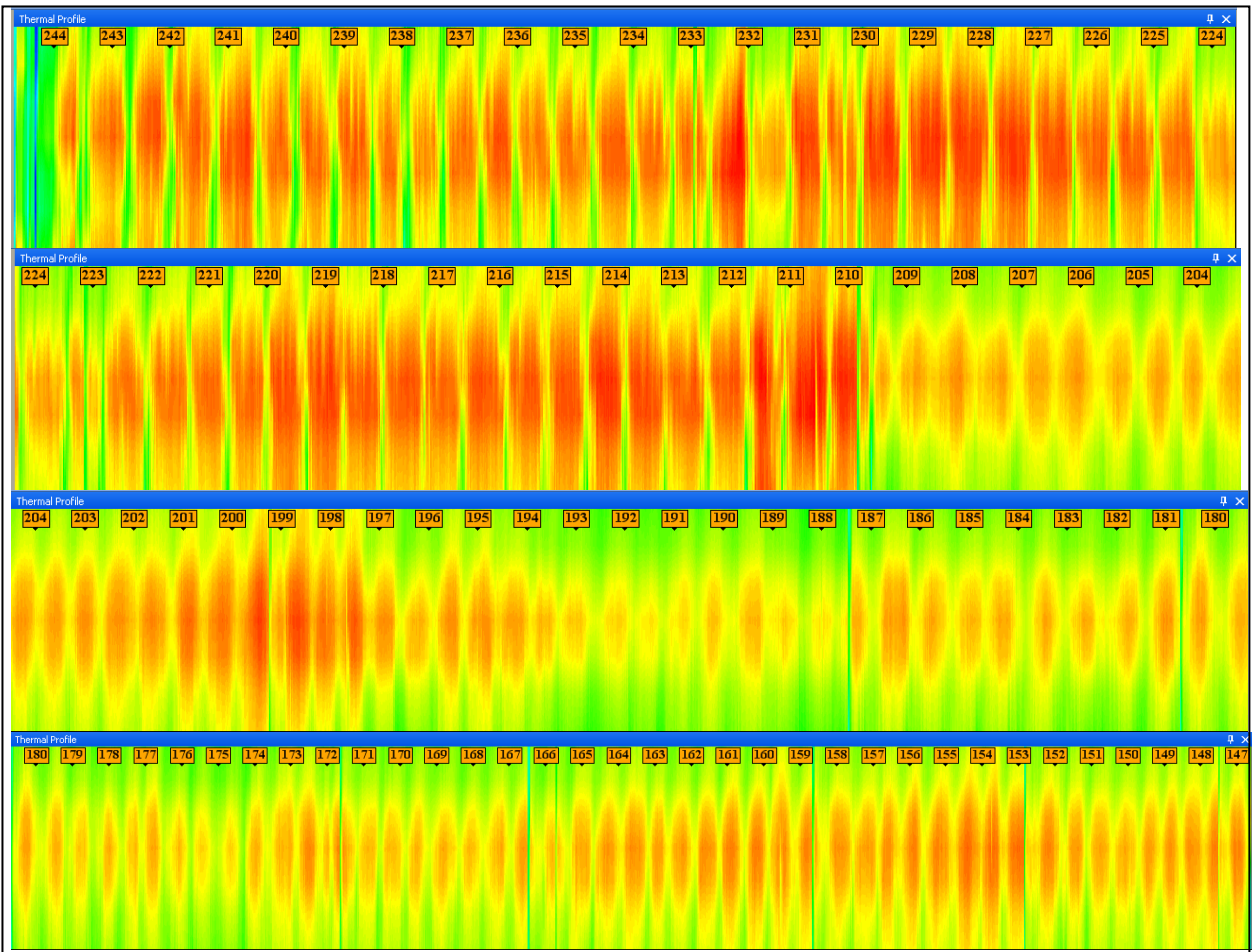


Figure 5.22 Graphical Display of Paving Mat Temperature on Project 2

A photo taken the day after paving in the vicinity of Station 220+00 is shown in Figure 5.23. This photo illustrates the end-of-truckload segregation. Darker regions correlate with the lighter sensor temperatures during paving. This temperature segregation was very difficult to visually detect during paving, including real-time Pave-IR display, and like many paving projects, more visible the day after paving.



Figure 5.23 End of Truckload Segregation on Project 2

At Station 209+80, two simultaneous changes occurred: (1) a replacement material transfer vehicle (MTV) was added to the paving train, and (2) mixing temperature reduced 10°F. Figure 5.22 illustrates this change with a reduction in red thermal areas from Station 209+80 to 147+00, downstation in the direction of paving. As mentioned earlier, at the start of paving the MTV developed a bent conveyor slat and was removed from the paving operation. Paving continued without the MTV until about mid-day when a replacement MTV arrived and begin transferring material at Station 209+80. The plant mixing temperature was also lowered 10°F prior to this location. Tables 5.4 and 5.5 summarize basic statistics without and with the MTV, respectively.

Table 5.4 Without-MTV IR Summary Statistics Sta. 242+00 to 209+80

Statistic	Sensor Number, Offset from Centerline						Overall Average
	#6 (right) 2.0 ft	#5 4.2 ft	#4 6.4 ft	#3 8.6 ft	#2 10.8 ft	#1 (left) 13.0 ft	
High Temp, °F	313	322	323	324	313	302	316
Low Temp, °F	241	240	251	258	255	254	250
Range, °F	72	82	72	66	58	48	66
Mean, °F	292	297	306	301	294	284	296
Std. Dev., °F	9.3	12.7	9.8	8.7	9.0	6.8	9.4
Coeff. Var., %	3.2	4.3	3.2	2.9	3.1	2.4	3.2
Sample size, n	3220	3220	3220	3220	3220	3220	3220

Table 5.5 With-MTV IR Summary Statistics Sta. 209+80 to 192+00

Statistic	Sensor Number, Offset from Centerline						Overall Average
	#6 (right) 2 ft	#5 4.2 ft	#4 6.4 ft	#3 8.6 ft	#2 10.8 ft	#1 (left) 13.0 ft	
High Temp, °F	299	307	314	314	306	296	306
Low Temp, °F	238	243	268	261	251	270	255
Range, °F	60	64	46	53	55	26	51
Mean, °F	283	293	301	300	289	282	291
Std. Dev., °F	5.5	6.2	5.2	5.1	6.1	4.8	5.5
Coeff. Var., %	2.0	2.1	1.7	1.7	2.1	1.7	1.9
Sample size, n	1780	1780	1780	1780	1780	1780	1780

When the MTV was added to the operation halfway through the day’s paving, the average mean temperature dropped 5°F, and the standard deviation was reduced in half 9.4°F to 5.5°F. The range also reduced from an average 66°F to 51 °F. Based on this data, material remixing equipment reduced variability in the mat temperature on this project.

5.3.1 Station 242+00, Start of Research Test Segment

A comparison was made among thermal measurements at Station 242+00 with summary results in Table 5.6. Thermal images to support the data from the truck box, paver hopper, and paver screed, are in respective Figures 5.24, 5.25, and 5.26. Observational notes are provided with each figure to understand the process.

Table 5.6 Thermal Measurement comparison at Station 242+00

Measurement	Minimum, °F	Maximum, °F	Δ Temp., °F
Camera-Truck	167	324	157
Camera-Hopper	152	316	164
Camera-Screed	250	303	53
Sensors	282	307	25

Unlike the first project, there was little difference in high temperature readings with the camera and sensors. As highlighted earlier, the range is much higher with the camera since the operator can choose specific points to sample (lowest if desired), while the sensors are at a fixed 13-in spacing (26-in spacing used on this project).

Without the material transfer vehicle at Station 242+00, there was no temperature variability reduction between the truck and hopper, in fact, the range increased from 157°F to 164°F. The range was then reduced from 164°F in the hopper to 53°F behind the screed, a range reduction ratio of about 3.1-to-1, somewhat similar to the first project. The overall

temperature range reduction ratio from the truck box to the screed was about 3.0-to-1 (157°F to 53°F). However, the final mat range was much high (53°F) than the previous projects with a remixer in the paving train.

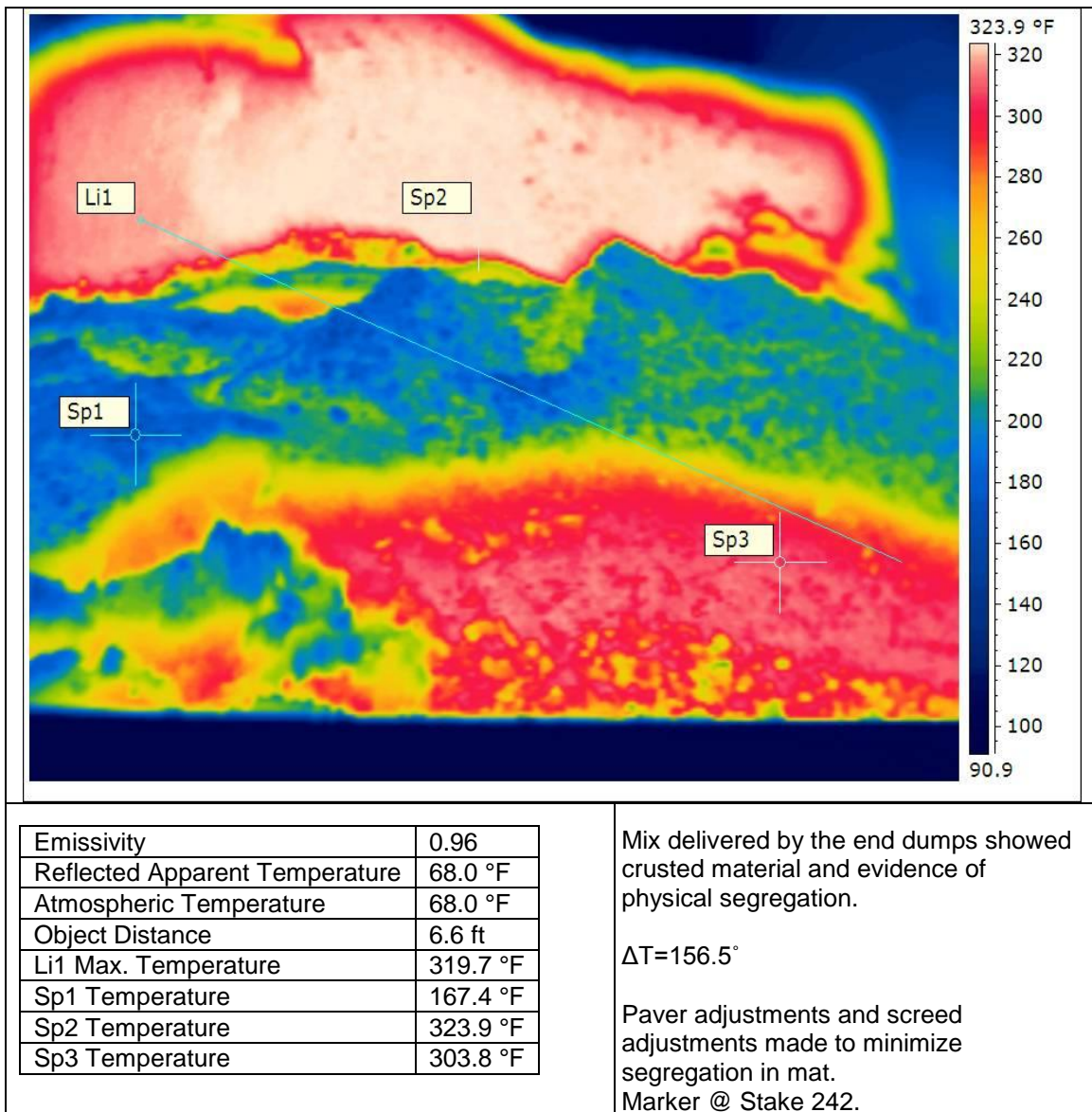


Figure 5.24 Station 242+00 Truck Box

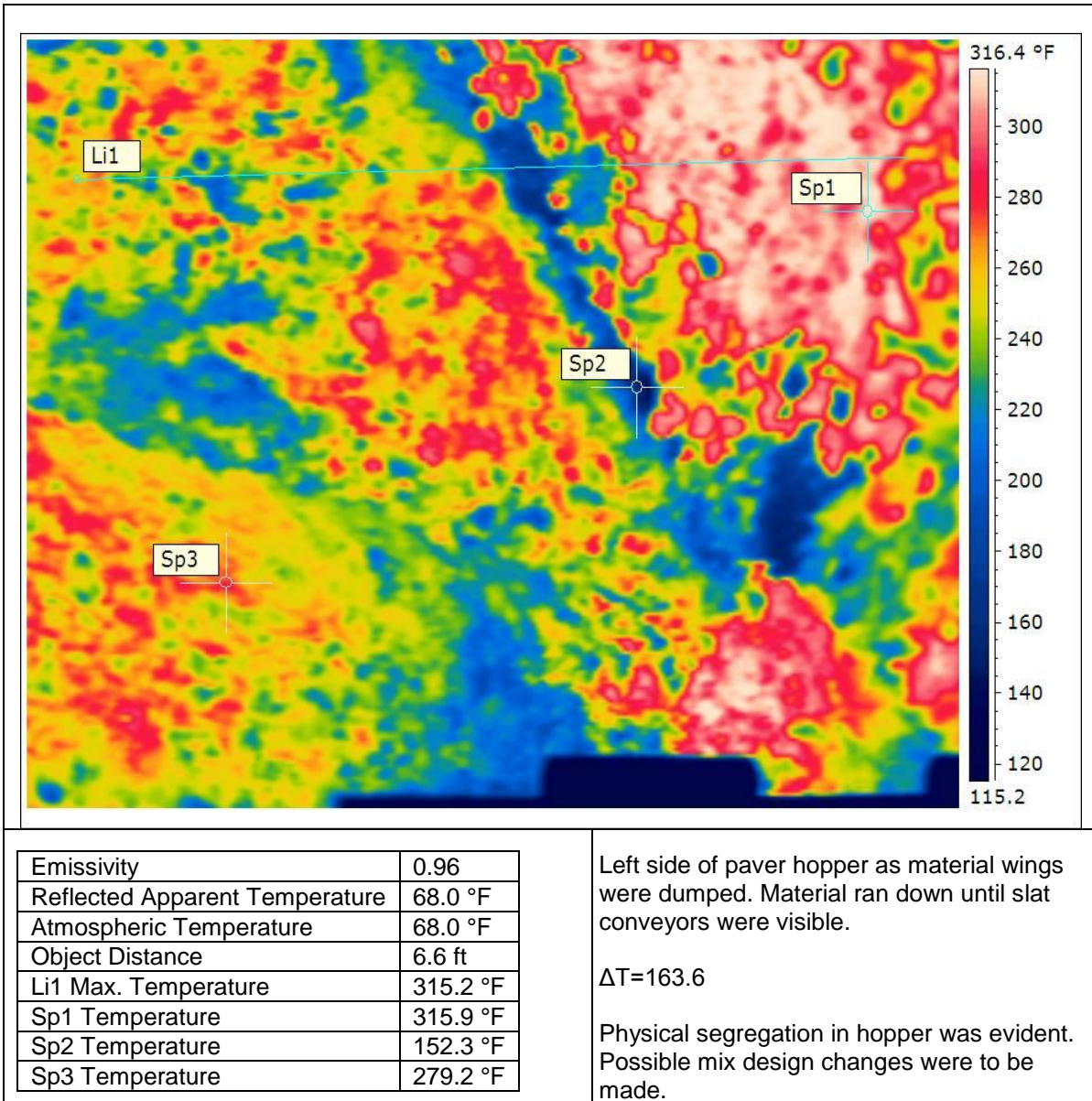


Figure 5.25 Station 242+00 Paver Hopper

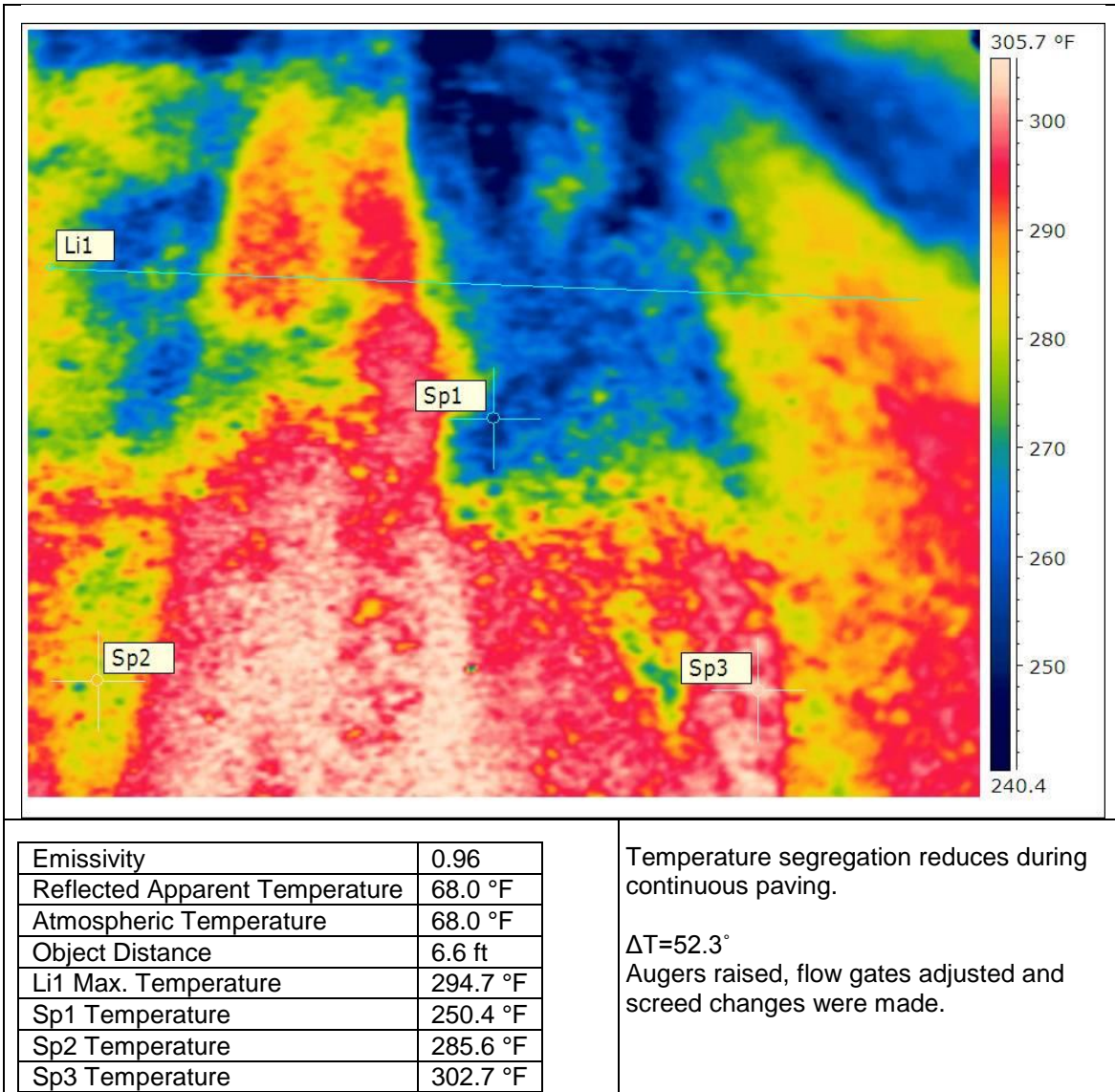


Figure 5.26 Station 242+00 Paver Screed

5.3.2 Station 235+00, 700 ft into paving Research Test Segment

A measurement comparison was made at Station 235+00 with summary results in Table 5.7. Thermal images to support the data from the truck box are shown in Figure 5.27 and the paver screed in Figures 5.28 and 5.29. No hopper images were recorded at this station. Observational notes are provided with each figure to understand the process.

Table 5.7 Thermal Measurement comparison at Station 235+00

Measurement	Minimum, °F	Maximum, °F	Δ Temp., °F
Camera-Truck	192	324	132
Camera-Hopper	n/a	n/a	n/a
Camera-Screed #1	259	295	36
Camera-Screed #2	236	286	50
Sensors	279	307	28

Here, high temperature readings behind the paver were slightly greater with the sensors, compared to the two camera images. Similar to before, the range was much higher with the camera, primarily since the operator chose specific points to sample, while the sensors were at a fixed 26-in spacing. From the truck to behind the screed, the range decreased from 132°F to 50°F (controlling value). This equates to a reduction ratio of 2.6-to-1, less than 3.1-to-1 at Station 242+00.

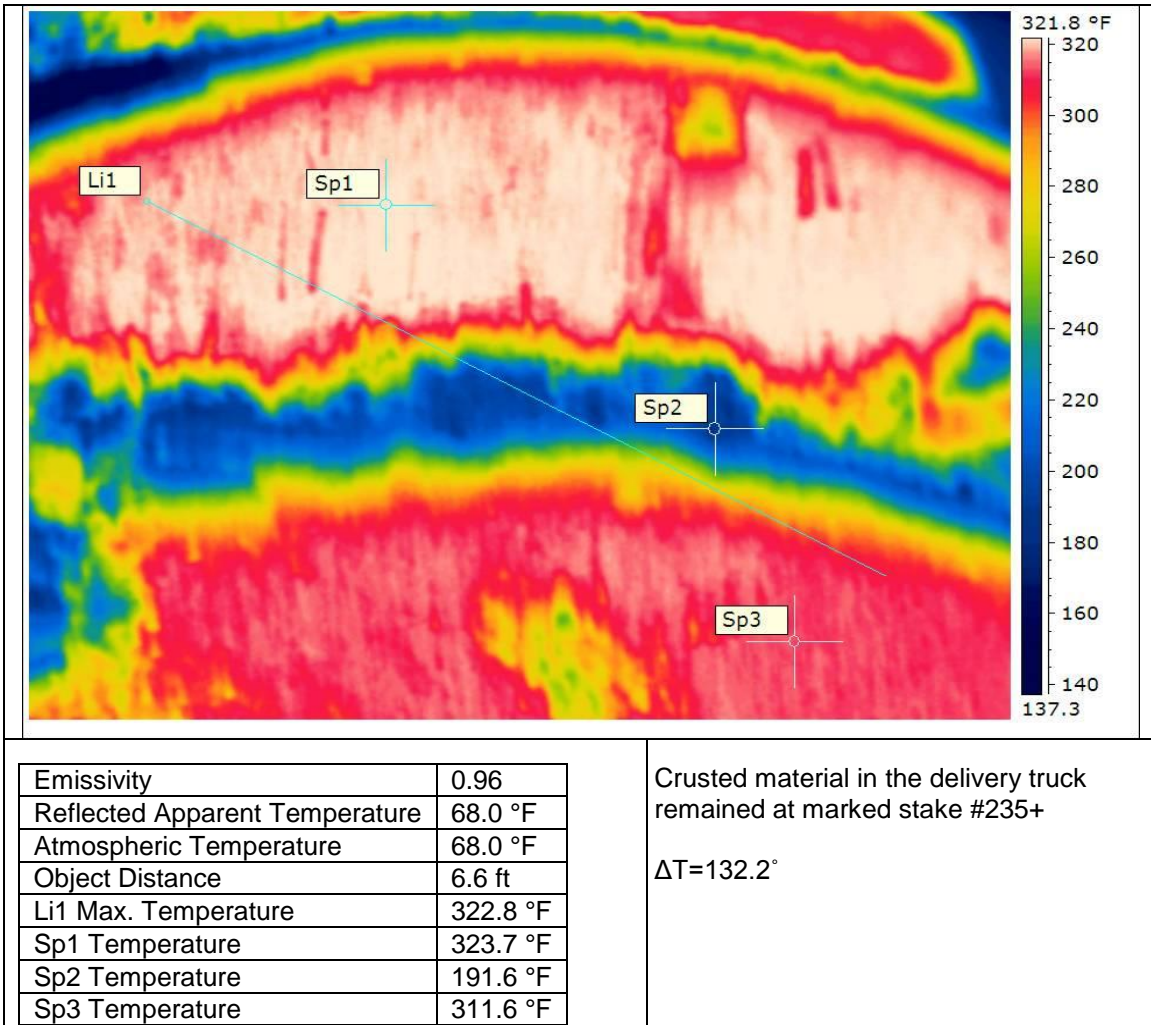


Figure 5.27 Station 235+00 Truck Box

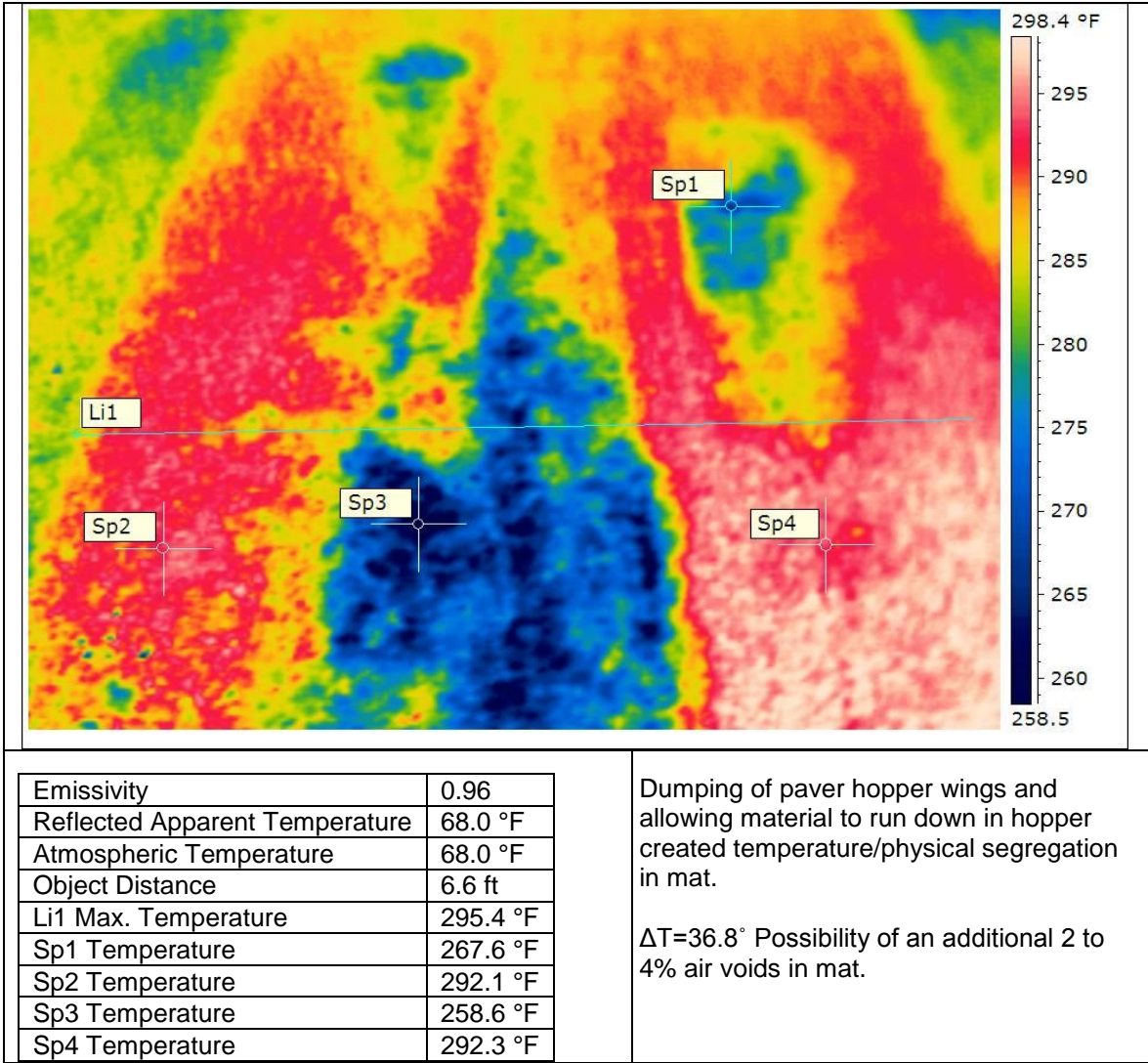


Figure 5.28 Station 235+00 Paver Screed (Image #1)

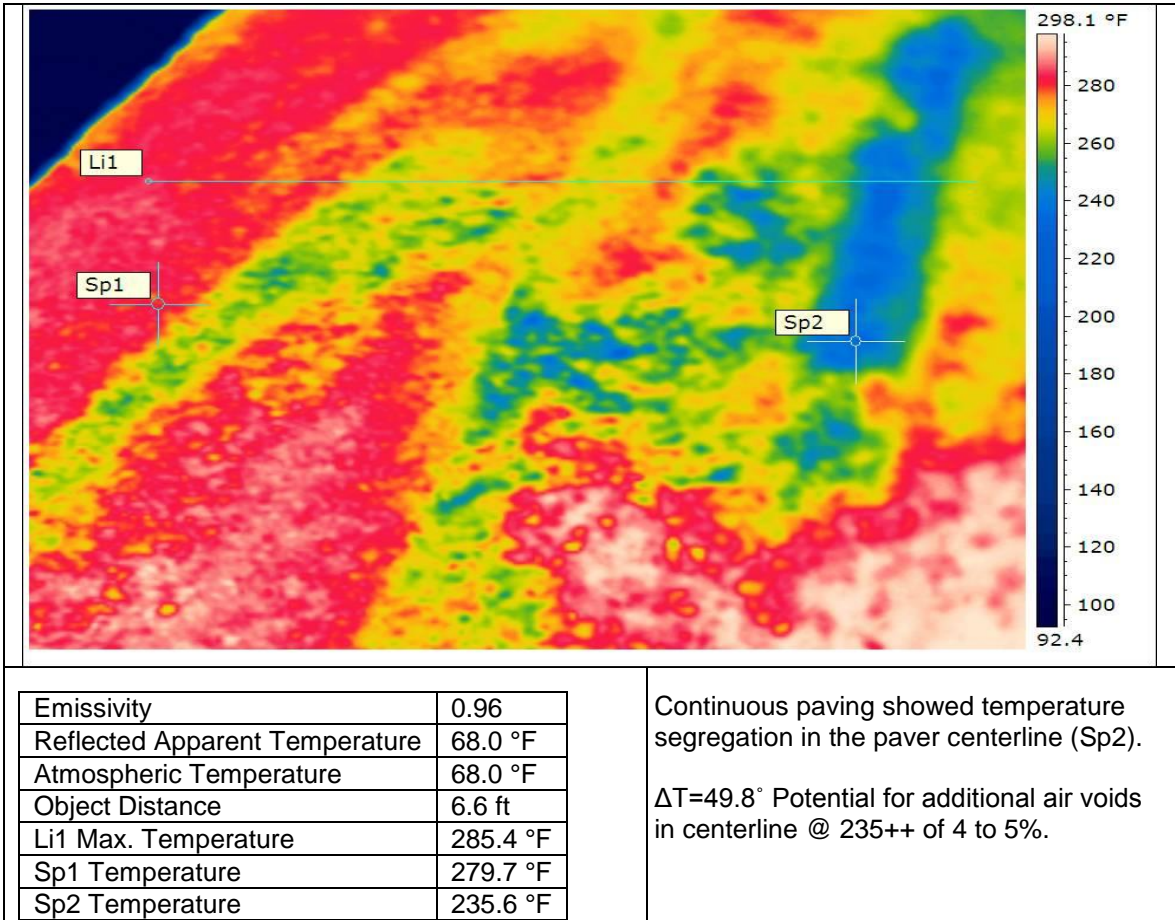


Figure 5.29 Station 235+00 Paver Screed (Image #2)

5.3.3 Station 230+00, 1200 ft into paving Research Test Segment

A comparison among measurements was conducted at Station 230+00 with summary results in Table 5.8. Thermal images to create the data from the truck box, paver hopper, and paver screed (left and right), are in respective Figures 5.30, 5.31, 5.32, and 5.33. Observational notes are provided with each figure to understand the process.

Table 5.8 Thermal Measurement comparison at Station 230+00

Measurement	Minimum, °F	Maximum, °F	Δ Temp., °F
Camera-Truck	159	315	167
Camera-Hopper	187	319	132
Camera-Screed left	261	302	41
Camera-Screed right	286	309	23
Sensors	293	315	22

There were slightly higher temperature readings behind the paver with the sensor bar than with the camera images. As before, the range was much higher with the camera since selective cooler and warmer points were sampled, while the sensors recorded at a fixed 26-in spacing.

The temperature variability reduction from the truck to the hopper decreased from 167°F to 132°F, a drop of 27%. The range was then reduced from 132°F in the hopper to 41°F the left side of the screed (controlling value), a reduction ratio of about 3.2-to-1, very similar to the previous two sampling locations. The overall temperature range reduction ratio from the truck box to the screed was about 4.1-to-1 (167°F to 41°F).

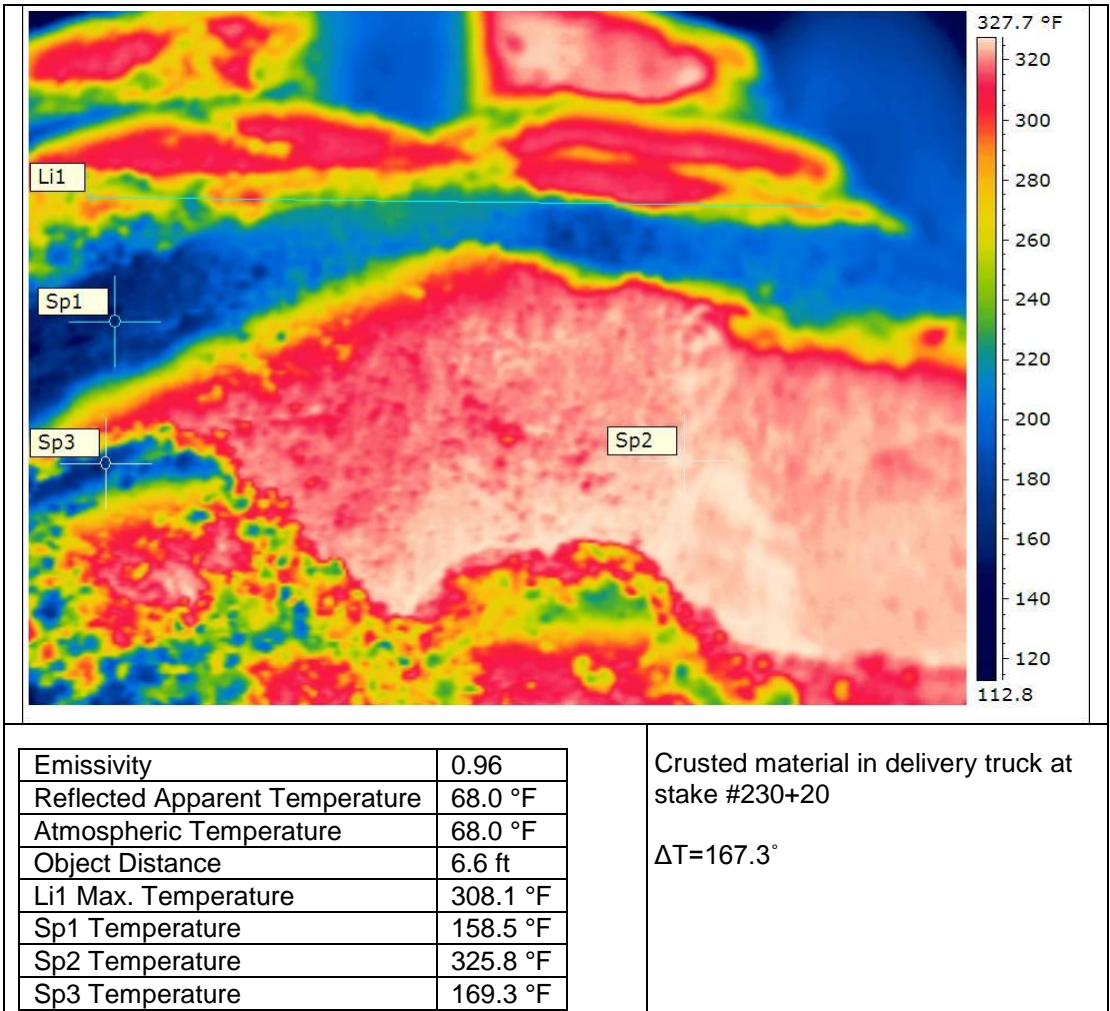


Figure 5.30 Station 230+00 Truck Box

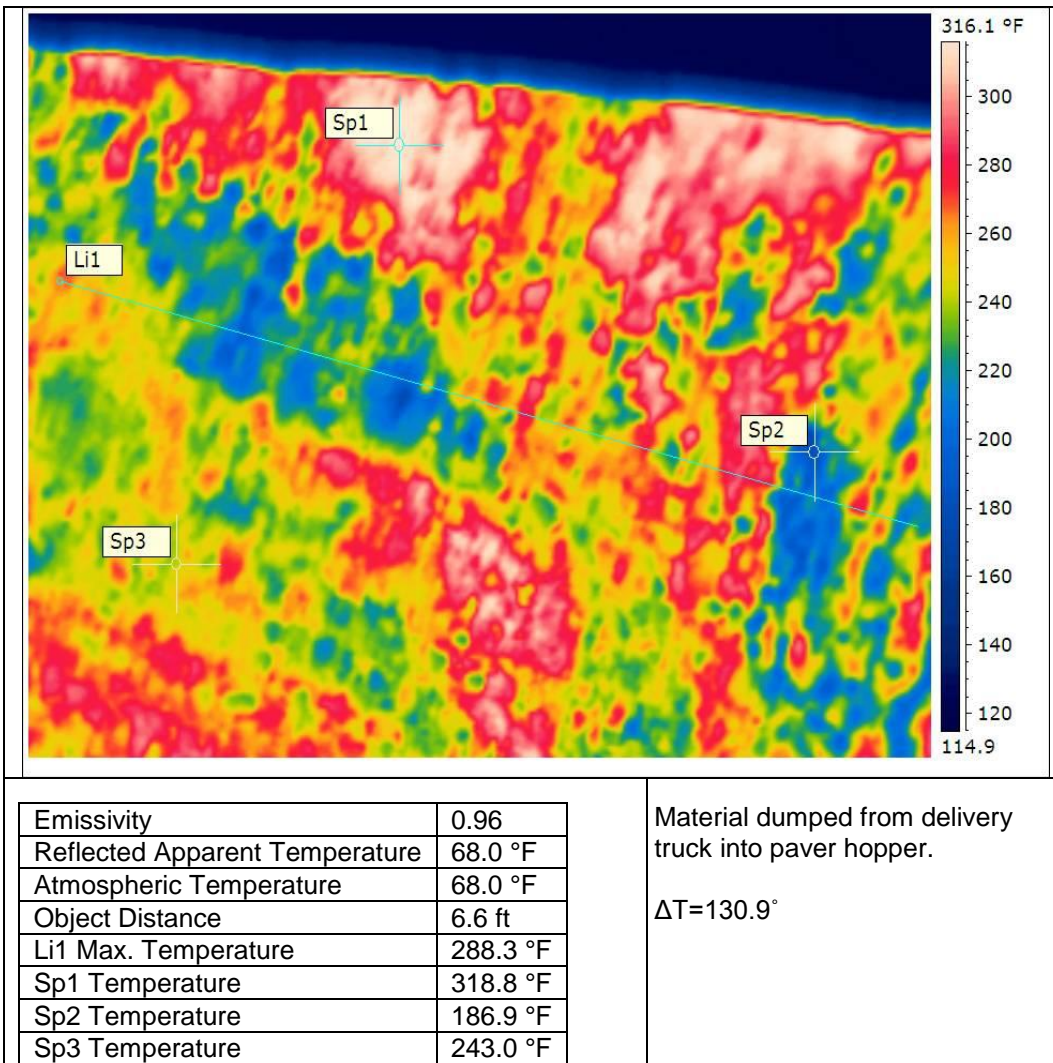
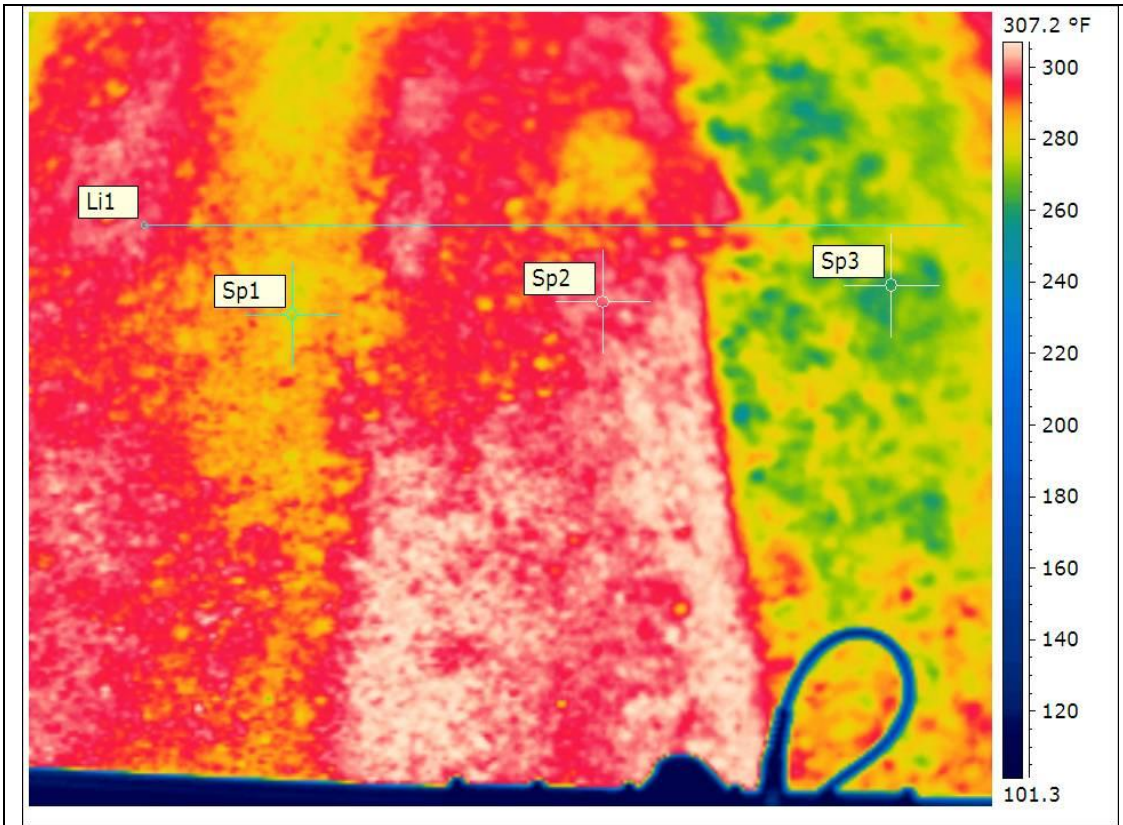


Figure 5.31 Station 230+00 Paver Hopper



Emissivity	0.96
Reflected Apparent Temperature	68.0 °F
Atmospheric Temperature	68.0 °F
Object Distance	6.6 ft
Li1 Max. Temperature	302.3 °F
Sp1 Temperature	274.5 °F
Sp2 Temperature	298.9 °F
Sp3 Temperature	261.4 °F

$\Delta T=40.9^\circ$ temperature segregation on the left side of the mat.

Texture difference from left screed extension. This is prior to mix design change and arrival of Roadtec Shuttle Buggy... At intersection

Figure 5.32 Station 230+00 Paver Screed (left side)

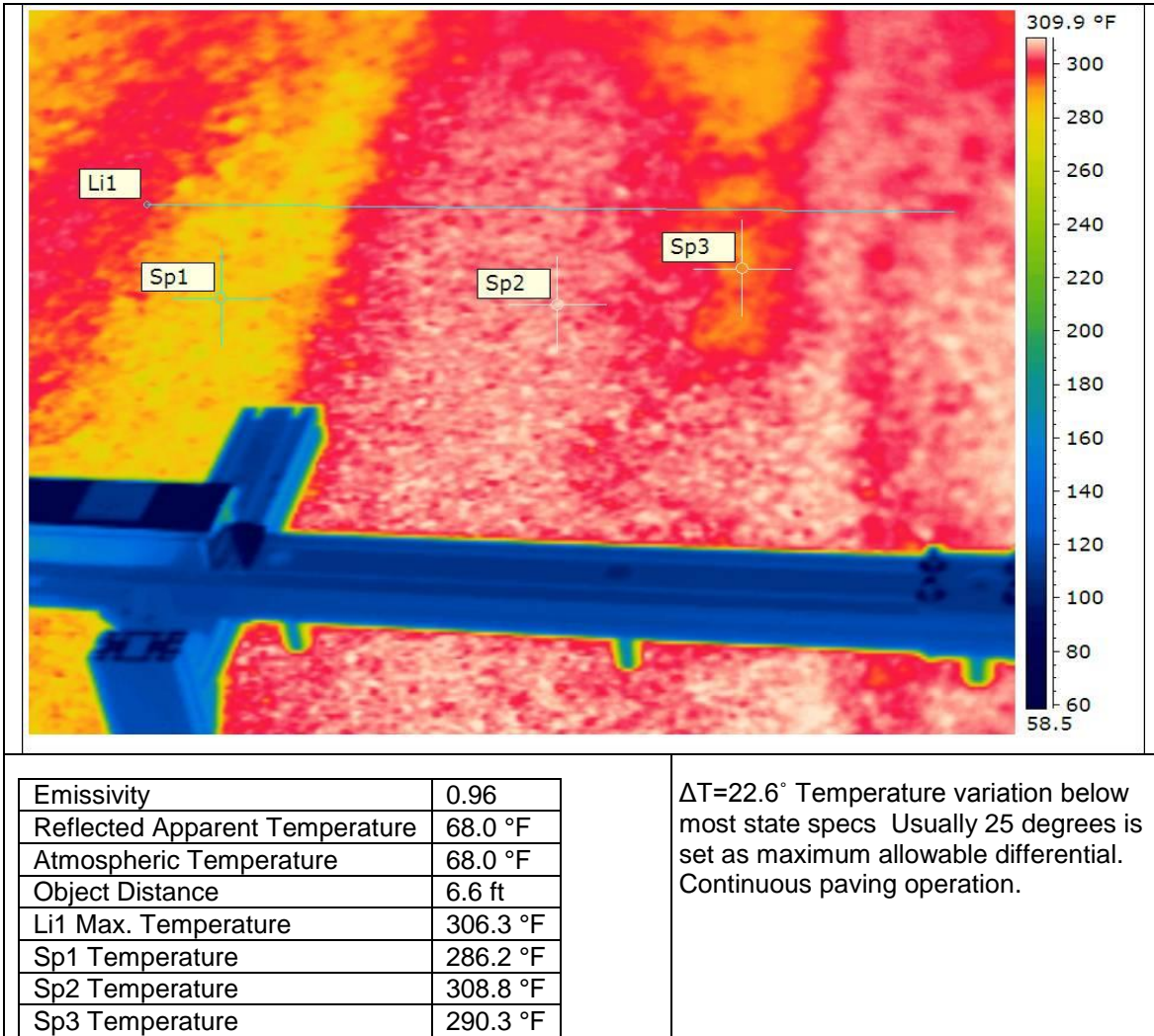


Figure 5.33 Station 230+00 Paver Screed (Right side)

5.3.4 Station 220+00, 2200 ft into paving Research Test Segment

A similar measurement comparison was conducted at Station 220+00 with summary results in Table 5.9. Thermal images to create the data from the truck box, paver hopper, and paver screed are shown in respective Figures 5.34, 5.35, and 5.36. Observational notes are provided with each figure to understand the process.

Table 5.9 Thermal Measurement comparison at Station 220+00

Measurement	Minimum, °F	Maximum, °F	Δ Temp., °F
Camera-Truck	195	306	111
Camera-Hopper	163	326	163
Camera-Screed	269	303	34
Sensors	293	315	22

The sensor measured a higher maximum value and lower range, very similar to the previous comparative locations. Again, the camera operator can choose the lowest and highest regions, or a line across the suspected differential region, while the sensors recorded at a fixed 26-in spacing.

The temperature range increased from the truck to the hopper from 111°F to 163°F, an increase of 52°F, or 47%. The reason for the increase may be explained by the ability to effectively sample the truck box and paver hopper, such as a given load of material or different sampling area. The temperature range was reduced from 163°F in the hopper to 34°F at the screed, a reduction ratio of about 4.8-to-1. The overall temperature range reduction ratio from the truck box to the screed was about 3.3-to-1 (111°F to 34°F).

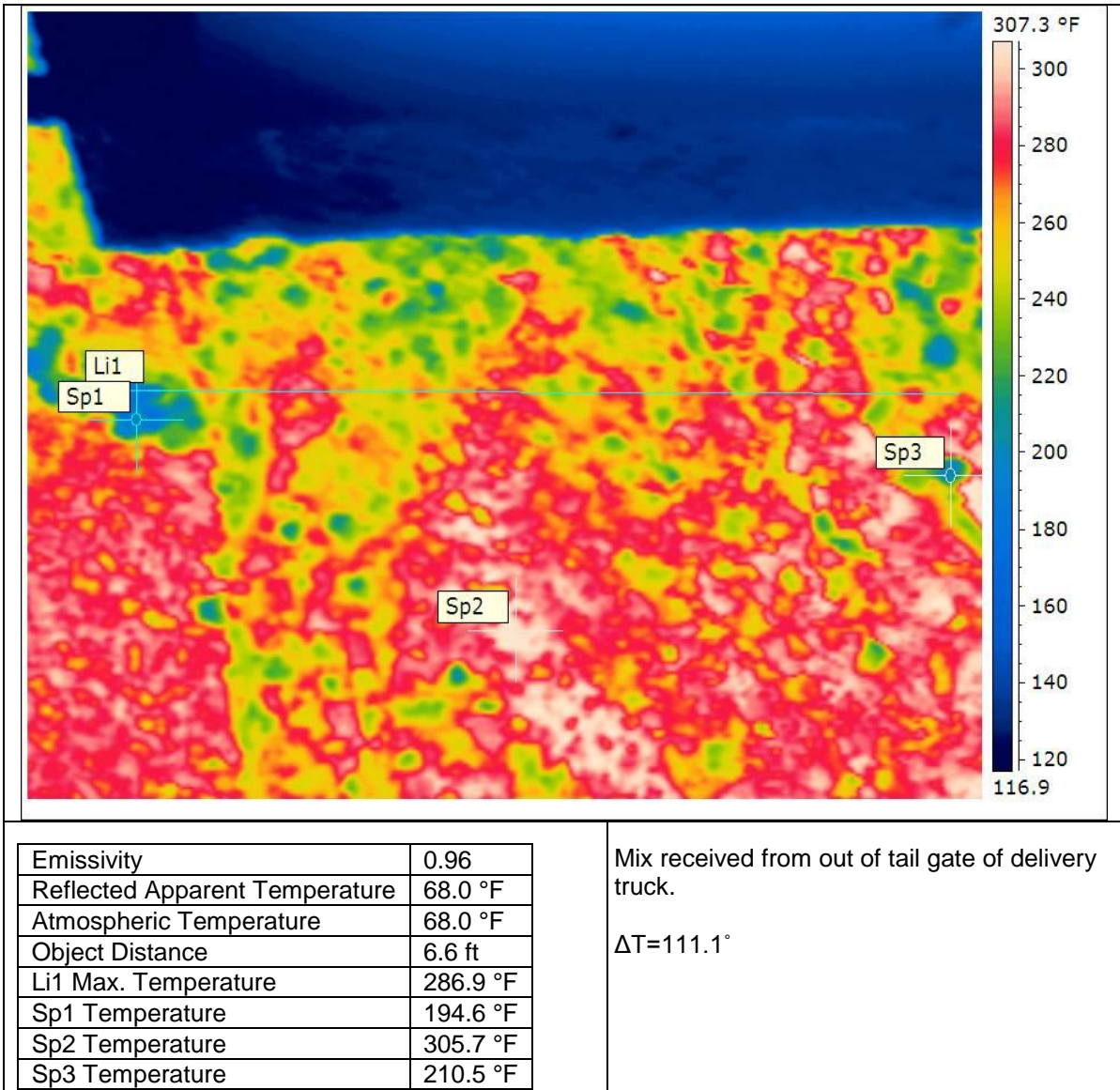


Figure 5.34 Station 220+00 Truck Box

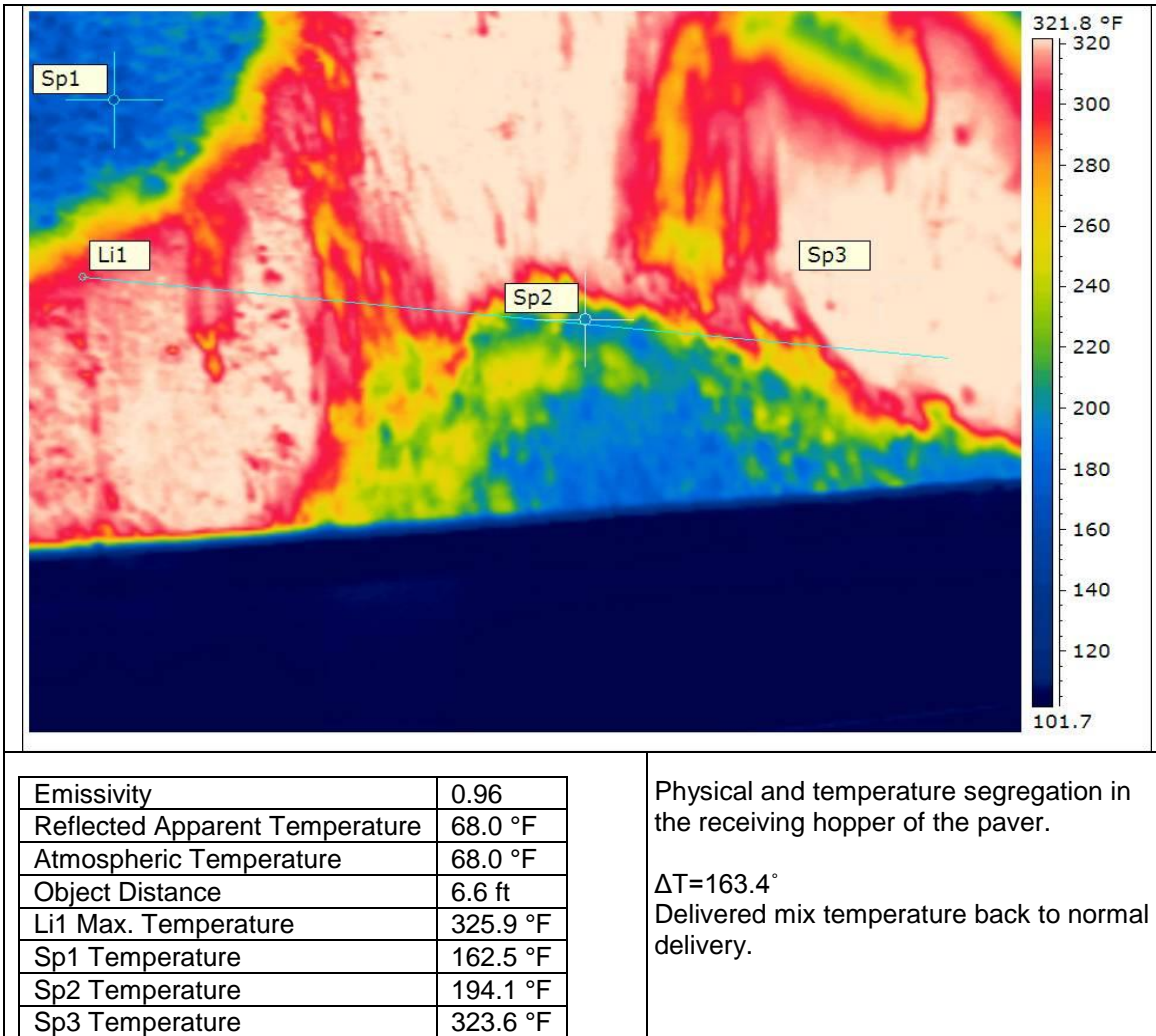


Figure 5.35 Station 220+00 Paver Hopper

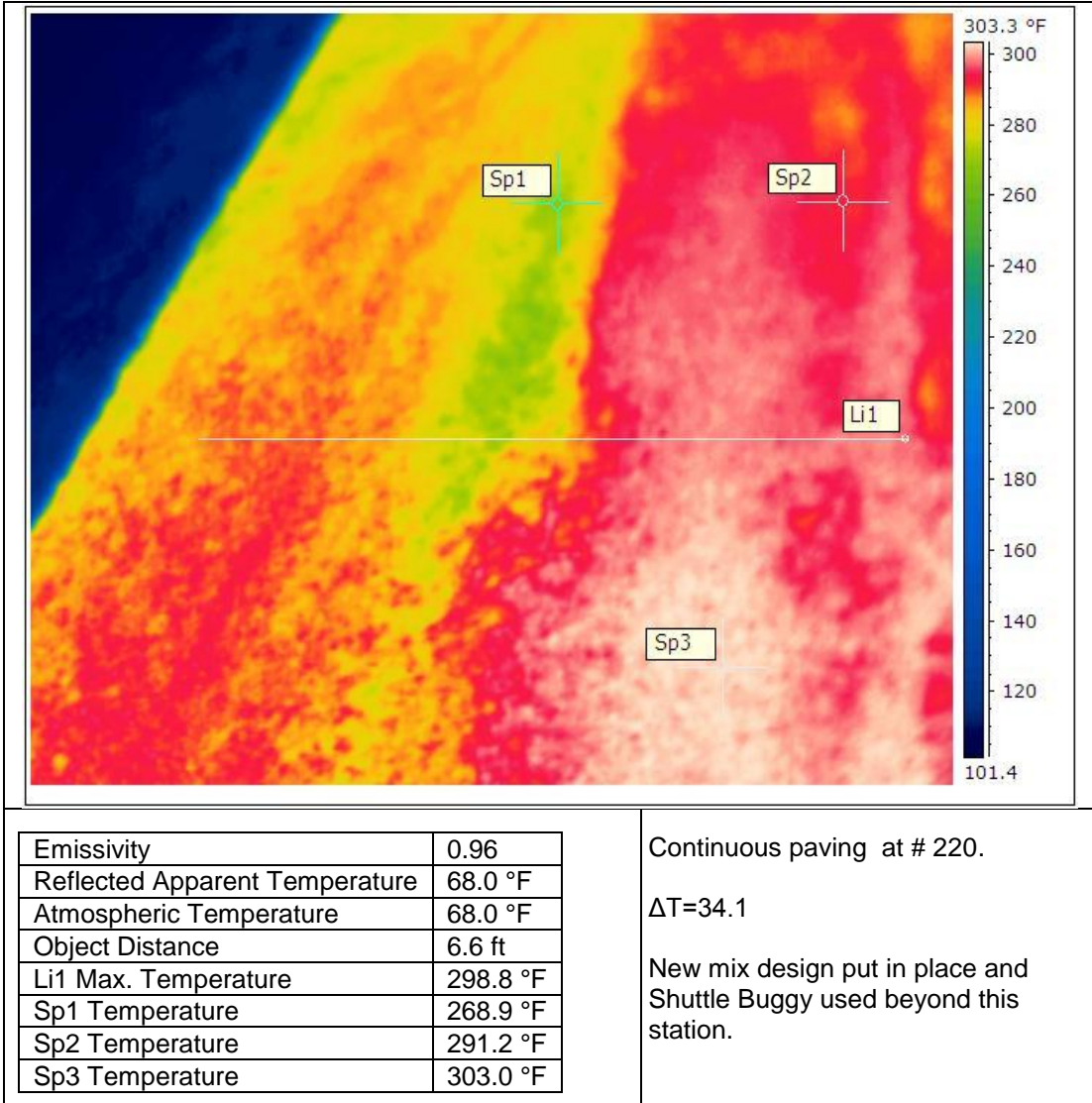


Figure 5.36 Station 220+00 Paver Screed

After Station 209+00 until the end of day, a material transfer vehicle was used to remix the asphalt from the truck to the paver. No thermal images were taken in the truck box, but one image was taken at the mat. Figure 5.37 measured a maximum range of 25°F. This indicates that the remixing operation was able to reduce final variability. This finding is further supported in earlier Tables 5.4 and 5.5.

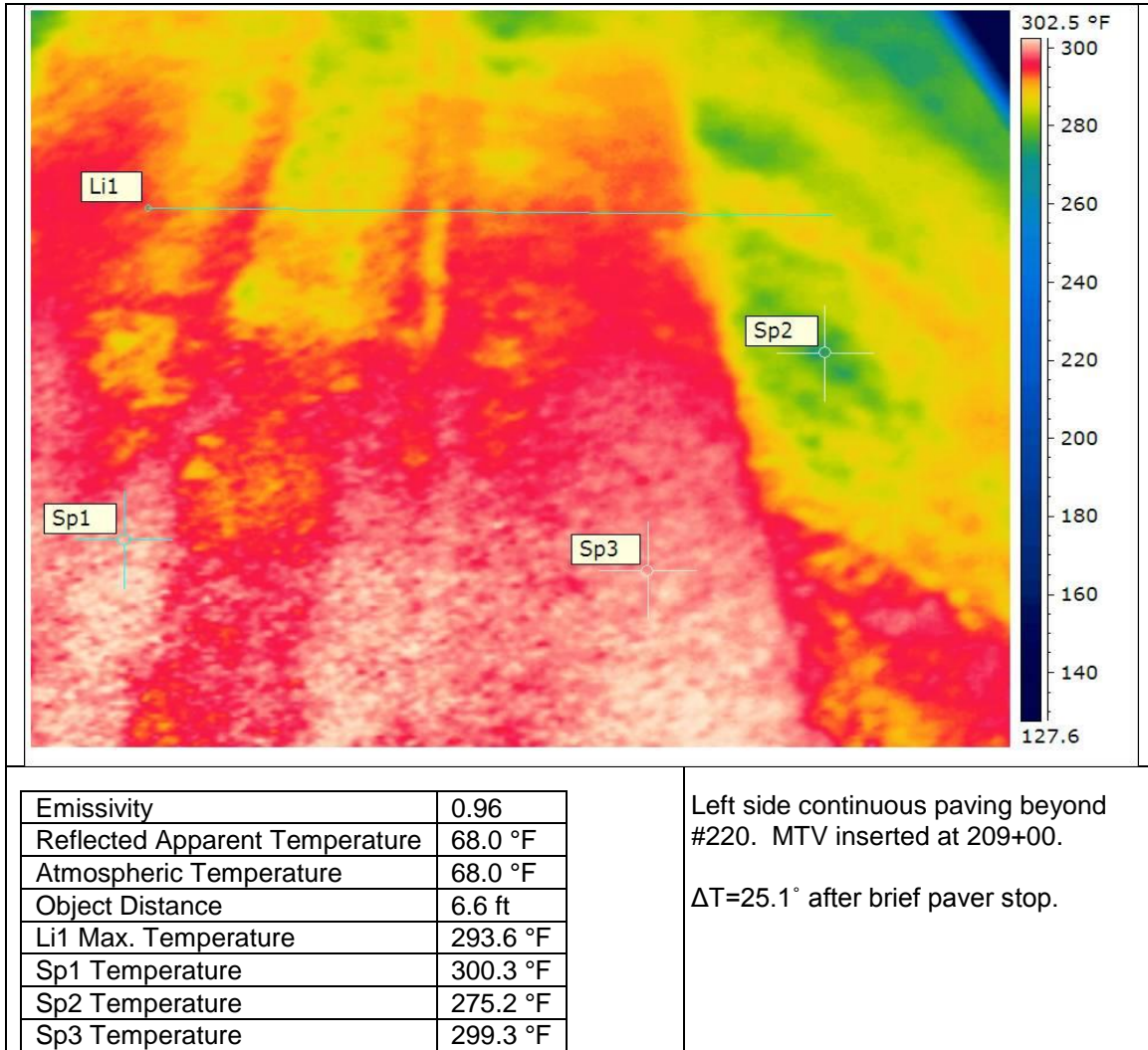


Figure 5.37 Station 209+00 Paver Screed (with MTV)

5.4 Project 3 Thermal Images

5.4.1 Stations 600+00 to 630+00

Paving was upstation with research testing beginning at 600+00 and ending at Station 660+00. Figures 5.38 through 5.40 illustrate the continuous temperatures behind the paver from Stations 604+00 to 632+00. This project included a material transfer vehicle between the truck box and paver hopper. Final surface layer paving consisted of a 15-ft wide, 1.75-in thick mat placed on a lower layer.

It is very apparent from these figures that the center-left and left side of the mat in direction of paving was much warmer. Data in the project summary statistics section in Chapter 4 reported higher average temperatures with Sensors 2, 5, and 6. Hand-held heat gun readings taken periodically during paving operation verified that these 3 sensors were out of calibration, and this particular Pave-IR hardware was sent back to the manufacturer after paving.

Aside from the out-of-calibration sensors, the figure illustrated end-of-truck segregation at an interval of about 135 ft. A 22-ton mix payload placed 1.75-in thick and 15-ft wide at compacted 150 lb/ft³ has a yield length of 135 ft. A distinct V-shaped pattern (light green) at intervals of 135 ft is slightly visible along the right side of the paver with cooler material spooling transversely as the paver moves forward longitudinally.

Paver movement was nearly continuous with no lengthy delays, so a speed diagram tab was selected to interpret paving rate. An initial rate of 30 ft/min was increased to a steady 40 ft/min rate.

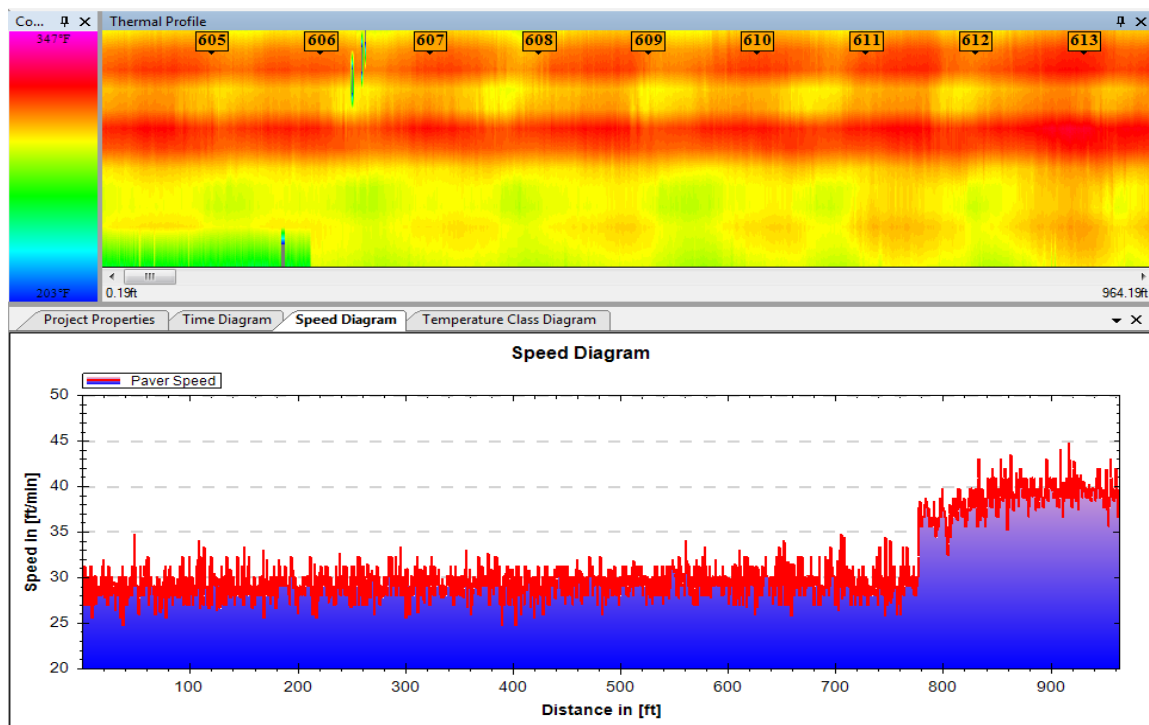


Figure 5.38 Pave-IR measurement from Station 604+00 to 613+00

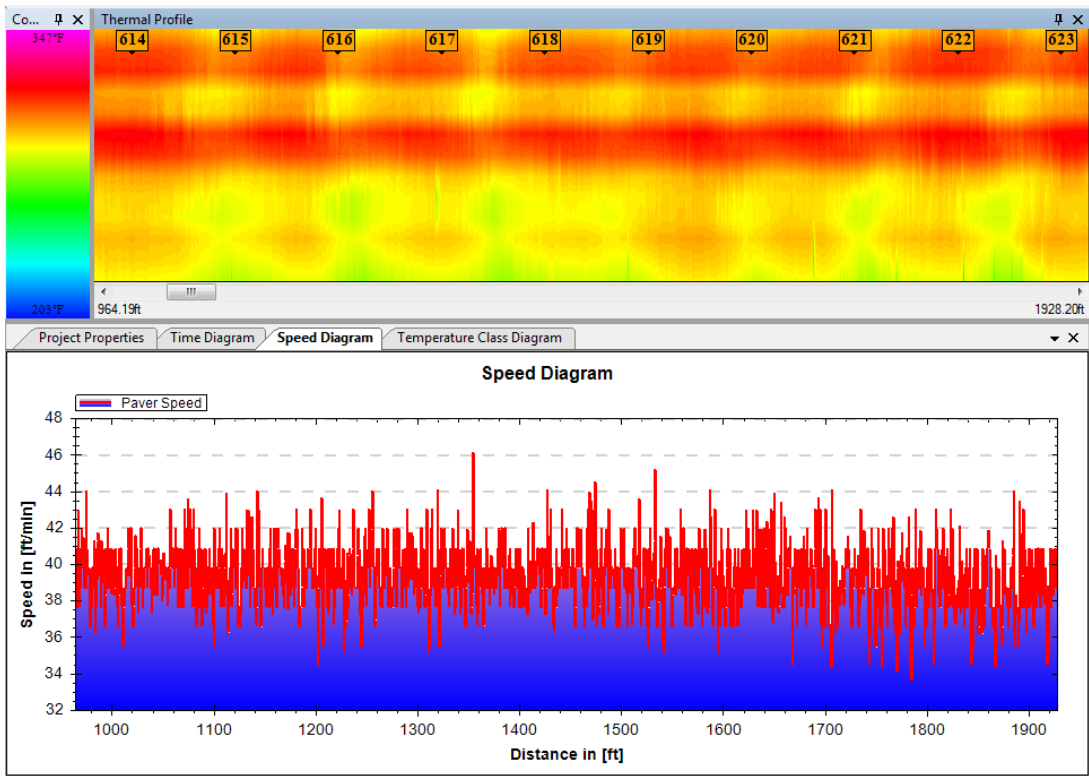


Figure 5.39 Pave-IR measurement from Station 614+00 to 623+00

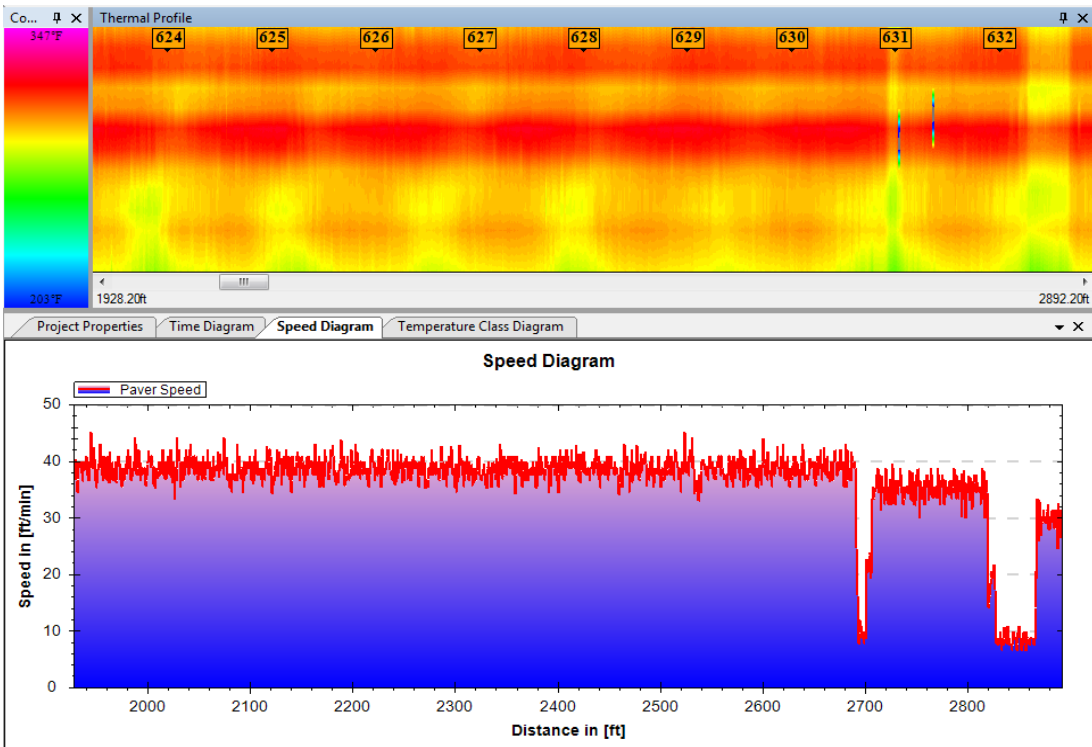


Figure 5.40 Pave-IR measurement from Station 624+00 to 632+00

A thermal measurement comparison was conducted at Station 628+00 with summary results in Table 5.10. Thermal images to create the data from the truck box and paver screed are shown in Figures 5.41 and 5.42, respectively. Images in the MTV were not possible.

Table 5.10 Thermal Measurement comparison at Station 628+00

Measurement	Minimum, °F	Maximum, °F	Δ Temp., °F
Camera-Truck	144	307	163
Camera-Screed	284	295	11
Sensors	287	328	41

The temperature range was reduced from 163°F in the truck box to 11°F at the screed, a reduction ratio of about 14.8-to-1. This ratio was over three times those values in the previous projects (3:1 to 4:1 ratios). The sensor measured a much higher maximum value and range than the camera image, largely due to the out-of-calibration sensors.

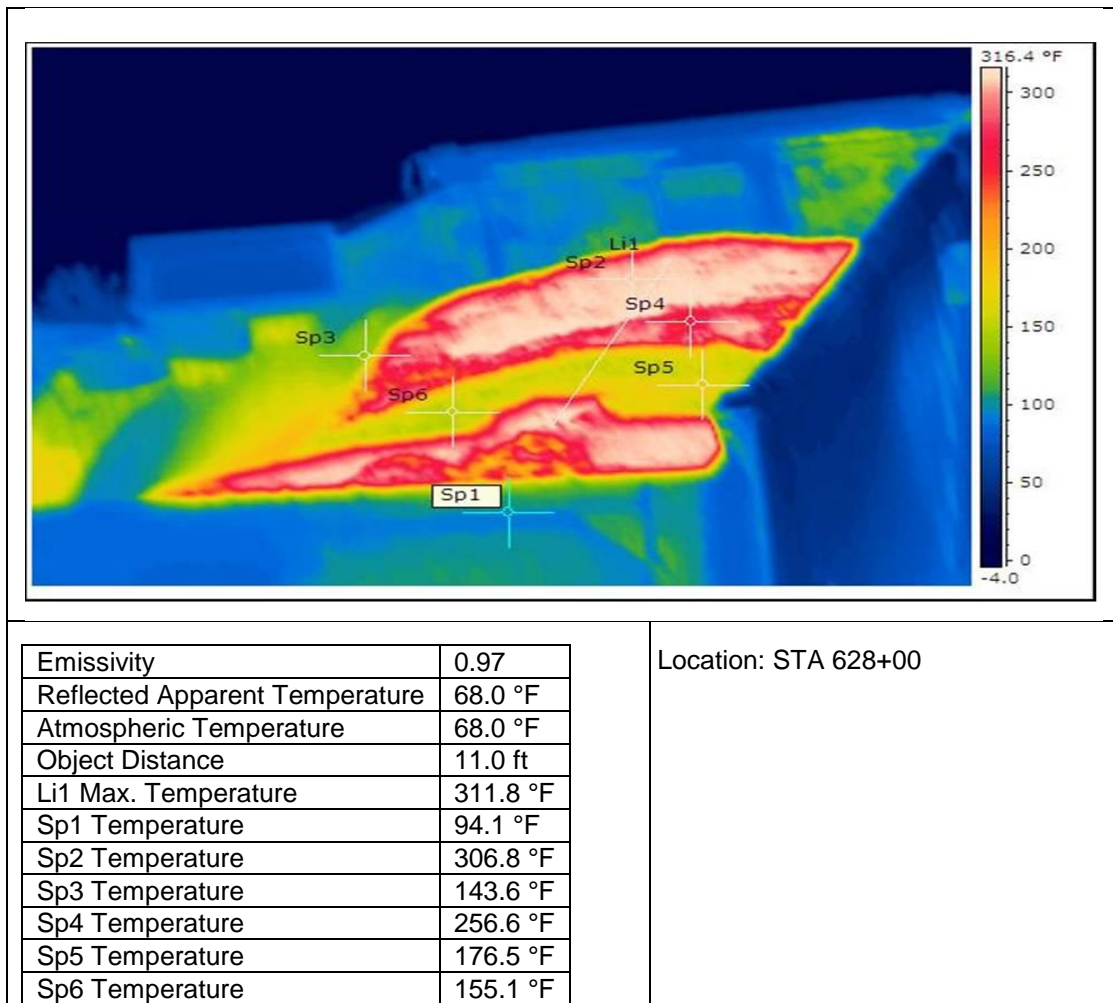


Figure 5.41 Station 628+00 Truck Box

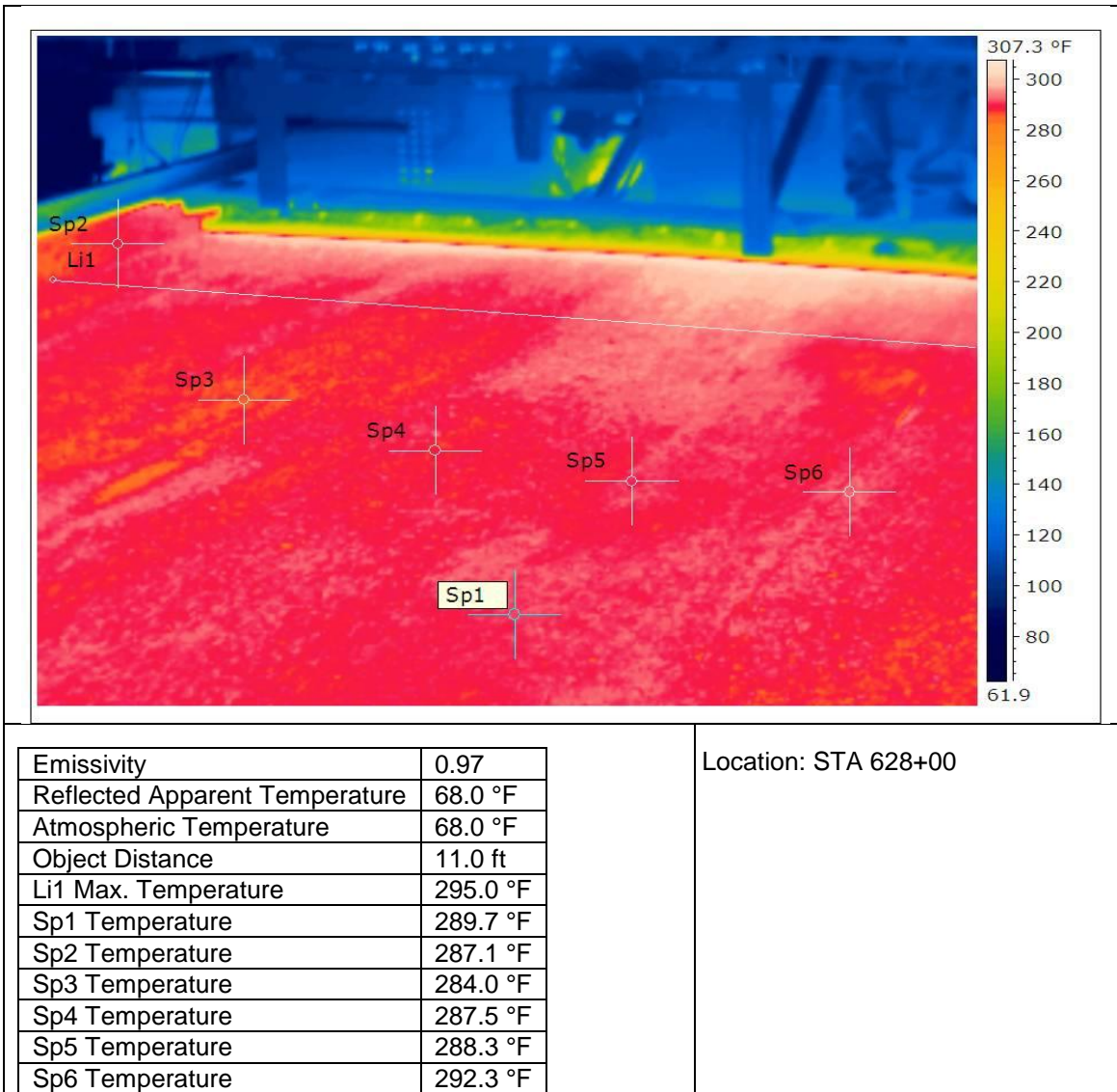


Figure 5.42 Station 628+00 Paver Screed

A measurement comparison between the sensors and image of the mat was conducted at Station 630+00 as shown in Table 5.11. The thermal image of the mat is shown in Figure 5.43. No images were taken in the truck box. The temperature range was 13°F at the screed, similar to 200 ft prior. The minimum and maximum readings were lower than Station 628+00, possibly explained by cooler end-of-truckload mix. The sensors again measured a much higher maximum value and range than the camera image due to the calibration bias.

Table 5.11 Thermal Measurement comparison at Station 630+00

Measurement	Minimum, °F	Maximum, °F	Δ Temp., °F
Camera-Screed	252	265	13
Sensors	287	325	38

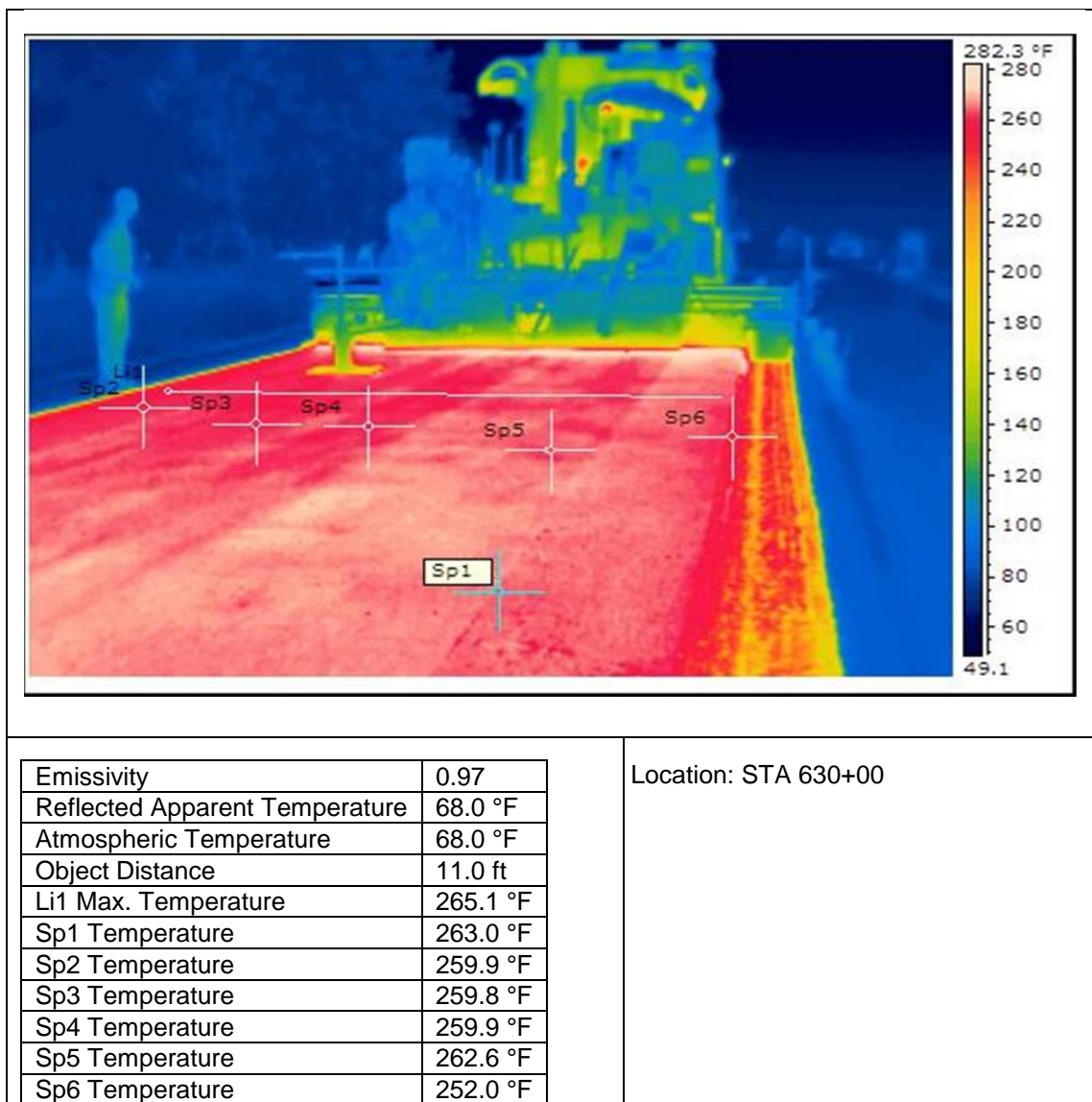


Figure 5.43 Station 630+00 Paver Screed

5.4.2 Stations 630+00 to 6??+00

Figures 5.44 through 5.46 illustrate the continuous temperatures behind the paver from Stations 634+00 to 661+00. These figures continue to illustrate the higher out-of-calibration sensors on the center-left and left side of the mat in direction of paving. The figures also illustrate end-of-truck cooler temperature segregation at an interval of about 135 ft. Paver rate generally fluctuated from 30 to 40 ft/min, with the exception of a few slower sections.

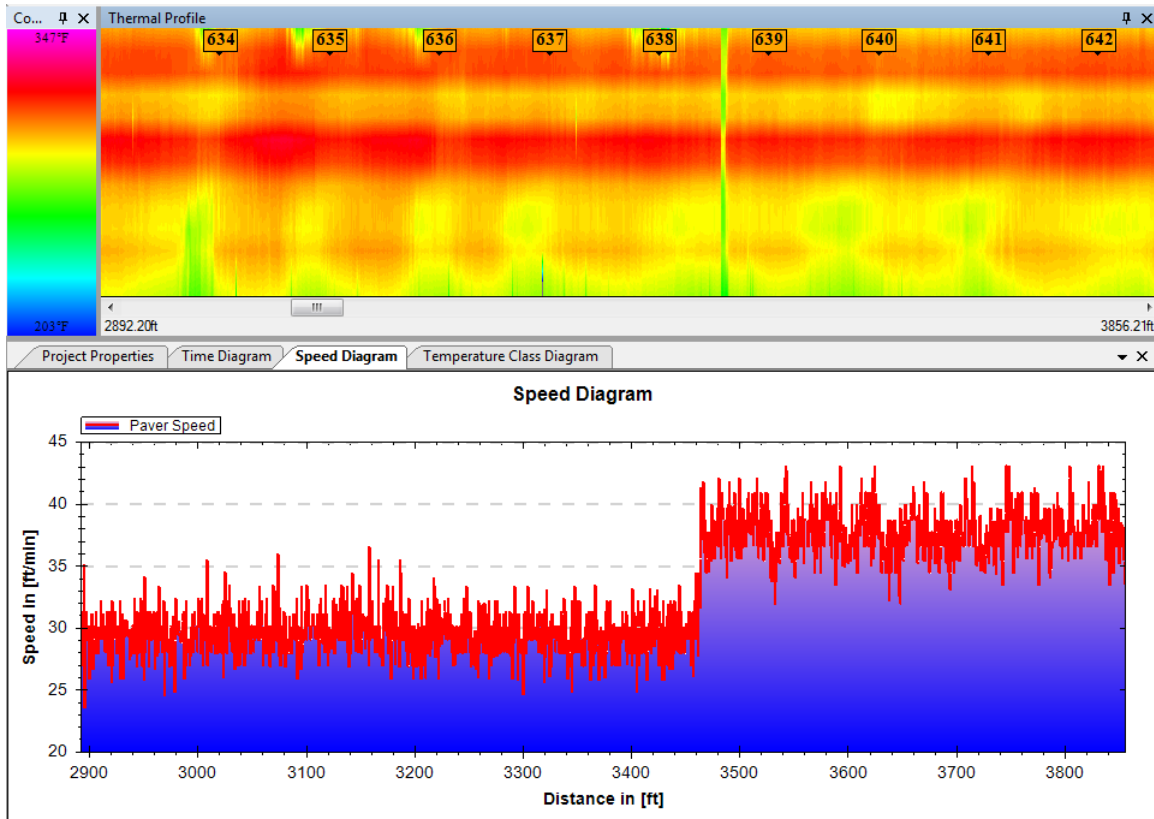


Figure 5.44 Pavement IR measurement from Station 634+00 to 642+00

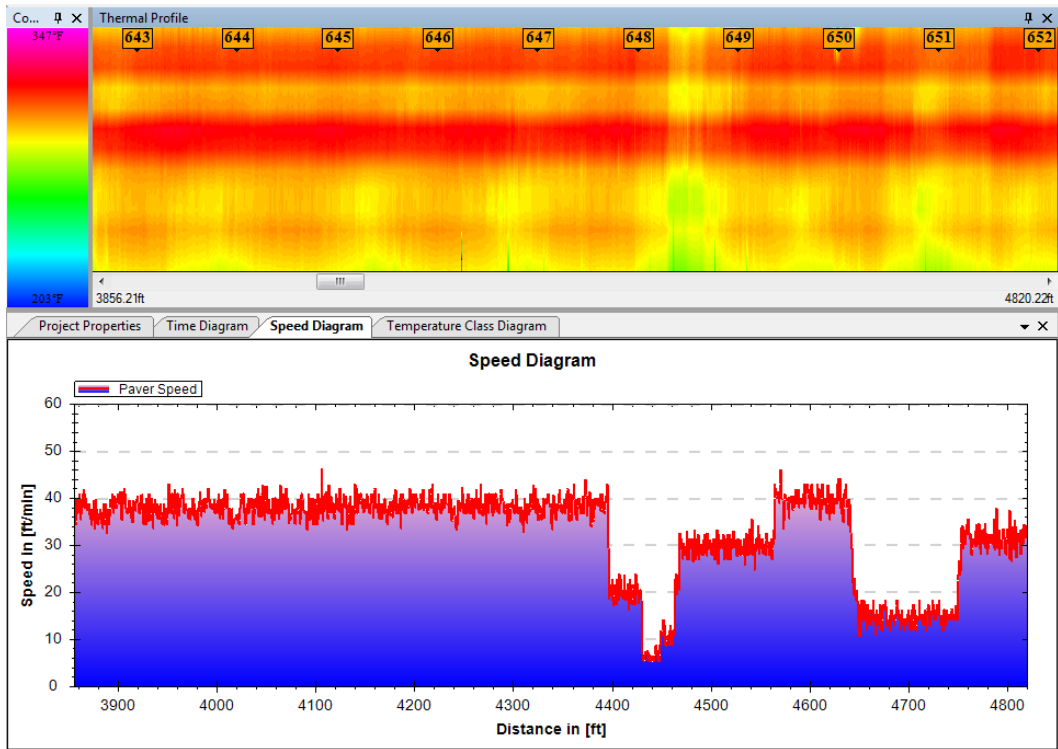


Figure 5.45 Pave-IR measurement from Station 643+00 to 652+00

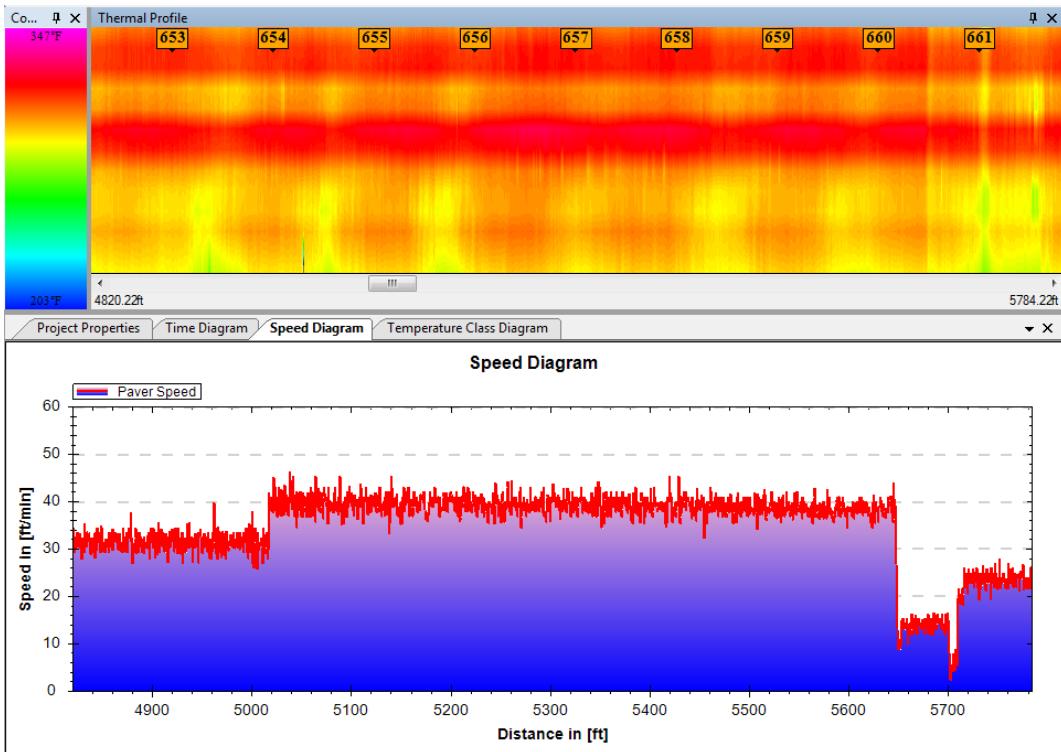


Figure 5.46 Pave-IR measurement from Station 653+00 to 661+00

A measurement comparison was conducted at Station 634+00 with results in Table 5.12. Here, thermal images were taken at the MTV discharge chute and at the paver screed shown in Figures 5.47 and 5.48, respectively.

Table 5.12 Thermal Measurement comparison at Station 634+00

Measurement	Minimum, °F	Maximum, °F	Δ Temp., °F
Camera-MTV Chute	144	307	163
Camera-Screed	284	295	11
Sensors	285	327	42

The temperature range at the discharge tremie exceeded 300°F, then ranged 9°F behind the paver from a high of 293°F and low of 284°F. This suggests a very consistent transverse temperature. The sensor measured a much higher maximum value and range than the camera image from out-of-calibration sensors.

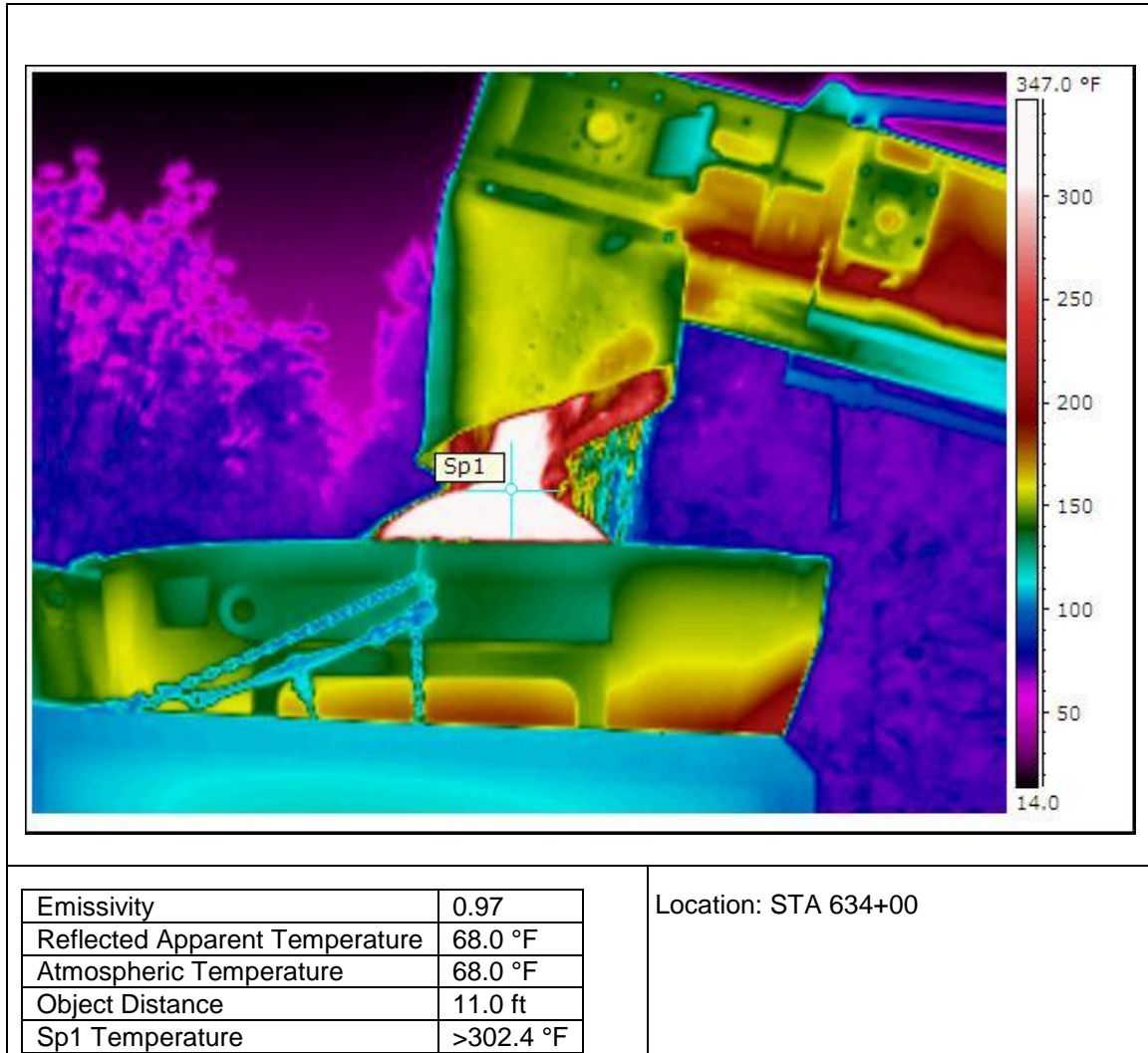


Figure 5.47 Station 634+00 MTV Discharge Chute

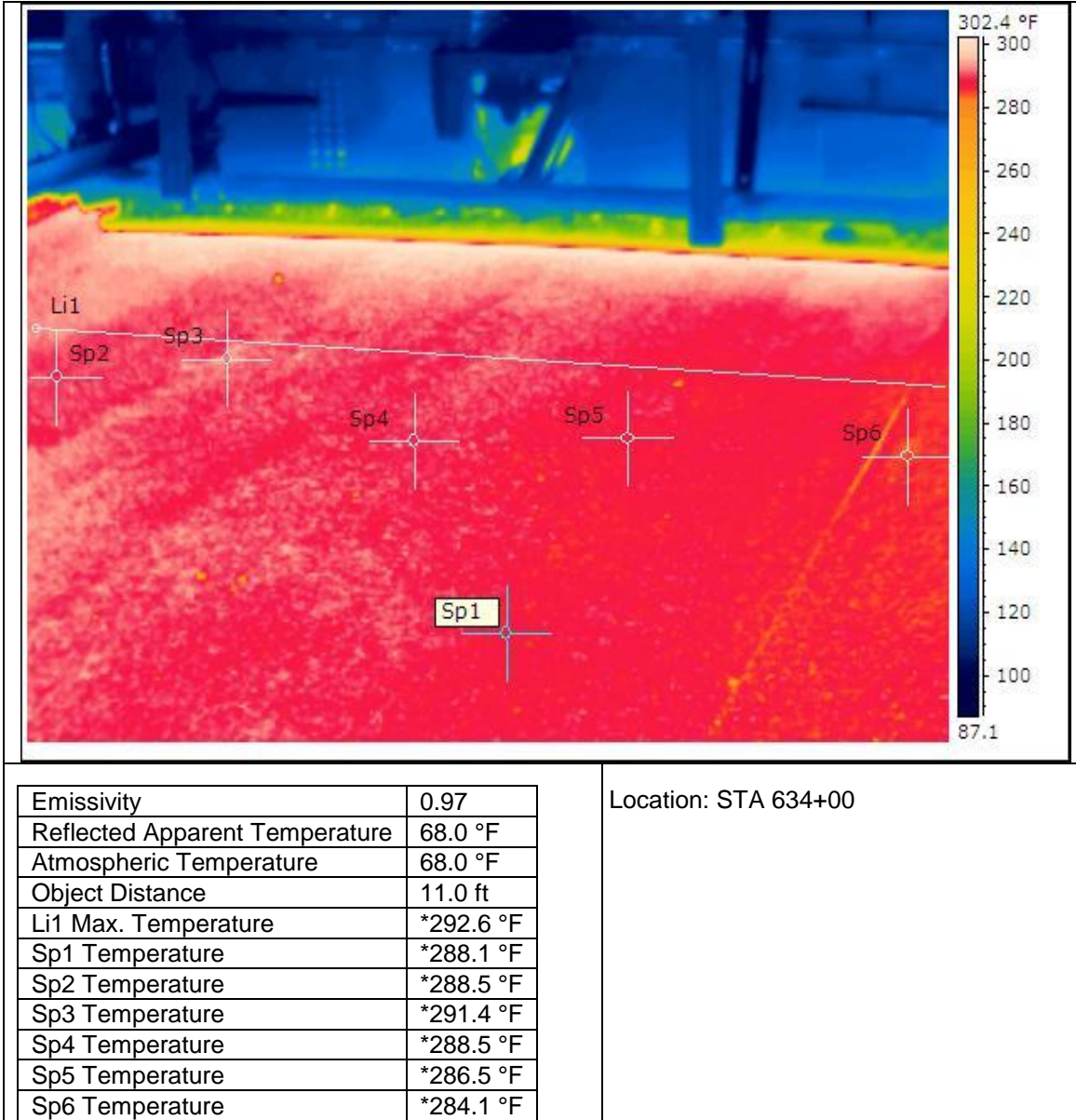


Figure 5.48 Station 634+00 Paver Screed

Comparison of temperature measurements was made at Station 637+50 with summary data in Table 5.13. Thermal images taken at the truck hopper and paver screed are shown in Figures 5.49 and 5.50, respectively. The temperature range was reduced from the truck box to paver screed by a reduction ratio of 10:1 (90°F to 9°F). This range is consistent with Stations 628+00 and 630+00. Again, the sensor measured a much higher maximum value and range than the camera image behind the paver.

Table 5.13 Thermal Measurement comparison at Station 637+50

Measurement	Minimum, °F	Maximum, °F	Δ Temp., °F
Camera-Truck	212	302	90
Camera-Screed	282	291	9
Sensors	288	329	41

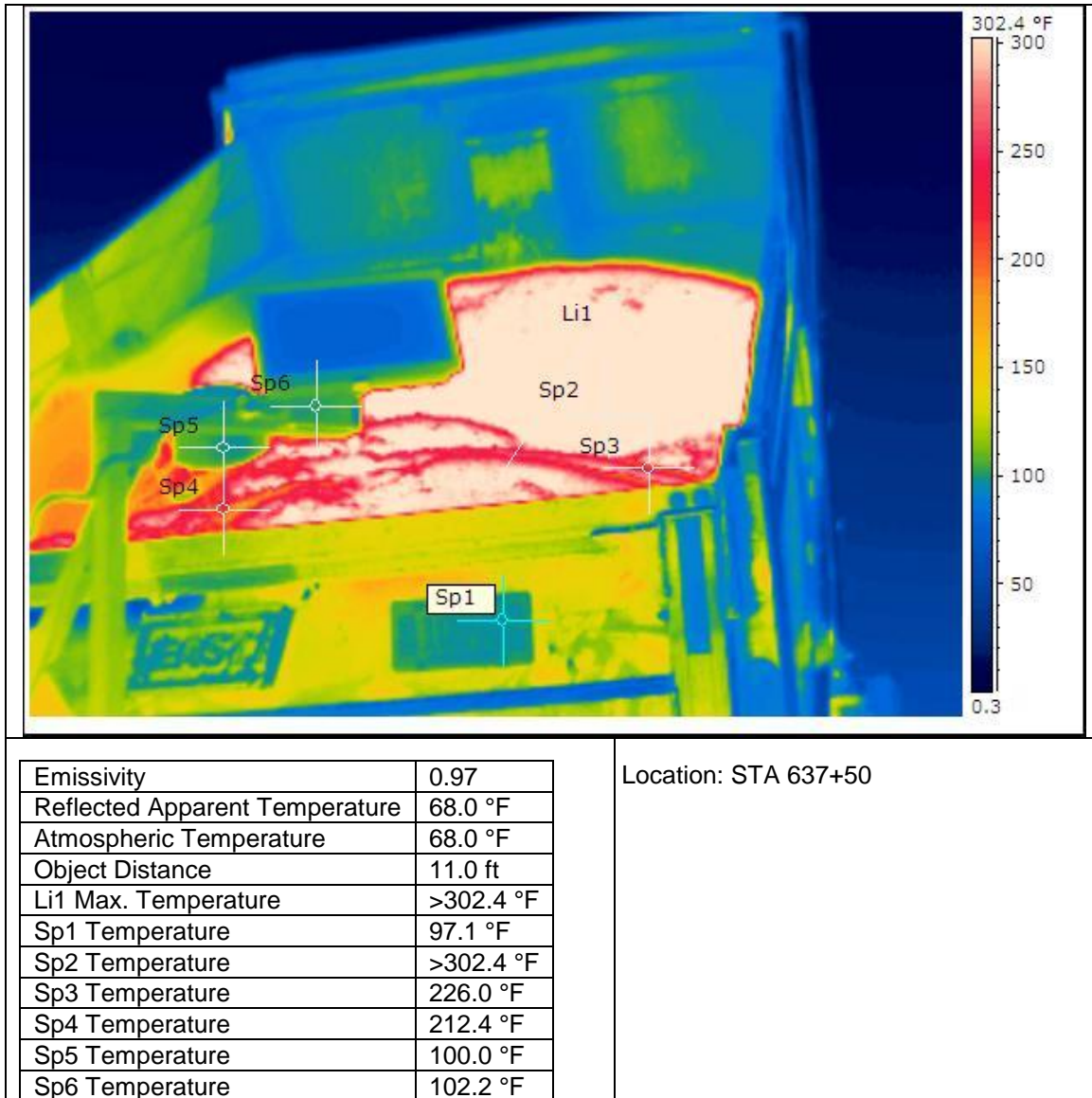


Figure 5.49 Station 637+50 Truck Box

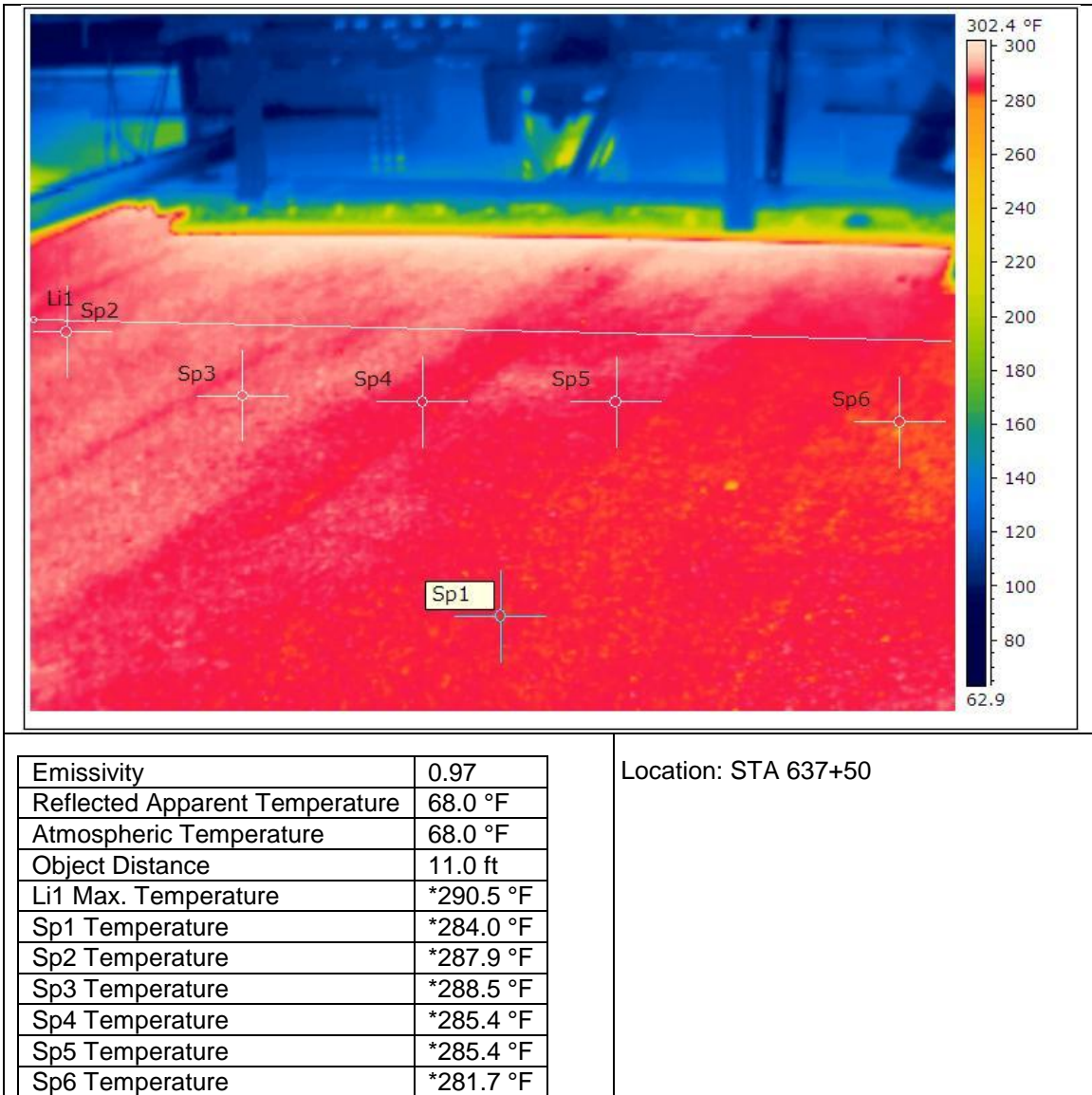


Figure 5.50 Station 637+50 Paver Screed

Additional mat-only thermal images were recorded beyond the research test section end point of 660+00 to evaluate consistency in the temperature range. Table 5.14 summarizes paving range temperatures behind the screed at Stations 673+00, 787+00, and 790+00, with images shown in Figures 5.51 through 5.53, respectively. The ranges were somewhat similar at Stations 673+00 and 787+00 at 8°F and 11°F, while 790+00 had a range of 16°F. The lower temperatures at 790+00 may be a between-truckload region.

Table 5.14 Thermal Image comparison at Stations 673, 787, and 790

Station	Measurement	Minimum, °F	Maximum, °F	Δ Temp., °F
673+00	Camera-Screed	286	294	8
787+00	Camera-Screed	281	292	11
790+00	Camera-Screed	266	282	16

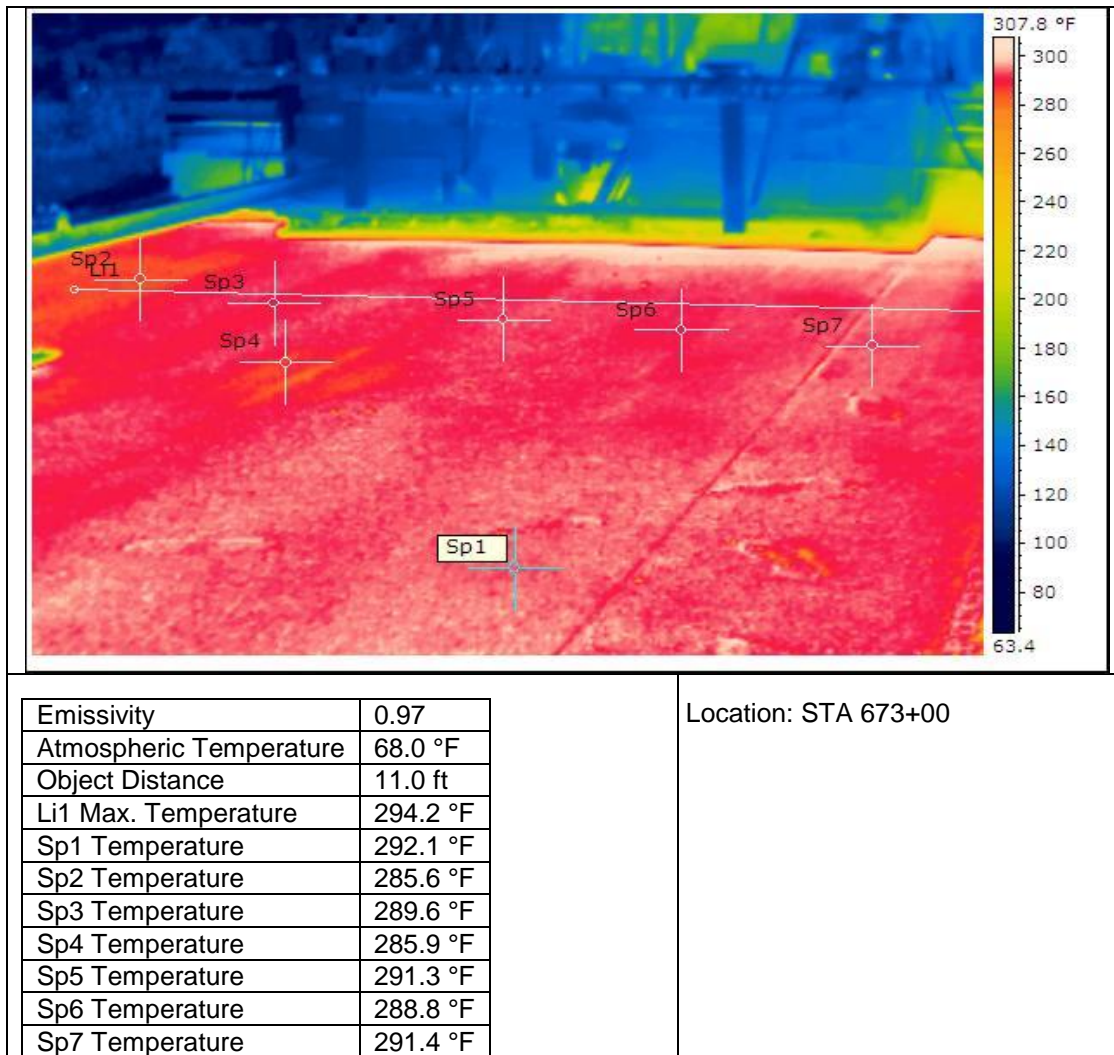


Figure 5.51 Station 673+00 Paver Screed

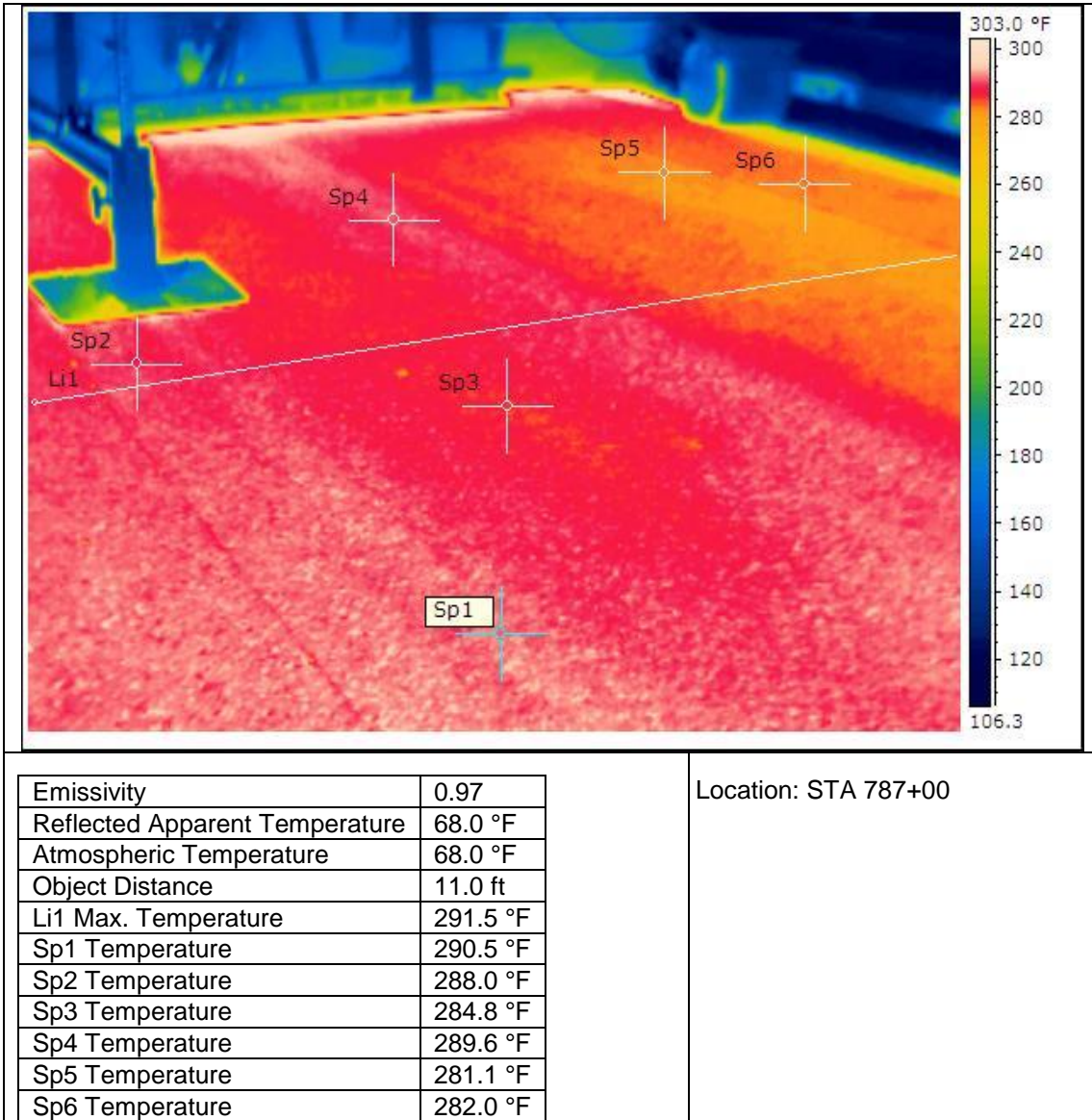
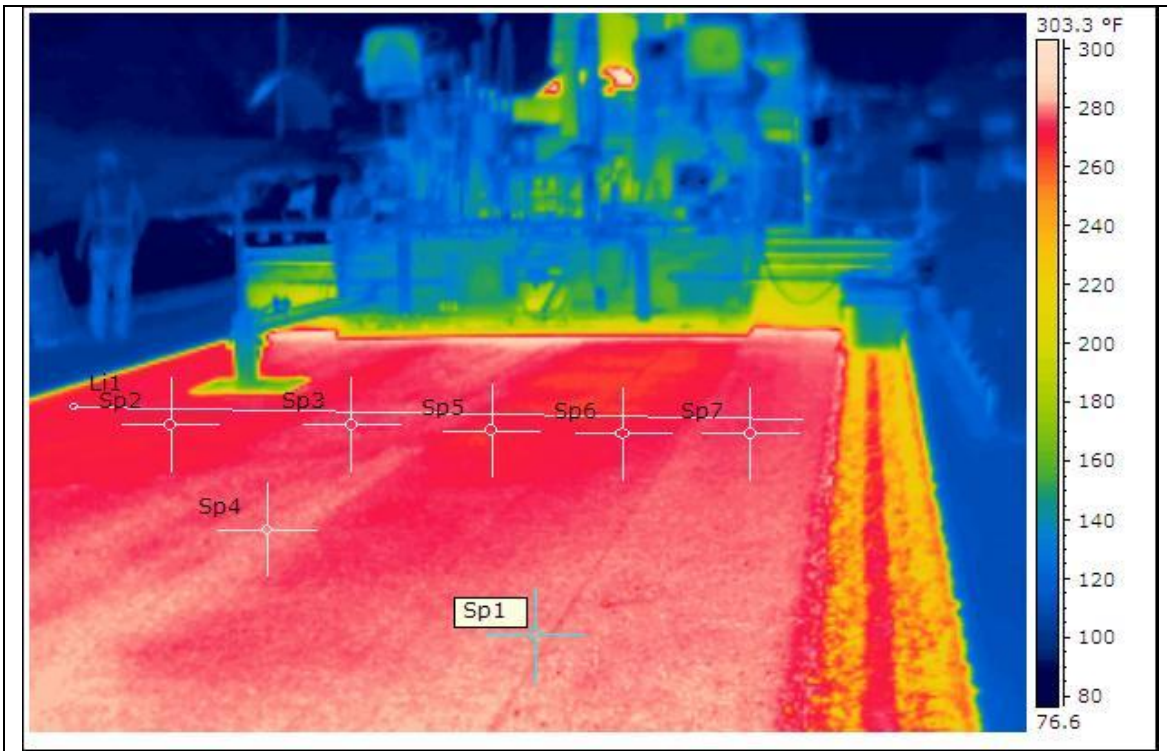


Figure 5.52 Station 787+00 Paver Screed



Emissivity	0.97	Location: STA 790+00
Reflected Apparent Temperature	68.0 °F	
Atmospheric Temperature	68.0 °F	
Object Distance	11.0 ft	
Li1 Max. Temperature	276.7 °F	
Sp1 Temperature	281.7 °F	
Sp2 Temperature	269.3 °F	
Sp3 Temperature	274.9 °F	
Sp4 Temperature	279.0 °F	
Sp5 Temperature	265.6 °F	
Sp6 Temperature	270.8 °F	
Sp7 Temperature	275.0 °F	

Figure 5.53 Station 790+00 Paver Screed

5.5 Comparison of Continuous Thermal and GPR Data

The previous section provided an analysis of thermal measurements using continuous readings with the Pave-IR system and point measures with the FLIR thermal imaging camera. In this section, the continuous Pave-IR readings are compared with the continuous GPR readings. The purpose was to determine if there was a change in GPR density with cooler and warmer locations on the mat, and to investigate whether these two NDT technologies used in parallel could demonstrate potential as quality control and acceptance tools.

IR sensor data were plotted against GPR densities at the closest centerline offset. Plots for the entire project length and select subplot groupings were prepared. The entire project length contains 5,000 to 6,000 comparison points, while subplots had 500 data points. Simple plots were created for each project in the following sections to provide a visual comparison.

5.5.1 Project 1, IR and GPR Comparison

As reported earlier, a difficulty with the Project 1 data was the bias in distance measurement instruments (DMI) between the paver and project stationing lathe. Initial data points among the IR and GPR may have been in a direct alignment, but there is lack of comparative data to accurately adjust subsequent locations. Thus, the data locations are unadjusted.

Figures 5.54 and 5.55 present data from the entire project length for offsets of approximately 2 ft and 6 ft, respectively. Approximately 100 points were excluded from the figures having lower 90°F temperature to provide better resolution on the remaining points. Both plots have a substantial clustering of points in the temperature range of 230°F to 260°F. The best-fit line, with a weak R^2 value, detects that higher IR temperatures led to lower densities. Statistics in Chapter 4 measured higher temperature variability closer to the longitudinal joint, and despite this variability, the trends are counter to what would be expected on a typical project.

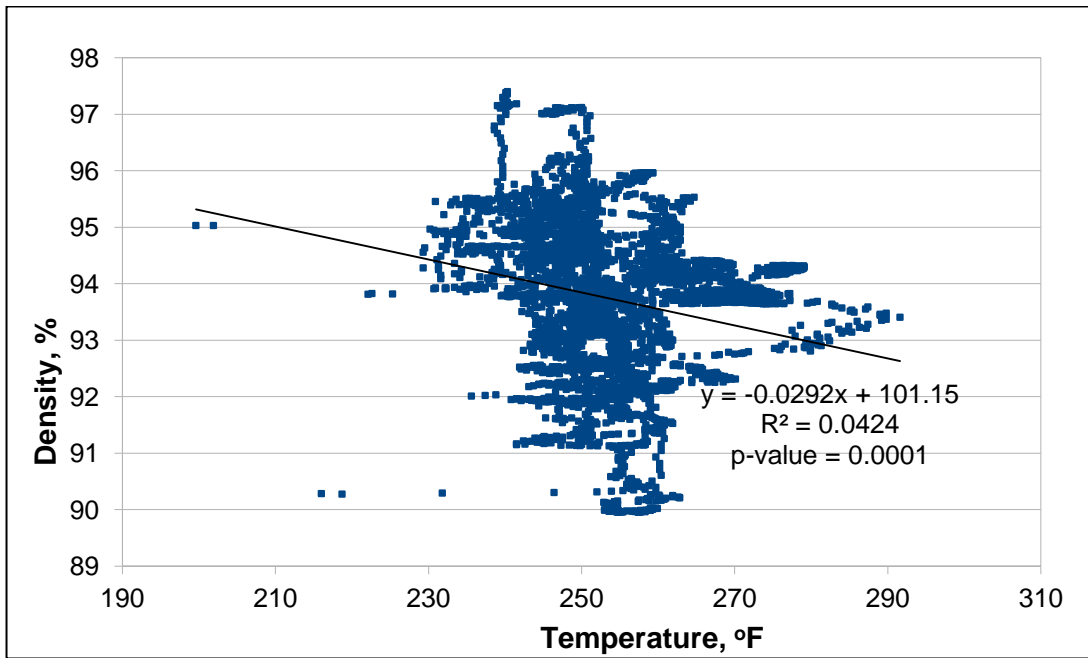


Figure 5.54 IR Temperature (2.1 ft) and GPR Density (2.5 ft) Project 1, Full Length

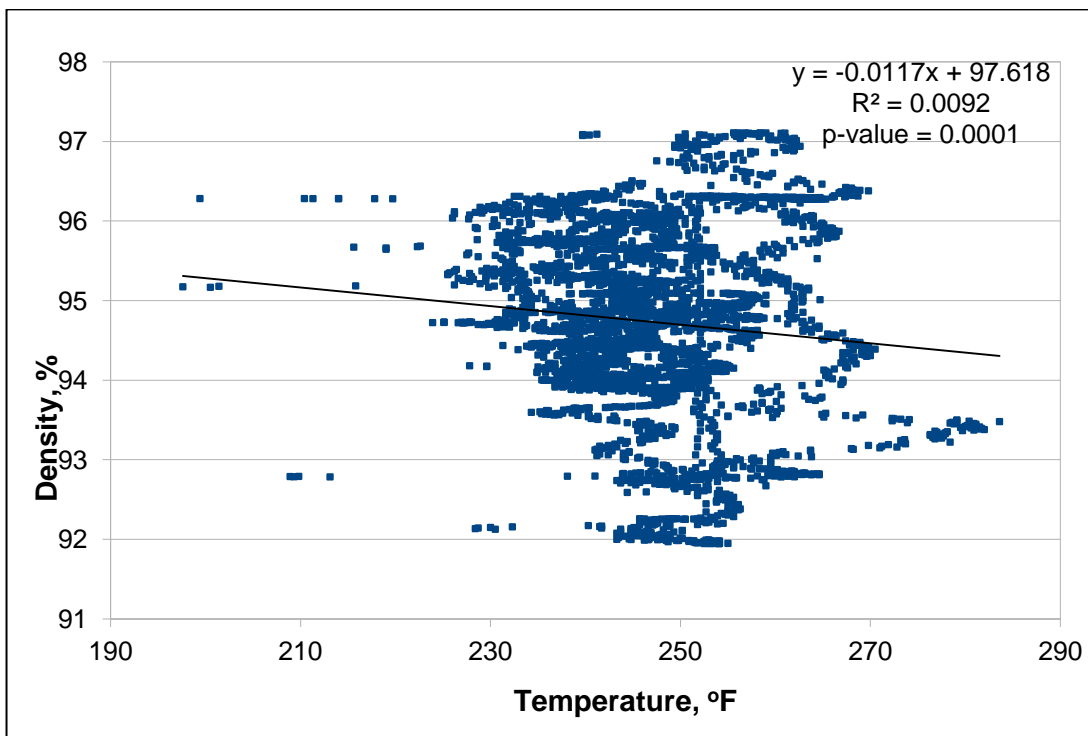


Figure 5.55 IR Temperature (6.4 ft) and GPR Density (6 ft) Project 1, Full Length

Figures 5.56 and 5.57 plot the IR and GPR data from the first 500 ft length of research testing for offsets of approximately 2 ft and 6 ft, respectively. Similar to the full length research data, there is some indication of a trend towards higher temperatures resulting in lower densities. The 2.5-ft offset had no clear visible trend with a scatter of points in the mid-temperature range, while the the 6-ft offset had a strong trendline higher temperatures having lower density, again, opposite of what would be expected.

Previous research pertaining to the ability to achieve field density has determined that number of passes is one of the most significant factors (Schmitt et al. 2009). The data set collected for this study did not include measurement of passes, as well as vibratory setting and roller type. A future experiment will want to incorporate all measures to create a holistic picture of variable influence. Thus, the IR temperature versus GPR density plots indicate no positive relationship between cooler temperatures and lower GPR densities, but rather higher temperatures generally resulted in lower GPR densities (not accounting for other factors).

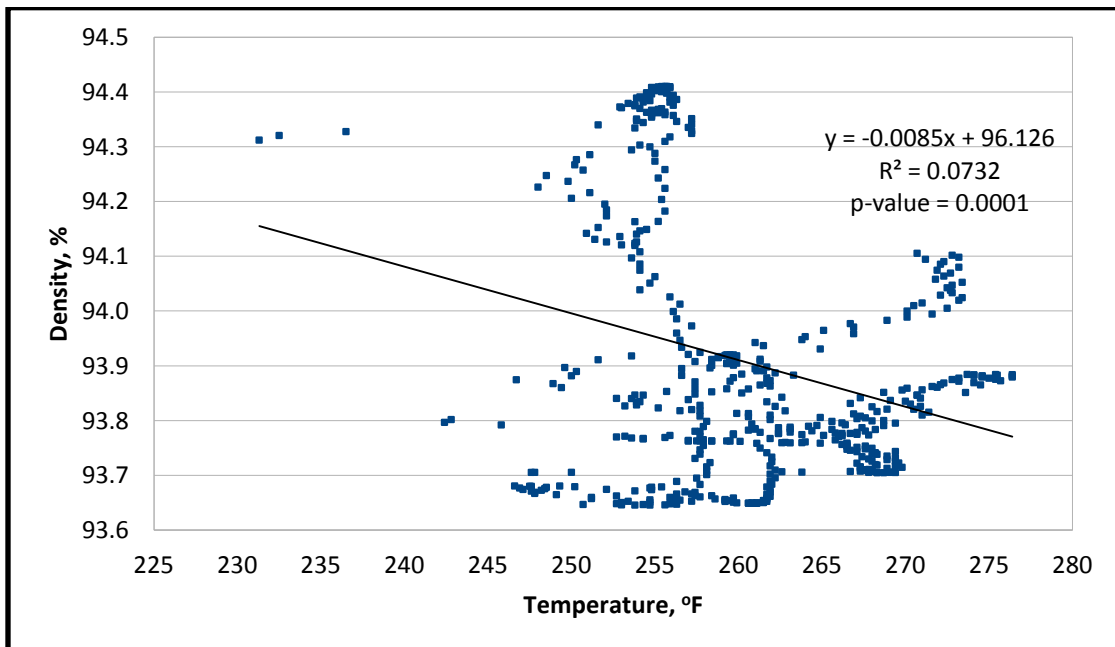


Figure 5.56 IR Temperature (2.1 ft) and GPR Density (2.5 ft) Project 1, Sublot 1

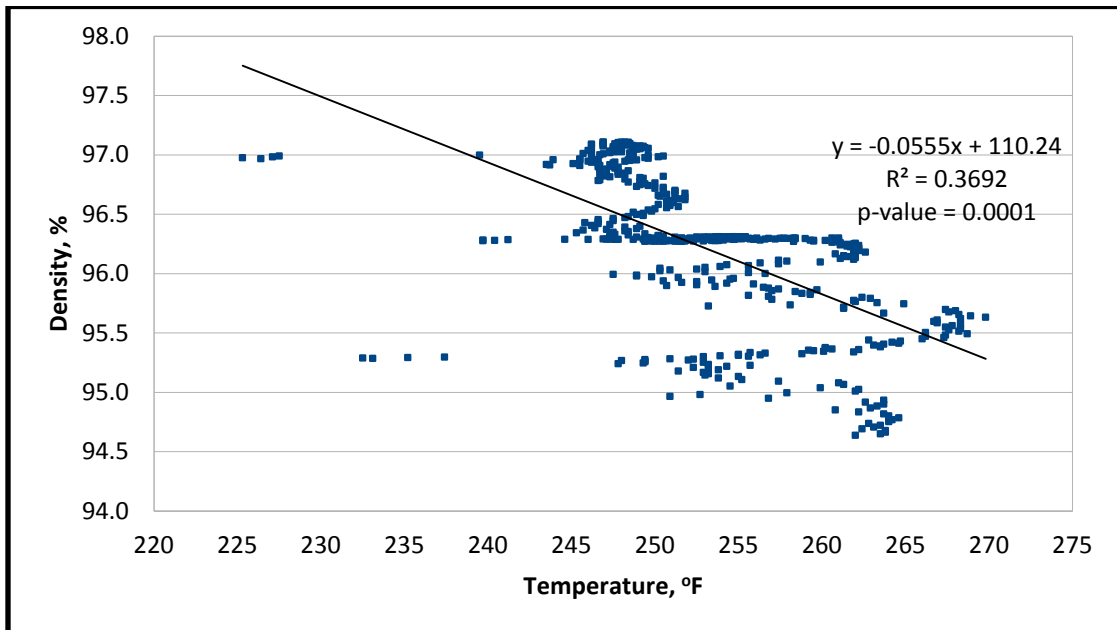


Figure 5.57 IR Temperature (6.4 ft) and GPR Density (6 ft) Project 1, Sublot 1

5.5.2 Project 2, IR and GPR Comparison

Unlike the first project, the IR and GPR distance measurement instruments (DMI) were in close agreement. Each was verified against project stationing lathe to ensure accuracy. During GPR traces, the offset was checked every 1,000 ft, and any disagreement was limited to 10 ft.

Figures 5.58 and 5.59 plot the IR and GPR data from the full 5,000 ft length of research testing for offsets of approximately 9 ft and 11 ft, respectively. With a grouping of nearly 5,000 data points per figure, there was no clear trend emerging from the plots with regards to a connection between temperatures at the time of paving and the final density measured by the GPR.

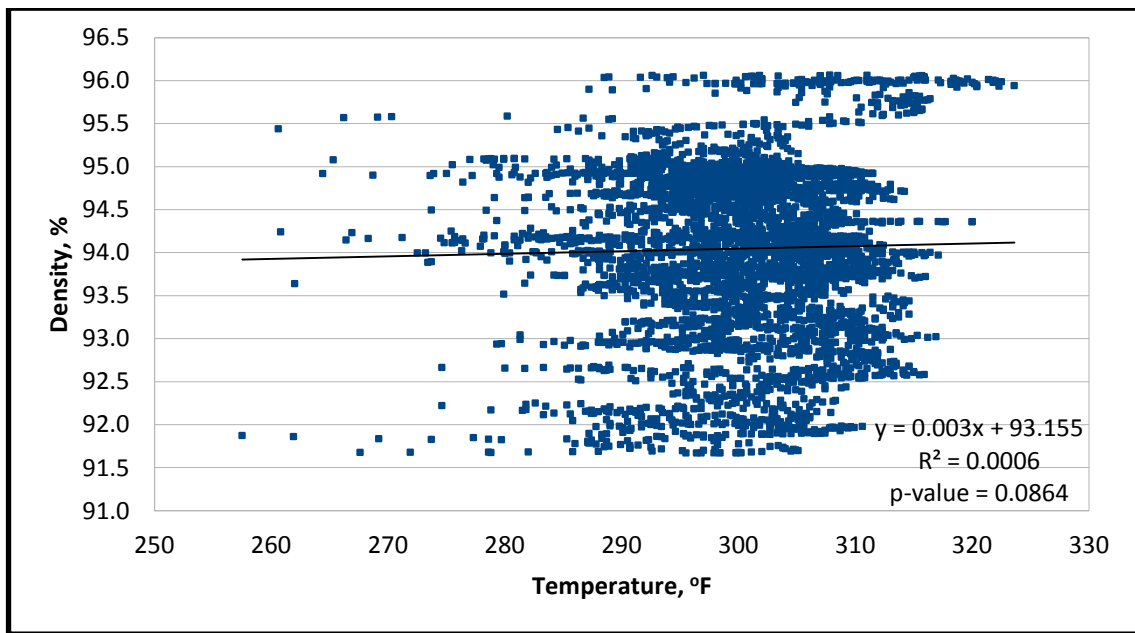


Figure 5.58 IR Temperature (8.6 ft) and GPR Density (9.5 ft) Project 2, Full Length

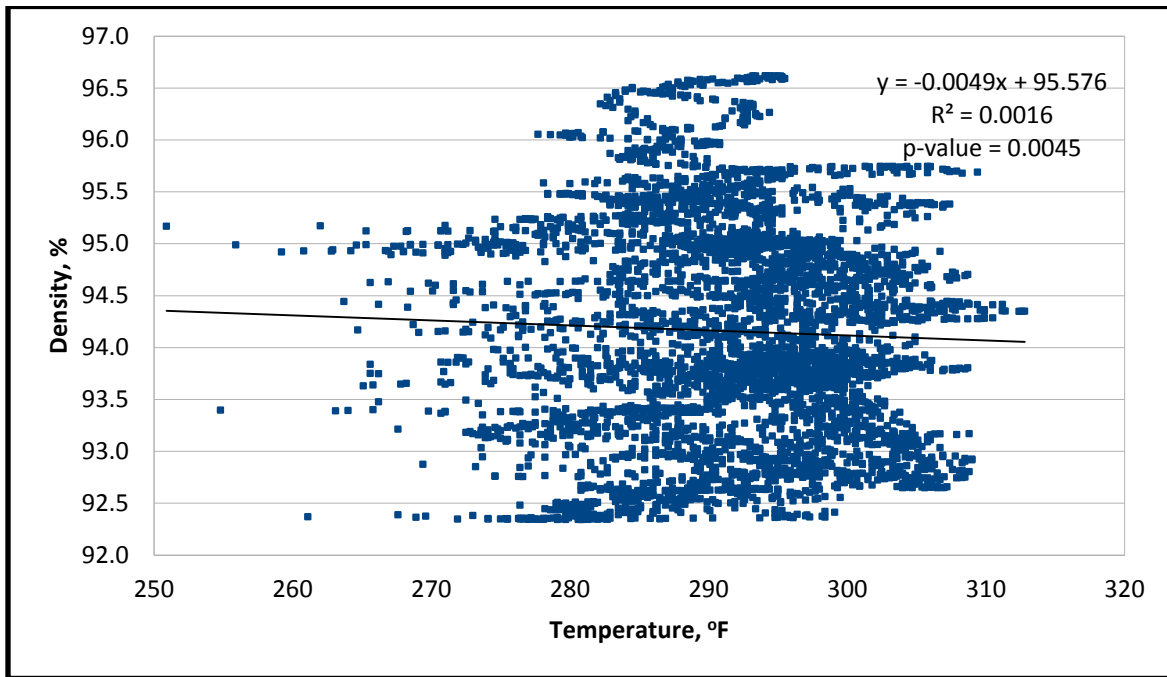


Figure 5.59 IR Temperature (10.8 ft) and GPR Density (11.5 ft) Project 2, Full Length

IR and GPR data from the first 500 ft length of research testing for the same offsets of approximately 9 ft and 11 ft and plotted in Figures 5.60 and 5.61, respectively. The data shown for the first subplot of the project illustrate no discernible trend regarding the relationship of initial mat temperature and final density. More scatter was observed at 9-ft offsets, while an S-shaped pattern emerged at the 11-ft offset.

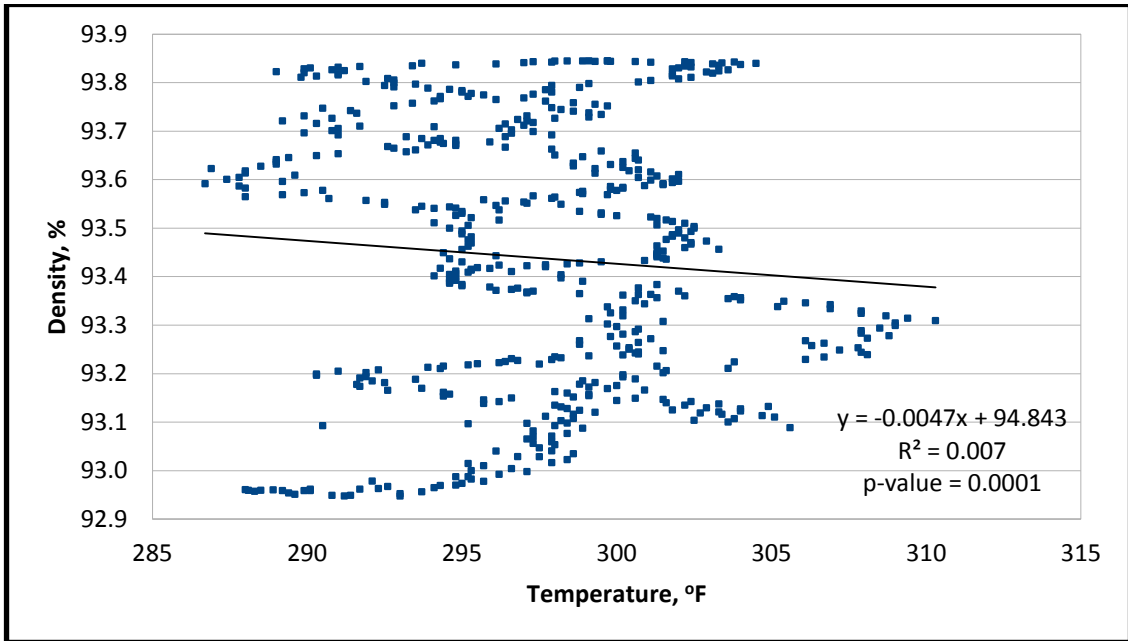


Figure 5.60 IR Temperature (8.6 ft) and GPR Density (9.5 ft) Project 2, Sublot 1

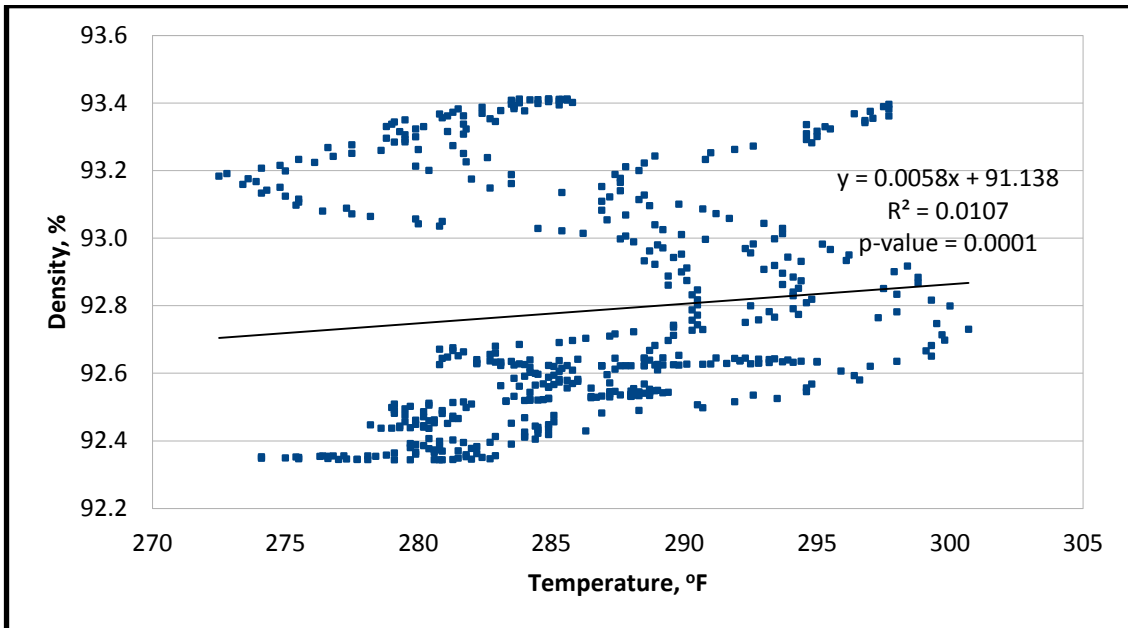


Figure 5.61 IR Temperature (10.8 ft) and GPR Density (11.5 ft) Project 2, Sublot 1

5.5.3 Project 3, IR and GPR Comparison

Similar to second project, the IR and GPR distance measurement instruments (DMI) were in close agreement. IR distances were verified periodically during paving against project stationing lathe to ensure accuracy. GPR distances were confirmed during traces with the comparison checked every 1,000 ft.

Figures 5.62 through 5.64 plot the IR and GPR data from the full 6,000 ft length of research testing for offsets of approximately 6 ft, 9 ft, and 11 ft, respectively. The plots identify a slight trend with higher density resulting from higher initial mat temperature with a range of less than 3% density. In order to provide a better illustration of this trend, 10 outlier points were removed. Lower GPR densities were the result of a low calibration to the nuclear density gauge, since density measured with the nuclear density gauge generally exceeded 92% on this project. However, from a relative point of view, there is appears to be a positive trend.

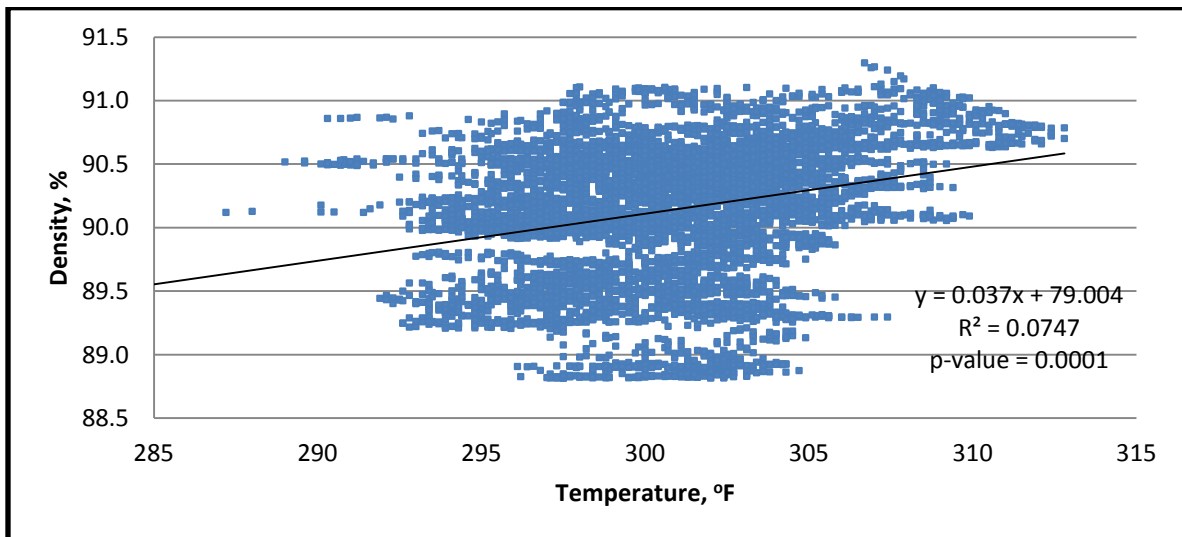


Figure 5.62 IR Temperature (6.4 ft) and GPR Density (6 ft) Project 3, Full Length

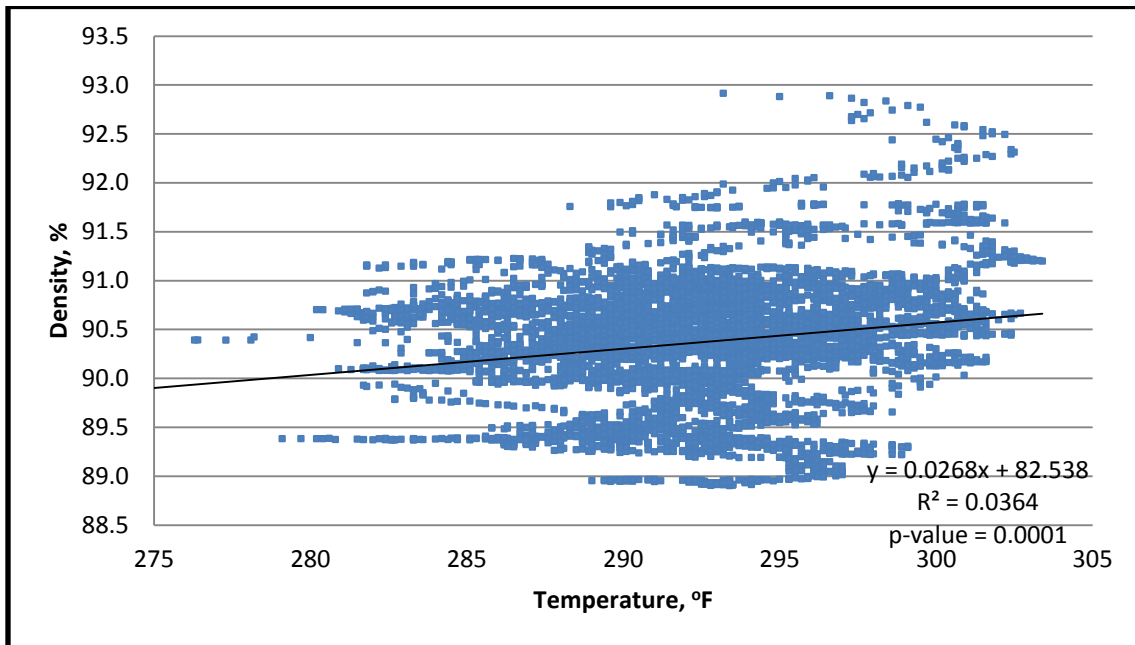


Figure 5.63 IR Temperature (9.7 ft) and GPR Density (9.5 ft) Project 3, Full Length

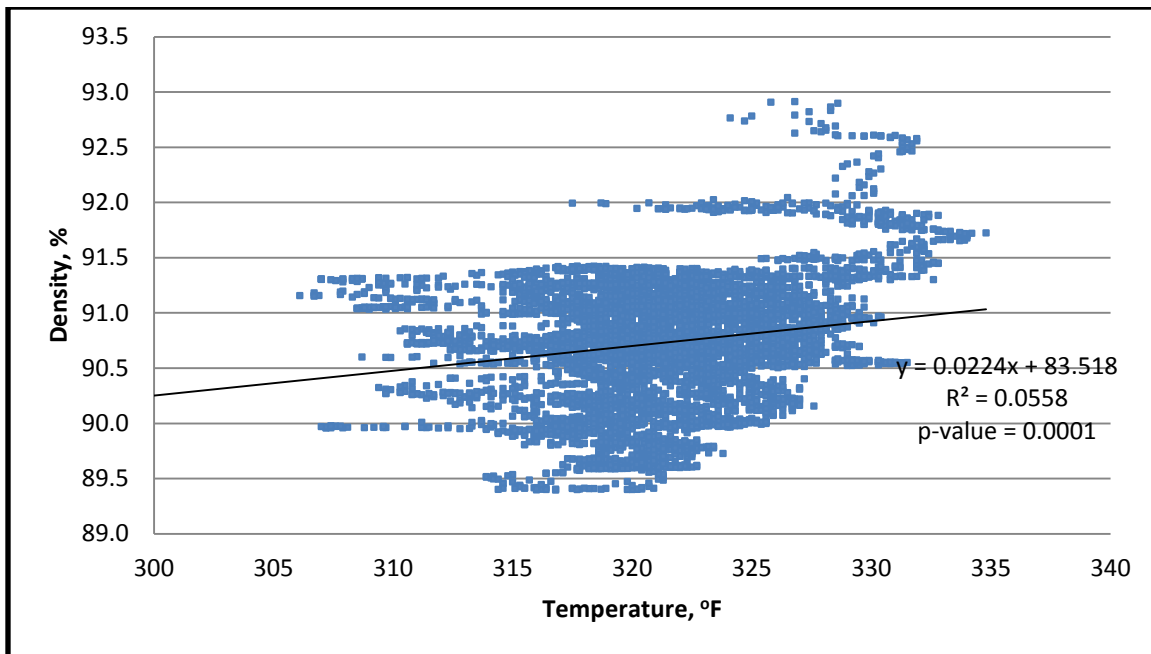


Figure 5.64 IR Temperature (11.8 ft) and GPR Density (11.5 ft) Project 3, Full Length

Figures 5.65 through 5.67 plot the IR and GPR data from the first 500 ft length of research testing for offsets of approximately 6 ft, 9 ft, and 11 ft, respectively. The 6-ft offset detected a positive trend of higher temperatures with higher densities, while the 9-ft

and 11-ft offsets had no trend. Despite any positive trend line, the figures generally indicate scatter with some level of dependency on another variable. Thus, based upon the plots for the three projects, there is no definitive relationship between continuous thermal temperatures behind the paver and final density measured by GPR.

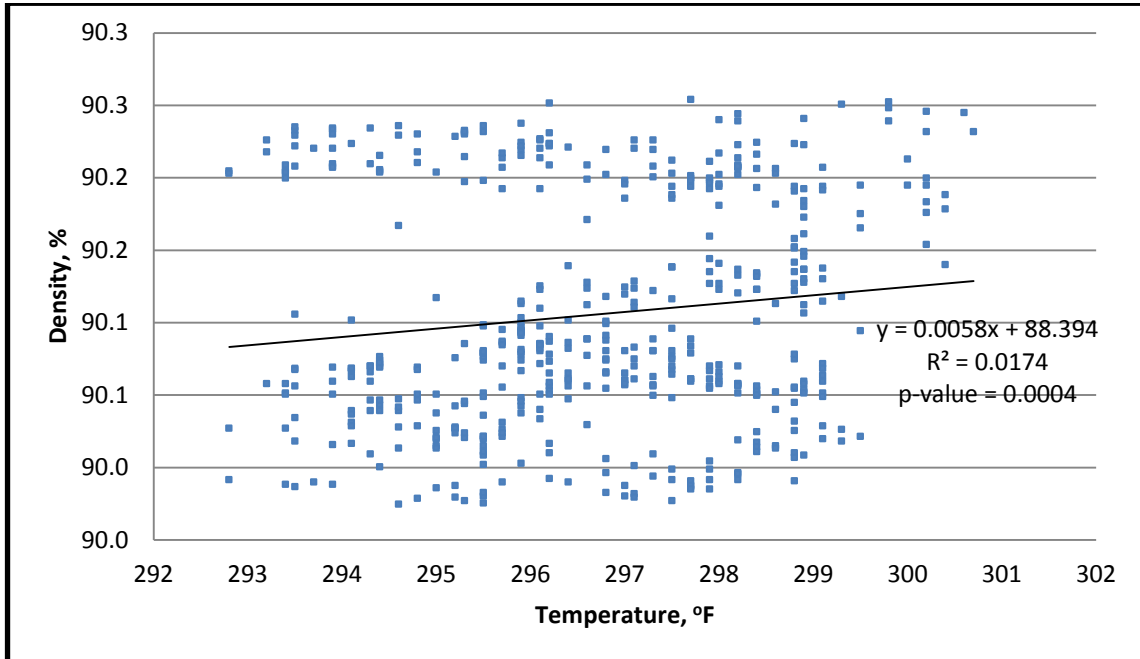


Figure 5.65 IR Temperature (6.4 ft) and GPR Density (6 ft) Project 3, Sublot 1

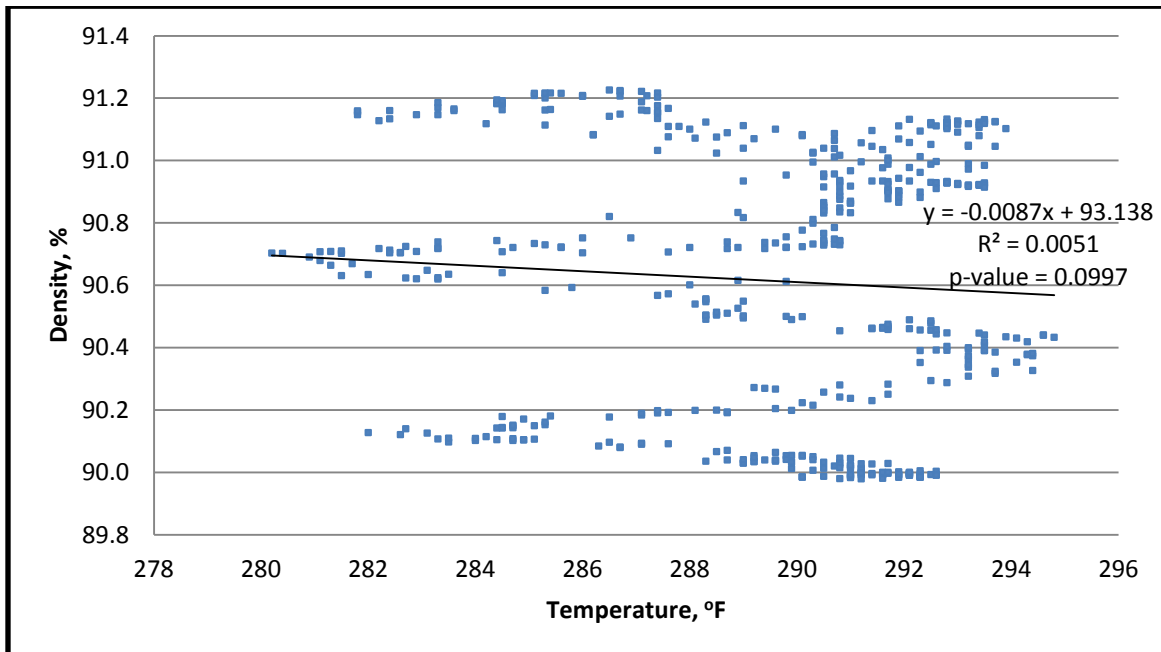


Figure 5.66 IR Temperature (9.7 ft) and GPR Density (9.5 ft) Project 3, Sublot 1

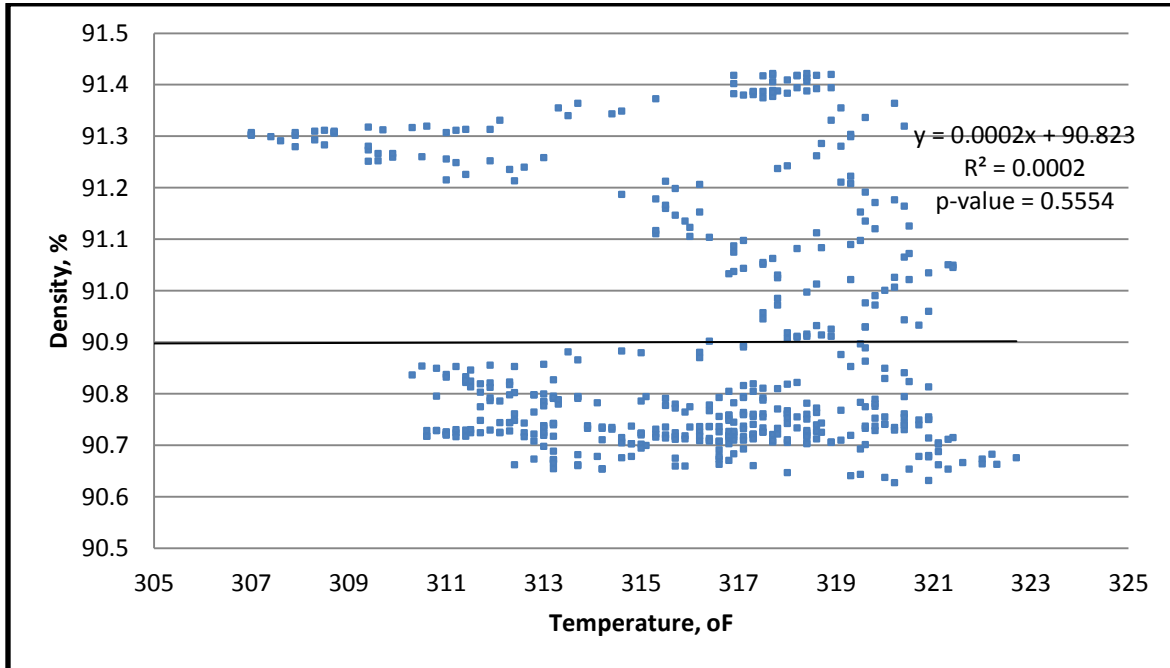


Figure 5.67 IR Temperature (11.8 ft) and GPR Density (11.5 ft) Project 3, Sublot 1

5.6 Correlations by Sublot Averaging

The previous section presented simple plots of continuous IR and GPR readings on the projects. In this section, the analysis is expanded to include a comparison of all NDT devices using statistical correlations and plots. For example, does the average nuclear density compare with the average thermal readings within a given 500-ft subplot length. To this end, subplot correlations were computed using the mean and standard deviation of these NDT measures:

- Infrared temperature with thermal bar
- GPR thickness
- GPR density
- Seismic modulus
- Nuclear density

The mean and standard deviation for these measures were computed using all samples within each subplot. Infrared and GPR sample sizes ranged from $n=1,000$ to $n=3,000$ depending on number of offsets, while nuclear density and seismic modulus readings were limited to $n=5$. (An investigation of point measures is provided in the next chapter).

With several significant correlations among NDT devices by subplot averages and/or standard deviations, Table 5.15 summarizes positive/negative correlation slope and R^2 among the two variables. There were inconsistent slopes among projects for any combination of variables, except for negative correlations between mean IR temperature and GPR thickness. This lack of consistency presents a challenge for using combinations of NDT tests, in their current form, as interrelated quality control and acceptance tools.

Table 5.15 Summary of Project Correlations

Variables	Project 1		Project 2		Project 3	
	Correlation	$R^2, \%$	Correlation	$R^2, \%$	Correlation	$R^2, \%$
IR Mean vs GPR Thickness Mean	↘	13.8	---	0	↘	20.1
IR Mean vs GPR Density Mean	↘	0.6	↘	2.6	↗	1.7
IR Mean vs Nuclear Density Mean	↗	10.2	↘	4.5	↘	65.1
IR Mean vs Seismic Modulus Mean	↘	84.6	↗	5.2	↘	55.7
GPR Density Std. Dev. vs GPR Thickness Std. Dev.	---	0	↗	31.2	---	0
Seismic Modulus Mean vs GPR Thickness Mean	↗	42.1	---	0	---	0
Seismic Modulus Std. Dev. vs GPR Thickness Std. Dev.	---	0	↗	27.2	↘	19.0
Nuclear Density Mean vs GPR Density Mean	↗	17.4	---	0	---	0
Nuclear Density Std. Dev. vs IR Temp. Std. Dev.	↗	7.5	---	0.1	↗	1.2
'---' denotes insignificant linear model with p-value > 10%. All other correlations significant at the 10% level.						

5.6.1 Project 1 Correlations

The average and standard deviation of the NDT measures were computed and are reported in Table 5.16. The sample sizes to compute these statistics by subplot are very unbalanced, where the infrared temperature and GPR were n=500, while nuclear density and seismic modulus were n=5. An error in GPR density processing in Sublot 3 yielded a sample size of n=0.

Table 5.16 Project 1 Statistics for Correlation Analysis

Sublot	Infrared Temp., °F		GPR Thick., in.		GPR Dens., %		Nuclear Dens., %		Modulus, ksi	
	Mean	Std. Dev.	Mean	Std. Dev.	Mean	Std. Dev.	Mean	Std. Dev.	Mean	Std. Dev.
1	235.0	26.80	1.79	0.173	95.5	0.820	93.1	0.94	2173.5	576.5
2	247.7	8.50	1.82	0.175	95.0	0.745	93.1	2.29	2207.3	367.2
3	245.9	7.49	1.79	0.118	94.8	1.137	93.5	0.61	2078.0	165.8
4	223.8	47.67	1.80	0.113	.	.	90.9	3.18	2492.7	404.4
5	247.7	7.28	1.81	0.182	93.8	0.967	92.9	0.96	2144.0	180.2
6	253.1	8.29	1.81	0.154	94.2	0.752	90.8	5.28	2004.0	55.7
7	250.0	8.89	1.78	0.154	92.6	1.194	92.2	0.81	2045.3	101.3
8	251.5	8.61	1.72	0.137	94.7	0.645	93.5	1.28	1859.3	241.4
9	262.6	13.26	1.78	0.114	92.7	0.919	92.5	0.93	1810.7	225.4
10	264.2	8.73	1.75	0.138	95.1	1.240	93.2	0.54	1627.3	550.4

Scatter plots were created for those mean correlation coefficients greater than 0.4 or less than -0.4 to capture marginal correlations beyond the 0.5/-0.5 cutoff threshold. For Project 1, Figure 5.68 shows that, while weak, there is a negative correlation between the GPR thickness and IR temperature, confirming earlier plots. There was no clear correlation between the GPR density and IR mean temperature, which is shown in Figure 5.69. There was a weak linear correlation between the nuclear density reading and the IR temperature in Figure 5.70, although the low accuracy of the trendline may be due to two sublots having relatively low densities.

There was a strong negative correlation between the seismic modulus and the infrared temperature readings with a very tight grouping of the points on the linear trendline shown in Figure 5.71. A positive correlation was observed in Figure 5.72 between the seismic modulus and the GPR thickness, although the points were not as close to the trendline as they were in Figure 5.71. A generally positive correlation was observed between the GPR density and the nuclear density after they were plotted against each other in Figure 5.73. This positive density correlation would be expected.

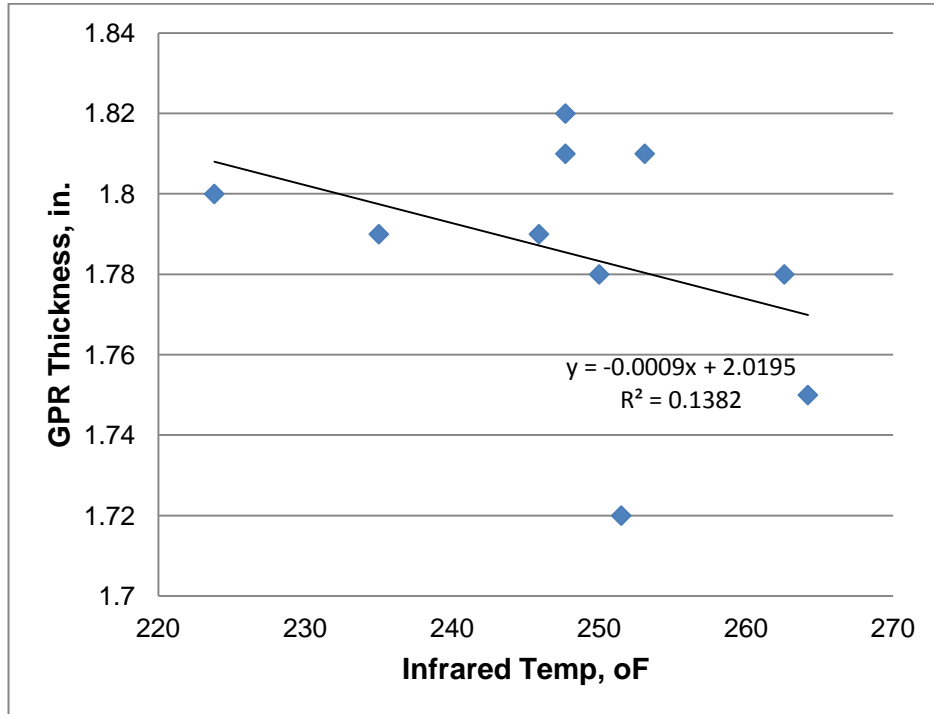


Figure 5.68 Correlation between Average GPR Thickness and IR Temperature on Project 1

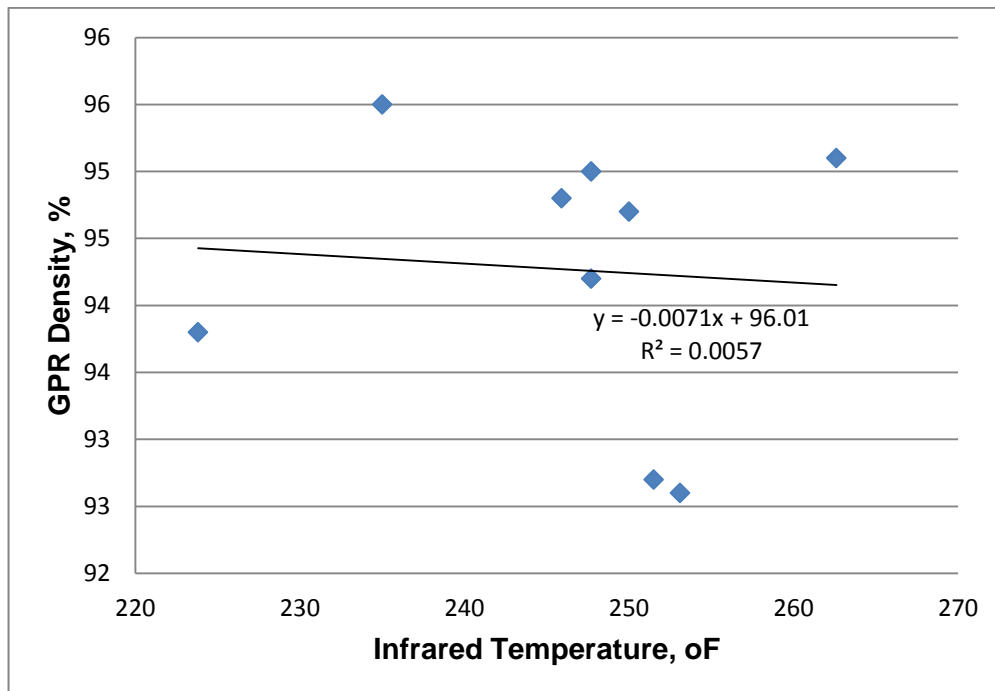


Figure 5.69 Correlation between Average GPR Density and IR Temperature on Project 1

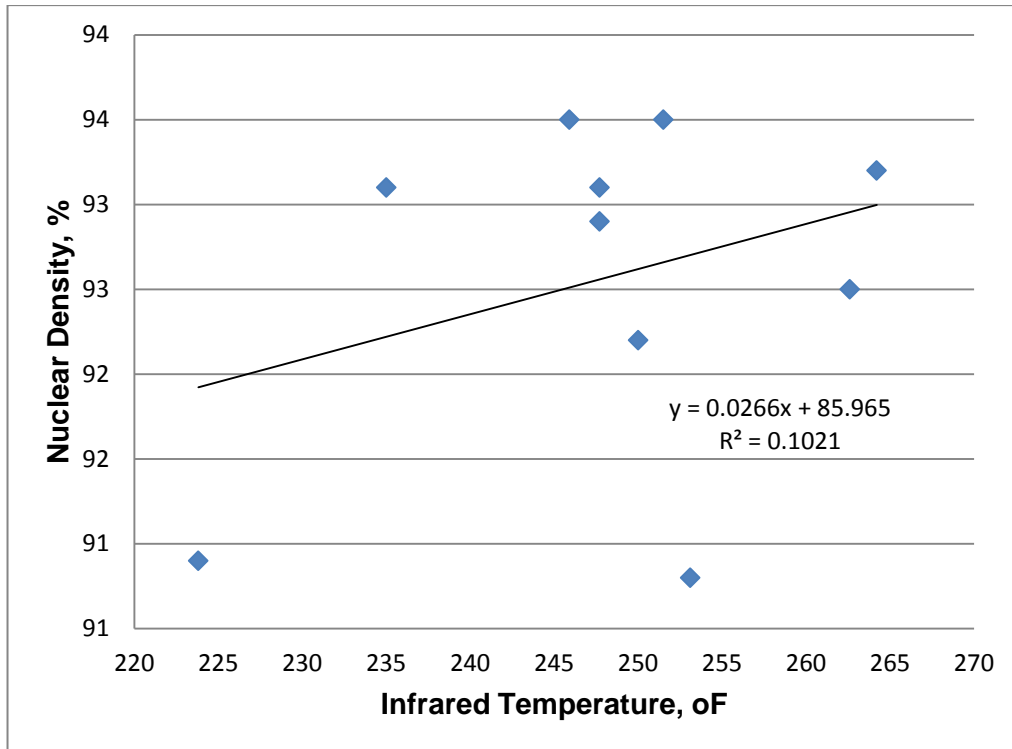


Figure 5.70 Correlation between Average Nuclear Density and IR Temperature on Project 1

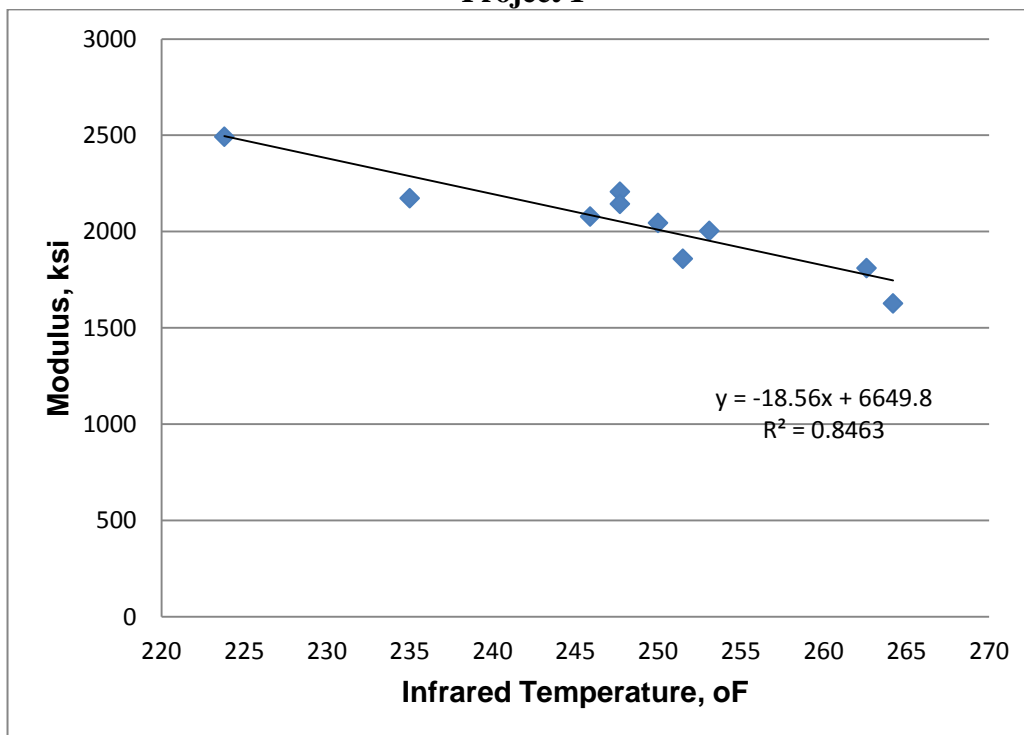


Figure 5.71 Correlation between Average Seismic Modulus and IR Temperature on Project 1

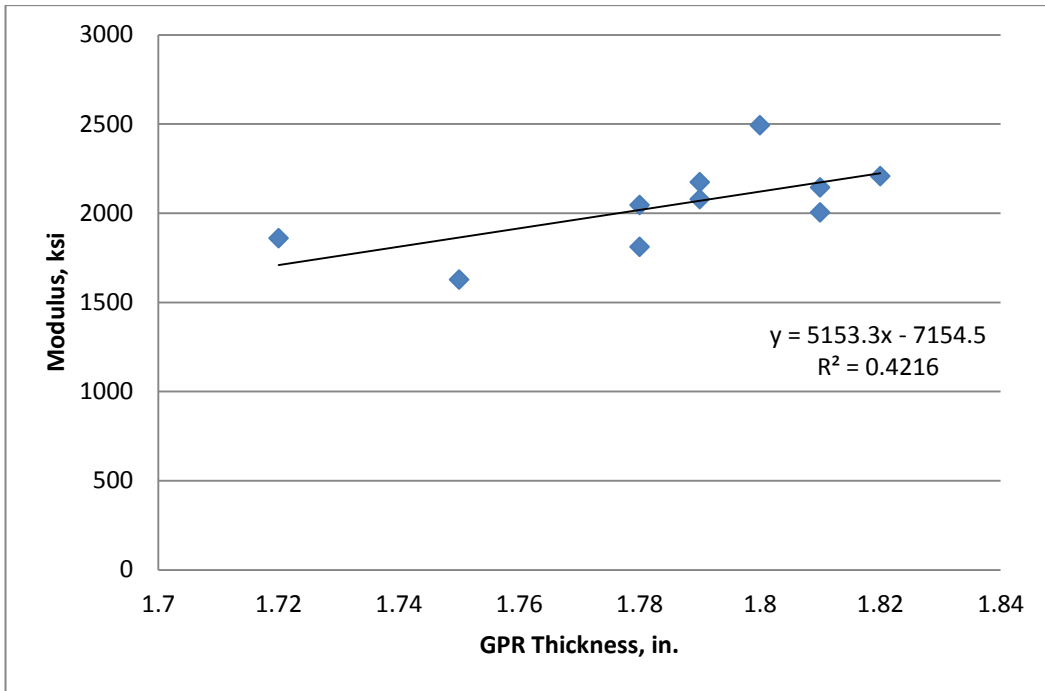


Figure 5.72 Correlation between Seismic Modulus and GPR Thickness on Project 1

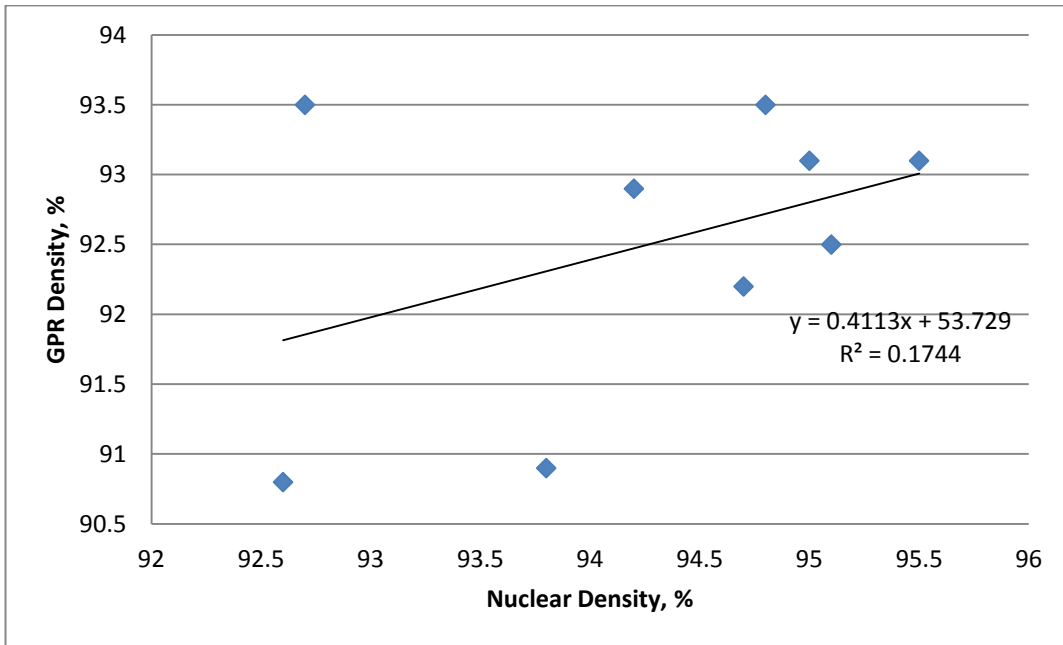


Figure 5.73 Correlation between Average GPR Density and Nuclear Density on Project 1

5.6.2 Project 2 Correlations

The average and standard deviation of the NDT measures were computed and are reported in Table 5.17. With respect to variability, there was a reduction for temperature variability while fluctuations were observed for GPR thickness, GPR density, nuclear density, and modulus.

Table 5.17 Project 2 Statistics for Correlation Analysis

Sublot	Infrared Temp., °F		GPR Thickness, in.		GPR Density, %		Nuclear Density, %		Modulus, ksi	
	Mean	Std. Dev.	Mean	Std. Dev.	Mean	Std. Dev.	Mean	Std. Dev.	Mean	Std. Dev.
1	293.3	12.8	2.6	0.2	95.0	0.3	92.3	1.83	2063.3	237.0
2	293.6	12.0	2.7	0.1	94.3	0.5	93.7	0.56	2001.3	195.1
3	298.1	11.2	2.6	0.2	93.3	0.5	92.0	1.83	1995.3	91.8
4	292.3	11.7	2.6	0.2	92.9	0.8	92.1	1.84	2108.7	161.2
5	297.1	10.3	2.5	0.2	94.2	0.5	92.0	2.59	1382.0	475.7
6	297.5	10.4	2.6	0.1	93.8	0.3	92.8	1.49	876.0	275.6
7	293.0	12.3	2.6	0.2	95.2	0.6	93.0	2.02	1137.7	745.2
8	288.8	8.1	2.6	0.2	95.1	0.6	92.4	2.11	864.3	251.1
9	294.0	8.7	2.5	0.2	94.2	0.9	93.1	1.17	864.0	433.9
10	289.0	9.4	2.6	0.2	93.1	0.4	92.9	1.08	1025.3	334.6

Project 2 data were similarly plotted in order to examine correlations between different measurements. Figure 5.74 shows a weak negative correlation between the GPR density reading and the IR temperature that was similar to Project 1. The correlation was weakened by the high variability in the data which reduced the R^2 value. There was also a weak negative correlation between the nuclear density and the IR temperature due to similar factors which are shown in Figure 5.75, which was opposite of Project 1. A weak positive correlation could be detected between the seismic modulus and the infrared temperature data present in Figure 5.76 which was opposite the strong trend on Project 1. The two correlations that were evaluated for the standard deviations on Project 2 both were fairly strong positive correlations. These were between the standard deviation of the GPR thickness with both the GPR density and the seismic modulus, as shown in Figures 5.77 and 5.78, respectively.

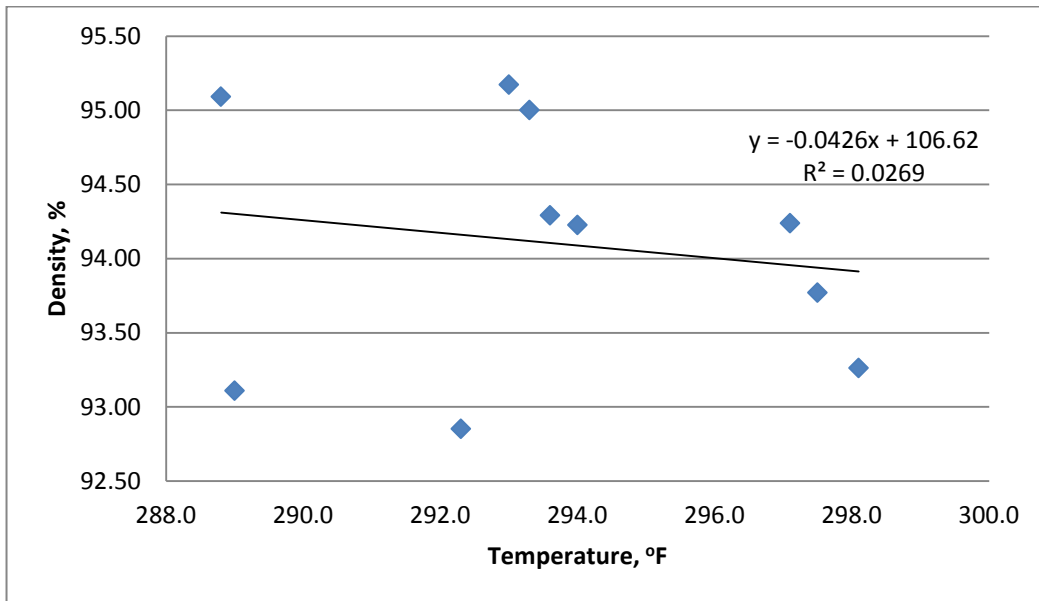


Figure 5.74 Correlation between Average GPR Density and IR Temperature on Project 2

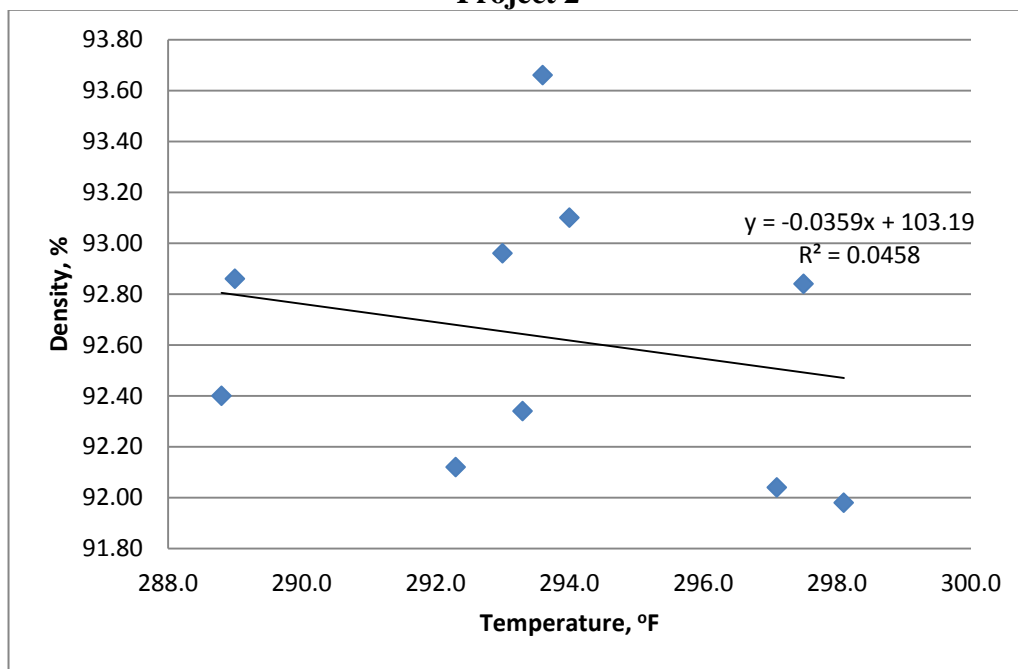


Figure 5.75 Correlation between Average Nuclear Density and IR Temperature on Project 2

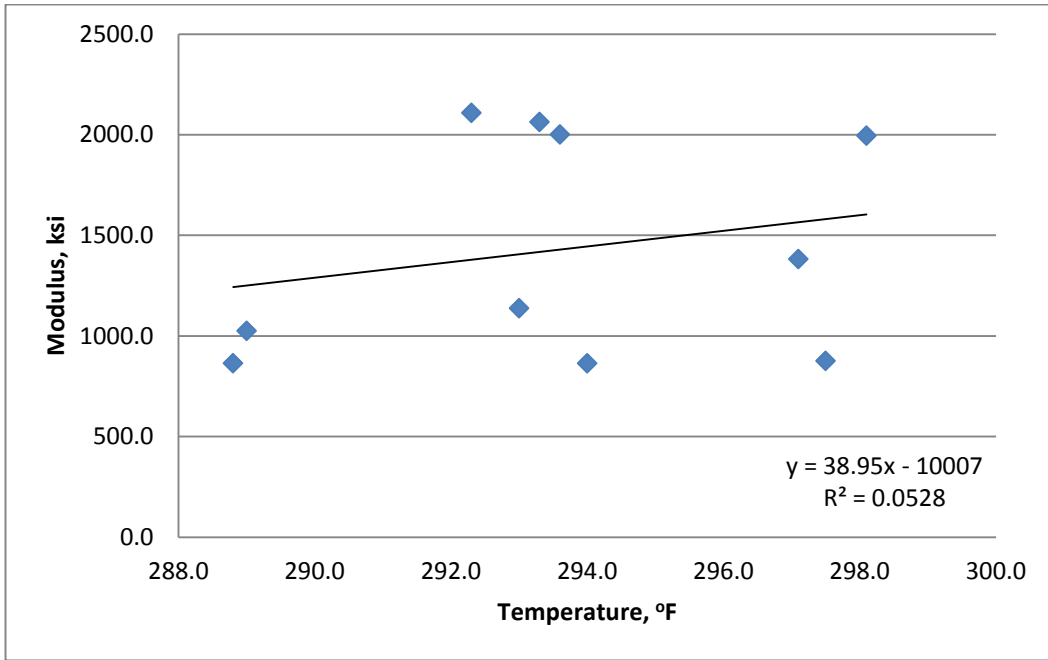


Figure 5.76 Correlation between Average Seismic Modulus and IR Temperature on Project 2

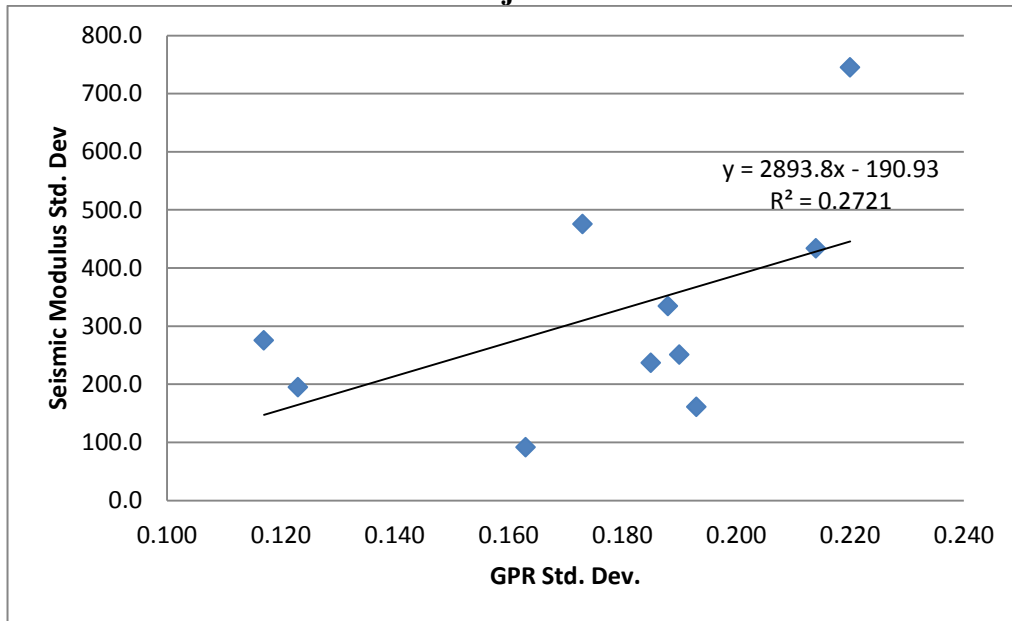


Figure 5.77 Correlation between Standard Deviations of Seismic Modulus and GPR Thickness on Project 2

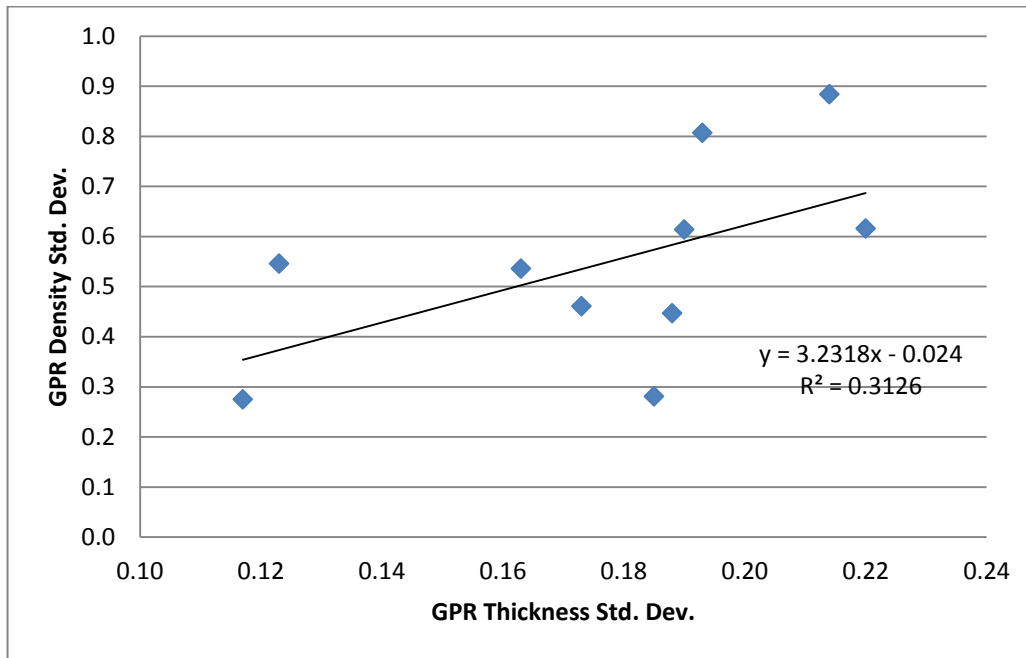


Figure 5.78 Correlation between GPR Density and Thickness Standard Deviations on Project 2

5.6.3 Project 3 Correlations

The average and standard deviation of the NDT measures were computed and are reported in Table 5.18. There were fluctuations in variability for all NDTs.

Table 5.18 Project 3 Statistics for Correlation Analysis

Sublot	Infrared Temp., °F		GPR Thickness, in.		GPR Density, %		Nuclear Density, %		Modulus, ksi	
	Mean	Std. Dev.	Mean	Std. Dev.	Mean	Std. Dev.	Mean	Std. Dev.	Mean	Std. Dev.
1	296.0	13.9	1.5	0.1	90.5	0.4	93.6	1.47	1544.0	253.9
2	299.7	12.2	1.6	0.1	90.1	0.5	93.2	1.06	1466.0	327.0
3	298.0	11.8	1.9	0.2	89.7	0.3	92.9	1.13	1611.3	254.4
4	300.1	12.3	1.4	0.1	89.9	0.4	92.5	0.75	1318.0	256.5
5	302.3	11.5	1.4	0.1	89.5	0.6	92.6	1.85	1505.3	307.8
6	299.9	13.8	1.5	0.1	90.6	0.4	92.9	2.01	1442.0	228.7
7	298.8	13.1	1.9	0.2	90.5	0.3	92.4	1.48	1558.7	74.4
8	300.7	12.4	1.5	0.1	90.6	0.3	92.1	1.52	1571.3	92.3
9	301.0	12.4	1.4	0.1	90.7	0.4	91.7	1.19	1447.3	291.2
10	302.3	12.3	1.5	0.1	90.6	0.4	92.5	0.67	1042.0	507.4
11	305.5	12.4	1.5	0.1	90.6	0.2	91.3	0.92	724.7	125.3
12	303.8	12.7	1.5	0.1	90.4	0.4	92.0	1.26	668.0	81.3

Project 3 correlations were also plotted and compared to the results of the first projects. Similar to Project 1, Figure 5.79 shows that there was a negative correlation between the GPR thickness and IR temperature, although it was slightly stronger on Project 3. It has been recognized that thicker mats harbor more thermal energy, so that explanation here is contradictory. The relationship may be confounded where the material along the centerline joint is thicker and has a greater conveyance length to the auger extensions and screed extensions.

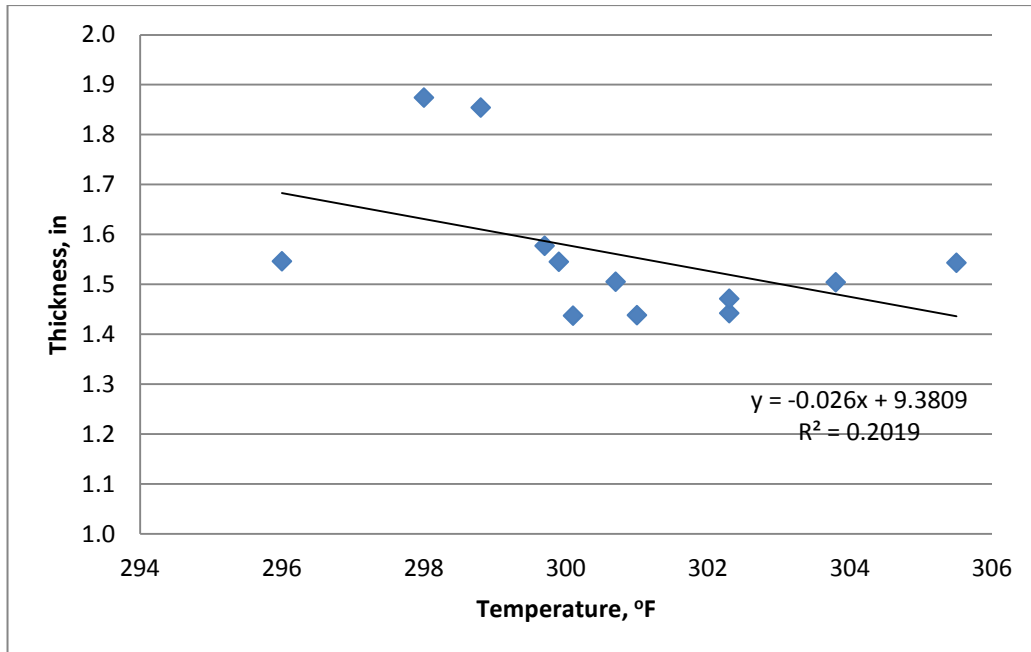


Figure 5.79 Correlation between Average GPR Thickness and IR Temperature on Project 3

Unlike the other projects, there was a weak positive correlation between the GPR density and the IR temperature, which is shown in Figure 5.80. The correlation between the nuclear density and the IR temperature in Figure 5.81 for Project 3 was strongly negative, which contrasted with the weak negative correlation on Project 2, and even more so with the weak positive correlation on Project 1. Projects 1 and 3 had very similar strong negative correlations between the seismic modulus and the IR temperature illustrated for Project 3 in Figure 5.82, although Project 2 showed a weak positive correlation. A negative correlation was observed in Figure 5.83 for the correlation between the seismic modulus standard deviation and the GPR thickness standard deviation, which was the opposite of what occurred on Project 2.

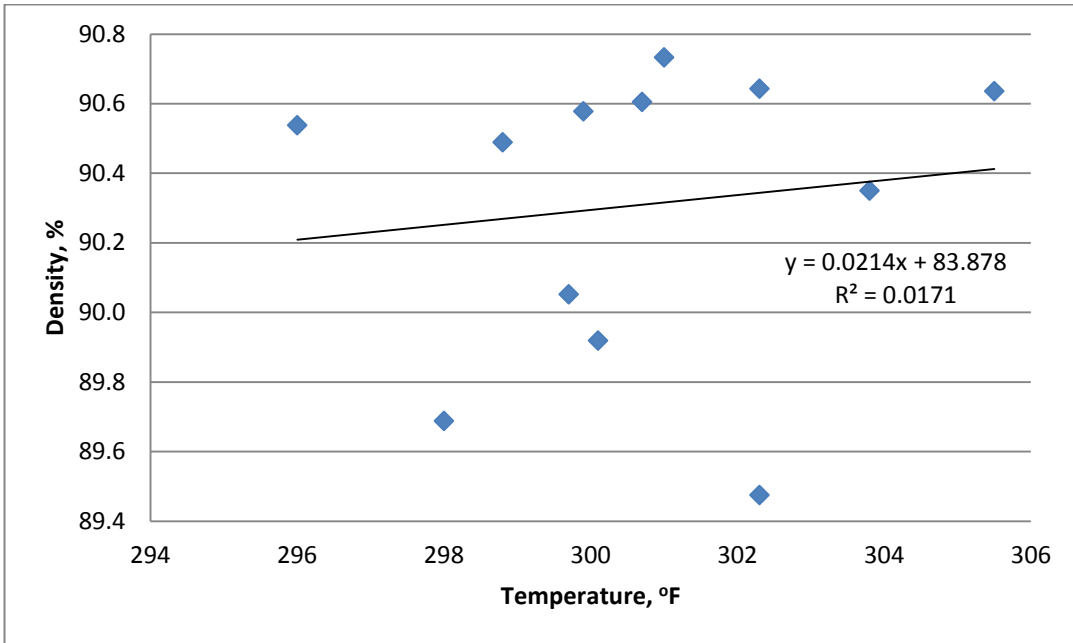


Figure 5.80 Correlation between Average GPR Density and IR Temperature on Project 3

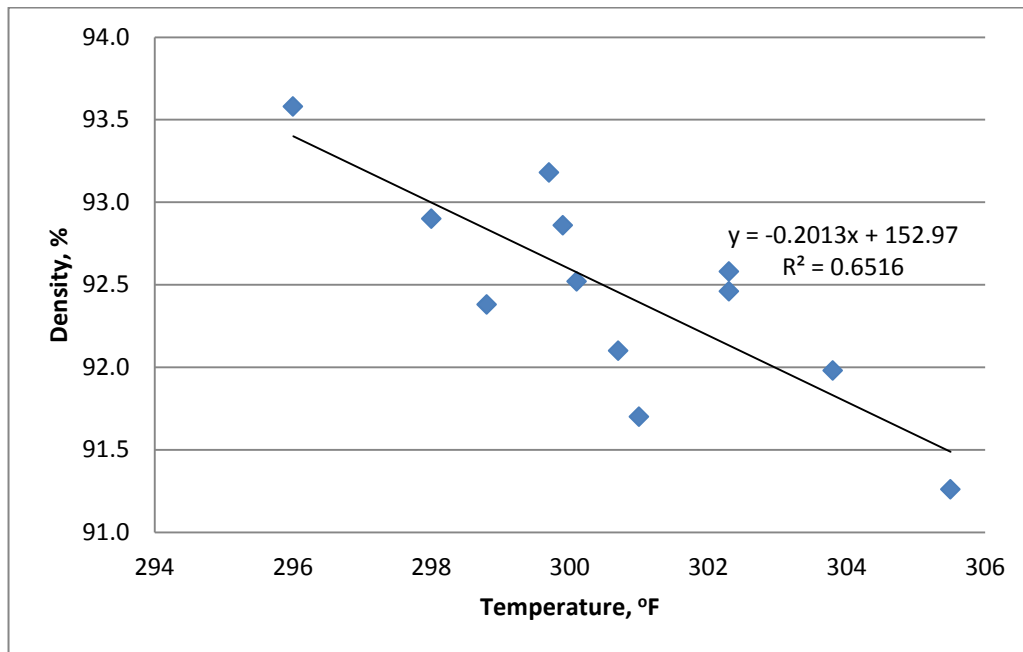


Figure 5.81 Correlation between Average Nuclear Density and IR Temperature on Project 3

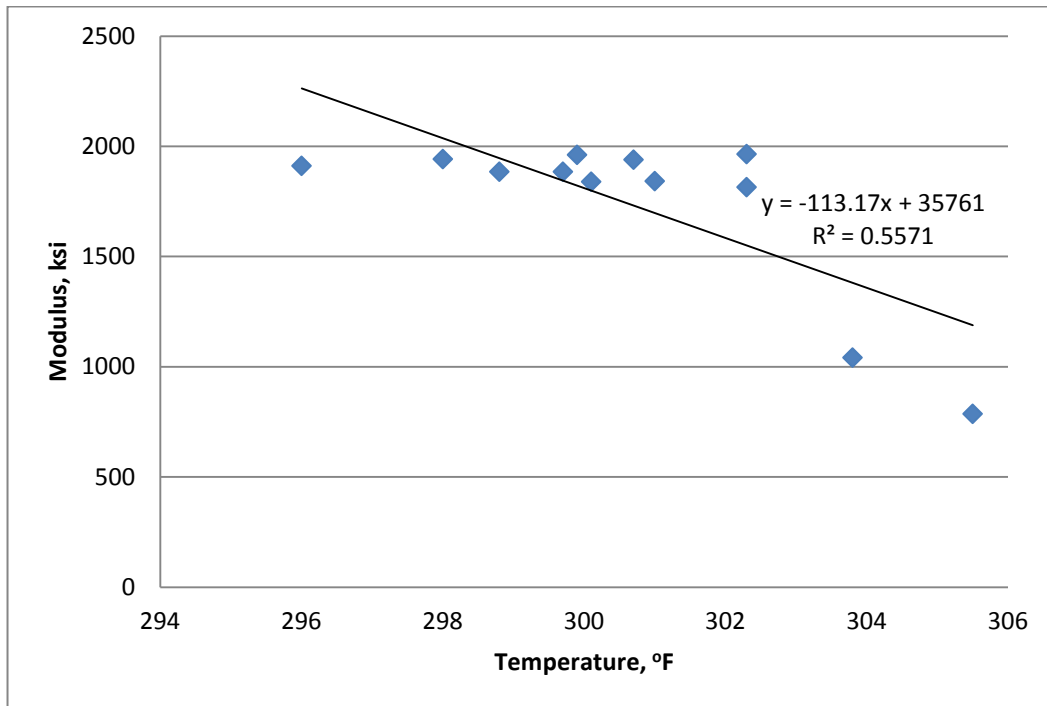


Figure 5.82 Correlation between Average Seismic Modulus and IR Temperature on Project 3

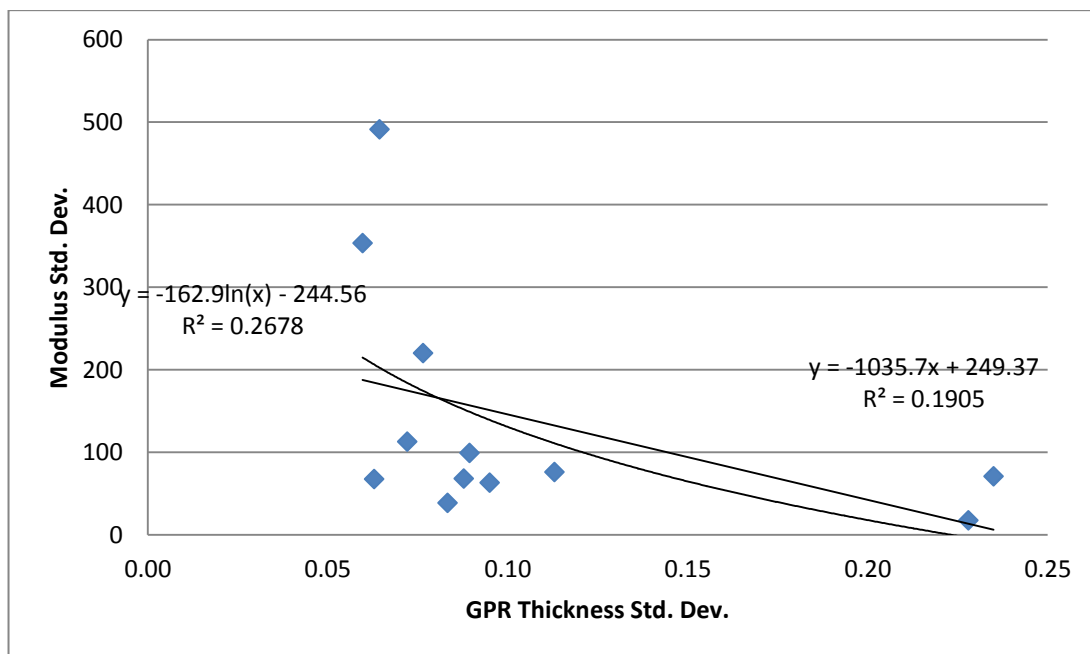


Figure 5.83 Correlation between the Standard Deviations of the Seismic Modulus and the GPRadar Thickness on Project 3

5.6.4 Correlation Summary

Figure 5.84 illustrates the standard deviations for nuclear density and IR temperature by project. Although the correlations were insignificant, it is necessary to illustrate that there was no relationship between variability in mat temperature and final density, again suggesting that final density is not a sole function of mat temperature. As discussed earlier, the number of passes, roller type, vibratory settings, project-specific mix properties, and other factors play an important role in final densification. Previous research by Washington DOT found that temperature differentials were found to lead to significant density differentials in the finished mat (Willoughby et al. 2001). In the state of Washington, over 40% of the observed projects had temperature differentials of 25°F or greater.

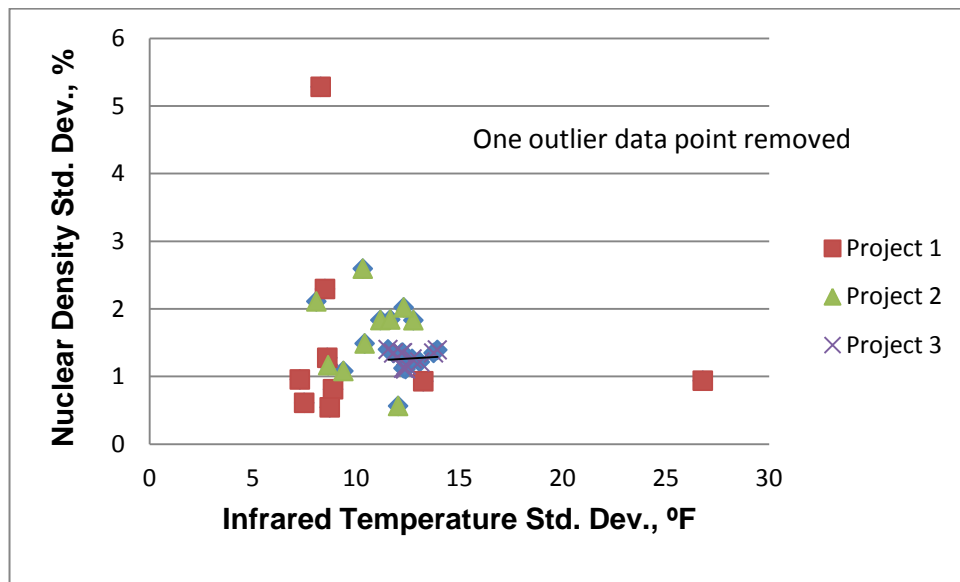


Figure 5.84 Correlation between Nuclear Density Variability and IR Temperature Variability

Based upon the plots from the three projects, there is no definitive relationship between continuous temperatures behind the paver and final density measured by the GPR.

5.7 Summary

This chapter presented a detailed analysis of thermal temperatures during paving with Pave-IR sensor data and FLIR imaging camera data. A comparison was made with continuous GPR thickness and density data, and then subplot averages and standard deviations among all NDTs. The following sections summarize the findings.

5.7.1 Thermal Data and Images

An evaluation of continuous thermal data and FLIR camera images concluded:

- (1) A distinctive V-shaped pattern at intervals the length of a truckload of mix were evident in all continuous thermal graphs. The distance between intervals ranged from 80 to 135 ft, depending on truck yield distance. The V-shaped pattern was caused by cooler material spooling transversely by the augers as the paver moved longitudinally forward.
- (2) On Project 1, there was a disagreement between the bar sensors and thermal camera of about 30°F to 50°F, where the camera recorded higher temperatures.
- (3) The paver chain case is a potential cause of segregation in the paving operation. Its close proximity to the mat and variable temperature from the mix passing overhead, along with the case in direct alignment with the articulation pin in the main screed, combine to potentially cause a linear low temperature streak in the mat. The sensor bar is unable to detect this linearly segregated section.
- (4) The MTV can reduce mat temperature variability behind the screed. On Project 2, the standard deviation was reduced in half 9.4°F to 5.5°F when the MTV was added to the operation. The range also reduced from an average 66°F to 51 °F.
- (5) Camera images of the truck box, material transfer vehicle (MTV), and paver screed illustrated the mix temperature range using selected points and lines. The range of the material in the truck box was approximately 100°F to 160°F. Material behind the screed measured by the camera ranged from 8°F to 53°F. Table 5.19 summarizes the ranges in the truck box and paver screed for the three projects and defined stations. When a pass/fail criteria is set at a range of 25°F, locations having an MTV are able to pass this requirement in 10 of 11 tests. Locations not having an MTV fail this requirement in 4 of 4 tests. Use of an MTV (remix hopper, or Shuttle Buggy™) reduces the material temperature range. The range reduction ratio, as measured by the ratio of the truck temperature range to mat temperature range (FLIR camera), was 2.1 to 14.8.
- (6) Comparisons of the temperature range with the FLIR thermal image camera and Pave-IR sensor bar from earlier chapter sections are summarized in Table 5.20. On the first two projects, the thermal camera image measured a higher range than the sensor bar, while the out-of-calibration sensor bar on the third project measured a range much higher than camera. A question of implementing the Pave-IR bar into practice is acknowledging this disparity, particularly if there is movement towards an allowable range, such as 25°F range. An additional consideration with the thermal camera is the sampling approach, whether the temperature points (Area, Line, or Spot) are selected. Cooler and warmer areas are of interest and are knowingly selected by the camera operator or other end-user. Randomization principles should be incorporated to ensure unbiased parameter estimates are obtained.

Table 5.19 Thermal Range and Pass/Fail Comparison by MTV

Project	Station	Truck Δ °F	Mat Δ °F	Range Reduction Ratio	Material Transfer Device Operating	Pass/Fail Mat Δ $\leq 25^\circ\text{F}$
1	429+00	149	25	6.0	Yes	Yes
	422+00	91	24	3.8	Yes	Yes
	402+00	91*	43	2.1	Yes	No
2	242+00	157	53	3.0	No	No
	235+00	132	50	2.6	No	No
	230+00	167	41	4.1	No	No
	220+00	111	34	3.3	No	No
	209+00	111*	25	4.4	Yes	Yes
3	628+00	163	11	14.8	Yes	Yes
	630+00	163*	13	12.5	Yes	Yes
	634+00	163*	11	14.8	Yes	Yes
	637+50	90	9	10.0	Yes	Yes
	673+00	90*	8	11.3	Yes	Yes
	787+00	90*	11	8.2	Yes	Yes
	790+00	90*	16	5.7	Yes	Yes

* Assumed value from previously measured truckload.

Table 5.20 Range Comparison of Thermal Camera and Sensor Bar

Project	Station	Image Δ °F	Sensor Δ °F	Image Δ – Sensor Δ , °F
1	432+00	38	24	14
	429+00	25	17	8
	422+00	24	17	7
	402+00	43	20	23
2	242+00	53	25	28
	235+00	50	28	22
	230+00	41	22	19
	220+00	34	22	12
	209+00	25	23	2
3*	628+00	11	41	-30
	630+00	13	38	-25
	634+00	11	42	-31
	637+50	9	41	-32

* Sensor bar out of calibration at Sensors #2, #5, and #6.

(7) The FLIR camera provides a full picture of mat temperature in a given location. It can also measure temperature differentials in the truck box and paver hopper.

Images from the camera were interpreted and shared with the crews to help with adjustments to construct a more uniform pavement. But, the FLIR camera is limited to intermittent sampling in the longitudinal direction.

- (8) Previous research by Washington DOT found that temperature differentials were found to lead to significant density differentials in the finished mat (Willoughby et al. 2001). Over 40% of the jobs observed had temperature differentials of 25°F or greater. In this project, there was a very weak or no correlation at all between variability in IR temperature and nuclear density.

5.7.2 Comparing Continuous Thermal and GPR Data

Continuous Pave-IR readings were plotted against continuous GPR density readings. Plots for the entire project length and 500-ft subplot groupings were created. The entire project length contained up to 5,000 or 6,000 comparison points, while sublots had 500 data points. Based upon the plots for the three projects, there was no definitive relationship between continuous thermal temperatures behind the paver and final density measured by GPR. The findings for the three projects are as follows:

Project 1: Best-fit line, with a weak R^2 value, detected that higher IR temperatures led to lower densities. In a shorter 500-ft subplot, the 2.5-ft offset had no clear visible trend while the 6-ft offset had a strong trendline with higher temperatures having lower density.

Project 2: For both the 5,000-ft full length and a 500-ft subplot, there was no clear trend between IR temperatures at the time of paving and the final GPR density.

Project 3: A slight positive trend using all data was detected with higher density resulting from higher initial mat temperature. The first 500-ft subplot had the 6-ft offset with a positive trend, while the 9-ft and 11-ft offsets had no trend.

5.7.3 Correlations among NDTs using the Average and Standard Deviation

The mean and standard deviation were computed for each NDT using all samples within the each 500-ft subplot. These statistics created data sets of $n=10$ for the first two projects and $n=12$ for the third project. Then, statistical correlations were computed and plotted using these relatively small sample sizes. Table 5.21 summarizes the correlation slope among variables. There were inconsistent slopes among projects for any combination of variables, except for negative correlations between mean IR temperature and GPR thickness. This lack of consistency presents a challenge for using combinations of NDT tests, in their current form, as interrelated quality control and acceptance tools.

Table 5.21 Summary of Project Correlations

Variable Combination	Correlation, ↗ positive ↘ negative		
	IR mean vs GPR Thickness mean	↘	---
IR mean vs GPR Density mean	↘	↘	↗
IR mean vs Nuclear Density mean	↗	↘	↘
IR mean vs Seismic Modulus mean	↘	↗	↘
GPR Density std. dev. vs GPR Thickness std. dev.	---	↗	---
Modulus mean vs GPR Thickness mean	↗	---	---
Modulus std. dev. vs GPR Thickness std. dev.	---	↗	↘
Nuclear Density mean vs GPR Density mean	↗	---	---
Nuclear Density std. dev. vs IR Temp. std. dev.	↗	---	↗

Chapter 6 Structural Analysis

6.1 Introduction

Chapter 4 estimated the variability in the measured properties for discrete testing of seismic modulus and nuclear density. In addition, the comparison in seismic modulus at two temperatures (warm and cold) confirmed temperature dependency following expected trend for a viscoelastic material. In this chapter, the analysis focuses on the ability of the proposed technologies to distinguish nonconforming sections of pavement. This is to establish the ability of the non-destructive technologies to serve as quality control and/or acceptance tools during pavement construction. The strategy for achieving this goal is to group conforming and nonconforming locations using nuclear density, then investigate the ability of the NDT technologies (PSPA, GPR, and IR) to discriminate conformance. The determinant in whether a location is conforming to the target quality is the nuclear density measurement. A location is considered conforming if the relative density is 92% G_{mm} or higher. As reported in the literature review, density is an indicator of segregation, as well as gradation and visual observation. This chapter will also explore the interrelationship between the different NDT technology measures and illustrate the presence of strong correlations applicable using point measures, thus building upon findings in the previous chapter.

6.2 Conforming with Quality Analysis

This section evaluates the ability of the different technologies to distinguish quality between the density conforming test points and those nonconforming. The following series of plots show the average values for the different outputs from the NDT technologies in this project.

Figure 6.1 compares density measurements as indicated by the nuclear device for all three projects. The average values for the densities for the conforming test points are consistently above 93% G_{mm} . On the other hand, the nonconforming test points range in values from 89.4 to 90.7% G_{mm} . This is a clear distinction in density values and is expected to allow for the different technologies to distinguish between variations in performance. For all projects about 20% of all test points are non-conforming. The numbers inside the columns reflect the number of test points contributing the reported averages.

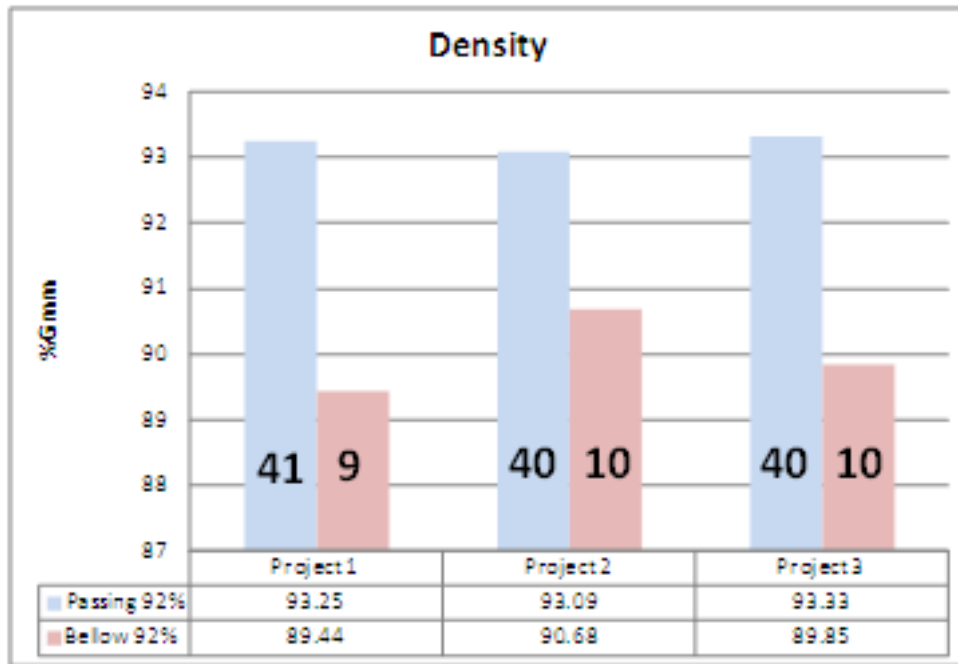


Figure 6.1 Average of Density Values for Conforming and Nonconforming Tests

Figure 6.2 is the average normalized modulus values for the density conforming and nonconforming test points. The modulus values for the subset passing 92% Gmm show a converging trend. Project 3 shows the biggest gap in modulus. This gap shrinks by half for Project 2 and almost disappears for Project 1. As mentioned earlier, the majority of the nonconforming test data are located at the left joint.

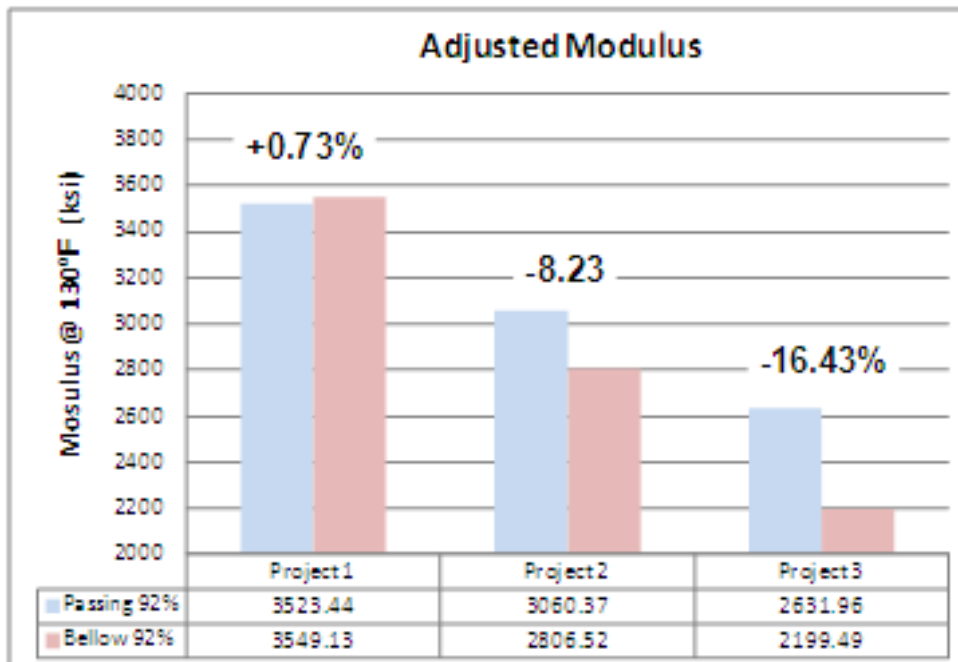


Figure 6.2 Average Modulus Values for Conforming and Nonconforming Tests

Figures 6.3 and 6.4 are similar graphs for the IR temperature and GPR thickness data when extracted at the specific test point. The measurements from the IR sensor bar and the GPR thickness do not indicate any noteworthy difference between the two groups.

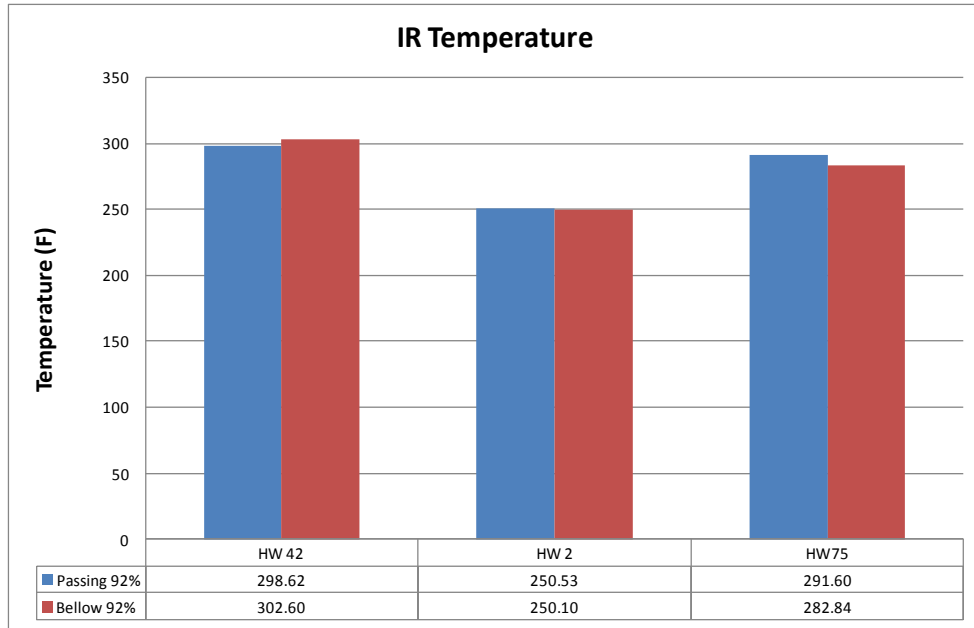


Figure 6.3 Average IR Temperature for Conforming and Nonconforming Tests

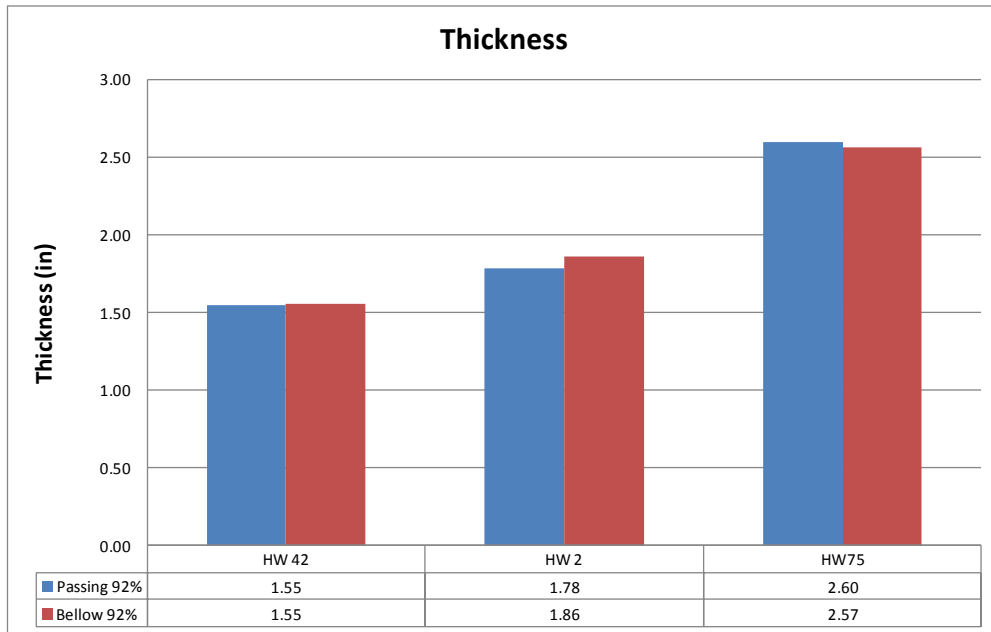


Figure 6.4 Average GPR Thicknesses for Conforming and Nonconforming Test Points

Based on the comparison of averages in the previous figures, a more detailed analysis is conducted to evaluate the differences in measurements for the potential of the NDTs to distinguish the quality during pavement construction.

6.2.1 Project 1, USH 2

For the first project, 9 of 50 test sites did not meet the 92% threshold (see Table 6.1). The range of values for the nonconforming locations is sorted ranging from 81.5% to 91.9%. It is important to note that the location of most nonconforming tests is 1 ft from centerline.

Table 6.1 Station and Offset for Nonconforming Tests on Project 1

Station	Offset, ft	Density, %
408+07	1	81.5
416+38	8	85.4
426+96	1	89.6
415+51	10	90.8
392+94	1	91.1
401+44	1	91.1
414+41	1	91.8
396+98	1	91.8
402+91	3	91.9

The results obtained from the other NDTs are used to investigate their ability to distinguish between these nonconforming locations and those conforming. Table 6.2 compares average values for multiple parameters separated by the location conforming to the 92% density threshold. The only distinguishable results are shaded in the table.

Table 6.2 shows the number of points conforming and nonconforming to the 92% density threshold. The other information listed in the table includes the PSPA modulus values, the GPR estimated density, the range of densities estimated by the GPR, the thickness of the pavement as measured by the GPR and range of thickness, the placement temperature as measured by the IR, and the range of temperatures.

Table 6.2 Quality Indicators for Conforming and Nonconforming Tests on Project 1

Measure	Passing (above 92% G_{mm})	Failing (below 92% G_{mm})
Sample Size, n	41	9
Offset Average, ft.	7.5	3.0
Density Average, %	93.2	89.4
Normalized Modulus Average, ksi	3523.4	3549.1
GPR Density Average, %	94.3	93.1
GPR Density Average Range, %	1.21	0.81
GPR Thickness Average, in.	1.78	1.86
GPR Thickness Average Range, in.	0.36	0.27
IR Temp. Average, °F	250.5	250.1
IR Temp Range Average, °F	27.2	24.8

The primary difference between the conforming and the nonconforming test sites is average offset for conforming is 7.5 ft, while the nonconforming average is 3 ft. This indicates that the middle of the lane, on average, had the most densification, while the centerline edge is less densified. With regard to all the other parameters, both sections show very similar results. It is important to note that all the paving locations studied in this research project were at least 15 ft wide, with a 12 ft driving lane and 3 to 5 ft integral shoulder. The driving lane outer edge was confined while the centerline was not.

6.2.2 Project 1, STH 75

For this project, 10 of 50 test points had density values below the 92% threshold, with the sites sorted in Table 6.3. The results continue to show that the centerline edge is less densified compared than the other pavement areas.

Table 6.3 Station and Offset for Nonconforming Tests on Project 2

Station	Offset, ft	Density, %
221+87	1	88.0
205+99	1	88.9
222+33	1	88.9
231+89	1	89.1
240+49	1	89.4
208+06	1	89.6
215+98	1	90.2
218+43	7	91.3
196+29	1	91.4
198+29	1	91.7

Table 6.4 reports the number of points conforming and nonconforming to the 92% density threshold, along a summary of the quality indicators. The data continue to support the difference in densification and modulus between the pavement centerline (1.6 ft offset) and full driving lane (7.8 ft offset). Note that the GPR density for this pavement section was not conducted at the pavement edge by the longitudinal joint due to difficulty straddling the centerline edge dropoff with the GPR test vehicle.

Table 6.4 Quality Indicators for Conforming and Nonconforming Tests on Project 2

Measure	Passing (above 92% G_{mm})	Failing (below 92% G_{mm})
Sample Size, n	40	10
Offset Average, ft.	7.8	1.6
Density Average, %	93.1	90.7
Normalized Modulus Average, ksi	3060.4	2806.5
GPR Density Average, %	94.2	N/A
GPR Density Average Range, %	0.56	0.87
GPR Thickness Average, in.	2.60	2.57
GPR Thickness Average Range, in.	0.39	0.42
IR Temp. Average, °F	291.6	282.8
IR Temp Range Average, °F	23.7	24.7

6.2.3 Project 3, STH 42

For the third project, 20 of 50 test points (20%) were nonconforming, the highest percentage of the three projects. Table 6.5 sorts the test sites by final density with reporting station and offset. The same observation is noted for this project where a majority of nonconforming test points are at the centerline edge of the pavement.

Table 6.5 Station and Offset for Nonconforming Tests on Project 3

Station	Offset, ft	Density, %
661+15	1	89.5
620+59	1	89.6
638+02	1	89.6
642+06	1	89.6
626+93	1	89.7
657+59	1	90.0
661+37	2	90.1
651+51	1	90.4
633+56	1	90.5
653+28	8	90.7

Table 6.6 summarizes the quality indicators for conforming and nonconforming points. The results indicate that the average nonconforming points are towards the pavement centerline (1.8 ft) while more are in the right wheel path (7.9 ft).

Table 6.6 Quality Indicators for Conforming and Nonconforming Tests on Project 3

Measure	Passing (above 92% G_{mm})	Failing (below 92% G_{mm})
Sample Size, n	45	20
Offset Average, ft.	7.9	1.8
Density Average, %	93.33	89.85
Normalized Modulus Average, ksi	2639.9	2199.4
GPR Density Average, %	90.2	90.4
GPR Density Average Range, %	0.71	0.65
GPR Thickness Average, in.	1.55	1.55
GPR Thickness Average Range, in.	0.19	0.12
IR Temp. Average, °F	298.6	302.6
IR Temp Range Average, °F	40.4	39.7

The results show that the modulus values of conforming points is about 16% higher than that of the nonconforming points. The other indicators show minimal differences between the conforming and nonconforming points.

6.3 Quality by Location

The previous sections illustrated the values captured by the different NDT technologies distributed by location to evaluate the quality. This analysis is further expanded to investigate dependency of the pavement quality on location, particularly by transverse offset.

Figure 6.5 is the bar graph of average density by transverse offset. For the density measurements, the results show a clear trend with densification at the centerline joint consistently lower than the other locations. The difference between the left joint and the left wheel path (LWP) density measurements is about 2 to 3 feet in distance, and more than 2% points in relative density. Average density was similar at the other offsets across the mat from the left wheel path to the right edge.

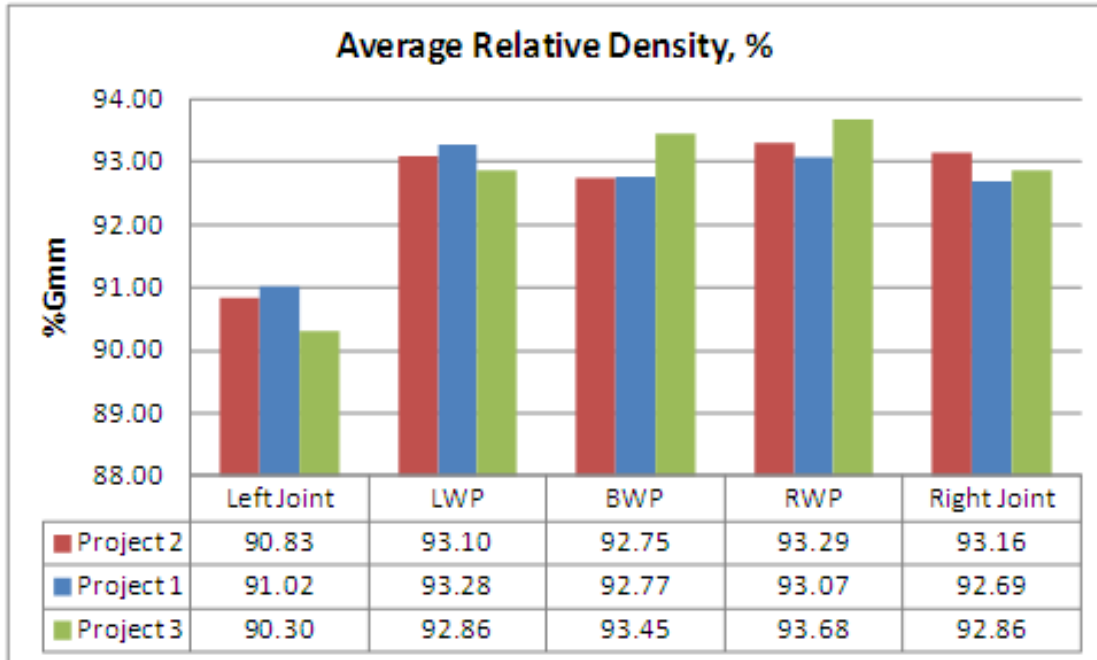


Figure 6.5 Density Average of all Projects by Transverse Locations

Figure 6.6 is a similar presentation for modulus. The PSPA predicted-modulus at 130°F followed the same trend indicating that in addition to lack of compaction at the longitudinal joint, the mechanical stability of the pavement at this location on average is not comparable to the rest of the pavement.

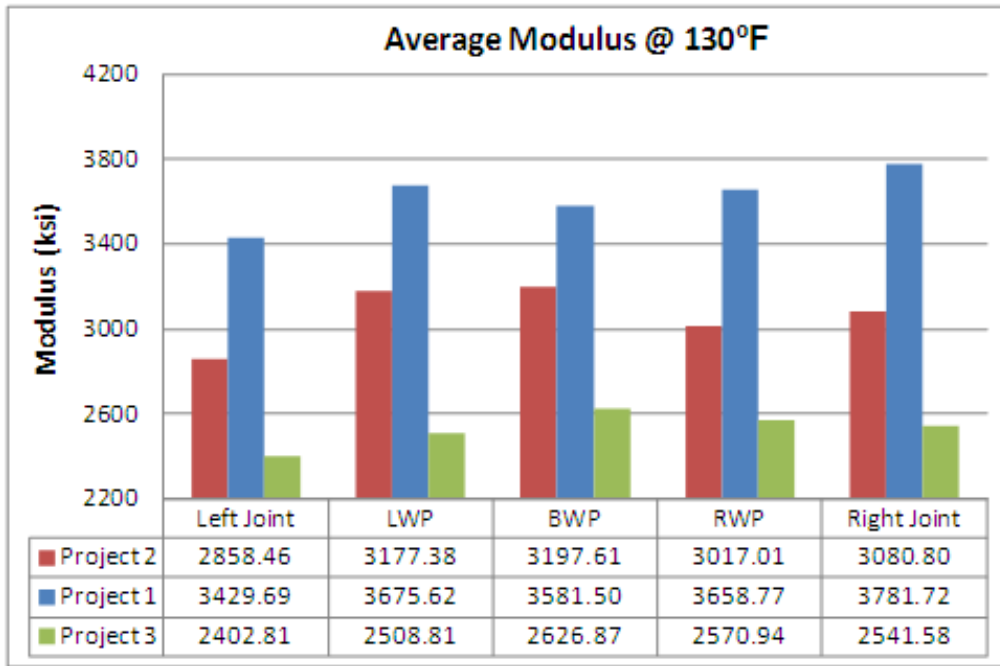


Figure 6.6 Modulus Values of all Projects by Transverse Locations

Figure 6.7 graphs the GPR pavement thickness average showing minimal changes by offset. For Hwy 2, the trend is showing a decreasing thickness towards the right side of the driving lane. Hwy 42 shows consistent average thickness of around 1.5 in. Hwy 75 shows a drop in the average thickness in the left wheel path; this project was paved on pulverized base with potential for a more variable thickness.

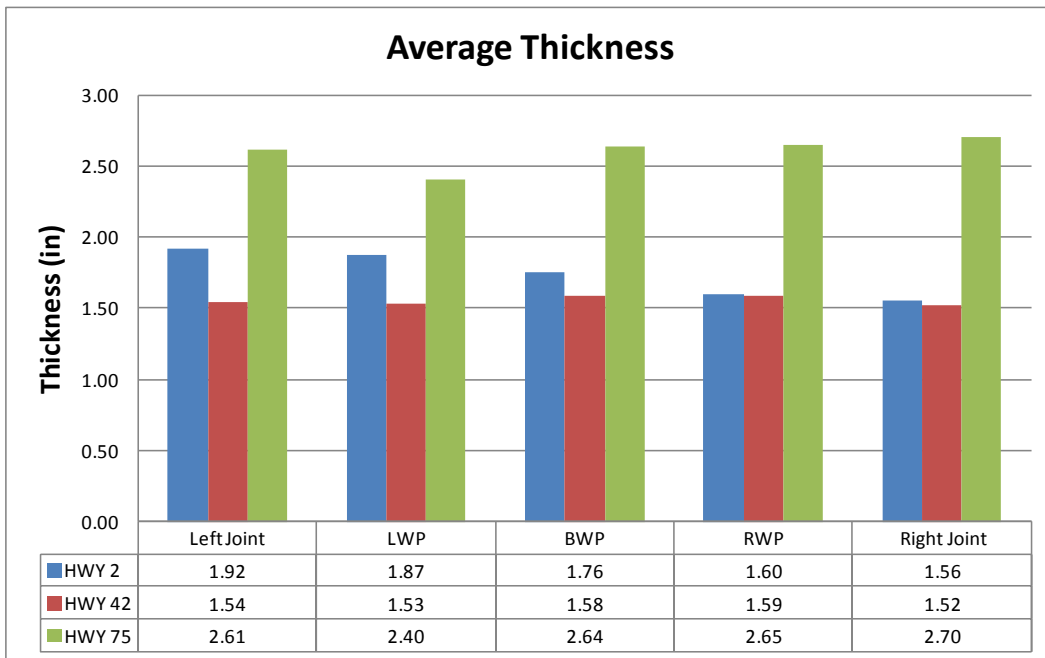


Figure 6.7 GPR Pavement Thickness of all Projects by Transverse Location

In Figure 6.8, the placement temperature values show minor differences by transverse offset indicating the mixture was rheologically uniform during laydown. The observed variability in density and modulus could be related to the state-of-practice where the compactors have more overlap in the middle of the lane.

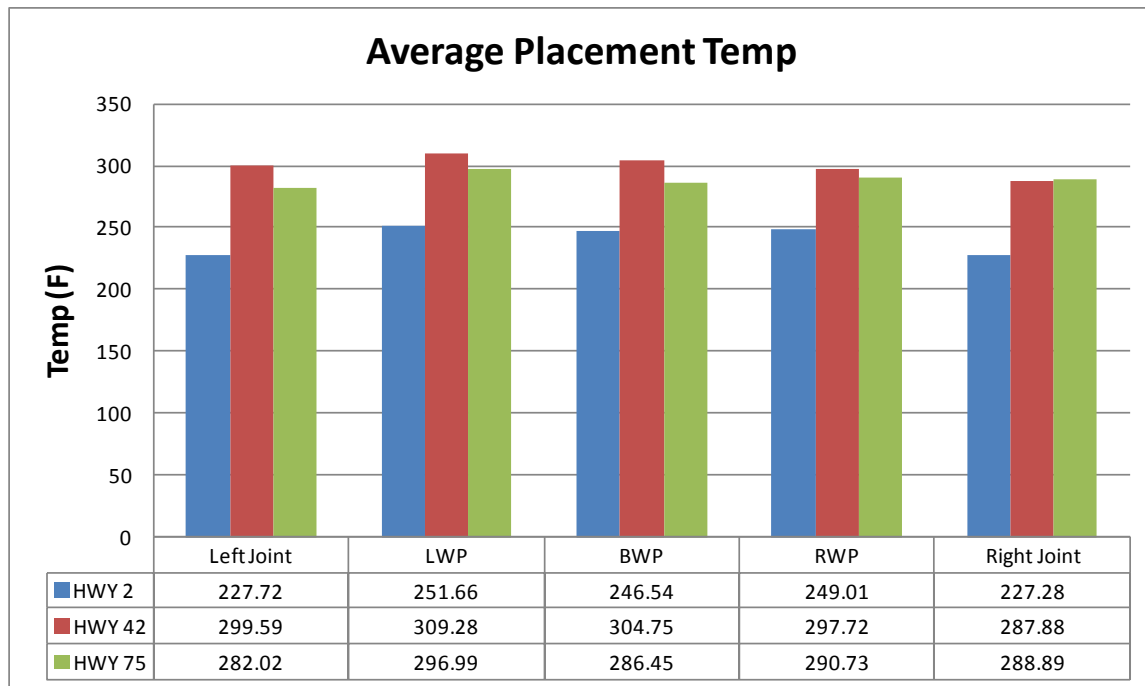


Figure 6.8 Pavement Placement Temperature of all Projects by Transverse Location

Earlier analysis showed that the placement temperature did not vary significantly. This means that the mixtures were brought to the site and paved at the same rheological condition assuming uniform mixtures. Therefore, the variability in the pavement quality indicators can only be related to the compaction process. Table 6.7 show the correlation coefficient for the linear regression with the modulus as the dependent variable and the temperature as the independent variable for projects Hwy 2, Hwy 42, and Hwy 75.

Table 6.7 Correlation Coefficient for Modulus at 130°F versus the Placement Temperature

Project	R-squared, %
Hwy 2	22.1
Hwy 75	2.3
Hwy 42	0.1

The data presented in the table show the lack of correlation between the placement temperature and the modulus. This is expected since in practice the targets the uniform relative density regardless of the placement temperature. If the temperature is a bit low,

more compaction effort is exerted, while if the temperature is higher than the target compaction temperature the crew would wait for it to cool down before compacting to the target density. Therefore, from the state of practice point of view, the placement temperature does not appear to influence the final product quality as measured by density. It is mainly serving as a process control tool for the contractor to maintain a uniform mix. It is well established that the modulus of the mixture will mainly rely on the collective structure of the compacted mix (aggregate structure bind by the asphalt binder).

6.4 Mix Properties

Mix properties among the three projects were analyzed next, using data in Table 3.3. It is important to note that the data findings are limited to three projects having a limited sample size.

Figures 6.9 plots VMA versus modulus, where the modulus showed positive dependency on VMA. The typical expected influence of the VMA on the mixture stability is that as the VMA increases, the stability is expected to improve. Then as the VMA increases further yet, the mix will experience lower stability. The mixes included in this study had a VMA range of 13.6 to 16.3%. It appears that this range begins very close to the minimum acceptable VMA value of 13% for 19mm and 14% for 12.5mm mixes.

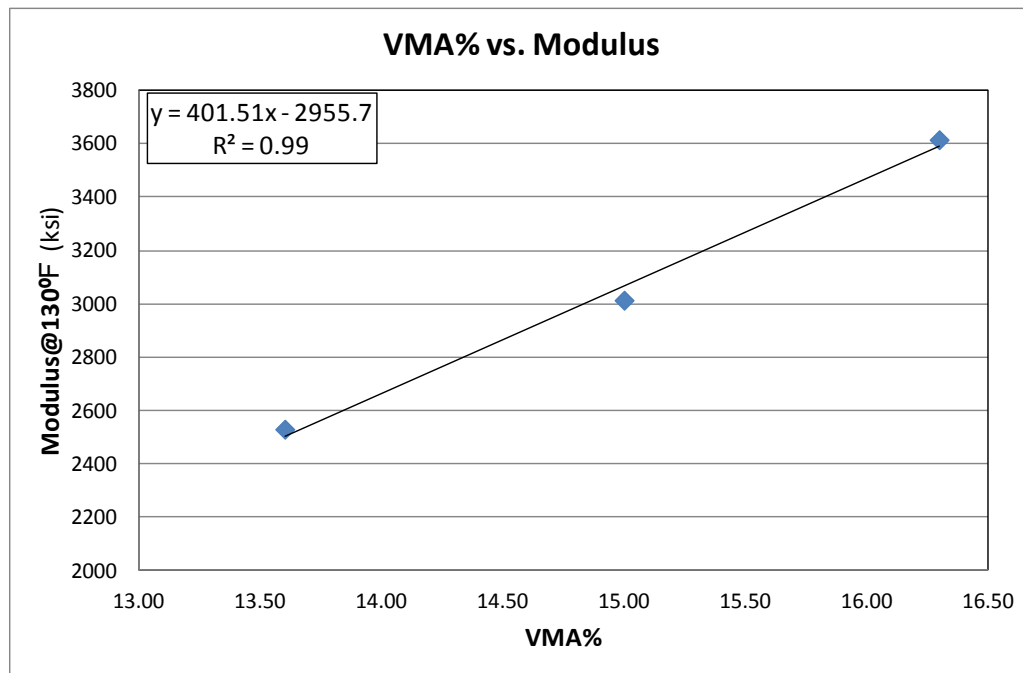


Figure 6.9 Comparison of Average Pavement Modulus and Mixture VMA

The effect of densification on the relationship of VMA with modulus is illustrated in Figure 6.10. The average data of the field projects are separated by compaction level as indicated by the 92% density cutoff value. The results for the average modulus show higher sensitivity of the under-compacted test points to VMA, as measured by the steeper slope values.

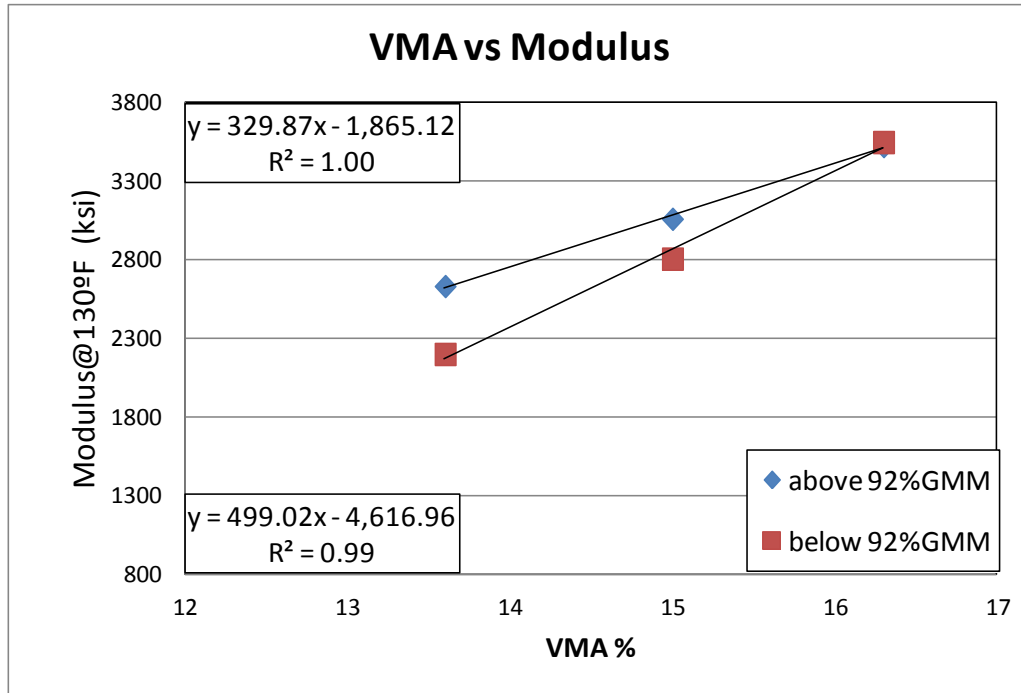


Figure 6.10 Comparison of Average Pavement Modulus and Mixture VMA for Compacted and Under-compacted Test Points

Finally, density is introduced into the comparison among mixture properties in Figure 6.11. The results of comparing the mixtures volumetric with measured field density show no correlation. This is expected, since the pavements are compacted to the same target density regardless of the laboratory volumetric values. But this observation compliments the previous observations regarding the use of modulus to achieve structural stability, where in-place density does not necessary reflect the optimum compaction of the mix. Therefore, the research strongly suggests extending this project to an additional phase focusing on testing projects that include both field seismic testing and laboratory testing using the asphalt mixture performance testing (AMPT) protocols to build a database capable of defining mutual findings among projects.

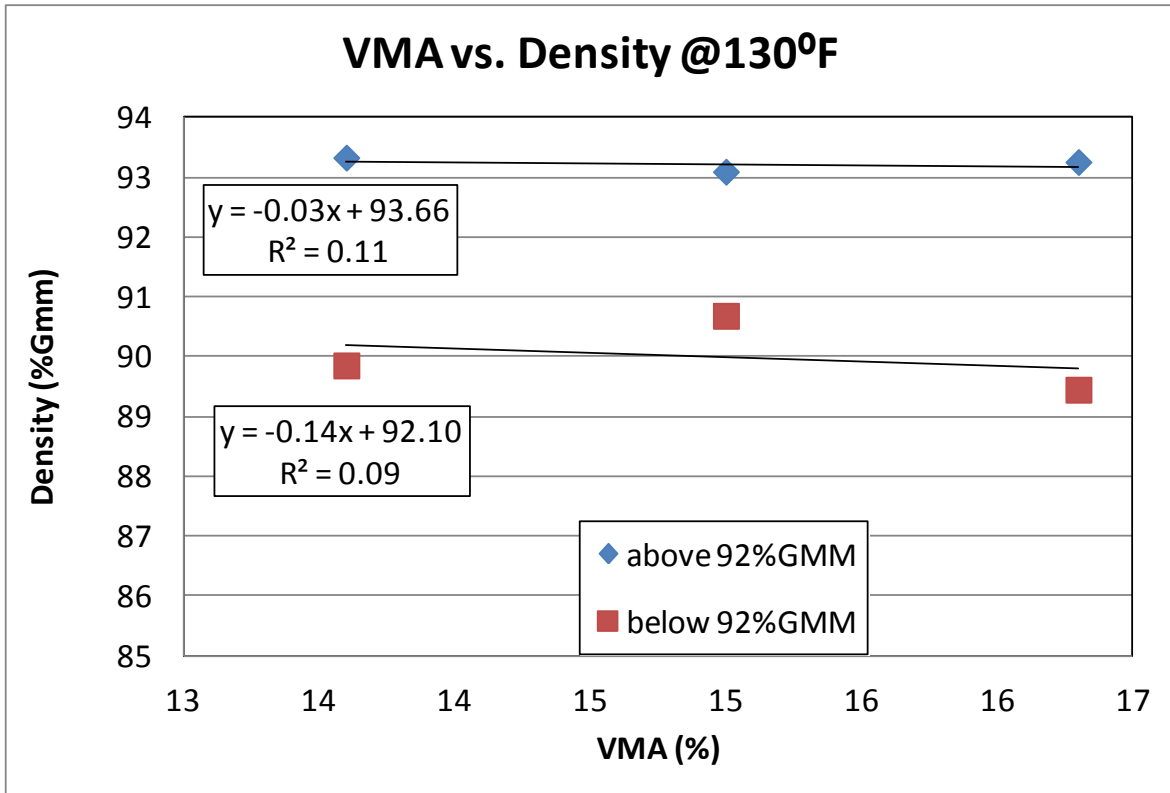


Figure 6.11 Comparison of Average Pavement In-Place Density and Mixture VMA, for Compacted and Under-compacted Test Points

6.5 Summary

The following is a summary based upon the findings in this chapter:

- (1) The majority of the nonconforming test points are at the outer edge of the pavement.
- (2) The average modulus for nonconforming test points is lower than that of conforming, except for Project 1 where the nonconforming modulus was higher by 0.73% indicating no change in results.
- (3) The results show that the for mixture with higher VMA and VFA, the influence of density diminishes. At lower VMA and VFA values, not meeting the target density resulted in a sharp decrease in the measured modulus as illustrated by the 16.43% drop in modulus for Project 2.
- (4) Placement temperature does not appear to affect measured modulus or density. This could be due to the fact that the mixture is placed at suitable temperature for compaction. Or adequate compaction effort was used to achieve the target density.
- (5) The results suggest that the final pavement quality is controlled by the compaction process behind the paver. This is very important, as it directs future focus on monitoring the compaction process closely.
- (6) It is highly recommended that this study be expanded to focus on compaction state-of-practice with respect to the outer edge.

Chapter 7 Implementation

7.1 Findings to Establish Guidelines

The purpose of this chapter is to present guidelines for implementing the NDT technologies into practice. These guidelines are a function of data findings from the study, as well as prior research and active specifications. For all technologies, more data are necessary to clearly define acceptable limits and thresholds for construction. However, at this stage, this chapter presents the framework for a “Non-Destructive Testing System” for controlling the quality of flexible pavements during construction. The system will be based on the findings of this research and on the vision of the research team on how the data collected from a system comprised of the three NDT evaluated in this study should be utilized in order to improve the quality of asphalt pavement construction.

This chapter will first establish a system of measuring the target properties. Then it will progress towards a detailed implementation strategy for corresponding devices. The purpose is to create a system that is dependent on the quality measure, instead of the testing technology. This approach provides the needed flexibility in the future for switching between different models or modes of testing to meet the quality measure as the technology advances further.

An important finding of this study is that the mixes evaluated in this study did not demonstrate sensitivity to placement temperature over the ranges measured in the field. Therefore, as a primary foundation of the proposed quality monitoring system for a verified adequate mixture that is delivered at an appropriate temperature, the system will focus on quality control for the mat behind the paver. This finding adds more emphasis on NDT testing since it is highly desirable to inspect the quality of the constructed mat with non-invasive approaches. The tasks will be expected to be conducted following the schematic in Figure 7.1.

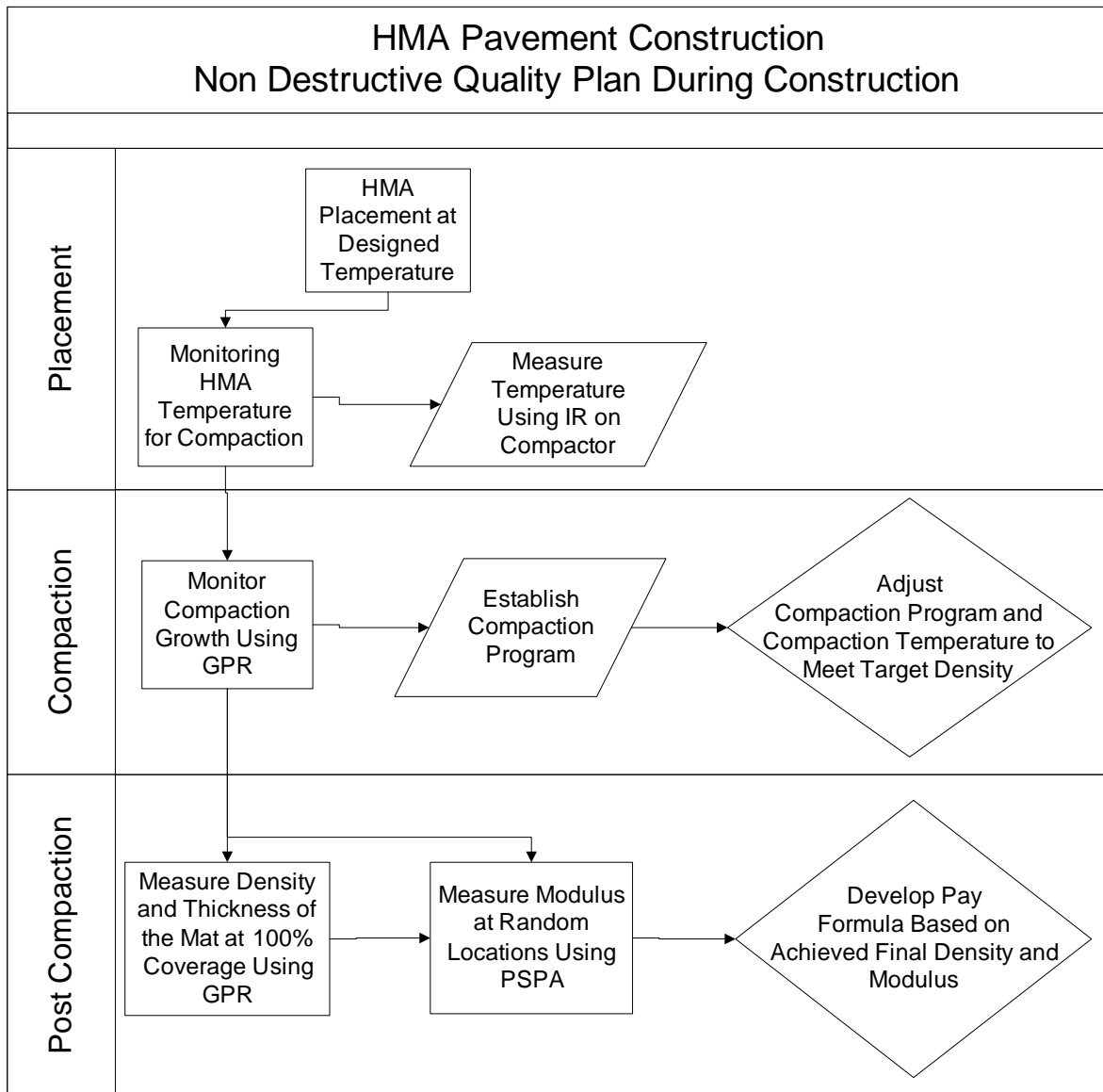


Figure 7.1 Flow Chart of NDT Quality Plan during HMA Pavement Construction

The proposed system focuses tracing the quality of the mix as it is being compacted after placement. The goal is provide a full coverage of the constructed mat using the studied technologies in this project. Therefore, the basic sequence of task to assure quality during construction is expected to be as follows:

- (1) Assure that compaction takes place at optimum temperatures using infrared technology.
- (2) Assure densification using the GPR.
- (3) Assure mechanical stability of the compacted mat using the PSPA.

It is important to point out that any implementation plan for this system must have primary goals. The first goal is to collect enough field data to establish acceptance limits applicable to the different classes of pavements. The second goal is to establish an

acceptable approach for corrective actions. This chapter proposes the framework for pursuing these goals.

Based on the findings of this study, the research team proposes to equip field compactors of temperature sensing technology to maintain the compaction process with the optimum temperature range. The implementation of this technology should limit the usage of different types of compactors (such as vibratory, static, pneumatic) to an acceptable range of temperatures to optimize their influence. The available information does not allow to proposing these limits at this stage.

With regard to densification, the proposed implementation should cover two main tasks:

Task 1: the first task is to allow the contractor to establish the densification growth for a given mix by using the GPR after every pass of the available compactors. This will give the contractor the opportunity to devise a compaction plan to achieve the target density. This plan will be set at the beginning of paving day at a test strip. The plan should be developed using at least three compaction points. The details for establishing this densification growth are provided in Section 7.3.

Task 2: the second task is concerned with establishing a density contour map of the finished product by having the GPR conduct a full scan of the paved mat. The information provided by the map should be used in the incentive pay formula where a given portion of the pavement (e.g., 90% density) is expected to meet the target density, and an incentive pay should be provided for every single additional percentage, and deduction of pay be taken for every single percent below threshold.

With regard to the mechanical stability of the finished product, the PSPA should be used to evaluate the seismic modulus of the pavement. This quality measure is expected to be phased into the QMP after developing a database of modulus values for multiple pavements. The database should contain in addition to the modulus values, mixture volumetric information (VMA, VFA) and field compaction densities. The database will be used to establish acceptance limits for pavement types. In addition, this database is expected to contain corresponding dynamic modulus values for the tested mixes using the AMPT. The goal is to calibrate the PSPA readings against the AMPT to establish acceptance limits based on the mix quality. This database will provide important tracking information for the quality of Wisconsin mixes beyond construction quality control goals.

The application of the PSPA test should be applied at random points in accordance to the Wisconsin DOT specifications for random testing. The selection of testing points should be in accordance to the current random testing used for the nuclear density gauge on pavements. The details of taking measurements at a given test point is provided in Section 7.4. Measured values of the seismic modulus shall be used in incentive payment for contractors. However, this will apply at a later stage after building the needed database.

7.2 Thermal Measurements

Specification parameters from Texas DOT procedure 244-F should be reviewed as the continuous thermal technology is used in practice. In addition, Washington DOT has included continuous thermal measurements in their construction manuals. Temperature uniformity has been documented to have an effect on pavement density in a study by Willoughby et al. (2001) where temperature differentials were found to lead to significant density differentials in the finished mat. Over 40% of the jobs observed a Washington DOT study had temperature differentials of 25°F or greater. However, in this study, there was a very weak correlation (projects 1 and 3) or no correlation (project 2) between variability in IR temperature and nuclear density.

An important consideration in interpreting the data in using the standard deviation or range. The standard deviation allows all readings equal weight in determining variability, while the range is substantially influenced by a single maximum or minimum value. In fact, placing an object between the sensor and mat, such as a tool or hand, immediately affects the range.

Several parameters in the TxDOT ‘Tex-244-F’ specification summarized by Angerhofer et al. (2011) include:

- Pave-IR profiles each 150 foot segment of paving.
- One profile per subplot.
- Excludes the outer 2 feet toward the edges.
- Determines “maximum baseline temperature” in first 20 feet of paving. This temperature will generally not be the absolute maximum from within a profile’s limits. This approach reduces the contractor’s risk.
- Locations of paver stops > 10 sec. are excluded from analysis. Using this approach eliminated irregular thermal signatures attributable to the paver stops in all cases examined.
- Omit hottest 1.5% of measurements to determine maximum baseline temperature.
- Omit coldest 1% of measurements to determine minimum profile temperature.
- Profile temperature differential is defined as: maximum – minimum.
- Engineer may reduce testing frequency.
- Engineer may also obtain as many thermal profiles as deemed necessary.
- Contractor must automatically process data.
- Pave-IR stores which sensors to ignore, and reports which sensors were not used in the temperature differential determination.

The operator must properly inspect the system geometry in relation to the paving width prior to initiating data collection. Before starting data collection, the operator selects which sensors are closer than 2 feet to the mat edges. Pave-IR will not use these sensors when calculating the temperature differential; however, the data from these sensors still is recorded for reference.

Researchers manually evaluated 380 profile segments for the specification. The hottest spot in the first 20 ft is typically 98.5% of the hottest spot in the entire profile

segment. Pave-IR ignores 1.5% of the hottest temperatures to determine the maximum baseline temperature.

Preventing ‘False Positives’ is an important component of the procedure, including:

- External factors could create artificial cold spots in data log files.
- Hand work, cooler spills, and hands/equipment in front of sensor can create problems.
- A “single point” approach for determining the minimum profile temperature would artificially inflate the temperature differential when these external factors are present in a profile

7.3 Ground Penetrating Radar

GPR scan data were collected from centerline offsets in this study. In order to evaluate pavement layer thickness and density at various locations in a lane, multiple survey lines were established at varying offset distances from the centerline. The lines were marked on the lower base or existing asphalt layer for the initial pre-paving scan, and on the freshly paved layer to align the start of each scan. While scanning, the driver visually maintained the desired centerline offset by periodically referencing the center longitudinal joint. There is the potential for lane wander during the scan, and this variability has been naturally built into the data set. It was not possible to scan all five offsets on each project due to opposing vehicle traffic near the centerline joint or layer edge drop off. Until this approach is incorporated in a compaction system on future projects, the following guidelines can be used.

Pre-survey

- Identify the locations where GPR survey vehicle can move back and forth perpendicular to the lane during the compaction, as shown in Figure 7.2.
- Communicate with the compactor operators before construction the compaction plans and the monitoring approach with GPR.

Equipment Selection

- An air-coupled antenna system should be used.
- An antenna system with a 2-GHz center frequency is recommended. This allows a good balance between accuracy and depth of GPR electromagnetic waves penetration depth. A 1-GHz antenna may be acceptable.
- One antenna system is needed.
- Distance Measuring Instrument (DMI) is not needed in this test.
- Other accessories such as Global Position System (GPS) and digital video recorder can also be used to obtain more information.

Equipment Setup

- The antennae should be mounted on either front or back side of the vehicle. Non-metallic materials should be used to support the antenna and connect it to the vehicle.

- The antennae should be placed 40-50 cm above the pavement surface and at 1-1.5 m away from the vehicle bumper. An example of the antenna setup is shown in Figure 7.2.



Figure 7.2 GPR setup for compaction status monitoring

Data Collection and Interpretation

- Two operators shall be available to perform pavement compaction monitoring. One drives the vehicle and the other operates the GPR system. With experience and further development, one person shall be able to perform the monitoring when the process becomes automated.
- Before any data collection, the GPR system shall be calibrated to ensure collecting good signal from the pavement.
- Record date, weather, operator names, file naming rules and other information related to the survey for future records.
- Move the vehicle until the antenna is 2 m away from the lane. Mark the location of the vehicle (e.g. front tire on the driver's side); an example is shown in Figure 7.3(b). This will be the *standby point*.
- Move the vehicle until the antenna is on top of the lane of interest and the antenna is above a desired location. Mark the location of the vehicle (e.g. front tire on the driver's side), as shown in Figure 7.3(a). This will be the *survey point*.
- After the compactor passes, move the vehicle to the *survey point* and collect GPR data for 100 scans, as shown in Figure 7.3(a). This process usually takes 5 to 10 sec.
- After the data collection, move the vehicle back to the *standby point* to avoid disturbing the compaction operation, as shown in Figure 7.3(b);
- Open the GPR compaction status monitoring software and load the collected data file. This allows monitoring the changes in the asphalt pavement density after each compaction pass.

- After each compaction pass, repeat the above three steps to collect and interpret data. The same *standby point* and *survey point* should be used during the compaction monitoring.
- The compaction curve can be viewed to monitor the compaction status in real time.

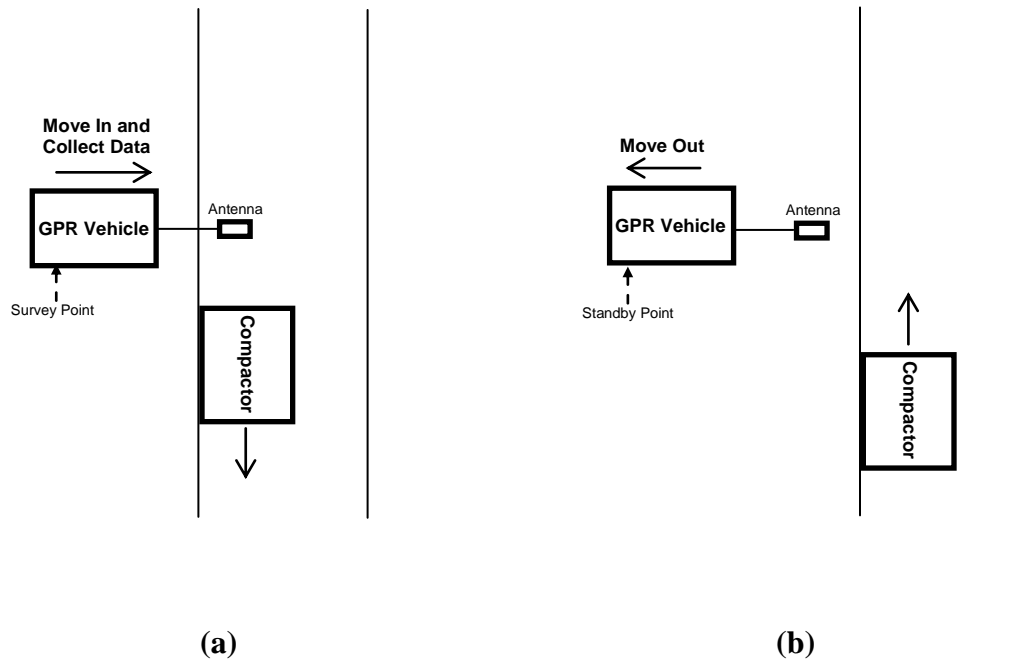


Figure 7.3 Procedure of compaction operation monitoring using GPR: collecting data between compactor passes.

7.4 Portable Seismic Pavement Analyzer

The PSPA modulus shows a strong correlation with the mix VMA and structural stability. However, the correlation is based on data from three projects only, without any supporting laboratory testing. The next stage for this effort is suggested to conduct a laboratory study to validate the results of the PSPA with mixture fundamental properties and structural stability. In addition, the dependency of the modulus values on temperature of the mat requires evaluating in the implementation process. Accordingly, the following areas are suggested to be the focus of the implementation period of this project.

- (1) Temperature dependency.
- (2) Validation of PSPA results with laboratory mixture testing.
- (3) Building a database containing, pavement mix properties, in-place density, in-place modulus, and laboratory performance testing.

The temperature dependency needs to incorporate the binder type, as well as the binder content. The preliminary results show that as the binder content increases, the rate of change in the modulus increases (Figure 7.4). This is a logical trend, since the asphalt binder is the only temperature dependent component in the mixture, and as the binder content increases, the thermal mass dependency is expected to increase.

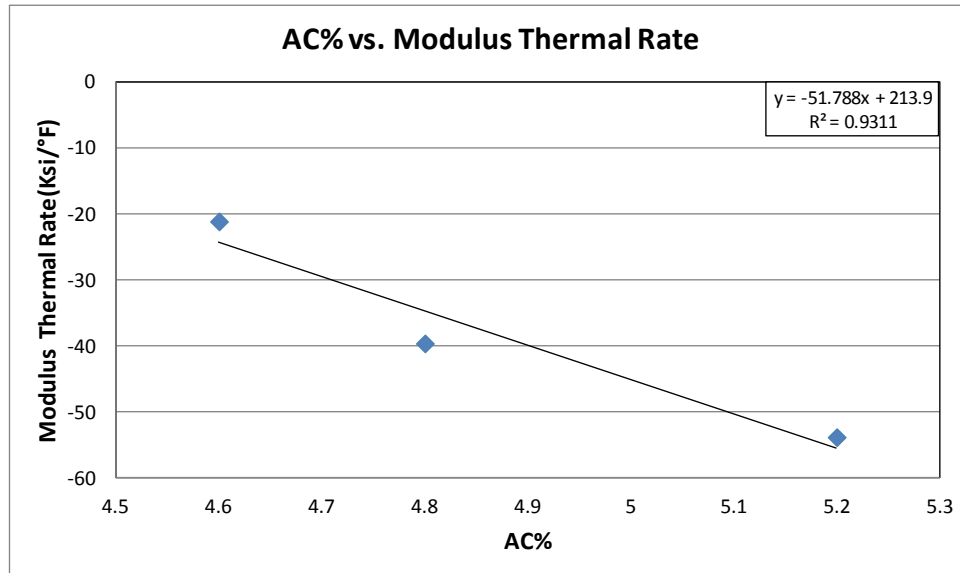


Figure 7.4 Comparison of Rate of Change in Modulus per Unit Temperature Increase and Asphalt Binder Content

The points mentioned above will serve to validate the results obtained in this study regarding the correlation of the PSPA modulus with the mixture stability. This can be done by setting a modulus threshold at which pavements should achieve to guarantee structural stability.

The following are the recommended guidelines for operating the PSPA device on site during the implementation process:

- (1) Five tests are required per testing location. The maximum and the minimum values to be omitted and the average of the remaining three tests is to be recorded.
- (2) Testing at the random location is to be conducted for the 5 runs without re-positioning the device. Consulting with the device manufacturer illustrated that re-positioning the device at the same location contributes to increasing the variability of the test.
- (3) Conduct testing at least at two different temperature ranges to establish temperature dependency
- (4) A temperature dependency model is required that takes into account the binder grade, binder content, and aggregate structure.
- (5) Conduct tests away from shaded areas, and joints to avoid interference with data.
- (6) Do not test the mat at temperatures above 140°F.
- (7) Randomize testing locations by longitudinal and transverse directions. Make sure to test near the longitudinal joint of the pavement.

- (8) Collect pavement mixture properties reflective of the tested sub-lot.
- (9) Obtain thickness information of pavement adjacent to longitudinal joints.
- (10) Collect loose mix for laboratory AMPT testing.
- (11) Record compaction passes by all rollers. Record number of passes and types of rollers.

Chapter 8 Conclusions & Recommendations

8.1 Conclusions

This report detailed Stage One and Stage Two of a research project to investigate and develop a non-destructive system to evaluate compaction. During the project, the objectives were modified to identify potential thermal segregation, measure pavement thickness and density using ground penetrating radar, and measure modulus of asphalt pavements after the compaction process. The following conclusions are summarized by project area.

8.1.1 Defining Critical Properties and Selecting NDT Technologies

Stage One research defined critical properties and non-destructive testing (NDT) technologies that have potential to assess the asphalt compaction. The identified critical characteristics are in-place compaction level, potential thermal segregation, and layer modulus. NDT technologies capable of assessing asphalt pavement during compaction were investigated including the following: Deflectometers, Ground Penetration Radar, Impact Echo, Ultrasonic Pulse Velocity, Infrared Thermography, Intelligent Compaction, Lasers, Permeameters, and Ultrasonic Seismic. Each technology was evaluated against 12 specific attributes: operational principle; measures and indicators; test equipment; portability of the test; complexity of execution in the field; time required to conduct each test; environmental limitations; reliability of collected data; committee-approved test protocols; degree of training required; cost; and states using the technology in practice.

Critical properties and characteristics were categorized in accordance with available NDTs for volumetric, structural, and functional features. A ranking was developed with an objective scoring system to determine the most appropriate NDTs for field evaluation. An overall score was calculated as the multiplicative score of the equipment properties and their ability to achieve the goals of the study. Based upon this ranking system, three higher-ranked NDTs were selected for field evaluation: Infrared Thermography (IR), Ground Penetrating Radar (GPR), and Portable Seismic Pavement Analyzer (PSPA). The nuclear density gauge was also used in the evaluation because it is a standard test for compaction evaluation in Wisconsin.

8.1.2 Field Data Collection

Using the three identified NDT devices, data were collected from three projects: USH 2 in Ashland County, STH 75 in Kenosha County, and STH 42 in Manitowoc County. The first and third projects used an E-3 mixture ($N_{des} = 75$), while the second used an E-1 mixture ($N_{des} = 60$); all were fine-graded mixes. All projects utilized a material transfer vehicle (MTV) in the paving process, except STH 75 during morning paving due a mechanical failure.

Research test section lengths were 5,000 ft to 6,000 ft. A spatial data collection plan was created where 500-ft subplot lengths were planned to manage data sampling and analysis. Five offsets from pavement centerline were established to evaluate measurements

at the two longitudinal joints, two wheel paths, and between the wheel paths. This approach offered the ability of the IR and GPR to continuously measure in a path and to detect any changes in both transverse and longitudinal directions.

8.1.3 Basic Statistical Summaries

Statistical data from each project were summarized by full research length and 500-ft subplot length. Plots illustrated where discrete point data were sampled for the PSPA and nuclear density gauge. The study was affected by project-specific factors, such as plant mixing temperature, delivered truck temperature, paver operation, and Pave-IR device calibration. The findings are discussed below.

Continuous Temperature Readings:

Table 8.1 summarizes the outcome of temperature measurements for the three projects.

Table 8.1 Project Continuous Thermal Readings

Similar Project Findings	Dissimilar Project Findings
<ul style="list-style-type: none"> • <u>Variability</u> was greater along the centerline side of the mat. <p>(Only one similar finding among the three projects).</p>	<ul style="list-style-type: none"> • <u>Average sensor temperatures</u> varied with first project ranging from 240 to 260°F, second project from 288 to 303°F, and third project from 287 to 327°F. Three sensors were out of calibration on the third project yielding higher pavement temperatures that exceeded neighboring sensors by about 25 to 40°F. • <u>Average temperature of neighboring sensors</u> were random (Project 1) or higher in the center and lower at the edges (Project 2). Project 3 had three sensors out of calibration. • <u>Variability</u> was similar between adjoining sensors (Project 3) but greater at the outer sensors (Project 1 and 2).

Continuous GPR Thickness and Density Prediction:

Project dependency for GPR thickness and density prediction was categorized in Table 8.2. Results showed consistency in GPR measurements; such as greater thickness and density variability closer to the centerline joint. The GPR density variability was half that of traditional nuclear density variability. The respective nuclear density standard deviations on the three projects were 2.21%, 1.66%, and 1.40%. By comparison, the respective project standard deviations for multiple GPR density prediction traces on a project were 1.4% and 1.1% (Project 1), 0.9% and 1.1% (Project 2), and 0.5% and 0.6% (Project 3). In other words, the GPR density standard deviation is about half that of nuclear density.

Table 8.2 Continuous GPR Measurements

Similar Project Findings	Dissimilar Project Findings
<ul style="list-style-type: none"> • <u>Thickness variability</u> and coefficient of variation close to the centerline joint was greater than other offsets. • <u>Density average</u> was similar at center and shoulder side of the mat. • <u>Density variability</u> was higher closer to the centerline joint than center of the mat. 	<ul style="list-style-type: none"> • <u>Thickness average</u> was more variable for a milled or pulverized base and more consistent over a previously paved layer. (This would be expected given the different base profiles). • <u>Density average</u> was lower at the centerline joint (Project 1).

Point Measurements for Modulus and Nuclear Density

The average nuclear density on the three projects was nearly identical, ranging from 92.4% to 92.6% and a varying standard deviations of 2.21%, 1.66%, and 1.40% on the three respective projects. Coefficient of variation for nuclear density was below 2.4% on all projects.

Average modulus constructed on Project 1 was 1,462 ksi, and Projects 2 and 3 nearly identical at about 1,270 ksi. The standard deviation was relatively high on all three projects with respective values of 382 ksi, 585 ksi, and 405 ksi. Respective COV values were also high at 27%, 64%, and 32%. This indicates that modulus variability is high when assessing pavement construction.

Modulus was investigated by offset location on the mat, as well as the sensitivity of the field test to pavement temperature (warm at about 120°F, and cool below 100°F). There was no effect on modulus by offset (centerline, between wheel path, right wheel path, etc.), but there was a reduction in modulus of 20 to 54 ksi per 1°F increase, reflecting the viscoelastic nature of asphalt pavements with temperature. This creates a complexity when measuring as-constructed modulus when the test is a function of the rapidly changing mat temperature.

8.1.4 Thermal Analysis

A detailed analysis of thermal temperature data collected by the Pave-IR sensors and the FLIR imaging camera provided a comparison among two thermal measurement methods. A comparison was also made with data from the other NDT devices including continuous GPR thickness and density prediction data, and point measures from PSPA modulus and nuclear density using subplot averages.

Pave-IR Sensors and the FLIR Imaging Camera

An evaluation of continuous thermal data and FLIR camera images resulted in the following:

- (1) A distinctive V-shaped pattern at intervals of a mix truckload length (80 to 135 ft spacing) was evident in the continuous thermal graphs from each project. The V-shaped pattern was caused by cooler material spooling transversely by the augers as the paver moved longitudinally forward.
- (2) On Project 1, there was a disagreement between the thermal bar sensors and thermal camera where the camera recorded temperatures 30°F to 50°F higher than the sensors.
- (3) The material transfer vehicle (MTV) can reduce mat temperature variability behind the screed. On Project 2, the standard deviation was reduced in half from 9.4°F to 5.5°F when the MTV was added to the operation. The average range was also reduced from 66°F to 51 °F.
- (4) Camera images of the truck box, MTV, and paver screed illustrated the mix temperature range using selected points and lines. The range of the material in the truck box was approximately 100°F to 160°F, and material temperature behind the screed ranged from 8°F to 53°F. When a pass/fail criterion was set at a range of 25°F, locations with MTV were able to pass the requirement in 10 of 11 tests. Locations not having an MTV failed the requirement in 4 of 4 tests. Use of an MTV reduced the material temperature variation range. The range reduction ratio, as measured by the ratio of the truck box temperature range to mat temperature range, was 2.1 to 14.8.
- (5) Comparisons of the temperature range with the FLIR thermal image camera and Pave-IR sensor bar found that the thermal camera image measured a higher range than the sensor bar of up to 28°F. If the thermal camera is adopted for quality control or acceptance, adherence to randomization principles is necessary to ensure that unbiased parameter estimates are obtained, hence, a sampling approach must be considered.

Comparing Continuous Thermal and GPR Data

Continuous Pave-IR readings were plotted against continuous GPR density readings. Plots for the entire project length and 500-ft subplot groupings were created. Based upon the plots for the three projects, there was no definitive relationship between continuous thermal temperatures behind the paver and final density measured by GPR. The findings from the three projects are as follows:

Project 1: Best-fit line, with a weak R^2 value, suggested that higher IR temperatures led to lower densities. In a shorter 500-ft subplot, the 2.5-ft offset had no clear visible trend; while the 6-ft offset had a strong trendline with higher temperatures and lower density.

Project 2: For both the 5,000-ft full length and a 500-ft subplot, there was no clear trend between IR temperatures at the time of paving and the final GPR density.

Project 3: A slight positive trend using all data was detected with higher density resulting from higher initial mat temperature. The first 500-ft subplot had the 6-ft offset with a positive trend, while the 9-ft and 11-ft offsets had no trend.

Correlations among NDTs Using the Average and Standard Deviation

The mean and standard deviation were computed for each NDT using all samples within the each 500-ft subplot. These statistics created data sets of n=10 for the first two projects and n=12 for the third project. Statistical correlations were computed and plotted using these relatively small sample sizes. Table 8.3 summarizes the correlation slope among variables, reporting inconsistent slopes among projects for any combination of variables, except for negative correlations between mean IR temperature and GPR thickness. This lack of consistency suggests that NDT technologies should be used as quality control for the intended parameters.

Table 8.3 Summary of Project Correlations

Variable Combination	Project correlation, ↗ positive ↘ negative		
	USH 2	STH 75	STH 42
IR mean vs GPR Thickness mean	↘	---	↘
IR mean vs GPR Density mean	↘	↘	↗
IR mean vs Nuclear Density mean	↗	↘	↘
IR mean vs Seismic Modulus mean	↘	↗	↘
GPR Density std. dev. vs GPR Thickness std. dev.	---	↗	---
Modulus mean vs GPR Thickness mean	↗	---	---
Modulus std. dev. vs GPR Thickness std. dev.	---	↗	↘
Nuclear Density mean vs GPR Density mean	↗	---	---
Nuclear Density std. dev. vs IR Temp. std. dev.	↗	---	↗

Research by Washington DOT found that temperature differentials were found to lead to significant density differentials in the finished mat (Willoughby et al. 2001). Over 40% of the jobs observed had temperature differentials of 25°F or greater. In this study, there was a very weak or no correlation between variability in IR temperature and nuclear density.

8.1.5 Structural Analysis of Point Measures

An investigation assessed the ability of the proposed technologies to distinguish nonconforming sections of pavement using nuclear density as the baseline indicator. The average values for the densities for the conforming test points are consistently above 93%, while nonconforming test points range in average density values of 89.4 to 90.7%. The majority of the nonconforming test points are at the outer edge of the pavement.

The average modulus for nonconforming test points is lower than that of conforming except for one project where the nonconforming modulus was higher by 6.5%. Modulus at the outer edge of pavement is dependent on the pavement thickness. Density of the outer edge did not correlate with the pavement thickness.

Placement temperature does not appear to affect measured modulus or density. This could be due to the fact that the mixture is placed at suitable temperature for compaction, as well as prior research that has identified number of the passes at warmer temperatures as a key factor in achieving density. The results suggest that the final pavement quality is controlled by the compaction process behind the paver.

8.2 Recommendations

Recommendations for future implementation of the considered NDT technologies are enumerated based upon findings from the field data and previous research, as well as details provided in Chapter 7. The following recommendations are provided for thermal readings, GPR thickness and density predictions, and PSPA modulus measurements.

8.2.1 Thermal Readings

Findings for thermal readings suggest that several issues must be addressed before implementing thermal readings into practice, including the following: (1) disparity between thermal sensor bar and thermal camera, (2) device calibration, (3) relationship between variability of temperature upon variability of density, and (4) relationship of thermal variability to performance. Each is briefly discussed with a plan for future research and development.

(1) First, comparisons of the temperature range with the FLIR thermal image camera and Pave-IR sensor bar found:

- Thermal camera image measured a higher range than the sensor bar of up to 28°F.

Recommendation: A ground ‘truth’ measurement should be established for thermal measurements.

- Both non-destructive tests use infrared technology, but use very different sampling approaches. Continuous Pave-IR readings offer a near-population estimate of temperature in the as-placed mat. Thermal cameras have a point-sample approach, whether the temperature points (Area, Line, or Spot) are selected. Cooler and warmer areas of interest can be knowingly selected by the camera operator or other end-user.

Recommendation: A statistically-based random sampling plan is necessary if thermal cameras are adopted for quality control and/or acceptance.

- Thermal cameras offer an excellent advantage for quality control where temperature gradients can be mapped and understood at primary tasks within the laydown process from truck box, to material transfer, to paver screed.

Recommendation: Design a future experiment to measure compaction system response within a project for a given crew and between projects for crews A, B, C, etc. Determine whether there is variability reduction using a statistical hypothesis test for variances within and between days of paving.

- (2) Second, device calibration is an issue with respect to the Pave-IR sensing system. It was observed at the start of paving on Project 3 that three temperature sensors were out of calibration with respect to the other sensors with 25°F to 40°F higher temperature than the neighboring sensors

Recommendation: A parallel comparison among sensors from future projects is necessary so that sensor calibration tolerances can be created.

- (3) Third, the relationship between variability of temperature upon variability of density found a very weak to no correlation. Research at the state of Washington found that temperature differentials were found to lead to significant density differentials in the finished mat (Willoughby et al. 2001). Recent research has found that number of passes is one of the most significant factors in achieving density gains in the mat (Schmitt et al. 2009).

Recommendation: Collect data from future projects and determine if there is a definitive relationship between variability in IR mat temperature and density. Based on the data in this study, the relationship is inconclusive.

- (4) Lastly, the correlations in this study did not find a consistent comparison between infrared temperature and GPR density across the projects. In fact, warmer temperatures led to lower GPR density, a finding that is contrary to conventional practice.

Recommendation: A performance study is necessary to investigate the relationship between thermal temperatures, both mean and variability, with performance. A range of performance-related distresses should be aligned with the as-placed mat temperature.

8.2.2 GPR Technology

The findings for GPR measurement of thickness and density suggest that GPR is state-of-the-art for HMA construction, with many states investigating its potential, but none

using in practice for quality control or acceptance. Immediate use in specifications and construction manuals should be delayed until these specific findings are addressed: (1) consistency of GPR readings with other quality control measures and (2) data collection.

- (1) First, statistical correlations of GPR measures with other field measures during compaction, including IR temperature and PSPA modulus, found inconsistent results. Variability in GPR measured density (as measured by standard deviation) was half of the nuclear density measurement method.

Recommendation. Decide if using the GPR density measurement method is acceptable when it measures half the variability of the nuclear density measurement method. This will require evaluation of specification values.

- (2) Second, GPR traces were conducted before paving and after paving, presenting a test window that must be factored into typical construction schedules.

Recommendation: The pre-paving scan is recommended to adjust raw readings from final compaction traces. Final compaction measurements must be made while the pavement is dry, due to the effects from electromagnetic pulses interacting with pavement moisture.

8.2.3 PSPA for Modulus

Findings from PSPA measurements suggest that this technology is state-of-the-art for HMA construction. This technology is of interest in determining pavement strength with a seismic wave technique. Future research and development is necessary to address these specific concerns: (1) relationship with nuclear density and stiffness, (2) minimizing the level of variability, (3) temperature dependency during data collection, and (4) confirm relationship with mixture volumetrics.

- (1) First, the ability of the PSPA to discriminate between conforming and nonconforming pavement sections resulted in a mixed outcome. Areas with insufficient densification would have average levels of modulus, suggesting the inability of the PSPA to identify lower densified and potentially underperforming areas in the mat. The modulus was primarily a function of pavement thickness, with the centerline joint having the greatest level of thickness variability, as measured by the GPR

Recommendation: Additional data should be collected to assess the ability of the PSPA to identify nonconforming areas in the pavement. Then, the performance can be tracked similar to the thermal readings experiment.

- (2) Measurement of modulus is a function of mat temperature, as would be expected for a viscoelastic material.

Recommendation: A temperature adjustment is necessary on all projects by developing a calibration curve similar to this study.

- (3) Modulus values measured show strong dependency on mixture volumetric. This relationship can provide the contractors with an essential tool to design mixes with optimum structural stability. This is a paradigm shift in mix design process, since traditionally design is geared towards achieving volumetric goal only.

Recommendation: A database of multiple mixes showing volumetric values and field modulus values is essential to establish clear target values for different classes of highways.

8.2.4 Technology Selection Process

It is recommended that the selection process for the chosen technologies be expanded to include performance parameters and impacts. Individual PCI performance parameters could be cross-listed in matrix form with the technology, such as longitudinal cracking with Pave-IR. The new selection process should incorporate existing and newly defined relationships between the technology and performance parameter and impacts. Several heuristic methods should be considered, such as neural networks, fuzzy logic, objective cost function, and sensitivity analysis of weighting factors using simulation. A comparison between methods is necessary to compare inputs and outputs.

References

- Al-Qadi, I.L., Leng, Z., Lahaour, S., and Baek, J. (2010). "In-place Hot-mix Asphalt Density Measurement Using Ground Penetrating Radar", *Journal of Transportation Research Record*, TRR 2152, pp.19-27.
- Al-Qadi, I.L., and Lahouar, S. (2005). "Measuring layer thicknesses with GPR-Theory to practice." *Construction and Building Materials*, 19(10), 763-772.
- Angerhofer, P., Lano, J., and Motak, G. (2010). "The Nuts and Bolts of Thermal Profiling with Pave-IR", Pave-IR Webinar Module 3, Moba Corporation, Fayette, GA.
- Asphalt Institute (2003). Asphalt Maintenance and Rehabilitation FAQs, <<http://www.asphaltinstitute.org/index.asp>> (Feb. 1, 2011).
- Brown, E.R., Hainin, M.R., Cooley, L.A. Jr., and Hurley, G. (2004). "Relationship of Air Voids, Lift Thickness, and Permeability of Hot Mix Asphalt Pavements," NCHRP Report 531, National Cooperative Highway Research Program, Transportation Research Board, Washington, D.C., September 2004.
- Brown, E.R., and Brownfield, J.R. (1988). "Investigation of Rutting and Segregation of Asphalt Mixtures in the State of Georgia." Georgia Department of Transportation, Atlanta, GA.
- Buchanan, M.S. and Cooley, L.A. (2003). "Investigation of Tender Zone in Compaction of Coarse-Graded Superpave® Hot-Mix Asphalt Mixtures," *Transportation Research Record: Journal of the Transportation Research Board*, No. 1861, 2003, pp. 29-36.
- Choubane, B., Page, G.C., and Musselman, J.A. (1998). "Investigation of Water Permeability of Coarse-Graded Superpave Pavements." *Journal of the Association of Asphalt Paving Technologists*, Volume 67, 1998.
- Cooley, L.A., Prowell, B.D., and Brown, E.R. (2002). "Issues Pertaining to the Permeability Characteristics of Coarse-Graded Superpave Mixes," NCAT Report No. 2002-06, National Center for Asphalt Technology, Auburn, AL.
- Cross, S.A.; and Brown, E.R. (1993). "Effect of Segregation on Performance of Hot-Mix Asphalt", *Transportation Research Record*, No. 1417, Transportation Research Board, Washington, D.C. pp. 117-126.
- Geomedia (2010). "Portable Seismic Property Analyzer for Nondestructive Testing", <<http://www.geomedia.us>>, (Dec. 20, 2010).
- Hand, A. (2009). "Material Selection and Construction of the Ideal Asphalt Pavement", *Journal of the Association of Asphalt Paving Technologists*, Symposium on the Ideal Asphalt Pavement, Vol 78, St. Paul, MN.

Kandhal, P.S., Ramirez, T.L., and Ingram, P.M. (2001). "Evaluation of Eight Longitudinal Joint Construction Techniques for Asphalt Pavements in Pennsylvania," *Transportation Research Record: Journal of the Transportation Research Board*, No. 1813, Transportation Research Board of the National Academies, Washington, D.C., 2001, pp. 87-94.

Lahouar, S., and Al-Qadi, I.L. (2008). "Automatic detection of multiple pavement layers from GPR data", *NDT and E International*, Vol. 41(2), pp. 69-81.

Lahouar, S. (2003). *Development of Data Analysis Algorithms for Interpretation of Ground Penetrating Radar Data*. Ph.D. Dissertation, Virginia Polytechnic Institute and State University, Blacksburg, VA.

Leng, Z., Al-Qadi, I.L., Baek, J., and Lahouar, S. (2009). "Selection of antenna type and frequency for pavement surveys using GPR." *88th Annual Meeting of the Transportation Research Board*, CD-ROM, Transportation Research Board of the National Academies, Washington, D.C.

Leng, Z., Al-Qadi, I.L., and Lahaour, S. (2011). "Development and Validation for In-situ Asphalt Mixture Density Prediction Model", *NDT&E International*, Elsevier, Vol. 44, No. 4, pp. 369-375.

Mahoney, J.P, and Backus, A.W. (1999). "QA Specification Practices", Washington State Transportation Center Research Report, Seattle, WA,
<<http://www.fhwa.dot.gov/pavement/smoothness/>> (Feb. 1 2011).

Moba Corporation (2011). "MOBA PAVE-IR - Paving the way to higher quality and efficiency", Moba Mobile Automation AG, Limburg, Germany, and Fayetteville, GA,
<<http://www.moba.de/en.html>> (Mar. 24, 2011).

Mohammad, L.N., Bae, A., Elseifi, M.A., Button, J.W., and Patel, N. (2010). "Effects of Pavement Surface Type and Sample Preparation Method on Tack Coat Interface Shear Strength", *Journal of the Transportation Research Board – No. 2180*, Washington, D.C., pp. 93-101.

Mohammad, L.N., Bae, A., Elseifi, M.A., Button, J.W., and Scherocman, J.A. (2009). Development of Pull-off Test Device and Methodology to Evaluate Bond Strength of Tack Coat Materials in the Field. *Journal of the Transportation Research Board - No. 2126*, Washington, D.C., pp. 1-11.

Monismith, C., and Harvey, J. (2009). "The Ideal Asphalt Pavements: Pavement Design", *Journal of the Association of Asphalt Pavement Technologists*, Symposium on the Ideal Asphalt Pavement, Vol. 78, St. Paul, MN.

Musselman, J.A., Choubane, B., Page, G.C., and Upshaw, P.B. (1998). "Superpave Field Implementation: Florida's Early Experience", *Transportation Research Record*, No. 1609, Washington, D.C.

Nazarian, S., Yuan, D., Tandon V., and Arellano, M. (2005). "Quality Management of Flexible Pavement Layers with Seismic Methods", Texas Department of Transportation, FHWA Research Report 0-1735, Washington, D.C.

Noureldin, S., Zhu, K., Harris, D., and Shuo, L. (2005). "Non- Destructive Estimation Of Pavement Thickness, Structural Number, and Subgrade Resilience Along InDOT Highways", Final sReport, FHWA/IN/JTRP-2004/35, SPR-2408.

Paye, B., and Bahia, H. (2001). "Minimum Pavement Lift Thickness for Superpave Mixtures", WisDOT Highway Research Study 0092-00-04. Wisconsin Department of Transportation, Madison, WI.

Russell, J., Bahia, H., Kanitpong, K., Croveti, J., and Schmitt, R. (2005). "Effect Of Pavement Thickness On Superpave Mix Permeability And Density", WisDOT Highway Research Study 0092-02-14. Wisconsin Department of Transportation, Madison, WI.

SAS (2010). "Correlation Analysis for SAS", SASTM v9.1 User's Guide, Statistical Analysis Software, Inc., Cary, NC.

Sayers, M.W., and Karamihas, S.M. (1998). "Little Book of Profiling". University of Michigan Transportation Research Institute, <<http://www.umtri.umich.edu/content/LittleBook98R.pdf>> (Jan. 11, 2011).

Schmitt, R.L, Bahia, H.U., Johnson, C., and Hanz, A. (2009), "Effects of Temperature and Compaction Effort on Field and Lab Densification of HMA", *Journal of the Association of Asphalt Paving Technologists 2009*, Vol. 78, St. Paul, MN.

Stroup-Gardiner, M., and Brown, E.R. (2000). *Segregation in Hot-Mix Asphalt Pavement*, National Cooperative Highway Research Program, Report 441, Transportation Research Board, Washington, D.C.

Von Quintus, H. (2009). "Performance Characteristics of the Ideal Asphalt Pavement", *Journal of the Association of Asphalt Pavement Technologists*, Symposium on the Ideal Asphalt Pavement, Vol. 78, St. Paul, MN.

UWP-Bloom (2011). "Investigation and Development of a Non-Destructive System to Evaluate Critical Properties of Asphalt Pavements during the Compaction Process - Interim Report", Wisconsin Highway Research Program, Internal Report, University of Wisconsin – Platteville and The Bloom Companies, LLC, April 21, 2011.

Von Quintus, H.L., Rao, C., Minchin, R.E. Jr., Nazarian, S., Maser, K., and Prowell, B. (2009). "NDT Technology for Quality Assurance of HMA Pavement Construction", NCHRP Report 626, Washington, D.C.

Williams, R.C., Duncan, G. Jr., and White, T.D. (1996). "Hot-Mix Asphalt Segregation: Measurement and Effects", *Transportation Research Record, No. 1543*. Transportation Research Board, Washington, D.C. pp. 97-105.

Willoughby, K.A., Mahoney, J.P., Pierce, L.M., Uhlmeyer, J.S., Anderson, K.W., Read, S.A., Muench, S.T., Thompson, T.R., and Moore, R. (2001). "Construction-Related Asphalt Concrete Pavement Temperature Differentials and the Corresponding Density Differentials", Washington State Transportation Center Final Report, Olympia, WA.

Appendix A – Infrared Thermography Sublot Data Summary

Project 1, USH 2

Table A.1 IR Basic Statistics for Project 1 Sublot 1 Sta. 435+00 to 430+00

Measure	N	Mean	Std. Dev.	Coeff. Var.	Maximum	Minimum	Range
Sensor 12 at 1.0 ft, °F	500	232.8	31.6	13.6	252.3	95.0	157.3
Sensor 11 at 2.1 ft, °F	500	235.9	30.3	12.9	252.7	98.4	154.3
Sensor 10 at 3.2 ft, °F	500	233.6	34.6	14.8	253.2	95.9	157.3
Sensor 9 at 4.3 ft, °F	500	225.6	34.8	15.4	247.5	85.1	162.4
Sensor 8 at 5.3 ft, °F	500	227.6	32.9	14.5	248.4	91.8	156.6
Sensor 7 at 6.4 ft, °F	500	231.2	25.4	11.0	248.2	96.8	151.4
Sensor 6 at 7.5 ft, °F	500	239.6	18.9	7.9	255.2	97.7	157.5
Sensor 5 at 8.6 ft, °F	500	240.1	15.2	6.3	253.0	96.3	156.7
Sensor 4 at 9.7 ft, °F	500	236.4	16.2	6.9	252.3	97.9	154.4
Sensor 3 at 10.8 ft, °F	500	233.9	17.5	7.5	248.0	91.9	156.1
Sensor 2 at 11.8 ft, °F	500	248.8	19.1	7.7	262.6	101.7	160.9
Sensor 1 at 12.9 ft, °F	500	242.5	5.0	2.1	253.4	227.5	25.9

Table A.2 IR Basic Statistics for Project 1 Sublot 2 Sta. 430+00 to 425+00

Measure	N	Mean	Std. Dev.	Coeff. Var.	Maximum	Minimum	Range
Sensor 12 at 1.0 ft, °F	500	247.7	6.1	2.5	257.2	198.3	58.9
Sensor 11 at 2.1 ft, °F	500	248.3	6.2	2.5	258.3	199.6	58.7
Sensor 10 at 3.2 ft, °F	500	248.3	8.4	3.4	259.9	201.2	58.7
Sensor 9 at 4.3 ft, °F	500	242.1	8.1	3.3	254.7	196.0	58.7
Sensor 8 at 5.3 ft, °F	500	243.9	7.7	3.1	256.3	197.6	58.7
Sensor 7 at 6.4 ft, °F	500	243.9	6.7	2.8	253.8	197.6	56.2
Sensor 6 at 7.5 ft, °F	500	249.2	6.7	2.7	261.5	205.0	56.5
Sensor 5 at 8.6 ft, °F	500	250.0	7.0	2.8	261.5	199.0	62.5
Sensor 4 at 9.7 ft, °F	500	245.6	8.1	3.3	258.6	198.0	60.6
Sensor 3 at 10.8 ft, °F	500	244.7	8.0	3.3	256.8	196.0	60.8
Sensor 2 at 11.8 ft, °F	500	259.9	7.7	3.0	271.9	205.3	66.6
Sensor 1 at 12.9 ft, °F	500	250.9	6.3	2.5	261.5	202.5	59.0

Table A.3 IR Basic Statistics for Project 1 Sublot 3 Sta. 425+00 to 420+00

Measure	N	Mean	Std. Dev.	Coeff. Var.	Maximum	Minimum	Range
Sensor 12 at 1.0 ft, °F	500	246.0	4.2	1.7	254.7	218.3	36.4
Sensor 11 at 2.1 ft, °F	500	246.9	4.4	1.8	255.4	222.1	33.3
Sensor 10 at 3.2 ft, °F	500	246.1	7.0	2.9	256.1	223.9	32.2
Sensor 9 at 4.3 ft, °F	500	238.5	6.9	2.9	250.0	214.7	35.3
Sensor 8 at 5.3 ft, °F	500	240.3	6.2	2.6	250.3	219.4	30.9
Sensor 7 at 6.4 ft, °F	500	241.2	5.1	2.1	250.7	215.6	35.1
Sensor 6 at 7.5 ft, °F	500	248.0	5.1	2.1	257.9	227.7	30.2
Sensor 5 at 8.6 ft, °F	500	246.6	4.7	1.9	256.8	225.7	31.1
Sensor 4 at 9.7 ft, °F	500	241.5	5.7	2.4	251.1	221.2	29.9
Sensor 3 at 10.8 ft, °F	500	241.8	7.0	2.9	252.3	216.7	35.6
Sensor 2 at 11.8 ft, °F	500	257.1	6.1	2.4	267.6	229.6	38.0
Sensor 1 at 12.9 ft, °F	500	249.0	4.4	1.8	257.0	224.8	32.2

Table A.4 IR Basic Statistics for Project 1 Sublot 4 Sta. 420+00 to 415+00

Measure	N	Mean	Std. Dev.	Coeff. Var.	Maximum	Minimum	Range
Sensor 12 at 1.0 ft, °F	500	223.8	50.3	22.5	256.1	97.0	159.1
Sensor 11 at 2.1 ft, °F	500	226.3	48.9	21.6	258.3	100.0	158.3
Sensor 10 at 3.2 ft, °F	500	228.0	47.6	20.9	261.5	100.9	160.6
Sensor 9 at 4.3 ft, °F	500	221.1	47.7	21.6	253.9	97.5	156.4
Sensor 8 at 5.3 ft, °F	500	221.8	45.1	20.3	254.1	103.6	150.5
Sensor 7 at 6.4 ft, °F	500	224.3	44.2	19.7	254.5	105.4	149.1
Sensor 6 at 7.5 ft, °F	500	229.0	46.7	20.4	264.4	106.2	158.2
Sensor 5 at 8.6 ft, °F	500	230.3	44.9	19.5	261.9	107.6	154.3
Sensor 4 at 9.7 ft, °F	500	223.7	44.1	19.7	256.1	105.1	151.0
Sensor 3 at 10.8 ft, °F	500	223.1	47.6	21.3	258.1	99.3	158.8
Sensor 2 at 11.8 ft, °F	500	236.0	51.2	21.7	270.1	102.9	167.2
Sensor 1 at 12.9 ft, °F	500	227.6	49.6	21.8	261.7	104.7	157.0

Table A.5 IR Basic Statistics for Project 1 Sublot 5 Sta. 415+00 to 410+00

Measure	N	Mean	Std. Dev.	Coeff. Var.	Maximum	Minimum	Range
Sensor 12 at 1.0 ft, °F	500	248.3	2.8	1.1	255.9	239.5	16.4
Sensor 11 at 2.1 ft, °F	500	249.0	3.1	1.3	257.9	239.9	18.0
Sensor 10 at 3.2 ft, °F	500	248.4	4.5	1.8	259.7	231.3	28.4
Sensor 9 at 4.3 ft, °F	500	240.7	4.5	1.9	251.1	225.7	25.4
Sensor 8 at 5.3 ft, °F	500	240.9	6.4	2.6	252.0	216.5	35.5
Sensor 7 at 6.4 ft, °F	500	242.4	3.7	1.5	252.1	231.3	20.8
Sensor 6 at 7.5 ft, °F	500	249.6	3.5	1.4	259.0	237.0	22.0
Sensor 5 at 8.6 ft, °F	500	248.5	3.8	1.5	262.8	234.7	28.1
Sensor 4 at 9.7 ft, °F	500	243.9	6.7	2.7	258.6	216.0	42.6
Sensor 3 at 10.8 ft, °F	500	242.1	6.7	2.8	255.7	207.5	48.2
Sensor 2 at 11.8 ft, °F	500	259.2	4.4	1.7	272.3	238.8	33.5
Sensor 1 at 12.9 ft, °F	500	250.0	3.9	1.6	257.2	234.0	23.2

Table A.6 IR Basic Statistics for Project 1 Sublot 6 Sta. 410+00 to 405+00

Measure	N	Mean	Std. Dev.	Coeff. Var.	Maximum	Minimum	Range
Sensor 12 at 1.0 ft, °F	500	255.0	5.5	2.1	263.3	214.3	49.0
Sensor 11 at 2.1 ft, °F	500	256.5	5.0	2.0	264.7	216.0	48.7
Sensor 10 at 3.2 ft, °F	500	255.9	6.5	2.5	268.3	214.9	53.4
Sensor 9 at 4.3 ft, °F	500	248.2	6.5	2.6	261.5	207.3	54.2
Sensor 8 at 5.3 ft, °F	500	248.8	8.3	3.3	262.4	187.3	75.1
Sensor 7 at 6.4 ft, °F	500	250.0	5.9	2.4	260.2	208.9	51.3
Sensor 6 at 7.5 ft, °F	500	257.0	6.6	2.6	268.9	209.7	59.2
Sensor 5 at 8.6 ft, °F	500	256.2	6.8	2.7	267.6	211.5	56.1
Sensor 4 at 9.7 ft, °F	500	250.3	8.4	3.3	263.8	206.8	57.0
Sensor 3 at 10.8 ft, °F	500	251.2	6.5	2.6	263.1	206.2	56.9
Sensor 2 at 11.8 ft, °F	500	267.2	6.4	2.4	280.8	219.7	61.1
Sensor 1 at 12.9 ft, °F	500	257.6	12.9	5.0	269.1	104.0	165.1

Table A.7 IR Basic Statistics for Project 1 Sublot 7 Sta. 405+00 to 400+00

Measure	N	Mean	Std. Dev.	Coeff. Var.	Maximum	Minimum	Range
Sensor 12 at 1.0 ft, °F	500	249.0	4.5	1.8	258.1	235.6	22.5
Sensor 11 at 2.1 ft, °F	500	249.8	4.4	1.7	258.4	239.7	18.7
Sensor 10 at 3.2 ft, °F	500	248.8	6.8	2.7	260.2	229.6	30.6
Sensor 9 at 4.3 ft, °F	500	241.2	5.6	2.3	252.0	223.0	29.0
Sensor 8 at 5.3 ft, °F	500	243.7	5.0	2.1	251.8	228.9	22.9
Sensor 7 at 6.4 ft, °F	500	243.4	4.2	1.7	252.0	234.3	17.7
Sensor 6 at 7.5 ft, °F	500	242.3	4.1	1.7	251.6	228.7	22.9
Sensor 5 at 8.6 ft, °F	500	249.5	4.5	1.8	263.8	235.2	28.6
Sensor 4 at 9.7 ft, °F	500	246.1	5.5	2.2	259.9	217.9	42.0
Sensor 3 at 10.8 ft, °F	500	243.8	4.9	2.0	254.7	234.1	20.6
Sensor 2 at 11.8 ft, °F	500	258.7	6.0	2.3	270.0	241.5	28.5
Sensor 1 at 12.9 ft, °F	500	256.3	4.9	1.9	266.7	243.1	23.6

Table A.8 IR Basic Statistics for Project 1 Sublot 8 Sta. 400+00 to 395+00

Measure	N	Mean	Std. Dev.	Coeff. Var.	Maximum	Minimum	Range
Sensor 12 at 1.0 ft, °F	500	254.5	5.1	2.0	266.7	228.9	37.8
Sensor 11 at 2.1 ft, °F	500	256.2	5.4	2.1	267.6	235.6	32.0
Sensor 10 at 3.2 ft, °F	500	256.2	7.9	3.1	270.9	225.5	45.4
Sensor 9 at 4.3 ft, °F	500	247.9	6.1	2.4	259.5	224.8	34.7
Sensor 8 at 5.3 ft, °F	500	250.9	5.5	2.2	263.8	227.3	36.5
Sensor 7 at 6.4 ft, °F	500	249.6	4.9	2.0	259.0	228.4	30.6
Sensor 6 at 7.5 ft, °F	500	247.8	10.9	4.4	259.9	120.2	139.7
Sensor 5 at 8.6 ft, °F	500	256.7	4.7	1.8	268.0	232.9	35.1
Sensor 4 at 9.7 ft, °F	500	251.9	7.7	3.1	265.6	225.1	40.5
Sensor 3 at 10.8 ft, °F	500	250.7	5.6	2.2	263.5	230.5	33.0
Sensor 2 at 11.8 ft, °F	500	265.9	6.5	2.5	280.2	243.9	36.3
Sensor 1 at 12.9 ft, °F	500	262.6	5.1	2.0	275.5	240.8	34.7

Table A.9 IR Basic Statistics for Project 1 Sublot 9 Sta. 395+00 to 380+00

Measure	N	Mean	Std. Dev.	Coeff. Var.	Maximum	Minimum	Range
Sensor 12 at 1.0 ft, °F	500	267.6	7.1	2.7	287.1	247.8	39.3
Sensor 11 at 2.1 ft, °F	500	269.4	7.6	2.8	291.6	245.7	45.9
Sensor 10 at 3.2 ft, °F	500	269.9	10.3	3.8	294.3	235.8	58.5
Sensor 9 at 4.3 ft, °F	500	261.0	8.7	3.3	284.5	232.3	52.2
Sensor 8 at 5.3 ft, °F	500	263.8	9.4	3.6	288.5	234.0	54.5
Sensor 7 at 6.4 ft, °F	500	262.2	7.1	2.7	283.6	243.7	39.9
Sensor 6 at 7.5 ft, °F	500	261.1	6.9	2.6	280.2	236.3	43.9
Sensor 5 at 8.6 ft, °F	500	270.7	7.7	2.8	295.5	252.5	43.0
Sensor 4 at 9.7 ft, °F	500	267.0	8.7	3.3	290.8	235.4	55.4
Sensor 3 at 10.8 ft, °F	500	264.2	7.8	2.9	285.6	242.4	43.2
Sensor 2 at 11.8 ft, °F	500	280.6	9.4	3.4	303.8	248.0	55.8
Sensor 1 at 12.9 ft, °F	500	277.6	8.1	2.9	302.0	249.6	52.4

Table A.10 IR Basic Statistics for Project 1 Sublot 10 Sta. 390+00 to 385+00

Measure	N	Mean	Std. Dev.	Coeff. Var.	Maximum	Minimum	Range
Sensor 12 at 1.0 ft, °F	500	258.9	7.3	2.8	274.1	229.3	44.8
Sensor 11 at 2.1 ft, °F	500	260.3	7.4	2.8	276.4	231.3	45.1
Sensor 10 at 3.2 ft, °F	500	259.3	9	3.5	281.3	233.8	47.5
Sensor 9 at 4.3 ft, °F	500	251.5	8.1	3.2	272.1	225.3	46.8
Sensor 8 at 5.3 ft, °F	500	253.2	7.6	3	273.6	227.7	45.9
Sensor 7 at 6.4 ft, °F	500	253.2	6.8	2.7	269.8	225.3	44.5
Sensor 6 at 7.5 ft, °F	500	253.2	7.5	2.9	271.4	225.5	45.9
Sensor 5 at 8.6 ft, °F	500	258.6	7.2	2.8	279.1	230.2	48.9
Sensor 4 at 9.7 ft, °F	500	254.6	8.2	3.2	274.6	227.7	46.9
Sensor 3 at 10.8 ft, °F	500	252.7	7.1	2.8	271.9	225.3	46.6
Sensor 2 at 11.8 ft, °F	500	269.1	8.6	3.2	291.6	239.2	52.4
Sensor 1 at 12.9 ft, °F	500	267.1	7.2	2.7	285.1	234.3	50.8

Project 2, STH 75

Table A.11 IR Basic Statistics for Project 2 Sublot 1 Sta. 242+00 to 237+00

Measure	N	Mean	Std. Dev.	Coeff. Var.	Maximum	Minimum	Range
Sensor 6 at 2.0 ft, °F	500	290.0	11.3	3.9	306.0	241.2	64.8
Sensor 5 at 4.2 ft, °F	500	291.9	15.5	5.3	309.9	239.9	70.0
Sensor 4 at 6.4 ft, °F	500	302.9	12.7	4.2	316.6	251.1	65.5
Sensor 3 at 8.6 ft, °F	500	298.0	8.4	2.8	313.0	264.4	48.6
Sensor 2 at 10.8 ft, °F	500	294.2	9.4	3.2	309.4	259.2	50.2
Sensor 1 at 13.0 ft, °F	500	282.7	7.1	2.5	294.3	257.7	36.6

Table A.12 IR Basic Statistics for Project 2 Sublot 2 Sta. 237+00 to 232+00

Measure	N	Mean	Std. Dev.	Coeff. Var.	Maximum	Minimum	Range
Sensor 6 at 2.0 ft, °F	500	289.0	9.1	3.2	308.7	251.2	57.5
Sensor 5 at 4.2 ft, °F	500	295.3	12.8	4.3	315.0	245.8	69.2
Sensor 4 at 6.4 ft, °F	500	305.3	9.3	3.1	323.1	262.9	60.2
Sensor 3 at 8.6 ft, °F	500	298.6	9.1	3.0	320.0	266.4	53.6
Sensor 2 at 10.8 ft, °F	500	291.3	9.2	3.1	312.8	263.7	49.1
Sensor 1 at 13.0 ft, °F	500	281.9	6.5	2.3	300.2	258.3	41.9

Table A.13 IR Basic Statistics for Project 2 Sublot 3 Sta. 232+00 to 227+00

Measure	N	Mean	Std. Dev.	Coeff. Var.	Maximum	Minimum	Range
Sensor 6 at 2.0 ft, °F	500	295.3	8.2	2.8	306.5	267.1	39.4
Sensor 5 at 4.2 ft, °F	500	299.1	11.6	3.9	311.5	253.9	57.6
Sensor 4 at 6.4 ft, °F	500	307.2	9.7	3.1	320.5	272.8	47.7
Sensor 3 at 8.6 ft, °F	500	304.2	7.9	2.6	316.9	273.4	43.5
Sensor 2 at 10.8 ft, °F	500	297	8.6	2.9	309	266.2	42.8
Sensor 1 at 13.0 ft, °F	500	286	6.3	2.2	295.9	262	33.9

Table A.14 IR Basic Statistics for Project 2 Sublot 4 Sta. 227+00 to 222+00

Measure	N	Mean	Std. Dev.	Coeff. Var.	Maximum	Minimum	Range
Sensor 6 at 2.0 ft, °F	500	288.8	8.5	2.9	300.6	257.5	43.1
Sensor 5 at 4.2 ft, °F	500	294.6	12.3	4.2	309.6	245.7	63.9
Sensor 4 at 6.4 ft, °F	500	303.1	9.7	3.2	313.5	262.4	51.1
Sensor 3 at 8.6 ft, °F	500	298.2	8.1	2.7	312.1	257.5	54.6
Sensor 2 at 10.8 ft, °F	500	288.5	8.3	2.9	303.4	254.8	48.6
Sensor 1 at 13.0 ft, °F	500	280.5	6.6	2.3	291.6	253.9	37.7

Table A.15 IR Basic Statistics for Project 2 Sublot 5 Sta. 222+00 to 217+00

Measure	N	Mean	Std. Dev.	Coeff. Var.	Maximum	Minimum	Range
Sensor 6 at 2.0 ft, °F	500	293.8	6.8	2.3	304.7	257.4	47.3
Sensor 5 at 4.2 ft, °F	500	299.7	9.6	3.2	311	261	50
Sensor 4 at 6.4 ft, °F	500	307.2	7.2	2.4	315.5	280.2	35.3
Sensor 3 at 8.6 ft, °F	500	302.5	7.4	2.5	314.2	260.8	53.4
Sensor 2 at 10.8 ft, °F	500	294.5	7.7	2.6	308.7	255.9	52.8
Sensor 1 at 13.0 ft, °F	500	284.8	5.4	1.9	295.2	256.5	38.7

Table A.16 IR Basic Statistics for Project 2 Sublot 6 Sta. 217+00 to 212+00

Measure	N	Mean	Std. Dev.	Coeff. Var.	Maximum	Minimum	Range
Sensor 6 at 2.0 ft, °F	500	292.7	7.7	2.6	304.7	261.3	43.4
Sensor 5 at 4.2 ft, °F	500	299.9	10	3.3	310.6	260.4	50.2
Sensor 4 at 6.4 ft, °F	500	307.6	7.4	2.4	317.7	274.5	43.2
Sensor 3 at 8.6 ft, °F	500	304.2	7.1	2.3	317.1	279.9	37.2
Sensor 2 at 10.8 ft, °F	500	294.1	7.2	2.4	305.8	265.6	40.2
Sensor 1 at 13.0 ft, °F	500	286.3	4.8	1.7	295.7	270.5	25.2

Table A.17 IR Basic Statistics for Project 2 Sublot 7 Sta. 212+00 to 207+00

Measure	N	Mean	Std. Dev.	Coeff. Var.	Maximum	Minimum	Range
Sensor 6 at 2.0 ft, °F	500	286.1	11.7	4.1	312.8	238.3	74.5
Sensor 5 at 4.2 ft, °F	500	293.0	12.2	4.2	321.8	243.3	78.5
Sensor 4 at 6.4 ft, °F	500	301.6	9.6	3.2	323.2	266.9	56.3
Sensor 3 at 8.6 ft, °F	500	302.1	8.5	2.8	323.6	260.6	63.0
Sensor 2 at 10.8 ft, °F	500	291.5	9.6	3.3	311.2	250.9	60.3
Sensor 1 at 13.0 ft, °F	500	283.5	8.3	2.9	302.2	260.2	42.0

Table 4.18 IR Basic Statistics for Project 2 Sublot 8 Sta. 207+00 to 202+00

Measure	N	Mean	Std. Dev.	Coeff. Var.	Maximum	Minimum	Range
Sensor 6 at 2.0 ft, °F	500	282.0	3.7	1.3	289.2	271.2	18.0
Sensor 5 at 4.2 ft, °F	500	289.6	4.9	1.7	297.9	276.8	21.1
Sensor 4 at 6.4 ft, °F	500	296.9	4.0	1.3	303.1	287.2	15.9
Sensor 3 at 8.6 ft, °F	500	297.6	3.9	1.3	304.7	286.2	18.5
Sensor 2 at 10.8 ft, °F	500	288.4	4.5	1.5	295.5	277.5	18.0
Sensor 1 at 13.0 ft, °F	500	278.6	3.2	1.1	285.3	270.1	15.2

Table A.19 IR Basic Statistics for Project 2 Sublot 9 Sta. 202+00 to 197+00

Measure	N	Mean	Std. Dev.	Coeff. Var.	Maximum	Minimum	Range
Sensor 6 at 2.0 ft, °F	500	286.4	5.0	1.8	298.6	264.2	34.4
Sensor 5 at 4.2 ft, °F	500	295.8	5.7	1.9	307.4	276.4	31.0
Sensor 4 at 6.4 ft, °F	500	302.2	5.4	1.8	314.1	281.5	32.6
Sensor 3 at 8.6 ft, °F	500	302.3	5.3	1.7	313.5	279.3	34.2
Sensor 2 at 10.8 ft, °F	500	292.9	5.5	1.9	305.8	270.7	35.1
Sensor 1 at 13.0 ft, °F	500	284.6	4.3	1.5	296.1	273.9	22.2

Table A.20 IR Basic Statistics for Project 2 Sublot 10 Sta. 197+00 to 192+00

Measure	N	Mean	Std. Dev.	Coeff. Var.	Maximum	Minimum	Range
Sensor 6 at 2.0 ft, °F	500	280.3	5.4	1.9	291.4	264.6	26.8
Sensor 5 at 4.2 ft, °F	500	290.8	5.5	1.9	304.3	278.1	26.2
Sensor 4 at 6.4 ft, °F	500	299.8	4.7	1.6	311.4	288.3	23.1
Sensor 3 at 8.6 ft, °F	500	297.5	4.7	1.6	310.3	286.7	23.6
Sensor 2 at 10.8 ft, °F	500	285.9	6.1	2.1	300.7	272.5	28.2
Sensor 1 at 13.0 ft, °F	500	279.7	4.8	1.7	292.3	270.9	21.4

Project 3, STH 42

Table A.21 IR Basic Statistics for Project 3 Sublot 1 Sta. 600+00 to 605+00

Measure	N	Mean	Std. Dev.	Coeff. Var.	Maximum	Minimum	Range
Sensor 12 at 1.0 ft, °F	500	279.8	18.3	6.5	288.5	83.8	204.7
Sensor 11 at 2.1 ft, °F	500	293.6	2.2	0.8	298.2	288.5	9.7
Sensor 10 at 3.2 ft, °F	500	289.3	2.6	0.9	294.3	284.4	9.9
Sensor 9 at 4.3 ft, °F	500	285.8	2.7	0.9	290.1	278.1	12.0
Sensor 8 at 5.3 ft, °F	500	291.0	2.1	0.7	295.0	284.2	10.8
Sensor 7 at 6.4 ft, °F	500	296.7	1.8	0.6	300.7	292.8	7.9
Sensor 6 at 7.5 ft, °F	500	320.9	2.8	0.9	325.8	313.0	12.8
Sensor 5 at 8.6 ft, °F	500	308.8	3.5	1.1	314.4	299.3	15.1
Sensor 4 at 9.7 ft, °F	500	289.5	3.4	1.2	294.8	280.2	14.6
Sensor 3 at 10.8 ft, °F	500	289.5	3.4	1.2	294.8	280.2	14.6
Sensor 2 at 11.8 ft, °F	500	315.0	13.9	4.4	322.7	91.2	231.5
Sensor 1 at 12.9 ft, °F	500	292.3	6.8	2.3	298.6	155.1	143.5

Table A.22 IR Basic Statistics for Project 3 Sublot 2 Sta. 605+00 to 610+00

Measure	N	Mean	Std. Dev.	Coeff. Var.	Maximum	Minimum	Range
Sensor 12 at 1.0 ft, °F	500	287.6	3.3	1.2	294.6	275.9	18.7
Sensor 11 at 2.1 ft, °F	500	297.3	3.2	1.1	305.2	291.0	14.2
Sensor 10 at 3.2 ft, °F	500	293.5	3.5	1.2	300.9	286.2	14.7
Sensor 9 at 4.3 ft, °F	500	289.1	3.4	1.2	296.4	281.5	14.9
Sensor 8 at 5.3 ft, °F	500	295.5	3.2	1.1	302.4	288.9	13.5
Sensor 7 at 6.4 ft, °F	500	300.4	2.7	0.9	307.4	294.3	13.1
Sensor 6 at 7.5 ft, °F	500	324.5	3.2	1.0	332.1	318.2	13.9
Sensor 5 at 8.6 ft, °F	500	310.7	4.2	1.4	318.0	300.6	17.4
Sensor 4 at 9.7 ft, °F	500	290.6	4.0	1.4	298.6	282.6	16.0
Sensor 3 at 10.8 ft, °F	500	290.6	4.0	1.4	298.6	282.6	16.0
Sensor 2 at 11.8 ft, °F	500	320.0	3.7	1.1	327.0	311.7	15.3
Sensor 1 at 12.9 ft, °F	500	296.8	3.3	1.1	303.4	290.1	13.3

Table 4.23 IR Basic Statistics for Project 3 Sublot 3 Sta. 610+00 to 615+00

Measure	N	Mean	Std. Dev.	Coeff. Var.	Maximum	Minimum	Range
Sensor 12 at 1.0 ft, °F	500	285.5	3.6	1.2	293.0	264.0	29.0
Sensor 11 at 2.1 ft, °F	500	295.9	3.1	1.0	302.4	288.0	14.4
Sensor 10 at 3.2 ft, °F	500	293.8	3.3	1.1	300.6	285.8	14.8
Sensor 9 at 4.3 ft, °F	500	287.6	3.3	1.2	294.3	273.9	20.4
Sensor 8 at 5.3 ft, °F	500	294.5	2.9	1.0	300.9	279.3	21.6
Sensor 7 at 6.4 ft, °F	500	297.6	2.5	0.8	303.6	291.9	11.7
Sensor 6 at 7.5 ft, °F	500	322.7	2.7	0.8	327.6	314.2	13.4
Sensor 5 at 8.6 ft, °F	500	308.1	3.1	1.0	314.2	298.4	15.8
Sensor 4 at 9.7 ft, °F	500	288.9	3.1	1.1	294.4	279.1	15.3
Sensor 3 at 10.8 ft, °F	500	288.9	3.1	1.1	294.4	279.1	15.3
Sensor 2 at 11.8 ft, °F	500	317.3	3.4	1.1	322.5	307.0	15.5
Sensor 1 at 12.9 ft, °F	500	295.3	3.2	1.1	301.1	286.5	14.6

Table A.24 IR Basic Statistics for Project 3 Sublot 4 Sta. 615+00 to 620+00

Measure	N	Mean	Std. Dev.	Coeff. Var.	Maximum	Minimum	Range
Sensor 12 at 1.0 ft, °F	500	286.6	3.6	1.2	292.3	268.5	23.8
Sensor 11 at 2.1 ft, °F	500	297.1	3.9	1.3	303.3	257.5	45.8
Sensor 10 at 3.2 ft, °F	500	295.3	3.8	1.3	301.8	286.5	15.3
Sensor 9 at 4.3 ft, °F	500	288.9	3.6	1.2	294.8	281.1	13.7
Sensor 8 at 5.3 ft, °F	500	296.7	3.0	1.0	302.5	289.2	13.3
Sensor 7 at 6.4 ft, °F	500	299.2	3.1	1.0	305.8	292.6	13.2
Sensor 6 at 7.5 ft, °F	500	325.6	3.4	1.0	331.2	318.7	12.5
Sensor 5 at 8.6 ft, °F	500	310.7	3.3	1.1	316.0	300.2	15.8
Sensor 4 at 9.7 ft, °F	500	291.5	3.3	1.1	296.2	282.0	14.2
Sensor 3 at 10.8 ft, °F	500	291.5	3.3	1.1	296.2	282.0	14.2
Sensor 2 at 11.8 ft, °F	500	320.2	3.0	0.9	325.6	311.0	14.6
Sensor 1 at 12.9 ft, °F	500	298.4	2.6	0.9	303.8	291.9	11.9

Table A.25 IR Basic Statistics for Project 3 Sublot 5 Sta. 620+00 to 625+00

Measure	N	Mean	Std. Dev.	Coeff. Var.	Maximum	Minimum	Range
Sensor 12 at 1.0 ft, °F	500	289.5	2.7	0.9	293.7	282.2	11.5
Sensor 11 at 2.1 ft, °F	500	300.3	2.7	0.9	304.3	293.5	10.8
Sensor 10 at 3.2 ft, °F	500	298.5	3.0	1.0	302.4	290.7	11.7
Sensor 9 at 4.3 ft, °F	500	292.1	2.8	1.0	296.1	284.2	11.9
Sensor 8 at 5.3 ft, °F	500	299.4	2.2	0.7	303.3	293.7	9.6
Sensor 7 at 6.4 ft, °F	500	300.7	2.1	0.7	304.9	295.9	9.0
Sensor 6 at 7.5 ft, °F	500	327.1	2.7	0.8	331.2	321.3	9.9
Sensor 5 at 8.6 ft, °F	500	313.3	2.0	0.6	317.7	308.3	9.4
Sensor 4 at 9.7 ft, °F	500	293.3	2.2	0.7	297.0	286.9	10.1
Sensor 3 at 10.8 ft, °F	500	293.3	2.2	0.7	297.0	286.9	10.1
Sensor 2 at 11.8 ft, °F	500	320.5	1.5	0.5	323.8	317.3	6.5
Sensor 1 at 12.9 ft, °F	500	299.4	1.7	0.6	304.2	295.7	8.5

Table A.26 IR Basic Statistics for Project 3 Sublot 6 Sta. 625+00 to 630+00

Measure	N	Mean	Std. Dev.	Coeff. Var.	Maximum	Minimum	Range
Sensor 12 at 1.0 ft, °F	500	285.1	5.3	1.8	291.9	261.5	30.4
Sensor 11 at 2.1 ft, °F	500	297.1	4.4	1.5	303.4	280.0	23.4
Sensor 10 at 3.2 ft, °F	500	295.9	4.7	1.6	302.0	273.4	28.6
Sensor 9 at 4.3 ft, °F	500	289.2	4.0	1.4	296.1	277.5	18.6
Sensor 8 at 5.3 ft, °F	500	298.5	3.9	1.3	305.6	287.4	18.2
Sensor 7 at 6.4 ft, °F	500	299.1	3.7	1.2	305.4	289.0	16.4
Sensor 6 at 7.5 ft, °F	500	325.2	14.8	4.6	333.5	100.6	232.9
Sensor 5 at 8.6 ft, °F	500	309.9	14.5	4.7	317.3	91.6	225.7
Sensor 4 at 9.7 ft, °F	500	291.4	3.8	1.3	297.5	280.9	16.6
Sensor 3 at 10.8 ft, °F	500	291.4	3.8	1.3	297.5	280.9	16.6
Sensor 2 at 11.8 ft, °F	500	319.5	4.1	1.3	327.4	308.5	18.9
Sensor 1 at 12.9 ft, °F	500	296.9	6.5	2.2	305.4	260.6	44.8

Table 4.27 IR Basic Statistics for Project 3 Sublot 7 Sta. 630+00 to 635+00

Measure	N	Mean	Std. Dev.	Coeff. Var.	Maximum	Minimum	Range
Sensor 12 at 1.0 ft, °F	500	282.8	4.4	1.6	291.2	257.4	33.8
Sensor 11 at 2.1 ft, °F	500	296.1	3.7	1.2	304.0	272.7	31.3
Sensor 10 at 3.2 ft, °F	500	295.9	3.8	1.3	303.3	276.6	26.7
Sensor 9 at 4.3 ft, °F	500	287.3	4.2	1.4	295.7	264.6	31.1
Sensor 8 at 5.3 ft, °F	500	297.3	3.5	1.2	304.0	275.0	29.0
Sensor 7 at 6.4 ft, °F	500	298.2	3.1	1.1	303.8	271.6	32.2
Sensor 6 at 7.5 ft, °F	500	326.1	3.3	1.0	331.2	300.9	30.3
Sensor 5 at 8.6 ft, °F	500	308.7	3.9	1.3	314.8	279.3	35.5
Sensor 4 at 9.7 ft, °F	500	289.2	3.0	1.0	293.9	267.8	26.1
Sensor 3 at 10.8 ft, °F	500	289.2	3.0	1.0	293.9	267.8	26.1
Sensor 2 at 11.8 ft, °F	500	319.1	3.2	1.0	323.8	292.1	31.7
Sensor 1 at 12.9 ft, °F	500	295.5	7.5	2.5	304.5	246.7	57.8

Table 4.28 IR Basic Statistics for Project 3 Sublot 8 Sta. 635+00 to 640+00

Measure	N	Mean	Std. Dev.	Coeff. Var.	Maximum	Minimum	Range
Sensor 12 at 1.0 ft, °F	500	287.9	3.6	1.2	293.9	276.1	17.8
Sensor 11 at 2.1 ft, °F	500	299.1	3.6	1.2	305.6	289.0	16.6
Sensor 10 at 3.2 ft, °F	500	296.9	3.6	1.2	303.1	285.8	17.3
Sensor 9 at 4.3 ft, °F	500	289.9	4.0	1.4	296.2	276.8	19.4
Sensor 8 at 5.3 ft, °F	500	298.2	3.3	1.1	303.6	290.1	13.5
Sensor 7 at 6.4 ft, °F	500	300.3	2.9	1.0	306.0	292.5	13.5
Sensor 6 at 7.5 ft, °F	500	328.1	2.8	0.9	334.0	320.4	13.6
Sensor 5 at 8.6 ft, °F	500	310.2	3.1	1.0	316.0	300.0	16.0
Sensor 4 at 9.7 ft, °F	500	290.6	2.8	1.0	295.5	282.9	12.6
Sensor 3 at 10.8 ft, °F	500	290.6	2.8	1.0	295.5	282.9	12.6
Sensor 2 at 11.8 ft, °F	500	320.1	2.3	0.7	324.5	313.5	11.0
Sensor 1 at 12.9 ft, °F	500	296.9	2.1	0.7	302.9	292.1	10.8

Table A.29 IR Basic Statistics for Project 3 Sublot 9 Sta. 640+00 to 645+00

Measure	N	Mean	Std. Dev.	Coeff. Var.	Maximum	Minimum	Range
Sensor 12 at 1.0 ft, °F	500	287.8	8.7	3.0	293.2	118.8	174.4
Sensor 11 at 2.1 ft, °F	500	299.2	3.8	1.3	304.9	275.5	29.4
Sensor 10 at 3.2 ft, °F	500	297.1	4.0	1.3	302.9	286.5	16.4
Sensor 9 at 4.3 ft, °F	500	290.2	4.1	1.4	296.6	276.4	20.2
Sensor 8 at 5.3 ft, °F	500	297.9	3.3	1.1	303.3	287.2	16.1
Sensor 7 at 6.4 ft, °F	500	300.6	2.9	1.0	305.4	287.2	18.2
Sensor 6 at 7.5 ft, °F	500	327.4	3.6	1.1	332.8	315.1	17.7
Sensor 5 at 8.6 ft, °F	500	310.1	3.4	1.1	315.9	297.9	18.0
Sensor 4 at 9.7 ft, °F	500	291.9	3.1	1.1	297.1	281.8	15.3
Sensor 3 at 10.8 ft, °F	500	291.9	3.1	1.1	297.1	281.8	15.3
Sensor 2 at 11.8 ft, °F	500	320.2	3.5	1.1	324.3	306.1	18.2
Sensor 1 at 12.9 ft, °F	500	297.8	4.4	1.5	302.5	262.8	39.7

Table A.30 IR Basic Statistics for Project 3 Sublot 10 Sta. 645+00 to 650+00

Measure	N	Mean	Std. Dev.	Coeff. Var.	Maximum	Minimum	Range
Sensor 12 at 1.0 ft, °F	500	288.7	3.8	1.3	295.5	271.0	24.5
Sensor 11 at 2.1 ft, °F	500	299.5	3.5	1.2	307.2	289.2	18.0
Sensor 10 at 3.2 ft, °F	500	297.5	3.6	1.2	304.5	288.1	16.4
Sensor 9 at 4.3 ft, °F	500	291.2	3.1	1.1	297.1	280.6	16.5
Sensor 8 at 5.3 ft, °F	500	299.0	2.8	0.9	305.4	290.8	14.6
Sensor 7 at 6.4 ft, °F	500	300.6	2.8	0.9	307.0	293.2	13.8
Sensor 6 at 7.5 ft, °F	500	328.9	3.1	1.0	334.6	319.8	14.8
Sensor 5 at 8.6 ft, °F	500	312.1	2.8	0.9	317.5	302.5	15.0
Sensor 4 at 9.7 ft, °F	500	292.8	3.0	1.0	298.8	285.8	13.0
Sensor 3 at 10.8 ft, °F	500	292.8	3.0	1.0	298.8	285.8	13.0
Sensor 2 at 11.8 ft, °F	500	321.4	2.6	0.8	326.1	314.8	11.3
Sensor 1 at 12.9 ft, °F	500	302.5	3.1	1.0	308.1	290.3	17.8

Table A.31 IR Basic Statistics for Project 3 Sublot 11 Sta. 650+00 to 655+00

Measure	N	Mean	Std. Dev.	Coeff. Var.	Maximum	Minimum	Range
Sensor 12 at 1.0 ft, °F	500	292.7	3.0	1.0	297.9	284.4	13.5
Sensor 11 at 2.1 ft, °F	500	302.9	3.5	1.1	309.0	294.6	14.4
Sensor 10 at 3.2 ft, °F	500	299.9	3.9	1.3	306.9	291.6	15.3
Sensor 9 at 4.3 ft, °F	500	293.9	3.4	1.2	300.7	285.4	15.3
Sensor 8 at 5.3 ft, °F	500	301.9	3.1	1.0	307.9	295.3	12.6
Sensor 7 at 6.4 ft, °F	500	303.6	2.2	0.7	309.4	293.9	15.5
Sensor 6 at 7.5 ft, °F	500	332.6	2.8	0.8	338.7	325.9	12.8
Sensor 5 at 8.6 ft, °F	500	315.1	2.2	0.7	320.4	307.0	13.4
Sensor 4 at 9.7 ft, °F	500	296.4	2.7	0.9	301.6	288.5	13.1
Sensor 3 at 10.8 ft, °F	500	296.4	2.7	0.9	301.6	288.5	13.1
Sensor 2 at 11.8 ft, °F	500	325.2	1.8	0.6	329.7	320.9	8.8
Sensor 1 at 12.9 ft, °F	500	305.9	2.3	0.8	310.3	301.3	9.0

Table A.32 IR Basic Statistics for Project 3 Sublot 12 Sta. 655+00 to 660+00

Measure	N	Mean	Std. Dev.	Coeff. Var.	Maximum	Minimum	Range
Sensor 12 at 1.0 ft, °F	500	290.5	3.7	1.3	299.1	276.6	22.5
Sensor 11 at 2.1 ft, °F	500	301.3	3.9	1.3	309.2	289.2	20.0
Sensor 10 at 3.2 ft, °F	500	299.2	4.6	1.5	307.9	286.2	21.7
Sensor 9 at 4.3 ft, °F	500	291.9	4.7	1.6	300.0	268.3	31.7
Sensor 8 at 5.3 ft, °F	500	300.9	4.0	1.3	310.1	287.6	22.5
Sensor 7 at 6.4 ft, °F	500	302.0	3.0	1.0	309.2	291.7	17.5
Sensor 6 at 7.5 ft, °F	500	331.2	4.5	1.4	341.6	320.4	21.2
Sensor 5 at 8.6 ft, °F	500	312.9	3.7	1.2	319.6	295.2	24.4
Sensor 4 at 9.7 ft, °F	500	294.2	4.1	1.4	300.9	276.3	24.6
Sensor 3 at 10.8 ft, °F	500	294.2	4.1	1.4	300.9	276.3	24.6
Sensor 2 at 11.8 ft, °F	500	323.1	3.4	1.0	329.5	308.7	20.8
Sensor 1 at 12.9 ft, °F	500	304.3	3.9	1.3	311.7	292.3	19.4

Appendix B – Ground Penetrating Radar Sublot Data Summary

Project 1, USH 2

Table B.1 GPR Basic Statistics for Project 1 Sublot 1 Sta. 435+00 to 430+00

Measure	N	Mean	Std. Dev.	Coeff. Var.	Maximum	Minimum	Range
Thickness at 0.5 ft, in.	500	2	0.1	4.3	2.3	1.9	0.3
Thickness at 2.5 ft, in.	500	1.8	0.1	6.4	2	1.7	0.3
Thickness at 6.0 ft, in.	500	1.7	0	2.3	1.8	1.7	0.2
Thickness at 9.5 ft, in.	500	1.6	0	2.5	1.7	1.5	0.2
Density at 2.5 ft, %	500	95.4	1	1.1	97.4	93	4.4
Density at 6.0 ft, %	500	95.5	0.5	0.5	96.3	94.6	1.7

Table B.2 GPR Basic Statistics for Project 1 Sublot 2 Sta. 430+00 to 425+00

Measure	N	Mean	Std. Dev.	Coeff. Var.	Maximum	Minimum	Range
Thickness at 0.5 ft, in.	500	2	0.1	4.3	2.2	1.6	0.6
Thickness at 2.5 ft, in.	500	1.9	0.1	3.3	2	1.7	0.3
Thickness at 6.0 ft, in.	500	1.8	0.1	3.7	1.9	1.7	0.2
Thickness at 9.5 ft, in.	500	1.6	0	1.5	1.6	1.5	0.1
Density at 2.5 ft, %	500	94.5	0.7	0.8	95.9	93.1	2.8
Density at 6.0 ft, %	500	95.5	0.4	0.4	96.5	94.8	1.7

Table B.3 GPR Basic Statistics for Project 1 Sublot 3 Sta. 425+00 to 420+00

Measure	N	Mean	Std. Dev.	Coeff. Var.	Maximum	Minimum	Range
Thickness at 0.5 ft, in.	500	1.9	0.1	5.6	2.1	1.6	0.5
Thickness at 2.5 ft, in.	500	1.9	0	2.7	2	1.7	0.2
Thickness at 6.0 ft, in.	500	1.7	0	2.7	1.9	1.6	0.2
Thickness at 9.5 ft, in.	500	1.6	0	0.9	1.7	1.6	0
Density at 2.5 ft, %	500	93.9	0.9	0.9	94.9	92.5	2.4
Density at 6.0 ft, %	500	95.6	0.6	0.6	96.3	94.7	1.7

Table B.4 GPR Basic Statistics for Project 1 Sublot 4 Sta. 420+00 to 415+00

Measure	N	Mean	Std. Dev.	Coeff. Var.	Maximum	Minimum	Range
Thickness at 0.5 ft, in.	100	1.9	0.2	8.5	2.2	1.8	0.5
Thickness at 2.5 ft, in.	500	1.9	0.1	3.3	2	1.7	0.3
Thickness at 6.0 ft, in.	500	1.8	0.1	4.3	2	1.7	0.4
Thickness at 9.5 ft, in.	500	1.7	0.1	3.9	1.9	1.7	0.2
Density at 2.5 ft, %	0
Density at 6.0 ft, %	0

Table B.5 GPR Basic Statistics for Project 1 Sublot 5 Sta. 415+00 to 410+00

Measure	N	Mean	Std. Dev.	Coeff. Var.	Maximum	Minimum	Range
Thickness at 0.5 ft, in.	500	2	0.1	3.7	2.2	1.9	0.3
Thickness at 2.5 ft, in.	500	1.9	0.1	3.7	2	1.8	0.3
Thickness at 6.0 ft, in.	500	1.8	0.1	3.2	2	1.7	0.3
Thickness at 9.5 ft, in.	500	1.6	0	2.7	1.7	1.5	0.2
Density at 2.5 ft, %	500	93.5	1.2	1.3	96.2	91.2	5
Density at 6.0 ft, %	500	94.2	0.2	0.2	94.5	94	0.5

Table B.6 GPR Basic Statistics for Project 1 Sublot 6 Sta. 410+00 to 405+00

Measure	N	Mean	Std. Dev.	Coeff. Var.	Maximum	Minimum	Range
Thickness at 0.5 ft, in.	500	2	0.1	5.2	2.2	1.7	0.4
Thickness at 2.5 ft, in.	500	1.8	0.1	3.4	2	1.7	0.2
Thickness at 6.0 ft, in.	500	1.7	0	2.5	1.8	1.7	0.2
Thickness at 9.5 ft, in.	500	1.7	0.1	3.4	1.8	1.5	0.3
Density at 2.5 ft, %	500	93.9	1	1	96.3	91.9	4.3
Density at 6.0 ft, %	500	94.4	0.3	0.3	94.8	93.6	1.2

Table B.7 GPR Basic Statistics for Project 1 Sublot 7 Sta. 405+00 to 400+00

Measure	N	Mean	Std. Dev.	Coeff. Var.	Maximum	Minimum	Range
Thickness at 0.5 ft, in.	500	1.8	0.3	14	2.4	1.5	0.9
Thickness at 2.5 ft, in.	500	1.8	0	2.4	1.9	1.7	0.2
Thickness at 6.0 ft, in.	500	1.8	0	1.9	1.9	1.7	0.2
Thickness at 9.5 ft, in.	500	1.6	0	1.1	1.7	1.6	0.1
Density at 2.5 ft, %	500	91.7	1	1.1	93.7	90	3.8
Density at 6.0 ft, %	500	93.5	0.5	0.5	94	92.7	1.3

Table B.8 GPR Basic Statistics for Project 1 Sublot 8 Sta. 400+00 to 395+00

Measure	N	Mean	Std. Dev.	Coeff. Var.	Maximum	Minimum	Range
Thickness at 0.5 ft, in.	500	1.7	0.2	10	2.4	1.6	0.8
Thickness at 2.5 ft, in.	500	1.8	0	2	1.9	1.8	0.2
Thickness at 6.0 ft, in.	500	1.8	0	2.2	1.9	1.7	0.2
Thickness at 9.5 ft, in.	500	1.6	0	2.4	1.6	1.5	0.1
Density at 2.5 ft, %	500	94.5	0.8	0.8	96	93.3	2.7
Density at 6.0 ft, %	500	94.9	0.4	0.5	96.2	94	2.2

Table B.9 GPR Basic Statistics for Project 1 Sublot 9 Sta. 395+00 to 390+00

Measure	N	Mean	Std. Dev.	Coeff. Var.	Maximum	Minimum	Range
Thickness at 0.5 ft, in.	500	1.9	0.1	7.5	2.3	1.6	0.7
Thickness at 2.5 ft, in.	500	1.8	0.1	2.9	2	1.7	0.3
Thickness at 6.0 ft, in.	500	1.8	0	1.9	1.9	1.7	0.3
Thickness at 9.5 ft, in.	500	1.6	0	1.1	1.7	1.6	0.1
Density at 2.5 ft, %	500	92.5	1	1.1	94.3	91.1	3.2
Density at 6.0 ft, %	500	92.9	0.8	0.8	94.6	92	2.7

Table B.10 GPR Basic Statistics for Project 1 Sublot 10 Sta. 390+00 to 385+00

Measure	N	Mean	Std. Dev.	Coeff. Var.	Maximum	Minimum	Range
Thickness at 0.5 ft, in.	500	1.9	0.1	5.1	2.1	1.6	0.5
Thickness at 2.5 ft, in.	500	1.8	0	1.9	1.8	1.7	0.1
Thickness at 6.0 ft, in.	500	1.7	0	2.5	1.8	1.7	0.2
Thickness at 9.5 ft, in.	500	1.6	0	2.5	1.6	1.5	0.2
Density at 2.5 ft, %	500	93.9	0.2	0.2	94.4	93.7	0.8
Density at 6.0 ft, %	500	96.2	0.6	0.6	97.1	94.6	2.5

Project 2, STH 75

Table B.11 GPR Basic Statistics for Project 2 Sublot 1 Sta. 242+00 to 237+00

Measure	N	Mean	Std. Dev.	Coeff. Var.	Maximum	Minimum	Range
Thickness at 0.5 ft, in.	500	2.6	0.1	3.8	2.8	2.3	0.4
Thickness at 2.5 ft, in.	500	2.4	0.2	9.8	2.7	2.0	0.7
Thickness at 6.0 ft, in.	500	2.5	0.2	7.4	2.7	2.0	0.7
Thickness at 9.5 ft, in.	500	2.7	0.1	2.6	2.8	2.5	0.2
Thickness at 11.5 ft, in.	500	2.7	0.1	2.2	2.8	2.6	0.2
Density at 9.5 ft, %	500	94.9	0.1	0.1	95.1	94.6	0.5
Density at 11.5 ft, %	500	95.1	0.4	0.4	95.8	94.6	1.2

Table B.12 GPR Basic Statistics for Project 2 Sublot 2 Sta. 237+00 to 232+00

Measure	N	Mean	Std. Dev.	Coeff. Var.	Maximum	Minimum	Range
Thickness at 0.5 ft, in.	500	2.7	0.1	2.6	2.8	2.5	0.2
Thickness at 2.5 ft, in.	500	2.6	0.2	6.6	2.8	2.2	0.6
Thickness at 6.0 ft, in.	500	2.6	0.1	5.4	2.7	2.2	0.6
Thickness at 9.5 ft, in.	500	2.7	0.0	0.7	2.7	2.7	0.1
Thickness at 11.5 ft, in.	500	2.7	0.0	0.5	2.8	2.7	0.1
Gmm at 9.5 ft, %	500	94.4	0.3	0.4	95.0	93.8	1.3
Gmm at 11.5 ft, %	500	94.2	0.7	0.7	95.1	92.9	2.1

Table B.13 GPR Basic Statistics for Project 2 Sublot 3 Sta. 232+00 to 227+00

Measure	N	Mean	Std. Dev.	Coeff. Var.	Maximum	Minimum	Range
Thickness at 0.5 ft, in.	500	2.7	0.1	3.0	2.8	2.5	0.3
Thickness at 2.5 ft, in.	500	2.6	0.1	4.8	2.7	2.2	0.5
Thickness at 6.0 ft, in.	500	2.5	0.2	9.7	2.7	2.1	0.6
Thickness at 9.5 ft, in.	500	2.6	0.1	4.8	2.8	2.3	0.4
Thickness at 11.5 ft, in.	500	2.7	0.1	3.1	2.8	2.5	0.2
Gmm at 9.5 ft, %	500	93.3	0.5	0.5	94.2	92.5	1.6
Gmm at 11.5 ft, %	500	93.2	0.6	0.6	94.6	92.7	1.9

Table B.14 GPR Basic Statistics for Project 2 Sublot 4 Sta. 227+00 to 222+00

Measure	N	Mean	Std. Dev.	Coeff. Var.	Maximum	Minimum	Range
Thickness at 0.5 ft, in.	500	2.6	0.1	3.6	2.8	2.5	0.3
Thickness at 2.5 ft, in.	500	2.3	0.2	8.0	2.7	2.0	0.7
Thickness at 6.0 ft, in.	500	2.5	0.1	5.9	2.7	2.3	0.5
Thickness at 9.5 ft, in.	500	2.7	0.0	1.5	2.7	2.6	0.2
Thickness at 11.5 ft, in.	500	2.7	0.0	1.7	2.8	2.6	0.2
Gmm at 9.5 ft, %	500	92.3	0.4	0.4	93.7	91.7	2.0
Gmm at 11.5 ft, %	500	93.5	0.6	0.7	94.6	92.4	2.2

Table B.15 GPR Basic Statistics for Project 2 Sublot 5 Sta. 222+00 to 217+00

Measure	N	Mean	Std. Dev.	Coeff. Var.	Maximum	Minimum	Range
Thickness at 0.5 ft, in.	500	2.5	0.1	4.2	2.8	2.4	0.4
Thickness at 2.5 ft, in.	500	2.4	0.1	5.3	2.7	2.1	0.6
Thickness at 6.0 ft, in.	500	2.4	0.1	5.4	2.7	2.2	0.5
Thickness at 9.5 ft, in.	500	2.7	0.0	1.8	2.7	2.6	0.2
Thickness at 11.5 ft, in.	500	2.8	0.0	0.9	2.8	2.7	0.1
Gmm at 9.5 ft, %	500	94.2	0.4	0.4	94.8	92.8	2.0
Gmm at 11.5 ft, %	500	94.2	0.5	0.5	95.0	93.7	1.4

Table B.16 GPR Basic Statistics for Project 2 Sublot 6 Sta. 217+00 to 212+00

Measure	N	Mean	Std. Dev.	Coeff. Var.	Maximum	Minimum	Range
Thickness at 0.5 ft, in.	500	2.6	0.1	4.3	2.8	2.4	0.4
Thickness at 2.5 ft, in.	500	2.5	0.1	5.1	2.7	2.2	0.5
Thickness at 6.0 ft, in.	500	2.6	0.1	3.7	2.7	2.4	0.4
Thickness at 9.5 ft, in.	500	2.7	0.0	1.8	2.7	2.5	0.2
Thickness at 11.5 ft, in.	500	2.7	0.1	2.7	2.8	2.5	0.3
Gmm at 9.5 ft, %	500	93.9	0.2	0.2	94.8	93.7	1.1
Gmm at 11.5 ft, %	500	93.6	0.3	0.3	94.2	93.1	1.1

Table B.17 GPR Basic Statistics for Project 2 Sublot 7 Sta. 212+00 to 207+00

Measure	N	Mean	Std. Dev.	Coeff. Var.	Maximum	Minimum	Range
Thickness at 0.5 ft, in.	500	2.5	0.1	3.8	2.7	2.4	0.4
Thickness at 2.5 ft, in.	500	2.2	0.1	5.6	2.5	2.0	0.5
Thickness at 6.0 ft, in.	500	2.7	0.0	1.7	2.7	2.6	0.2
Thickness at 9.5 ft, in.	500	2.6	0.1	2.4	2.7	2.5	0.3
Thickness at 11.5 ft, in.	500	2.8	0.0	0.5	2.8	2.7	0.0
Gmm at 9.5 ft, %	500	95.2	0.6	0.6	96.1	94.4	1.7
Gmm at 11.5 ft, %	500	95.1	0.6	0.7	96.2	94.2	2.0

Table B.18 GPR Basic Statistics for Project 2 Sublot 8 Sta. 207+00 to 202+00

Measure	N	Mean	Std. Dev.	Coeff. Var.	Maximum	Minimum	Range
Thickness at 0.5 ft, in.	500	2.6	0.1	4.8	2.8	2.4	0.4
Thickness at 2.5 ft, in.	500	2.3	0.1	6.3	2.5	2.0	0.5
Thickness at 6.0 ft, in.	500	2.7	0.0	1.3	2.8	2.6	0.1
Thickness at 9.5 ft, in.	500	2.7	0.1	2.7	2.8	2.5	0.3
Thickness at 11.5 ft, in.	500	2.7	0.0	1.2	2.8	2.7	0.1
Gmm at 9.5 ft, %	500	94.7	0.2	0.2	95.2	94.2	1.0
Gmm at 11.5 ft, %	500	95.4	0.7	0.7	96.6	94.3	2.3

Table B.19 GPR Basic Statistics for Project 2 Sublot 9 Sta. 202+00 to 197+00

Measure	N	Mean	Std. Dev.	Coeff. Var.	Maximum	Minimum	Range
Thickness at 0.5 ft, in.	500	2.5	0.1	3.9	2.7	2.3	0.4
Thickness at 2.5 ft, in.	500	2.2	0.1	6.2	2.5	2	0.4
Thickness at 6.0 ft, in.	500	2.6	0.1	3.4	2.7	2.4	0.3
Thickness at 9.5 ft, in.	500	2.7	0.1	2.2	2.8	2.6	0.2
Thickness at 11.5 ft, in.	500	2.7	0.1	0.8	2.8	2.7	0.1
Gmm at 9.5 ft, %	500	94.1	0.9	1.0	95.5	92.8	2.7
Gmm at 11.5 ft, %	500	94.4	0.8	0.9	95.7	93.4	2.3

Table B.20 GPR Basic Statistics for Project 2 Sublot 10 Sta. 197+00 to 192+00

Measure	N	Mean	Std. Dev.	Coeff. Var.	Maximum	Minimum	Range
Thickness at 0.5 ft, in.	500	2.6	0.1	4.6	2.8	2.3	0.4
Thickness at 2.5 ft, in.	500	2.3	0.1	6.0	2.6	2.0	0.5
Thickness at 6.0 ft, in.	500	2.6	0.1	4.2	2.7	2.4	0.3
Thickness at 9.5 ft, in.	500	2.7	0.0	1.0	2.8	2.6	0.1
Thickness at 11.5 ft, in.	500	2.7	0.0	1.4	2.8	2.6	0.1
Gmm at 9.5 ft, %	500	93.4	0.3	0.3	93.9	93.0	0.9
Gmm at 11.5 ft, %	500	92.8	0.3	0.4	93.4	92.3	1.1

Project 3, STH 42

Table B.21 GPR Basic Statistics for Project 3 Sublot 1 Sta. 600+00 to 605+00

Measure	N	Mean	Std. Dev.	Coeff. Var.	Maximum	Minimum	Range
Thickness at 2.5 ft, in.	500	1.5	0.1	5.8	1.6	1.4	0.3
Thickness at 6.0 ft, in.	500	1.6	0.1	5.8	1.8	1.4	0.4
Thickness at 9.5 ft, in.	500	1.6	0.1	6.0	1.7	1.4	0.3
Thickness at 11.5 ft, in.	500	1.6	0.1	5.3	1.7	1.4	0.3
Gmm at 6.0 ft, %	500	90.1	0.1	0.1	90.3	90.0	0.3
Gmm at 9.5 ft, %	500	90.6	0.4	0.5	91.2	90.0	1.2
Gmm at 11.5 ft, %	500	90.9	0.2	0.3	91.4	90.6	0.8

Table B.22 GPR Basic Statistics for Project 3 Sublot 2 Sta. 605+00 to 610+00

Measure	N	Mean	Std. Dev.	Coeff. Var.	Maximum	Minimum	Range
Thickness at 2.5 ft, in.	500	1.5	0.0	3.2	1.7	1.4	0.2
Thickness at 6.0 ft, in.	500	1.6	0.1	5.3	1.9	1.5	0.4
Thickness at 9.5 ft, in.	500	1.6	0.1	7.9	2.0	1.5	0.5
Thickness at 11.5 ft, in.	500	1.6	0.1	8.7	2.0	1.4	0.5
Gmm at 6.0 ft, %	500	89.7	0.4	0.4	90.5	89.3	1.2
Gmm at 9.5 ft, %	500	90.1	0.4	0.4	90.8	89.5	1.3
Gmm at 11.5 ft, %	500	90.4	0.2	0.2	90.8	90.1	0.7

Table B.23 GPR Basic Statistics for Project 3 Sublot 3 Sta. 610+00 to 615+00

Measure	N	Mean	Std. Dev.	Coeff. Var.	Maximum	Minimum	Range
Thickness at 2.5 ft, in.	500	1.6	0.1	7.3	1.9	1.4	0.5
Thickness at 6.0 ft, in.	500	1.9	0.2	11.2	2.4	1.6	0.8
Thickness at 9.5 ft, in.	500	1.9	0.2	10.0	2.2	1.6	0.7
Thickness at 11.5 ft, in.	500	2.0	0.2	10.2	2.4	1.6	0.8
Gmm at 6.0 ft, %	500	89.5	0.1	0.2	89.7	89.2	0.5
Gmm at 9.5 ft, %	500	89.6	0.3	0.3	90.3	89.2	1.1
Gmm at 11.5 ft, %	500	90.0	0.3	0.4	90.8	89.4	1.4

Table B.24 GPR Basic Statistics for Project 3 Sublot 4 Sta. 615+00 to 620+00

Measure	N	Mean	Std. Dev.	Coeff. Var.	Maximum	Minimum	Range
Thickness at 2.5 ft, in.	500	1.4	0.1	5.6	1.5	1.3	0.3
Thickness at 6.0 ft, in.	500	1.5	0.1	5.5	1.6	1.3	0.3
Thickness at 9.5 ft, in.	500	1.5	0.1	5.4	1.6	1.3	0.3
Thickness at 11.5 ft, in.	500	1.4	0.1	5.1	1.6	1.3	0.3
Gmm at 6.0 ft, %	500	89.5	0.2	0.2	89.8	89.2	0.6
Gmm at 9.5 ft, %	500	90.3	0.4	0.4	90.8	89.5	1.3
Gmm at 11.5 ft, %	500	90.0	0.1	0.1	90.3	89.8	0.5

Table B.25 GPR Basic Statistics for Project 3 Sublot 5 Sta. 620+00 to 625+00

Measure	N	Mean	Std. Dev.	Coeff. Var.	Maximum	Minimum	Range
Thickness at 2.5 ft, in.	500	1.4	0.1	5.6	1.6	1.3	0.3
Thickness at 6.0 ft, in.	500	1.5	0.0	3.2	1.6	1.4	0.2
Thickness at 9.5 ft, in.	500	1.5	0.0	3.1	1.6	1.4	0.2
Thickness at 11.5 ft, in.	500	1.4	0.0	3.4	1.5	1.4	0.2
Gmm at 6.0 ft, %	500	89.1	0.4	0.4	90.4	88.8	1.6
Gmm at 9.5 ft, %	500	89.3	0.3	0.3	90.2	88.9	1.3
Gmm at 11.5 ft, %	500	90.0	0.5	0.6	91.2	89.6	1.6

Table B.26 GPR Basic Statistics for Project 3 Sublot 6 Sta. 625+00 to 630+00

Measure	N	Mean	Std. Dev.	Coeff. Var.	Maximum	Minimum	Range
Thickness at 2.5 ft, in.	500	1.5	0.0	3.0	1.6	1.4	0.2
Thickness at 6.0 ft, in.	500	1.6	0.1	4.1	1.7	1.4	0.3
Thickness at 9.5 ft, in.	500	1.6	0.1	7.2	1.9	1.5	0.4
Thickness at 11.5 ft, in.	500	1.5	0.1	4.6	1.7	1.4	0.3
Gmm at 6.0 ft, %	500	90.5	0.2	0.3	91.0	90.1	0.9
Gmm at 9.5 ft, %	500	90.1	0.1	0.2	90.5	90.0	0.5
Gmm at 11.5 ft, %	500	91.1	0.1	0.1	91.3	91.0	0.3

Table B.27 GPR Basic Statistics for Project 3 Sublot 7 Sta. 630+00 to 635+00

Measure	N	Mean	Std. Dev.	Coeff. Var.	Maximum	Minimum	Range
Thickness at 2.5 ft, in.	500	1.7	0.1	8.1	2.0	1.4	0.6
Thickness at 6.0 ft, in.	500	1.9	0.2	8.2	2.2	1.6	0.6
Thickness at 9.5 ft, in.	500	2.0	0.3	16.6	2.5	1.5	1.0
Thickness at 11.5 ft, in.	500	1.9	0.2	10.1	2.3	1.5	0.8
Gmm at 6.0 ft, %	500	90.4	0.4	0.4	91.1	89.9	1.2
Gmm at 9.5 ft, %	500	90.4	0.1	0.2	90.7	90.2	0.5
Gmm at 11.5 ft, %	500	90.7	0.3	0.3	91.2	90.2	1.0

Table B.28 GPR Basic Statistics for Project 3 Sublot 8 Sta. 635+00 to 640+00

Measure	N	Mean	Std. Dev.	Coeff. Var.	Maximum	Minimum	Range
Thickness at 2.5 ft, in.	500	1.5	0.1	4.2	1.7	1.4	0.2
Thickness at 6.0 ft, in.	500	1.6	0.1	5.3	1.7	1.4	0.3
Thickness at 9.5 ft, in.	500	1.5	0.1	4.7	1.6	1.4	0.2
Thickness at 11.5 ft, in.	500	1.4	0.1	4.8	1.6	1.3	0.2
Gmm at 6.0 ft, %	500	90.3	0.1	0.1	90.5	90.2	0.3
Gmm at 9.5 ft, %	500	90.7	0.3	0.3	91.0	90.3	0.7
Gmm at 11.5 ft, %	500	90.8	0.3	0.3	91.3	90.4	0.9

Table B.29 GPR Basic Statistics for Project 3 Sublot 9 Sta. 640+00 to 645+00

Measure	N	Mean	Std. Dev.	Coeff. Var.	Maximum	Minimum	Range
Thickness at 2.5 ft, in.	500	1.4	0.1	4.9	1.6	1.4	0.2
Thickness at 6.0 ft, in.	500	1.5	0.1	4.4	1.6	1.4	0.2
Thickness at 9.5 ft, in.	500	1.4	0.1	3.9	1.6	1.3	0.2
Thickness at 11.5 ft, in.	500	1.4	0.1	5.0	1.7	1.3	0.3
Gmm at 6.0 ft, %	500	90.3	0.2	0.2	90.7	89.9	0.8
Gmm at 9.5 ft, %	500	90.9	0.4	0.4	91.6	90.4	1.2
Gmm at 11.5 ft, %	500	91.1	0.2	0.3	91.4	90.6	0.8

Table B.30 GPR Basic Statistics for Project 3 Sublot 10 Sta. 645+00 to 650+00

Measure	N	Mean	Std. Dev.	Coeff. Var.	Maximum	Minimum	Range
Thickness at 2.5 ft, in.	500	1.5	0.1	6.7	1.8	1.3	0.4
Thickness at 6.0 ft, in.	500	1.5	0.1	4.1	1.7	1.4	0.3
Thickness at 9.5 ft, in.	500	1.5	0.1	3.5	1.6	1.4	0.2
Thickness at 11.5 ft, in.	500	1.4	0.1	5.0	1.6	1.4	0.3
Gmm at 6.0 ft, %	500	90.1	0.2	0.2	90.5	89.9	0.6
Gmm at 9.5 ft, %	500	90.7	0.2	0.2	91.1	90.5	0.6
Gmm at 11.5 ft, %	500	91.1	0.2	0.2	91.4	90.7	0.7

Table B.31 GPR Basic Statistics for Project 3 Sublot 11 Sta. 650+00 to 655+00

Measure	N	Mean	Std. Dev.	Coeff. Var.	Maximum	Minimum	Range
Thickness at 2.5 ft, in.	500	1.5	0.1	3.8	1.7	1.4	0.3
Thickness at 6.0 ft, in.	500	1.6	0.0	3.0	1.7	1.5	0.2
Thickness at 9.5 ft, in.	500	1.5	0.0	2.9	1.6	1.4	0.2
Thickness at 11.5 ft, in.	500	1.5	0.0	3.1	1.6	1.4	0.2
Gmm at 6.0 ft, %	500	90.5	0.1	0.1	90.8	90.3	0.5
Gmm at 9.5 ft, %	500	90.5	0.2	0.3	90.9	90.1	0.8
Gmm at 11.5 ft, %	500	90.8	0.2	0.2	91.1	90.6	0.5

Table B.32 GPR Basic Statistics for Project 3 Sublot 12 Sta. 655+00 to 660+00

Measure	N	Mean	Std. Dev.	Coeff. Var.	Maximum	Minimum	Range
Thickness at 2.5 ft, in.	500	1.5	0.1	3.8	1.6	1.4	0.2
Thickness at 6.0 ft, in.	500	1.5	0.1	4.0	1.7	1.4	0.2
Thickness at 9.5 ft, in.	500	1.5	0.1	3.9	1.6	1.4	0.2
Thickness at 11.5 ft, in.	500	1.5	0.1	4.0	1.6	1.4	0.2
Gmm at 6.0 ft, %	500	90.6	0.1	0.1	90.8	90.4	0.4
Gmm at 9.5 ft, %	500	90.0	0.4	0.5	90.5	89.2	1.3
Gmm at 11.5 ft, %	500	90.5	0.3	0.3	91.0	90.0	1.0

Figure 5.68 presents the correlation matrix of the averages and standard deviations from Project 1. Of interest are those correlation coefficients having a p-value greater than 0.5 (or for negative correlations, -0.5) for certain combinations of means and combinations of standard deviations. There are several significant correlations in Figure 5.68, having a p-value > 0.5 , or p-value < -0.5 .

Appendix C – Project Correlations

Correlations were computed using the Pearson product-moment correlation. The basic correlation is a parametric measure of association for two variables assessing the strength and the direction of a linear relationship. If one variable X is an exact linear function of another variable Y, a positive relationship exists if the correlation equals 1 and a negative relationship exists if the correlation equals -1. If there is no linear predictability between the two variables, the correlation is 0. If the two variables are normal with a correlation 0, the two variables are independent. However, correlation does not imply causality because, in some cases, an underlying causal relationship might not exist (SAS 2010).

The formula for the population Pearson product-moment correlation, denoted ρ_{xy} , is shown by Equation C.1:

$$\rho_{xy} = \frac{\text{Cov}(x,y)}{\sqrt{\text{V}(x)\text{V}(y)}} = \frac{\text{E}((x - \text{E}(x))(y - \text{E}(y)))}{\sqrt{\text{E}(x - \text{E}(x))^2 \text{E}(y - \text{E}(y))^2}} \quad (\text{C.1})$$

Where,

Cov = Covariance of two variables, x and y;

V = Variance of a variable, x or y; and

E = Expected value of the entry in the vector X or Y.

The sample correlation, such as a Pearson product-moment correlation or weighted product-moment correlation, estimates the population correlation. The formula for the sample Pearson product-moment correlation is shown by Equation C.2:

$$r_{xy} = \frac{\sum_i ((x_i - \bar{x})(y_i - \bar{y}))}{\sqrt{\sum_i (x_i - \bar{x})^2 \sum_i (y_i - \bar{y})^2}} \quad (\text{C.2})$$

Where,

\bar{x} = sample mean of x ; and

\bar{y} = sample mean of y .

The formula for a weighted Pearson product-moment correlation is shown by Equation C.3:

$$r_{xy} = \frac{\sum_i w_i (x_i - \bar{x}_w)(y_i - \bar{y}_w)}{\sqrt{\sum_i w_i (x_i - \bar{x}_w)^2 \sum_i w_i (y_i - \bar{y}_w)^2}} \quad (\text{C.3})$$

Where,

w_i = weight;

\bar{x}_w = weighted mean of x ; and

\bar{y}_w = weighted mean of y .

Probability values for the Pearson correlation are computed by Equation C.4, and indicate the significance of the correlation:

$$t = (n - 2)^{1/2} \left(\frac{r^2}{1 - r^2} \right)^{1/2} \quad (\text{C.4})$$

Where,

- t = computation from *t* distribution;
- n = sample size with (*n* – 2) degrees of freedom; and
- r* = sample correlation.

Each combination of the mean and standard deviation (2 statistics) for each NDT device (5 devices) yields 10 ‘X’ variables. Then, 100 correlations were computed for 10 ‘X’ variables and 10 ‘Y’ variables.

	IR_Mean	IR_Std Dev	GPRThk_ Mean	GPRThk_ StdDev	GPRDens_ Mean
IR_Mean	1.00000	-0.80109 0.0053	-0.37173 0.2902	-0.03037 0.9336	-0.39270 0.2958
IR_StdDev	-0.80109 0.0053	1.00000	0.16821 0.6423	-0.31469 0.3758	0.28444 0.4582
GPRThk_Mean	-0.37173 0.2902	0.16821 0.6423	1.00000	0.36846 0.2948	-0.07590 0.8461
GPRThk_StdDev	-0.03037 0.9336	-0.31469 0.3758	0.36846 0.2948	1.00000	0.23678 0.5396
GPRDens_Mean	-0.39270 0.2958	0.28444 0.4582	-0.07590 0.8461	0.23678 0.5396	1.00000
GPRDens_StdDev	0.29025 0.4487	-0.21097 0.5858	-0.05564 0.8869	-0.28019 0.4652	-0.25379 0.5099
Nuc_Mean	0.31950 0.3682	-0.48908 0.1514	-0.42718 0.2182	0.18308 0.6127	0.44635 0.2285
Nuc_StdDev	-0.23817 0.5076	0.23731 0.5091	0.43887 0.2045	0.03069 0.9329	0.04484 0.9088
Mod_Mean	-0.91991 0.0002	0.65850 0.0384	0.64926 0.0422	0.14686 0.6856	0.11828 0.7618
Mod_StdDev	-0.24205 0.5005	0.46745 0.1731	-0.16387 0.6510	0.06547 0.8574	0.65806 0.0540
	GPRDens_ StdDev	Nuc_Mean	Nuc_Std Dev	Mod_Mean	Mod_Std Dev
IR_Mean	0.29025 0.4487	0.31950 0.3682	-0.23817 0.5076	-0.91991 0.0002	-0.24205 0.5005
IR_StdDev	-0.21097 0.5858	-0.48908 0.1514	0.23731 0.5091	0.65850 0.0384	0.46745 0.1731
GPRThk_Mean	-0.05564 0.8869	-0.42718 0.2182	0.43887 0.2045	0.64926 0.0422	-0.16387 0.6510
GPRThk_StdDev	-0.28019 0.4652	0.18308 0.6127	0.03069 0.9329	0.14686 0.6856	0.06547 0.8574
GPRDens_Mean	-0.25379 0.5099	0.44635 0.2285	0.04484 0.9088	0.11828 0.7618	0.65806 0.0540
GPRDens_StdDev	1.00000	0.12869 0.7414	-0.53157 0.1408	-0.29576 0.4397	0.03871 0.9212
Nuc_Mean	0.12869 0.7414	1.00000	-0.80691 0.0048	-0.40875 0.2409	0.28399 0.4265
Nuc_StdDev	-0.53157 0.1408	-0.80691 0.0048	1.00000	0.35085 0.3202	-0.28070 0.4321
Mod_Mean	-0.29576 0.4397	-0.40875 0.2409	0.35085 0.3202	1.00000	0.02691 0.9412
Mod_StdDev	0.03871 0.9212	0.28399 0.4265	-0.28070 0.4321	0.02691 0.9412	1.00000

Figure C.1 Project 1 Correlation Matrix

	IR_Mean	IR_StdDev	GPRThk_Mean	GPRThk_StdDev	GPRDens_Mean
IR_Mean	1.00000	0.31744 0.3714	0.05389 0.8825	-0.45934 0.1817	-0.16383 0.6511
IR_StdDev	0.31744 0.3714	1.00000	0.24860 0.4886	-0.17091 0.6369	0.05998 0.8693
GPRThk_Mean	0.05389 0.8825	0.24860 0.4886	1.00000	-0.77169 0.0089	-0.05715 0.8754
GPRThk_StdDev	-0.45934 0.1817	-0.17091 0.6369	-0.77169 0.0089	1.00000	0.23437 0.5146
GPRDens_Mean	-0.16383 0.6511	0.05998 0.8693	-0.05715 0.8754	0.23437 0.5146	1.00000
GPRDens_StdDev	-0.24945 0.4870	-0.29113 0.4144	-0.46632 0.1743	0.55908 0.0929	-0.12993 0.7205
Nuc_Mean	-0.21407 0.5526	0.00051 0.9989	0.29526 0.4075	-0.21576 0.5494	0.22503 0.5319
Nuc_StdDev	0.18633 0.6063	0.00239 0.9948	-0.46720 0.1734	0.35511 0.3140	0.24742 0.4907
Mod_Mean	0.22975 0.5231	0.74763 0.0129	0.34141 0.3343	-0.20541 0.5692	-0.24440 0.4962
Mod_StdDev	-0.06689 0.8543	-0.01273 0.9722	-0.58350 0.0766	0.52165 0.1220	0.49756 0.1434
	GPRDens_StdDev	Nuc_Mean	Nuc_StdDev	Mod_Mean	Mod_StdDev
IR_Mean	-0.24945 0.4870	-0.21407 0.5526	0.18633 0.6063	0.22975 0.5231	-0.06689 0.8543
IR_StdDev	-0.29113 0.4144	0.00051 0.9989	0.00239 0.9948	0.74763 0.0129	-0.01273 0.9722
GPRThk_Mean	-0.46632 0.1743	0.29526 0.4075	-0.46720 0.1734	0.34141 0.3343	-0.58350 0.0766
GPRThk_StdDev	0.55908 0.0929	-0.21576 0.5494	0.35511 0.3140	-0.20541 0.5692	0.52165 0.1220
GPRDens_Mean	-0.12993 0.7205	0.22503 0.5319	0.24742 0.4907	-0.24440 0.4962	0.49756 0.1434
GPRDens_StdDev	1.00000	0.08993 0.8049	-0.08221 0.8214	-0.05354 0.8832	0.12931 0.7218
Nuc_Mean	0.08993 0.8049	1.00000	-0.80810 0.0047	-0.26942 0.4516	0.25480 0.4774
Nuc_StdDev	-0.08221 0.8214	-0.80810 0.0047	1.00000	-0.03157 0.9310	0.26374 0.4616
Mod_Mean	-0.05354 0.8832	-0.26942 0.4516	-0.03157 0.9310	1.00000	-0.53256 0.1130
Mod_StdDev	0.12931 0.7218	0.25480 0.4774	0.26374 0.4616	-0.53256 0.1130	1.00000

Figure C.2 Project 2 Correlation Matrix

	IR_Mean	IR_StdDev	GPRThk_Mean	GPRThk_StdDev	GPRDens_Mean
IR_Mean	1.00000	-0.41992 0.1741	-0.44932 0.1428	-0.56951 0.0532	0.13158 0.6835
IR_StdDev	-0.41992 0.1741	1.00000	0.06887 0.8316	0.01732 0.9574	0.60539 0.0370
GPRThk_Mean	-0.44932 0.1428	0.06887 0.8316	1.00000	0.96015 <.0001	-0.16363 0.6113
GPRThk_StdDev	-0.56951 0.0532	0.01732 0.9574	0.96015 <.0001	1.00000	-0.22408 0.4838
GPRDens_Mean	0.13158 0.6835	0.60539 0.0370	-0.16363 0.6113	-0.22408 0.4838	1.00000
GPRDens_StdDev	-0.18078 0.5739	-0.09367 0.7722	-0.40292 0.1941	-0.27752 0.3825	-0.43907 0.1533
Nuc_Mean	-0.80721 0.0015	0.31794 0.3139	0.23162 0.4688	0.30429 0.3362	-0.36270 0.2466
Nuc_StdDev	-0.51780 0.0846	0.10458 0.7464	0.12070 0.7087	0.14563 0.6516	-0.70458 0.0105
Mod_Mean	-0.74635 0.0053	0.04573 0.8878	0.13979 0.6648	0.34802 0.2676	-0.26558 0.4041
Mod_StdDev	0.75988 0.0041	0.02770 0.9319	-0.25575 0.4224	-0.43662 0.1559	0.34451 0.2728
	GPRDens_StdDev	Nuc_Mean	Nuc_StdDev	Mod_Mean	Mod_StdDev
IR_Mean	-0.18078 0.5739	-0.80721 0.0015	-0.51780 0.0846	-0.74635 0.0053	0.75988 0.0041
IR_StdDev	-0.09367 0.7722	0.31794 0.3139	0.10458 0.7464	0.04573 0.8878	0.02770 0.9319
GPRThk_Mean	-0.40292 0.1941	0.23162 0.4688	0.12070 0.7087	0.13979 0.6648	-0.25575 0.4224
GPRThk_StdDev	-0.27752 0.3825	0.30429 0.3362	0.14563 0.6516	0.34802 0.2676	-0.43662 0.1559
GPRDens_Mean	-0.43907 0.1533	-0.36270 0.2466	-0.70458 0.0105	-0.26558 0.4041	0.34451 0.2728
GPRDens_StdDev	1.00000	0.47650 0.1173	0.51851 0.0841	0.48257 0.1121	-0.24809 0.4369
Nuc_Mean	0.47650 0.1173	1.00000	0.77736 0.0029	0.66286 0.0188	-0.58022 0.0480
Nuc_StdDev	0.51851 0.0841	0.77736 0.0029	1.00000	0.38939 0.2109	-0.42064 0.1733
Mod_Mean	0.48257 0.1121	0.66286 0.0188	0.38939 0.2109	1.00000	-0.89394 <.0001
Mod_StdDev	-0.24809 0.4369	-0.58022 0.0480	-0.42064 0.1733	-0.89394 <.0001	1.00000

Figure C.3 Project 3 Correlation Matrix



WHRP

Wisconsin Highway Research Program
University of Wisconsin-Madison
1415 Engineering Drive
2204 Engineering Hall
Madison, WI 53706
608.890.4966
<http://wisdotresearch.wi.gov/whrp>